Study of Hippo effectors, Yap1 et Wwrt1, during proepicardium formation

Laia Ortiz López

UNIVERSITÉ DE STRASBOURG

ÉCOLE DOCTORALE

DES SCIENCES DE LA VIE ET DE LA SANTE

Institut de génétique et de biologie moléculaire et cellulaire (IGBMC)
UMR 7104/UMR_S 1258

THÈSE présentée par :

Laia ORTIZ LÓPEZ

soutenue le : **26 mars 2021**

pour obtenir le grade de : **Docteur de l'université de Strasbourg**

Discipline/ Spécialité : Biologie

Étude des effecteurs de la voie Hippo, Yap1 et Wwrt1, pendant la formation du proépicarde

THÈSE dirigée par :

Dr. VERMOT Julien	DR2, Université de Strasbourg – IGBMC, FR
Dr. FAHRBACH Florian	Leica Microsystems, DE

RAPPORTEURS :

Dr. TORRES Miguel	PR – CNIC, SP
Dr. JOPLING Chris	DR – IGF, FR

AUTRES MEMBRES DU JURY :

Dr. GODIN Juliette	DR – IGBMC, FR

“Causa admiración como trabaja el corazón”

Late el corazón – Amanece que no es poco

“I de vegades una tonteria de sobte ens indica que ens en sortim”

Captatio Benevolentiae – Manel

Acknowledgements

First, I would like to thank the members of my jury Dr. Juliette Godin, Dr. Miguel Torres and Dr. Chris Jopling for accepting to evaluate my work.

Next, I would like to thank my advisors Dr. Julien Vermot and Dr. Florian Fahrbach for the continuous support of my PhD study and related research and for their patience, motivation and knowledge.

I thank my labmates for the discussions and constant support: Elena, Helene, Renee, Pedro, Rita, Nathalie and Hajime. Especially I would like to thank Marina for all her support, knowledge, help, guidance and friendship during my PhD.

I would also like to thank Dr. Jens Kroll and his laboratory members for allowing me to use their fish facility and for having me in their lab meetings, sharing my research and learning about theirs. It was nice to learn that the zebrafish is more than a heart.

Also, I thank all the people form the platforms of IGBMC and my co-workers from Leica Microsystem for their help.

I would like to thank to the other members of the 4D Heart: Elena, Paul, Eleonora, Tiago and Morena. It was a pleasure to have you by my side during this project and I hope that we really do in the future all the things that we said we should.

Also, I thank the Spanish gang for being always there: Bea, Arantxa, Xenia, Jordi, Pau, Roberto, Raquel and Rafa.

Finalment, m'agradaria agrair-li a la meva família que sempre han cregut en mi més que ningú i als meus amics a Barcelona i a l'Alemanya, especialment a l'Anna, la Carolina, la Laura i al Marc.

And in case I forgot someone, thank you to you too.

Table of contents

List of publications, posters and oral communications

Publications

- Peralta, M., Ortiz Lopez, L., Jerabkova, K., Lucchesi, T., Vitre, B., Han, D., Guillemot, L., Dingare, C., Sumara, I., Mercader, N., Lecaudey, V., Delaval, B., Meilhac, S. and Vermot, J., 2020. Intraflagellar Transport Complex B Proteins Regulate the Hippo Effector Yap1 during Cardiogenesis. *Cell Reports*, 32(3), p.107932.

- In preparation: Yap/Wwtr1-Tead activity during proepicardial cluster formation

Posters

- Symposium Israel-Unistra-Académie des Sciences, Strasbourg, 24th October 2018.
  Title: In vivo actin dynamics during proepicardial formation in zebrafish
  Authors: Laia Ortiz López, Marina Peralta, Julien Vermot

- European Developmental Biology Congress, Alicante, 23rd – 26th October 2019.
  Title: YAP/WWTR1-TEAD activity during proepicardial cluster formation
  Authors: Laia Ortiz López, Marina Peralta, Elena Remacha, Nadia Mercader, Florian Fahrbach, Julien Vermot

Oral presentations

- 4D Heart conference: Quantitative in vivo imaging, 3rd June 2020
  Title: Molecular mechanism of proepicardium formation in zebrafish via multiple inhibitions of Tead activity

- 2020 Tri-Regio Developmental Biology and Stem Cell Meeting, Online Conference, 15th – 16th October.
  Title: Yap/Wwtr1-Tead activity during proepicardial cluster formation

Outreach activities

- Poster in European Researchers' Night 2019. 27th September.
  Title: Quantification of cardiac development using optical manipulation
  Authors: Laia Ortiz López, Marina Peralta, Elena Remacha, Florian Fahrbach, Julien Vermot

- Declics (Dialogues Entre Chercheurs et Lycéens pour les Intéresser à la Construction des Savoirs). Cercle Fser. 21 December 2018.
  Visit to the Lycée Marie Curie.

Others

- Using a Rotation Device for DLS Sample Mounting: TCS SP8 DLS Digital LightSheet Protocol (https://www.leica-microsystems.com/science-lab/using-a-rotation-device-for-dls-sample-mounting/)

- Advertisement feature. M. Julia Roberti, Laia Ortiz Lopez, Giulia Ossato, Irmtraud Steinmetz, Petra Haas, Frank Hecht, Luis A. J. Alvarez. Application note: TauSense: a fluorescence lifetime-based tool set for everyday imaging. *Nature Methods*

List of figures

Introduction

In vivo heart imaging with Leica TCS SP8 DLS

Figure 9. Placing the FEP tube in the rotation device (first step).

Figure 10. Placing the FEP tube in the rotation device (final step).

Figure 11. TCS SP8 DLS scanning stage with rotation device.

Figure 12. Drosophila embryo observed from different sides. Single planes were taken from 3D image stacks.

Intraflagellar Transport Complex B Proteins Regulate the Hippo effector Yap1 during Cardiogenesis

Graphical abstract.

Figure 1. IFT Complex B Proteins Regulate Proepicardial Development in Zebrafish and Mice

Figure 2. BMP Signaling Is Increased in *ift88*, *elipsa/ift54*, and *Ift20* Mutants

Figure 3. Yap1-Tead Activity Is Increased in *ift88*, *elipsa/ift54*, and *Ift20* Mutants during Proepicardium Development

Figure 4. IFT88 and IFT20 Are Physically Associated to YAP1, and IFT88 Modulates YAP1 Activity

Figure S1. *IFT complex B* mutants show increased proepicardialsize without affecting Islet1 cell number in zebrafish. Related to Figures 1 and 2.

Figure S2. Cilia protruding into the pericardial cavity are distributed heterogeneously in zebrafish during proepicardial development. Related to Figures1 and 3 and STAR methods.

Figure S3. Ift20 KO mice proepicardial cells lack cilia. Related to Figures1 and 2.

Figure S4. bmp4 is overexpressed in *ift88, elipsa/ift54*, and *Ift20* mutants. Related to Figure 2.

Figure S5. Yap1 activity is increased in the myocardium of *ift88* and *elipsa/ift54* zebrafish mutants and AMOTL1 activity is increased in IFT20 KO mice proepicardium. Related to Figure 3.

Figure S6. IFT88-GFP co-localize with YAP1 in the cytoplasm. Related to Figure 4.

Figure S7. IFT88 and IFT20 regulate YAP1 activity. Related to Figure 4.

Study of Yap1/Taz-Tead activity during PE cluster formation

Figure 1. Yap1/Taz-Tead in the dorsal pericardium.

Figure 2. Yap1/Taz-TEAD in vivo activation during PE cluster formation.

Figure 3. Modifying Yap1/Taz-Tead activity chemically impacts PE cluster formation.

Figure Supplementary 3. Dexamethasone increases GFP intensity in 4xGTIIC:d2GFP embryos but Yap1 mutations is not affecting PE formation.

Figure 4. Description of *lkb1* mutants at key points of PE cluster formation.

Figure Supplementary 4. Description of *lkb1* mutants at key points of PE cluster formation.

How is PE cluster formation affected by changes in fluid forces?

Figure 1. Modifying heartbeat affects PE cluster formation.

Figure 2. PE cluster in Yap1 injected with *tnnt2a* MO and changes in *4xGTIIC:d2GFP* after BDM treatment.

Looking for possible mechanoregulators of PE cluster formation

Figure 1. Study of PE cluster in mutants with primary cilia defects.

Figure 2. Study of PE cluster in *Klf2a/b* mutants.

List of abbreviations

CHD: Congenital heart disease
CVD: Coronary vascular disease
CC: Cardiac crescent
HT: Heart tube
FHF: first heart field
SHF: second heart field
AVC: atrio-ventricular canal
PE: proepicardium/proepicardial
Wt1: Wilms' tumor suppressor 1
Tbx18: T-box transcription factor 18
HPF: hours post-fertilization
DP: dorsal pericardium/dorsal pericardial
VP: venus pole
AP: arterial pole
BMP: bone morphogenetic protein
acvr1l: Activin A receptor type 1
HPSC: human pluripotent stem cells
EMT: epithelial-to-mesenchymal transition
Lkb1: liver kinase B1
IFT: intraflagellar transport
Kif3a: Kinesin family member
CUP: curly up
LPM: late plate mesoderm
MO: morpholino
Klf2a: Krüppel like factor 2a
DPF: days post-fertilization
ECM: extracellular matrix

PhD thesis outline

The epicardial layer is essential for heart development and proper heart function. Without the epicardium, embryonic development fails due to the failure of the coronary vessels and myocardium to form. It is also a key player during cardiac regeneration. The epicardium arises from an extracardiac cell cluster called proepicardium (PE). Proepicardial cells emerge from the dorsal pericardium, undergoing major cell shape changes. Despite the importance of the PE and the epicardial layer, there are many steps in PE development that are still not understood. In my PhD project, we aimed to explore the role of Yap/Taz-Tead activity in PE formation, as well as pinpoint new regulators important for this process.

To achieve these aims, we defined the following objectives:

- Describe Yap1/Taz-Tead activation in the dorsal pericardium, the PE, and the epicardial layer *in vivo*.
- Study the role of Yap1/Taz-Tead signalling during PE cluster formation, as well as study models of Yap1/Taz-Tead activity upregulation and dowregulation.
- Find new regulators of PE cluster formation.
- Study possible mechanosensors involved during PE cluster formation.

These objectives are reflected in the structure of this thesis as follows:

- Introduction
- Materials and methods
- *In vivo* imaging with Leica TCS SP8 DLS
- *Intraflagellar Transport Complex B Proteins Regulate the Hippo effector Yap1 during Cardiogenesis*
- Study of Yap1/Taz-Tead activity during PE cluster formation
- How is PE cluster formation affected by changes in fluid forces?
- Looking for possible mechanoregulators of PE cluster formation

Finally, Annex I contains an advertisement feature that I helped to create while I was working at Leica Microsystem. I contributed to the feature by imaging the fish embryos and by taking part in the writing process.

Plan de la thèse de doctorat

La couche épicardique est essentielle au développement du cœur et à son bon fonctionnement. Sans l'épicarde, le développement embryonnaire échoue en raison de l'absence de formation des vaisseaux coronaires et du myocarde. Il est également un acteur clé lors de la régénération cardiaque. L'épicarde naît d'un groupe de cellules extracardiaques appelé proépicarde (PE). Les cellules proépicardiques émergent du péricarde dorsal, subissant d'importants changements de forme cellulaire. Malgré l'importance du PE et de la couche épicardique, de nombreuses étapes du développement du PE ne sont toujours pas comprises. Dans mon projet de thèse, nous avons cherché à explorer le rôle de l'activité de Yap/Taz-Tead dans la formation du PE, ainsi qu'à identifier de nouveaux régulateurs importants pour ce processus.

Pour atteindre ces buts, nous avons défini les objectifs suivants :

- Décrire l'activation de Yap1/Taz-Tead dans le péricarde dorsal, le PE et la couche épicardique *in vivo*.
- Étudier le rôle de la signalisation Yap1/Taz-Tead pendant la formation du PE, ainsi qu'étudier les modèles d'upregulation et de dowregulation de l'activité Yap1/Taz-Tead.
- Trouver de nouveaux régulateurs de la formation du PE.
- Étudier les mécanosenseurs possibles impliqués dans la formation du PE.

Ces objectifs sont reflétés dans la structure de cette thèse comme suit:

- Introduction
- Matériel et methods
- Imagerie *in vivo* avec Leica TCS SP8 DLS
- Les protéines du complexe de transport intraflagellaire B régulent l'effecteur Hippo Yap1 pendant la cardiogenèse
- Étude de l'activité de Yap1/Taz-Tead pendant la formation du PE
- Comment la formation du PE est-elle affectée par les changements des forces fluides?
- Recherche de mécanorégulateurs possibles de la formation du PE

Enfin, l'annexe I contient une fonctionnalité publicitaire que j'ai contribué à créer lorsque je travaillais chez Leica Microsystem. J'ai contribué à la réalisation de ce reportage en réalisant des images d'embryons de poissons et en prenant part au processus de rédaction.

Introduction

The heart is the first organ to acquire its function in the developing embryo, providing the forming organs with oxygen and nutrients. Heart development is a complex, highly regulated process that when dysregulated results in congenital heart disease (CHD). In the human population, 1% of live births present CHD, and heart malformations explain around 30% of fetus loss during gestation (Bruneau 2008). Furthermore, cardiovascular disease (CVD) is the leading cause of death worldwide, responsible for 16% of the world's total deaths (WHO 2016). Specifically, 4 out of 5 CVD deaths are caused by heart attacks and strokes (WHO 2016). For all these reasons, a better understanding of heart development might open new avenues for regenerative medicine after myocardial infarction that are based on enhancing pathways active during embryogenesis to promote cardiac regeneration (Xin, Olson, and Bassel-Duby 2013; Tzahor and Poss 2017).

Heart development

In adult humans, the heart lies in the anterior part of the body in the middle compartment of the chest. It is surrounded by the pericardium, which contains a small amount of fluid, and it is nourished by the coronary vessels. The heart is divided into four chambers: right atrium, right ventricle, left atrium and left ventricle. Between chambers, we find the heart valves: these structures can be closed or opened, maintaining the flow in a single direction and preventing backflow (Figure 1A). The right atrium receives deoxygenated blood from the vena cava and it passes to the right ventricle. Blood is then pumped to the pulmonary circulation. It is oxygenated in the lungs and it returns to the left atrium, passing through the left ventricle first and then the left atrium, where it is pumped to the systemic circulation to provide the whole body with oxygen and nutrients.

The heart is composed of three layers: the epicardium, the myocardium, and the endocardium. The endocardium is an endothelial layer in direct contact with the blood. The myocardium is the cardiac muscle, responsible for heart contraction. The epicardium is the outermost layer covering the heart. Oxygen

and nutrient supply, as well as the removal of metabolic waste, is performed in the heart by the coronary vasculature.

1. Heart development in model organisms

In order to improve our knowledge and understanding of heart development and cardiovascular diseases, several animal models are currently used. It is important to define which question we would like to address before choosing a model. In chickens and mice, as in humans, the heart is composed of 4 chambers (Figure 1B). In zebrafish, the heart has only 2 chambers: a single atrium and a single ventricle (Figure 1C). In all of these animal models the heart comprises the 3 same layers as the human heart (Figure 1D).

The mouse embryo is a mammalian model well established for heart development. There are a large amount of genetic tools available in the mouse embryo, such as gene editing. However, since mice embryonic development occurs *in utero*, it is very challenging to follow heart development *in vivo*. Although mice are more similar to humans, the zebrafish offers several advantages for studying heart development (Stainier, Lee, and Fishman 1993). Zebrafish embryos are not completely dependent on a functional cardiovascular system in the early steps of heart development, since embryos without blood circulation can still obtain oxygen by passive diffusion and survive until 7 days post fertilization (dpf) (Sehnert et al. 2002). This allows the analysis of embryos with severe cardiovascular defects that is not possible with other animal models. Moreover, the optical transparency of zebrafish embryos, as well as their external development, facilitates *in vivo* imaging of heart development. Combined with new transgenic technologies, zebrafish is an animal model widely used for the study of heart development (Bakkers 2011).

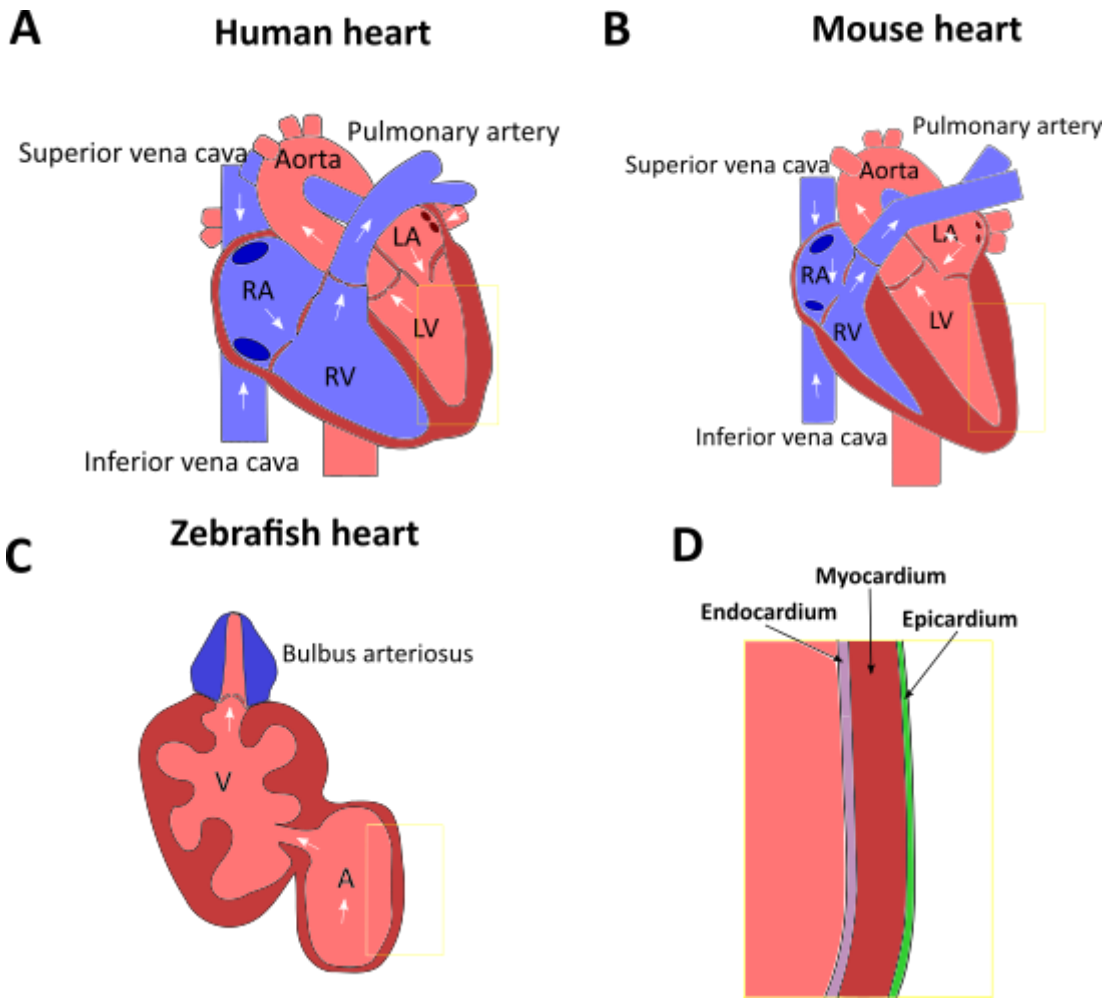

Figure 1. The heart in various animal models. (A) Frontal view of a human heart (B) Frontal view of a mouse heart (C) Frontal view of a zebrafish heart. In the mammalian and the avian heart we have 4 chambers. The zebrafish heart is composed of 2 chambers. White arrows indicate the blood flow direction. (D) The walls of the heart consist of three layers: the endocardium, the myocardium and the epicardium. RA: Right Atrium; RV: Right Ventricle; LA: Left Atrium; LV: Left Ventricle; A: Atrium; V: Ventricle.

2.1. Heart development in the mouse

Heart development in mice starts shortly after gastrulation (Meilhac and Buckingham 2018; Vincent and Buckingham 2010). Fate mapping showed that the first cardiac progenitors are located in the anterior region of the primitive streak. After gastrulation, cardiac precursors in the mesoderm differentiate into cardiomyocytes and form a bilateral structure called cardiac crescent (cc). By a complex morphogenetic process, the cc transforms into a primitive heart tube (HT) which rapidly begins to pump blood (Vincent and Buckingham 2010). The mature heart is formed by 2 main populations of progenitor cells: the first heart field (FHF) and the second heart field (SHF). The primitive HT (FHF) will give rise to the left ventricle. The SHF contributes to the elongation of the arterial and the venous pole of the heart (Buckingham, Meilhac, and Zaffran 2005), giving rise to the right ventricle, the left and right atrium, and the outflow tract (Figure 2) (Meilhac and Buckingham 2018; Ivanovitch, Temiño, and Torres 2017).

Progenitor FHF cells have not any specific gene marker, as it is hard to distinguish genes expressed in the cardiac crescent that are beginning to differentiate into cardiomyocytes (Meilhac and Buckingham 2018).

Cells from the SHF, on the other hand, express characteristic markers. *Fgf10* and *Fgf8*, for instance, are required for the correct formation of the right ventricle and outflow region of the heart. Another known marker is Isl1. *Isl1*-mutant mice show defects at the venous pole in the atria, as well as at the arterial pole in right ventricular and outflow tract development (Meilhac and Buckingham 2018).

As the cardiac tube elongates, it undergoes rightward looping and the poles of the heart tube converge and become juxtaposed. The cardiac chamber then grows out from the looping tube in a process called ballooning, leading to the formation of the right and left ventricles and the atria (Vincent and Buckingham 2010).

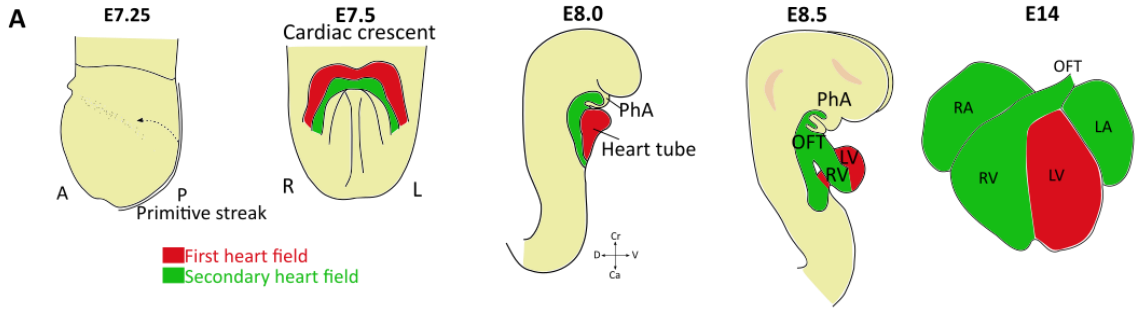

Figure 2. Heart development in mouse. First progenitor cells are found in the primitive streak. Then cardiac precursors differentiate into cardiomyocytes and form the cardiac crescent. A: anterior; P: posterior; R: right; L: left; PhA: pharyngeal arches; OFT: outflow tract; LV: left ventricle; RV: right ventricle; LA: left atrium; RA: right atrium. Adapted from (Meilhac and Buckingham 2018)

While the endocardium develops in close association with the myocardium, the epicardium emerges from the proepicardium, a transitory mesenchymal structure that forms at the posterior end of the heart tube at E9.5 (Vincent and Buckingham 2010).

Endocardial cells come from a subset of cardiac progenitor cells mapped in the primitive streak stage. It is not yet known whether endocardial cells derive from cells in close proximity to the cardiomyocytes in the primitive streak or if there is a common progenitor (Nakano et al. 2016; Meilhac and Buckingham 2018).

2.2. Heart development in the zebrafish

Although the zebrafish heart comprises 2 chambers, it recapitulates the main development steps during embryonic heart formation in mouse (Liu and Stainier 2012). First, cardiac progenitors can be found at the blastula stage. The ventricular pool resides more dorsally and closer to the margin than the atrial pool, while endocardial progenitors are located across the lateral margin without any specific spatial organization (Figure 3). During gastrulation, these progenitors migrate to reside in the posterior half of the anterior lateral plate mesoderm (LPM) by 15 hpf (Figure 3).

As they differentiate, the bilateral populations of myocardial precursors start to migrate toward the embryonic midline. After making contact, the two populations merge to form the cardiac cone (Figure 3) (Stainier, Lee, and

Fishman 1993). The embryonic heart starts to beat at 22 hpf. By 24 hpf, the cardiac cone has evolved into a linear HT, where the endocardial precursor stream medially and posteriorly, coating the HT. (Sainier, Lee, and Fishman 1993). The HT gradually grows and loops rightwards. Next, the V and At form by ballooning out. At 48 hpf, the ventricle and the atrium are separated by the constriction of the atrio-ventricular canal (AVC) and the heart starts to grow through the addition of cardiac progenitors from the arterial and venous pole (Bakkers 2011). Like in mammals and birds, the SHF population contributes to the arterial pole myocardium after the initial heart tube formation (Hami et al. 2011). Several signalling pathways are important for SHF cell fate determination. Fgf8, for instance, is required for cardiomyocyte differentiation at the arterial pole (de Pater et al. 2009). Hippo pathway is also involved in SHF cell fate determination. An increase in activity of Hippo pathway effectors Yap1/Wwtr1 promotes the size of the SHF while inhibiting Yap1/Wwrt1 restricts it. This regulation happens through the BMP pathway. Yap1/Wwrt1 promotes Bmp2 expression and this promotes venous pole identity and increases atrial CM number (Fukui et al. 2018).

At 72 hpf, differentiated cardiomyocytes in the myocardium start to protrude towards the lumen, generating small clusters of cells. These clusters of cells will form the trabeculae, highly organized sheet-like muscular structures that form as a result of the extrusion and expansion of differentiated cardiomyocytes into the lumen of the ventricular chambers. Cardiac trabecular formation is essential for proper heart development and failures in trabeculae formation can result in embryonic lethality or cardiomyopathies (Liu et al. 2010).

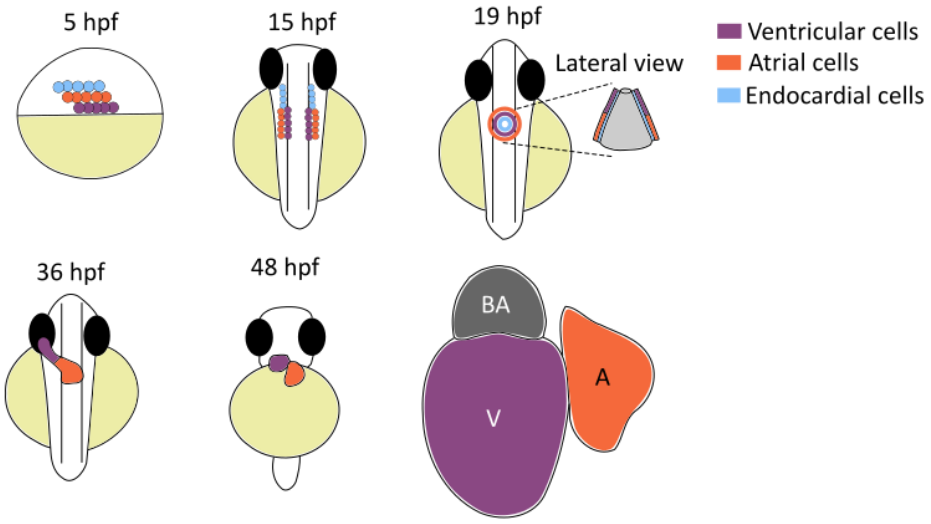

Figure 3. Heart development in zebrafish. In early timepoints, cardiac progenitors are placed in bilateral pools in the late plate mesoderm. Atrial, ventricular and endocardial progenitors are separated. Cells then migrate to the midline were myocardial fuse and form the cardiac tube, while the endocardial cells start to migrate inside the cone. This later forms the heart tube, which, starting at 48 hpf, will change its shape in a heartbeat-dependent process involving both looping of the tube and ballooning of the cardiac chambers. Finally, the heart will be formed by an atrium, ventricle, and the bulbus arteriosus. V: ventricle; A: atrium; BA: bulbus arteriosus. Adapted from (Brown et al. 2016; Bakkers 2011).

During heart development, physical forces generated by cardiac contractility and blood flow play an essential role. From the onset of heartbeat, blood flows through the cardiac lumen and this influences heart development at several steps, such as chamber formation (Granados-Riveron and Brook 2012), the progression of trabeculation, and chamber differentiation (Rasouli and Stainier 2017; Peshkovsky, Totong, and Yelon 2011; Staudt et al. 2014). In particular, mechanical forces are needed for proper valve development.

Several mechanosensors are important in this process. For instance, the opening of mechanosensitive channels like TRP or Piezo families is associated with calcium fluxes, which initiate intracellular signalling cascades (Steed, Boselli, and Vermot 2016). Two TRP channels, Pkd2 and Trpv4, regulate the expression of the transcription factor *Krüppel like factor 2a* (*Klf2a*). Klf2a regulates the expression of flow-resposible genes in endothelial cells, which

promote the formation of cardiac valves (Heckel et al. 2015; Vermot et al. 2009). Piezo channels, on the other hand, are necessary for proper outflow tract valves formation (Duchemin, Vignes, and Vermot 2019).

3. The Proepicardium

The epicardium is a single layer of flat mesothelium covering the myocardium. It starts to form at the time of heart looping. It is important for myocardial maturation (Männer 1993; Pennisi, Ballard, and Mikawa 2003) and gives rise to the coronary vasculature (Mikawa and Fischman 1992) and the intracardiac fibroblasts (Wessels et al. 2012). Importantly, the epicardium plays a key role in heart regeneration (J. Cao and Poss 2018).

The epicardium derives from the proepicardium (PE), a cluster of mesothelial cells in a cauliflower-like shape that forms close to the venous pole of the cardiac tube (Männer 1999). Interestingly, the PE was already known among embryologists of the 19th century. In 1909, Kurkiewicz identified the PE as the source for epicardial cells in the chick embryonic heart (Kurkiewicz and T 1909). This theory was not taken into account until it was rediscovered in the 1970s (Bodmer and Wassarman 2008). The PE has been described in several vertebrates, from fish to human (Hirakow 1992; Fransen and Lemanski 1990; Komiyama, Ito, and Shimada 1987; Kuhn and Liebherr 1988; Nesbitt et al. 2006; Icardo et al. 2009; Jahr et al. 2008; Serluca 2008). In mice, the PE is a cluster formed by a mixture of cells, including cells derived from epithelial and mesenchymal lineages, located in close proximity to the septum transversum (Viragh and Challice 1981). In zebrafish, the PE is composed of two clusters located both in the dorsal pericardium (DP). One cluster, which we will refer to as the avcPE, is located in the atrioventricular channel area, and the other one, which we will refer to as the vpPE, is located close to the venous pole. There is an additional source of cells, the apPE, close to the arterial pole area that can also contribute to the epicardium (Peralta et al. 2013).

Different molecular markers are used to define epicardial and PE identity, such as Wilms' tumor suppressor 1 (Wt1), T-box transcription factor 18 (Tbx18), and

the transcription factor Tcf21 (Carmona et al. 2001; Kraus, Haenig, and Kispert 2001; Tanaka and Tickle 2004; Robb et al. 1998).

3.1. PE formation

In the zebrafish, PE cluster formation begins around 48 hpf (Figure 4A) (Serluca 2008). Live imaging using a *wt1a* reporter line showed that mesothelial cells from the DP migrate collectively towards a midline between the venous pole area and the outflow tract area. Some cells of the DP rearrange their actin network, round up and form the PE cluster in a process reminiscent of epithelial apical extrusion (Figure 4B-C) (Andrés-Delgado et al. 2019). This process is dependent on actomyosin network, since it has been shown that BDM treatment, which disrupts the network, avoids PE cluster formation. While there is no cell division in cells from the midline, it is thought that the process whereby cells converge to the midline is driven by the proliferation of cells in the DP located far from the midline (Andrés-Delgado et al. 2019). PE cells remain loosely attached to neighbouring DP cells (Andrés-Delgado et al. 2019) (Figure 4C). Then, cells from the vpPE and the avcPE are released and are advected into the flow until they attach to the myocardium, while cells from the apPE migrate directly to the myocardium without being released.

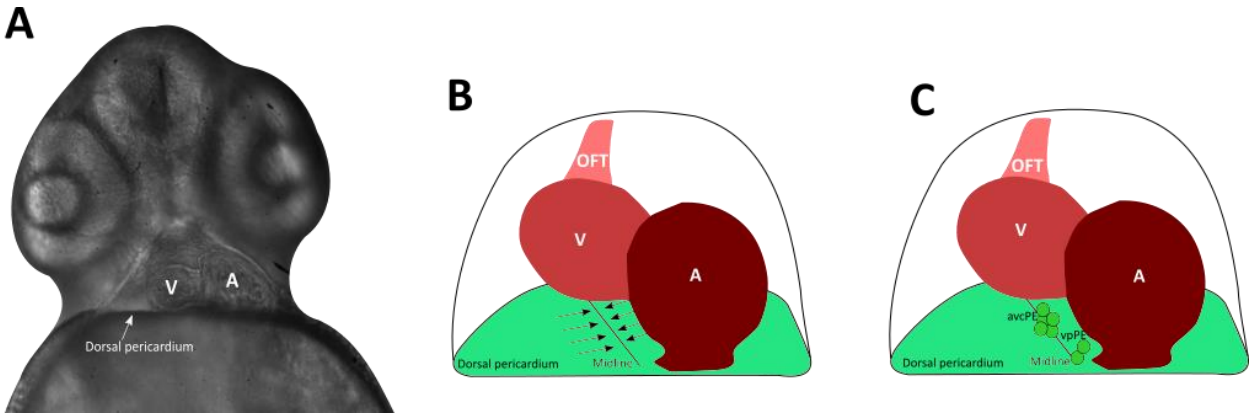

Figure 4. PE cluster formation in zebrafish. (A) Brightfield image of a zebrafish at 48 hpf, when PE cluster formation starts. (B) Cells from the dorsal pericardium converge through the midline. (C) 2 PE clusters can be found in later stages in the midline: the avcPE and the vpPE. V:ventricle; A:atrium; OFT: outflow tract. Adapted from (Andrés-Delgado et al. 2019; Peralta et al. 2013).

In mice live imaging does not allow yet a detailed description of PE cluster formation. The PE cluster is initially present in E9.0 through E9.75 and appears as an outgrowth of mesothelial cells adjacent to the liver bud and the sinus venosus (Cossette and Misra 2011). Starting at E9.5, cells from the PE delaminate and are released into the pericardial coelom. Then, they attach to the myocardium and migrate to cover the surface of the heart. There is also a contribution by migrating proepicardial cells directly over the adjacent myocardium (Viragh and Challice 1981).

3.2. Origin of the PE and mechanisms inducing PE formation

Genetic mapping in mice has shown that PE cells express *Nkx2.5* and *isl1* at some point in their development. These both genes are expressed in the primary and secondary heart fields, respectively, suggesting that the PE arises from the LPM (Maya-Ramos et al. 2013). In zebrafish, it has been described that a defect in midline migration of the lateral plate mesoderm results in cardia bifida. Interestingly, each of the hearts has its own PE. The presence of bilaterial PE suggests that the origin of the epicardium in zebrafish also lies in the LPM (Serluca 2008). Genetic mapping in the chick mapped the origin of the PE cells in the LPM, adjacent but not mixed to the cardiogenic mesoderm (Bressan, Liu, and Mikawa 2013).

It is still largely unknown how PE cell identity is induced. In chick, ectopic implantation of quail liver bud induces expression of *wt1, tbx18,* and *tcf21* in adjacent host tissue. In zebrafish lacking mature hepatocytes (*hnf1ba* mutants), *wt1, tbx18,* and *tcf21* are expressed at wild-type levels, indicating that the liver is not necessary for PE molecular induction (Maya-Ramos et al. 2013). The *T-box transcription factor 18* is strongly expressed in the PE and in the epicardium (Kraus, Haenig, and Kispert 2001; Tanaka and Tickle 2004). *Tbx18* inactivation in the mouse embryo causes defects in the epicardium, coronary vasculature, and the venous pole (Pérez-Pomares and de la Pompa 2011).

Wt1 is a known epicardial marker, already expressed in PE cells, that regulates the expression of important genes for epicardium development (Kirschner et al. 2006). In mutant mice lacking Wt1, the epicardium fails to cover the entire heart (Moore et al. 1999).

Tcf21 is a basic helix-loop-helix transcription factor expressed in the PE, the epicardium, and the pericardium. In Xenopus, when *tcf21* is lacking, epicardial cells fail to form a cohesive polarized sheet and are retained in a proepicardial state (Tandon et al. 2013). In chick and mice, *tcf21* depletion results in epicardial blistering (Braitsch et al. 2012).

Studies in zebrafish show that bone morphogenetic protein (BMP) plays a role in PE cluster formation (Liu and Stainier 2010). Zebrafish mutants lacking Activin A receptor type 1 (acvr1l), a functional type I BMP receptor, lose *tbx18* and *tcf21* expression in the heart (Liu and Stainier 2012).

The importance of BMP during epicardial development was also described in a paper from 2015 where they differentiated functional epicardial cells from human pluripotent stem cells (HPSC) (Iyer et al. 2015). In this study, HPSC cells were first differentiated to an early mesoderm. After Bmp4 treatment, cells increased the expression of epicardial markers. In addition to Bmp, RA and Wnt signaling was also promoted to obtain differentiated epicardial cells. These HPSC-derived epicardial cells not only resembled human fetal epicardial cells, but they were also able to contribute to the coronary vasculature of a developing chicken (Iyer et al. 2015).

In zebrafish, actomyosin dynamics driving PE morphogenesis are regulated by Bmp. In this context, Bmp promotes actin polymerization, dynamics and/or stability. When the actomyosin network is disrupted using BDM, Bmp2b stabilizes F-actin and recuperates PE formation. Bmp2 might be rescuing the F-actin tension by modulating the expression of other non-conventional myosins, such as Myh9 or non-muscle myosin Va, or by promoting the expression of proteins involved in actomyosin dynamics (Andrés-Delgado et al. 2019). Besides being important for actomyosin network regulation, BMP is an upstream effector of the zinc-finger transcription factor Gata4 in the LPM (Rojas et al. 2005). This factor is also important for PE, since it has been described that Gata4 mutant mice lack PE and have severe heart defects (Watt et al. 2004). This phenotype is not fully recovered with the expression of other members of the Gata family, such as Gata6, as the PE is smaller than in wild-

type, there are fewer epicardial cells attached, and the expression of *tbx18* is decreased (Borok, Papaioannou, and Sussel 2016).

Another known regulator of PE formation is *Tbx5*. In zebrafish, *tbx5a* is expressed in the LPM and when lacking, the expression of *tbx18* and *tcf21* is strongly decreased. It has also been proposed that *Tbx5a* expression allows LPM cells to have the ability to respond to Bmp signals and initiate PE formation (Liu and Stainier 2010). In chick, epicardial cells in early development express *tbx5*. When the cluster is formed, proepicardial cells are *tbx5* negative until they get close to the myocardium, when some of them reactivate *tbx5* expression. This suggests that factors from the myocardium might be regulating PE cluster formation (Bimber, Dettman, and Simon 2007). In humans, *tbx5* is expressed in the coronary vasculature and in the epicardium (Hatcher et al. 2004). Loss of *tbx5* expression accounts for Holt-Oram syndrome, a rare autosomal dominant disease which is characterized by upper limb malformations and cardiac septation defects (OMIM 2006).

Hand2 is another transcription factor expressed in the LPM that is critical for the differentiation of LPM derivatives and that seems to be important for PE cluster formation. In *hand2* zebrafish mutants, the PE cluster is completely absent, suggesting that it is required for the differentiation of mesodermal cells into PE cells. However, *hand2* mutants have severe cardiac malformation and the phenotype could be due to myocardial defects (Liu and Stainier 2010).

Genes involved in left-right assymmetry also influence the development of the proepicardium. In chick, the proepicardium forms from bilaterally symmetric structures that develop asymmetrically, as the proepicardium forms just on the right side of the cavity. When right-sided gene expression determintants, such as *fgf8* or *snai1* are disrupted, there is a loss of *tbx18* expression in the right inflow (Svensson 2010; Schlueter, Brand, and Martin 2009). In mice, however, left-right asymmetry genes do not seem to be regulating PE formation, as both right and left proepicardial precursors will develop equally and fuse in the midline to generate the proepicardium (Svensson 2010) . In zebrafish, both proepicardial primordia develop to form the PE cluster (Serluca 2008).

In mice, the Hippo signaling components are expressed during epicardium formation (Singh et al. 2016). Their expression in the PE has not yet been described, but mice where both *Yap* and *Taz* have been knocked out specifically in the PE and the epicardium show embryonic lethality, suggesting that the PE cluster does not form properly in these mice. Moreover, Yap and Taz regulate *Wt1* and *Tbx18* expression (Singh et al. 2016). In zebrafish, epicardial cells also express the Hippo signaling component Taz (or Wwtr1) (Lai et al. 2018).

3.3. Transfer of PE cells to the myocardium during epicardium formation

There are two main mechanisms of PE cell transfer to the myocardium: the formation of a transient bridge between the PE and the myocardium (Figure 5A), and the release of PE cells to the pericardial cavity followed by their progressive attachment to the myocardial surface (Figure 5B). Depending on the species, PE cell transfer occurs via one of the two mechanisms or via both mechanisms (Rodgers et al. 2008).

In *Xenopus*, the PE cluster establishes a firm contact with the developing ventricle and a bridge is established. Once the bridge is established, the PE cells transfer to the heart and spread over the myocardial surface to form a primitive epicardium (Jahr et al. 2008). A similar mechanism occurs in chick (Schulte et al. 2007).

In mice, however, a bridge does not seem to form. Instead, cells of the PE cluster are released into the pericardial cavity, after which they adhere to the myocardial surface, forming a primitive epicardium (Schulte et al. 2007).

In zebrafish, both methods have been observed. Cells from the apPE transfer directly to the myocardium, similarly as in birds and *Xenopus.* Cells from the other avcPE and vpPE cluster, however, are released into the pericardial cavity and are advected with a periodical motion coupled to the heartbeat. Epicardial cells preferentially adhere first to the distal half of the ventricle and later colonize the proximal half. The distal half of the ventricle is the area where the cells are advected at the lowest speed in the pericardial cavity, which suggests that PE cell attachment is a process resulting from the balance between PE cell

adhesiveness to the myocardium and the differential flow forces. Finally, the myocardium is fully covered at around 6 dpf (Peralta et al. 2013).

A proposed hypothesis is that differences in PE cell attachment to the myocardium are due to the differences in coelomic cavities. In chicken and *Xenopus*, at the time of PE formation, the cavity is not closed and the bridge ensures that cells are not lost. In mammals and zebrafish, the pericardial cavity is lost and PE cell release is predominant (Peralta et al. 2014) .

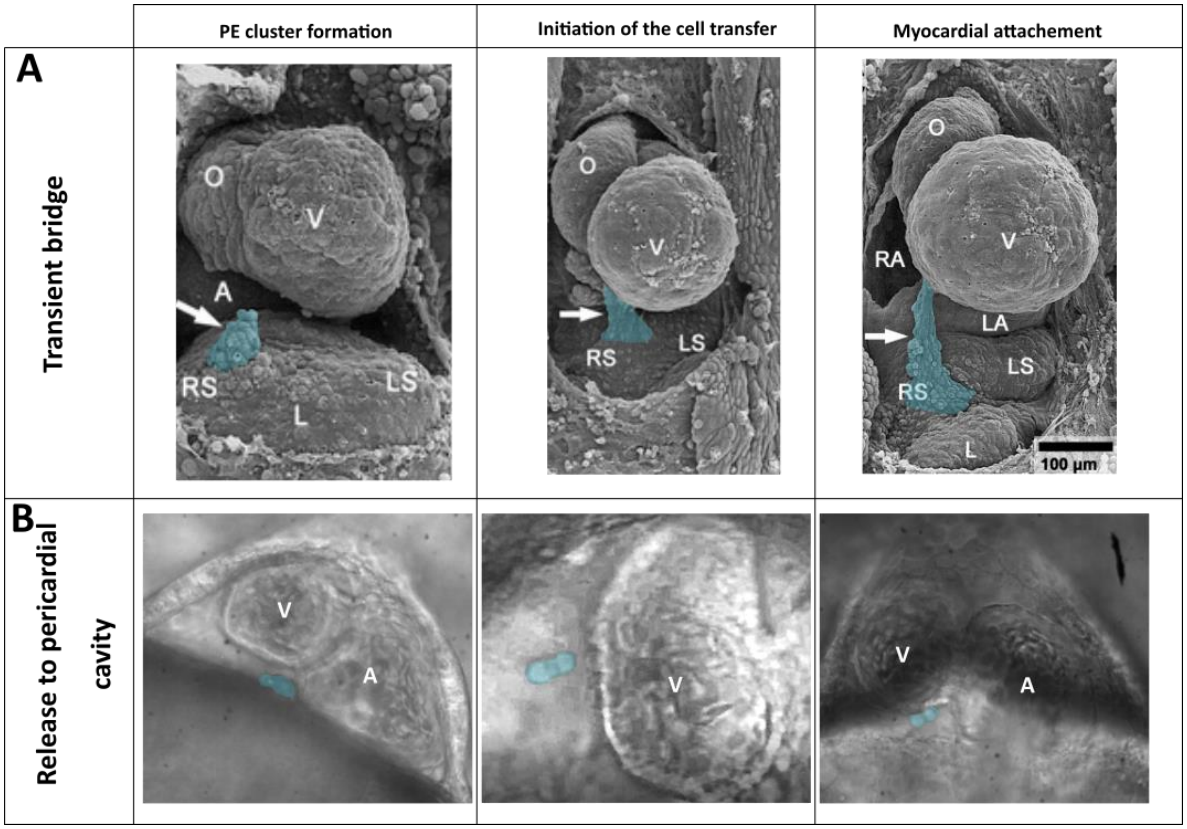

Figure 5. PE cell transfer to the myocardium. (A) An example of transient bridge formation. Electron microsocopy image showing PE cell transfer in Xenopus. The PE cluster is formed in the right sinus horn. In later timepoints, the PE cluster acquires a conical shape and attaches to the myocardium transferring the proepicardial cells. (B) An example of the release of PE cells into the pericardial cavity. Brightfield images of a zebrafish heart. The PE cluster forms in the atrioventricular channel area. Cells from the proepicardium are released and float in the pericardial cavity until they eventually attach to the myocardium. O: outflow tract; A: atrium; LS: left sinus horn; L: pericardial surface of the liver forming the bottom of the pericardial cavity; RA: right atrium; LA: left atrium; V: ventricle. Proepicardial and epicardial cells are marked in blue. Adapted from (Jahr et al. 2008; Peralta et al. 2013).

4. YAP and TAZ, effectors of the Hippo pathway

The Hippo signalling pathway was discovered in *Drosophila* and has been shown to be conserved in vertebrates (Huang et al. 2005; Dong et al. 2007). The Hippo signalling pathway was first described as a regulator of organ size (Dong et al. 2007), but since then more roles, such as being a regulator of cell proliferation, differentiation, migration, or EMT, have been described (Cheng et al. 2020; Varelas 2014) (Cheng et al. 2020). The main effectors of the Hippo pathway in mammals are YAP and TAZ.

Traditionally, nuclear localization of YAP is linked to the activation of pro-growth transcriptional programs through association with the TEAD family of transcription factors (Dupont et al. 2011; Zhao et al. 2007).

Several mechanisms regulate YAP localization, therefore controlling Yap-dependent gene transcription. The Hippo pathway is the main YAP regulator (Piccolo, Dupont, and Cordenonsi 2014), but other regulators such as Amot proteins are also important (Ragni et al. 2017). Importantly, these different mechanisms can coexist in a cell and it is not possible to exclude interplay between them.

4.1. Hippo pathway

The Hippo pathway is dysregulated in a broad range of cancers, and it is frequently correlated with cancer progression, but at the same time, it is key for proper embryonic development. Further knowledge of Hippo pathway might offer new insight into mechanisms of cancer progression as well as congenital diseases.

The Hippo pathway in *Drosophila* is based on a conserved kinase cascade that comprises the Hippo kinase, the Warts kinase, and the adaptor proteins Salvador and Mob. Activation of these signals promotes phosphorylation of the transcriptional regulator Yorkie by the Warts kinase, resulting in its exclusion from the nucleus. Nuclear Yorkie associates with Scalloped and promotes proliferation and inhibits apoptosis (Figure 6) (Huang et al. 2005).

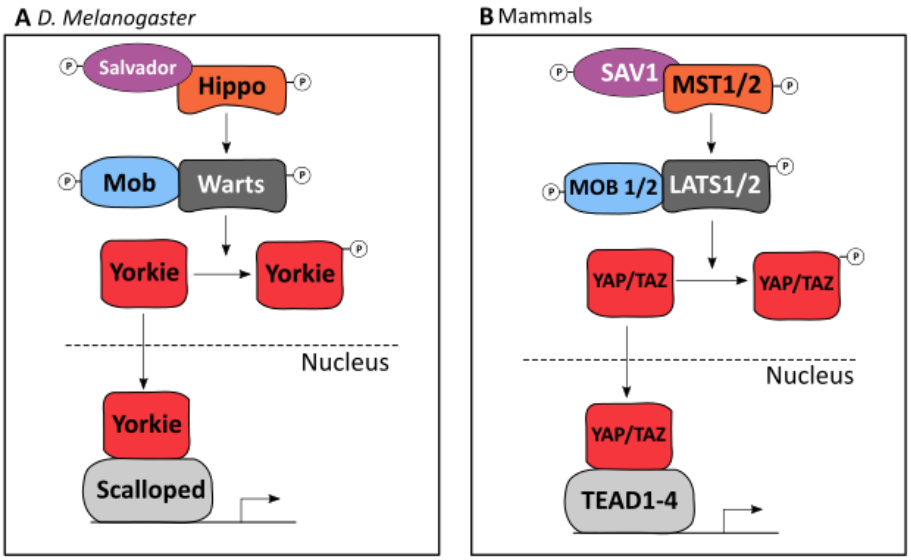

Figure 6. Canonical Hippo pathway. (A) Hippo pathway in Drosophila Melanogaster. (B) Hippo pathway in mammals. Adapted from (Taha, Janse van Rensburg, and Yang 2018; Varelas 2014).

The Hippo pathway is conserved throughout the eukaryotic kingdom. Since the Hippo pathway is essential for correct organ growth, it has been proposed that the emergence of the Hippo pathway is associated and conserved within animals that have an organized body plan that incorporates distinct organs and tissues (Hilman and Gat 2011). In mammalian model systems, YAP is a functional homolog of the transcriptional regulator Yorkie (Dong et al. 2007). TAZ or Wwrt1 has also been characterized as a paralog of YAP. LATS1 and LATS2 kinases are homologs of Warts. These kinases can phosphorylate YAP and TAZ, resulting in nuclear exclusion, cytoplasmatic sequestration and/or proteasomal degradation (Piccolo, Dupont, and Cordenonsi 2014). Most upstream components of the canonical Hippo pathway are also conserved in mammals, such as MST1 and MST2 kinases (homologs of Hippo), SAV1 (homolog of Salvador), and MOB1A and MOB1B (homologs of Mob). When YAP or TAZ are active, they can translocate into the nucleus and bind to transcription factors of the TEAD transcription factor family (homolog of Scalloped) and induce the expression of a wide range of genes, such as *ctgf* (Meng, Moroishi, and Guan 2016). Both YAP and TAZ have a shared domain in the N-terminal region that mediates the binding to TEAD transcription factors. Although most of the domain is conserved between the two proteins, in YAP

there is a PxxΦP motif that is lacking in TAZ. This suggests that there are some differences in TEAD activation between the two proteins, but the *in vivo* implications are not known yet (Varelas 2014).

4.2. Other YAP and TAZ regulators

Angiomotins (Amot) are a family of proteins known to bind to tight-junction proteins and F-actin that regulate YAP and TAZ nuclear localization (Zhao et al. 2011). Amot proteins have a Yap-binding motif. In mice, it has been shown that Amot depletion compromises development, as there is an increased percentage of embryo loss compared to wild-type embryos (Leung and Zernicka-Goetz 2013). In embryos lacking LATS1 and LATS2, there is an increase of proteins expressing Cdx2 (transcription factor downstream of TEAD) at the morula stage that is recovered by the expression of Amot (Leung and Zernicka-Goetz 2013). In zebrafish, *Amotl2a* is essential to restrict the number of cells in the posterior lateral line by inhibiting proliferation. Amotl2a physically interacts with Yap and Taz, sequestering them in the cytoplasm and inhibiting their proliferation-promoting transcriptional activity (Agarwala et al. 2015).

Mechanical and cytoskeletal inputs also regulate YAP and TAZ activity (Dupont et al. 2011). YAP and TAZ have a PDZ-binding motif, which mediates interactions with proteins that are usually transmembrane or cytoskeleton-associated (Varelas 2014). The cytoskeletal adaptation of spread cells (including the formation of F-actin stress fibers) causes YAP and TAZ nuclear accumulation. When cell shape is rounded and compact, YAP and TAZ are excluded from the nucleus. This is the case of contact inhibition of proliferation, a process by which cultured cells stop dividing then they become confluent. YAP and TAZ are nuclear in cells growing in low density and relocate to the cytoplasm when cells are in confluence (Zhao et al. 2007; Elosegui-Artola et al. 2017).

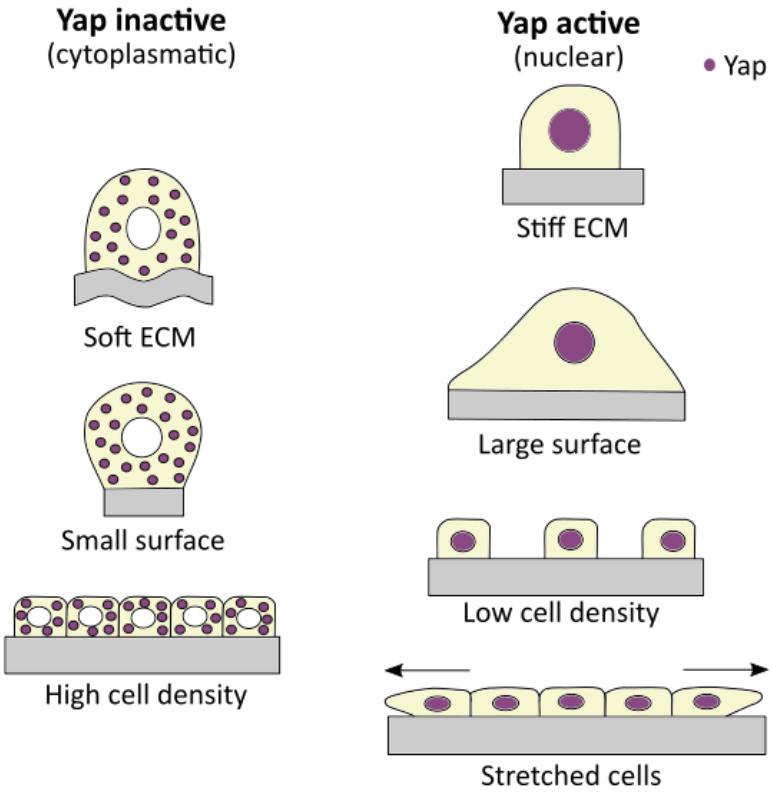

Figure 7. Non canonical Hippo pathway. Differences in cell mechanical properties affect Yap nuclear translocation. Adapted from (MB INFO 2016).

YAP and TAZ also respond to changes in extracellular matrix (ECM) stiffness: rigid ECM keeps more active YAP/TAZ to the nucleus than a softer ECM (Figure 7) (Piccolo, Dupont, and Cordenonsi 2014). YAP activation due to ECM stiffness can also induce EMT (Park et al. 2019).

Mechanical cues are regulators of Rho-GTPases, a family of GTPases that influence actin cytoskeleton dynamics and ROCK activity (a downstream Rho-GTPase effector). At the same time, YAP and TAZ activity can be regulated by them. Inhibition of Rho-GTPase function inhibits YAP and TAZ activity (Piccolo, Dupont, and Cordenonsi 2014) and activation of Rho-kinase (downstream of Rho-GTPase) promotes nuclear YAP/TAZ activity (Varelas 2014).

Alterations in F-actin also affect YAP and TAZ localization. F-actin capping proteins inhibit YAP and TAZ nuclear localization, as when these proteins are lacking there is an increase in YAP and TAZ activity (Aragona et al. 2013).

The liver kinase B1 (LKB1) also seems to have an important role in regulating YAP and TAZ nuclear translocation, since it is a known tumour suppressor and *in vitro* studies with several types of cells have shown that *Lkb1* expression increases Yap phosphorylation and consequent nuclear exclusion (Qiu et al. 2018)(Nguyen et al. 2013)(Mohseni et al. 2014).

4.3. Hippo pathway in zebrafish heart development

There are several tools available to study the Hippo pathway during zebrafish development.

It is possible to follow YAP and TAZ activity *in vivo* using different reporter lines. The *4xGTIIC:d2GFP* line contains the *4xGTIIC* promoter driving expression of d2GFP. The *4xGTIIC* promoter contains 4 GTIIC sequences which are consensus Tead binding sites responsive to Yap/Taz-Tead activity. Co-staining *4xGTIIC:d2GFP* embryos with Yap antibody show a strong correlation between nuclear located Yap and GFP expression. The same results are obtained when staining with ctgf antibody. Overall, these results confirm that this transgenic line faithfully reports endogenous Yap-Tead activity (Miesfeld and Link 2014). *Tg(Hsa.CTGF:nlsmCherry)* is another useful line for following Yap/Taz activity *in vivo.* In this line, they use a fragment of the human *CTGF* gene promoter, which contains three Yap/Taz/Tead-binding sites conserved in the zebrafish *ctgfa* promoter (Astone et al. 2018).

There are several different ways to modulate Yap activity in zebrafish. It is possible to manipulate Yap functionally using heat-shock transgenic lines, such as the *hsp70:RFP-CAyap*. Fish from this line have a mutation in the motif in Yap that is recognized by Lats 1/2, preventing its inactivation through phosphorylation and consequently promoting its translocation to the nucleus. Another line that allows us to modify Yap activity is the *hsp70:RFP-DNyap* line. A truncated form of the Yap protein is used, in which the transcriptional activation domain is removed but the Tead binding domain is intact. This allows Yap to bind to its DNA partner but it does not activate its targets (Mateus et al. 2015).

Yap activity can also be regulated with the use of some drugs. XAV939 is a trankyrase inhibitor that suppresses Yap activity. Trankyrases recognize poly-ADP ribosylation sites and can change the subcellular localization of the substrate or cause its proteasome-dependent degradation. Trankyrases are positive regulators of YAP, as they bind to Amot proteins, resulting in more free Yap that are able to translocate to the nucleus. When trankyrases are targeted, Amot protein levels are increased and YAP activity is downregulated (W. Wang et al. 2015).

Verteporfin is a second-generation photosensitizer that is also able to suppress Yap activity. Verteporfin decreases nuclear YAP levels and activity as a consequence of increasing 14-3-3σ protein levels. 14-3-3 proteins sequestrate phosphorylated proteins in the cytosol, targeting for degradation in the proteasome. When these proteins are upregulated, YAP is trapped in the cytosol (C. Wang et al. 2016).

Dexamethasone is a synthetic glucocorticoid that promotes the nuclear activity of Yap *in vitro* and *in vivo* in zebrafish (Astone et al. 2018). It has been described that activation of glucocorticoid receptors activated Yap via actin cytoskeleton remodelling in breast cancer cells (Sorrentino et al. 2017).

Yap1 also seems to be involved in OFT valve formation (Duchemin, Vignes, and Vermot 2019). Yap1 regulates cell fate determination of cardiac precursor cells into smooth muscle cells via a process that involves *elastin b* (Moriyama et al. 2016). Moreover, Yap1 is also localized in the nucleus of endothelial and smooth muscle cells of the OFT and a significant fraction of *Yap1* mutants have abnormal or not recognizable outflow tract valves (Duchemin, Vignes, and Vermot 2019).

Wwtr1 also has an important role in cardiomyocyte development and proliferation during trabecular morphogenesis (Lai et al. 2018).

5. Primary Cilia

Primary cilia are membrane protrusions, with an antenna-like shape. They consist of a microtubule-based ciliary axoneme assembled from a basal body and they are surrounded by a lipid bilayered membrane (Venkatesh 2017). According to the internal arrangement, primary cilia have a 9 +0 axoneme (Hildebrandt, Benzing, and Katsanis 2011) (Figure 8A). Inside the cilium, kinesins and dynein motor proteins transport intraflagellar transport (IFT) proteins and cargo towards the tip or back to the basal body and the cell, respectively (Ishikawa and Marshall 2011). The IFT machinery is composed of two biochemically distinct subcomplexes, IFT- complex A and IFT-complex B (Taschner, Bhogaraju, and Lorentzen 2012). Primary cilia are present in several types of cells, as a single primary cilium is found on the apical surface of the majority of cells in the human body (Berbari et al. 2009). Primary cilia sense chemical or mechanical signals and transduce them into cell responses such as proliferation, polarity, or differentiation (Berbari et al. 2009). It is proposed that through bending, cilia can initiate downstream mechanotransduction signal cascades, including ionic fluxes within the cilium (R Ferreira et al. 2019).

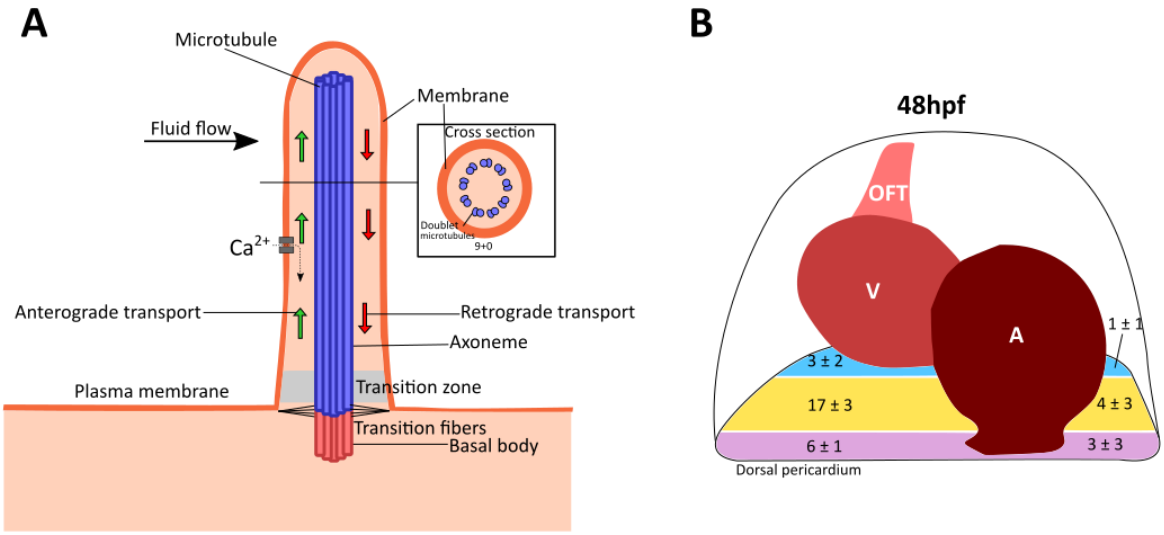

Figure 8. Primary cilia. (A) Schematic representation of a primary cilia. (B) Cilia quantification in dorsal pericardium of zebrafish at 48 hpf. Dorsal pericardium is divided in 3 areas. Adapted from (Peralta et al. 2020; Hsiao, Tuz, and Ferland 2012; Higgins, Obaidi, and McMorrow 2019).

Primary cilia have been reported in the embryonic pericardium of the chick and the mouse (Rash, Shay, and Biesele 1969). In zebrafish, *in vivo* analysis of the pericardial cavity shows that there are primary cilia and that they are heterogeneously distributed in the dorsal pericardium (Peralta et al. 2020). At 48 hpf, the right half of the sinus venosus presents a higher number of cilia than the left half. The PE region in the dorsal pericardium also has differences between the right and left side. The right side, where the PE cluster will form, shows higher cilia number. Heartbeat triggers motion of these primary cilia and their movement is different depending on the position of each cilium. Overall, there are more cilia in the right side of the avc area, where the PE cluster will form (Peralta et al. 2020) (Figure 8B).

Materials and methods

Zebrafish (ZF) husbandry and embryo treatments:

Animal experiments were approved by the Animal Experimentation Committee of the Institutional Review Board of the IGBMC. ZF lines used in the study were:

- *4xGTIIC:d2GFP* (Miesfeld and Link 2014)
- *Et(-26.5Hsa.WT1-6451gata2:EGFP)cn1*(Peralta et al. 2013)
- *lkb1Y261* (van der Velden et al. 2011)
- *tcf21:nls-GFP* (J. Wang et al. 2011)
- *actb2:lifeAct-RFP* (Behrndt et al. 2012)
- Yap^{fu48} (Agarwala et al. 2015)
- *Kif3a* (Pooranachandran and Malicki 2016)
- *Pkd2* (Schottenfeld, Sullivan-Brown, and Burdine 2007)
- *Klf2a* (Heckel et al. 2015)
- *Klf2b* (Generated in the Vermot Lab)

All animals were incubated at 28.5°C for 24 hours before treatment with 1-phenyl-2-thiourea (PTU) (Sigma Aldrich) to prevent pigment formation.

Drug treatments were performed as followed:

- Dexamethasone treatment: embryos were exposed to a solution containing 25 µM of dexamethasone during the time needed for the experiment.
- XAV939 treatment: embryos were exposed to a solution containing 5 µM of XAV939 from 36 to 55 hpf.
- Caffeine treatment: embryos were exposed to a solution containing 100 µM of caffeine from 50 to 55 hpf.
- Isoprenaline treatment: embryos were exposed to a solution containing 300 µM of isoprenaline from 50 to 55 hpf.

In vivo imaging:

Zebrafish embryos were staged and anaesthetised with 0.02% tricaine solution.

Brightfield imaging was performed on a Leica DMIRBE inverted microscope using a Photron SA3 high-speed CMOS camera (Photron, San Diego, CA) and

water immersion objective (Leica 20X, NA 0.7). Image sequences were acquired at a frame rate of 125 frames per second.

For confocal imaging, embryos were mounted in 0.7% low melting-point agarose (Sigma Aldrich). Confocal imaging was performed on a Leica SP8 confocal microscope. Images were acquired bidirectionally with a low-magnification water immersion objective (Leica HCX IRAPO L, 25X, N.A. 0.95). For time lapse, z-stacks were acquired each 15 or 30 min, depending on the experiment. The optical plane was moved 5 µm between the z-sections.

For lightsheet imaging, two mounting methods were used: 3D printed molds to create a phytagel structure, where the fish stay in direct contact with the medium, and U-shaped glass capillaries, where the fish is embedded in 0.7%low melting-point agarose (Sigma Aldrich). Lightsheet imaging was performed on a Leica TCS SP8 DLS with water immersion detection objective (HC Fluotar L 25 0.95 2.5 Water) with a TwinFlect of 5mm and with an illumination objective HC PL Fluotar 2.5 0.007.

Whole mount immunohistochemistry:

Embryos were fixed overnight with 4% Paraformaldehyde in PBS overnight at 4°C, washed with Tween 0.1% in PBS and permeabilized with 0.5% Triton-X100 in PBS for 20 min at room temperature.

After several steps of washing with Tween 0.1% in PBS, samples were blocked for 2h at RT with 5% goat serum, 5% BSA and 20mM MgCl2 in PBS followed by overnight incubation with the primary antibodies diluted in the blocking solution at 4°C. After several washes, secondary antibodies diluted 1:500 in PBS were incubated overnight at 4°C. Nuclei were counterstained with DAPI 1:1000 in PBS for 15 minutes at 4°C.

The antibodies for immunofluorescence detection were as follows: anti-GFP (Aves Lab) at 1:500, anti-ctgf (Abcam) at 1:100, anti-Yap/Taz (specific for Taz in zebrafish) at 1:100 (Cell signaling), anti-Yap (Lecaudey laboratory). Secondary antibodies and stains were: goat anti-chicken Alexa Fluor 488 IgY (H+L)

(Invitrogen), goat anti-rabbit Alexa Fluor 647 (Thermo Fisher Scientific), Phalloidin 568 (Thermo Fisher Scientific) and DAPI (Thermo Fisher Scientific).

In some experiments, *4xGTIIC:d2GFP* embryos were only labelled with phalloidin and DAPI and endogenous GFP was imaged.

Embryos were mounted and imaged with a Leica SP8 confocal microscope fitted with a dipping immersion objective (Leica HCX IRAPO L, 25X, N.A. 0.95). Z-stacks were taken every 5 µm. Maximal projections of images were 3D reconstructed in whole-mount views using IMARIS software (Bitplane Scientific Software).

Microinjection:

MOs from Genetools Inc were injected in 1 to 8 cell stage embryos.

The following MOs were used:

- Taz MO: 5'-CTGGAGAGGATTACCGCTCATGGTC-3' (Voltes et al. 2019) at 2ng concentration.
- tnnt2a MO: 5'-CATGTTTGCTCTGATCTGACACGCA-3' (Sehnert et al. 2002) at 5.8ng concentration.

Video analysis and statistical analysis:

ImageJ was used to manually quantify cell number, as well as fluorescence intensity.

Statistical tests were performed using GraphPad Prism 7.

RNAscope:

Embryos were fixed overnight at 4ºC in 4% paraformaldehyde in PBS and were dehydrated to 100% methanol gradually. RNAscope was performed using ctgf-C3 and from RNAscope Fluorescent Multiplex kit (Advanced Cell Diagnostics). TSA Plus fluorescein (PerkinElmer) and were used at 1:600 dilution. Embryos were kept for 3 days in 1:50 phalloidin 647 (Thermo Fisher Scientific) at 4ºC

after the RNAscope protocol to stain F-actin. Embryos were imaged using a Leica SP8 confocal microscope with a Leica HCX IRAPO L, × 25, NA0.95 water immersion objective.

In vivo heart imaging with Leica TCS SP8 DLS

Preface

In order to perform live imaging, lightsheet imaging is broadly used. Lightsheet microscopy, or selective plane illumination microscopy, is a technique that uses a focused light-sheet to illuminate the specimen from the side. This technique is used in live imaging because it can achieve good resolution at high penetration depths and because it is minimally invasive (Huisken and Stainier 2009).

The basis of lightsheet microscopy is to illuminate a well-defined volume around the focal plane of the detection optics from the side. In the Leica TCS SP8 DLS (called DLS from here), the sheet of light is formed by the fast scanning of a laser beam during the acquisition time of the camera (Köster and Haas 2015).

Although a traditional lightsheet has a perpendicular setup where the illuminating and the detection objectives are arranged at a 90° angle to each other, the DLS has a vertical setup that uses a mirror device (TwinFlect mirrors) to deflect the light sheet at a 90º angle. The module is fully integrated into the vertical axis of the inverted microscopy stand (Köster and Haas 2015). This vertical axis allows for horizontal mounting. The sample needs to be placed between the TwinFlect mirrors, as the light sheet has to be reflected into the sample and to be placed in the focal plane of the detection objective (Haas 2017) (Figure I A).

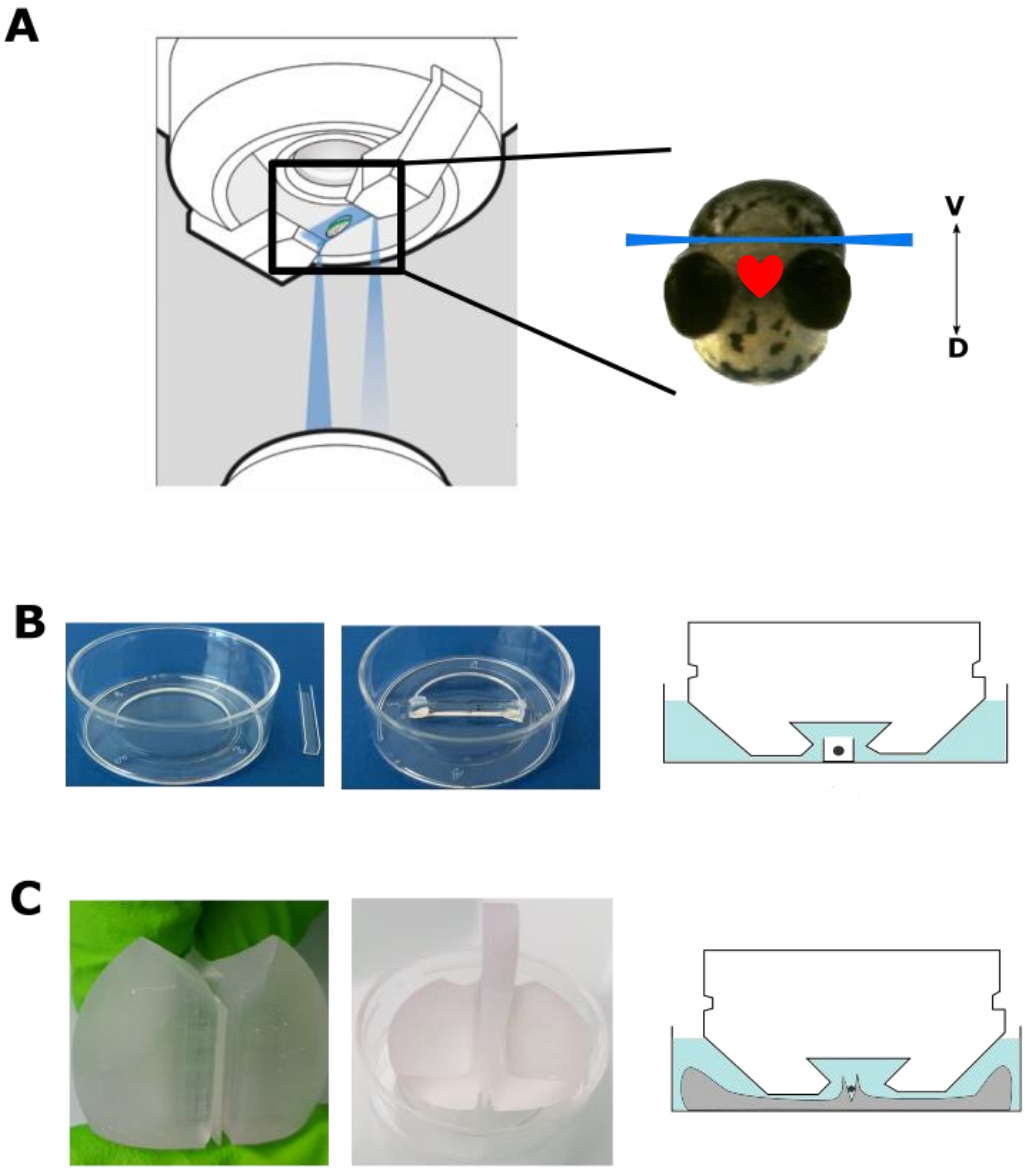

Figure I. In vivo imaging with Leica TCS SP8 DLS. A) Vertical setup of the microscope. B) Sample mounting with phytagel molds. C) Sample mounting with U-shaped glass capillaries.

For the *in vivo* imaging of this thesis, larvae were first transferred to fish water containing 0.2 mg/ml tricaine and 0.0033% PTU. Then, three different types of sample mounting have been used:

1) Phytagel molds designed at the IGBMC. Special 3D printed stamps were designed at the IGBMC. Placing the stamps in a bottom glass petri dish and adding phytagel at concentration 1% creates a pocket-like structure

between the mirrors, where the fish is kept still and in direct contact with the medium (Figure IB).

2) U-shaped capillary glass. U-shaped glass capillaries, customized for the different mirror sizes, are attached to the bottom of the bottom glass petri dish. The zebrafish embryo is embedded with agarose and placed in the U-shape capillary (Figure IC).
3) Rotation device, explained in the tutorial below, published in Leica Microsystems webpage (Haas et al. 2019). Leica Microsystems designed and created the rotation design and Dr. Remacha and I prepared the published protocol.

Préface en français

Pour réaliser des images en direct, l'imagerie par feuille de lumière est largement utilisée. La microscopie à feuille de lumière, ou microscopie à illumination plane sélective, est une technique qui utilise une feuille de lumière focalisée pour éclairer le spécimen par le côté. Cette technique est utilisée pour l'imagerie vivante car elle permet d'obtenir une bonne résolution à des profondeurs de pénétration élevées et parce qu'elle est peu invasive (Huisken et Stainier 2009).

La base de la microscopie à feuille de lumière est d'éclairer un volume bien défini autour du plan focal de l'optique de détection depuis le côté. Dans le Leica TCS SP8 DLS (appelé DLS à partir d'ici), la feuille de lumière est formée par le balayage rapide d'un faisceau laser pendant le temps d'acquisition de la caméra (Köster et Haas 2015).

Bien qu'une feuille de lumière traditionnelle ait une configuration perpendiculaire où les objectifs d'éclairage et de détection sont disposés à un angle de 90° l'un par rapport à l'autre, le DLS a une configuration verticale qui utilise un dispositif de miroirs (miroirs TwinFlect) pour dévier la feuille de lumière à un angle de 90º. Le module est entièrement intégré dans l'axe vertical du statif de microscopie inversé (Köster et Haas 2015). Cet axe vertical permet un montage horizontal. L'échantillon doit être placé entre les miroirs TwinFlect, car la feuille de lumière doit être réfléchie dans l'échantillon et être placée dans le plan focal de l'objectif de détection (Haas 2017) (Figure I A).

Pour l'imagerie in vivo de cette thèse, les larves ont d'abord été transférées dans de l'eau de poisson contenant 0,2 mg/ml de tricaine et 0,0033% de PTU. Ensuite, trois différents types de montage des échantillons ont été utilisés:

1) Les moules Phytagel conçus à l'IGBMC. Des tampons spéciaux imprimés en 3D ont été conçus à l'IGBMC. En plaçant les tampons dans une boîte de Pétri en verre de fond et en ajoutant du phytagel à la concentration de 1%, on crée une structure en forme de poche entre les miroirs, où le poisson est maintenu immobile et en contact direct avec le milieu (Figure IB).

2) Capillaires en verre en forme de U. Des capillaires en verre en forme de U, adaptés aux différentes tailles de miroir, sont fixés au fond de la boîte de Pétri en verre. L'embryon de poisson zèbre est enrobé d'agarose et placé dans le capillaire en forme de U (Figure IC).

3) Dispositif de rotation, expliqué dans le tutoriel ci-dessous, publié sur la page Web de Leica Microsystems (Haas et al. 2019). Leica Microsystems a conçu et créé le dispositif de rotation et le Dr Remacha et moi-même avons préparé le protocole publié.

Using a Rotation Device for DLS Sample Mounting
TCS SP8 DLS Digital LightSheet Protocol

The TCS SP8 DLS microscope utilizes the innovative concept of integrating Light Sheet Microscopy technology into a confocal microscope. Due to its unique optical architecture, specimens/samples can be mounted on standard glass bottom petri dishes, as for standard confocal imaging, but require only a few adaptations when compared to conventional mounting procedures.

Images were acquired in the framework of the 2018 EMBO Lightsheet Course at MPI CBG in Dresden with expert support of Bruno Cossermelli Vellutini (MPI CBG), Pavel Tomancak (MPI CBG), and Emmanuel Reynaud (UCD).

Authors: Petra Haas, Dr[1], Elena Remacha Motta [1], Laia Ortiz Lopez[2], Bruno Cossermelli Vellutini, Dr [3], Pavel Tomancak, Dr[3], Emmanuel Reynaud, Dr[4]

[1] Leica Microsystems

[2]IGBMC – Institute of Genetics and Molecular and Cellular Biology, France

[3]Max Planck Institute of Molecular Cell Biology and Genetics (MPI-CBG), Dresden, Germany

[4]University College Dublin (UCD), Belfield, Dublin 4, Ireland

Introduction

For image acquisition, the specimen preparation has two major requirements. The specimen needs to be placed into the focal plane of the detection objective in between the two mirrors of the cap. In addition, it needs to be slightly elevated from the petri dish bottom for the mirrors/light sheet to reach the specimen's distal part.

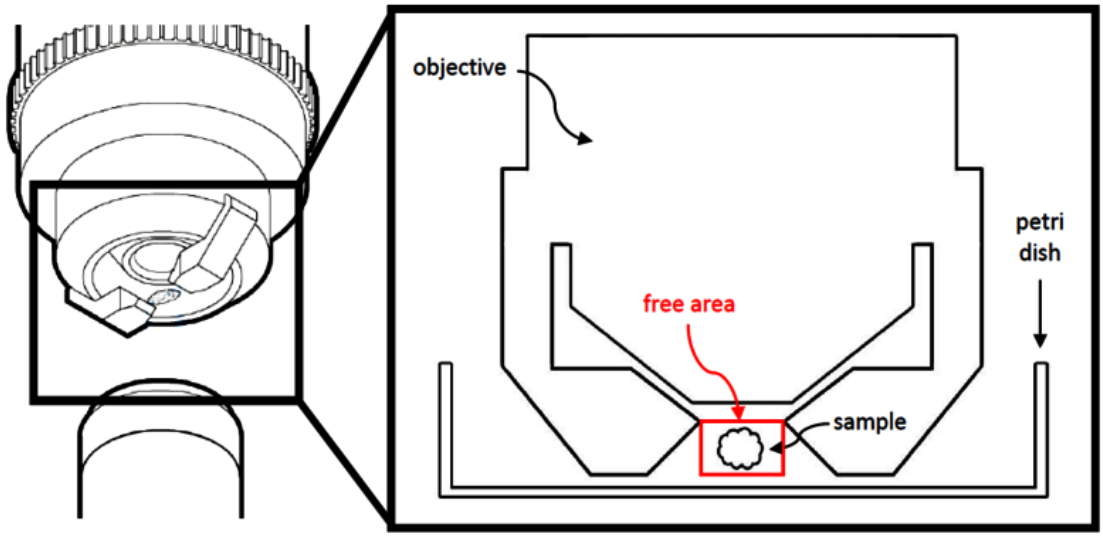

Figure 1: DLS objective: Positioning of specimens in the free area of the sample space.

One convenient way to position specimens in the free area of the sample space (see figure above) is by using FEP (fluorinated ethylene propylene) tubes (see figure below). With a refractive index, n, of 1.338, FEP is well suited for imaging specimens immersed in aqueous solutions (at least when using objectives with moderate numerical apertures [NAs]).

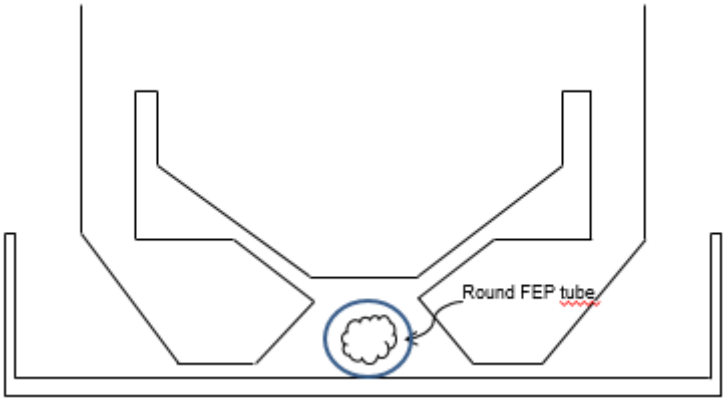

Figure 2: DLS objective: Sample positioning by using FEP (fluorinated ethylene propylene) tubes.

For SP8 DLS imaging, specimens can be positioned and fixed in place using an FEP tube (see diagram below).

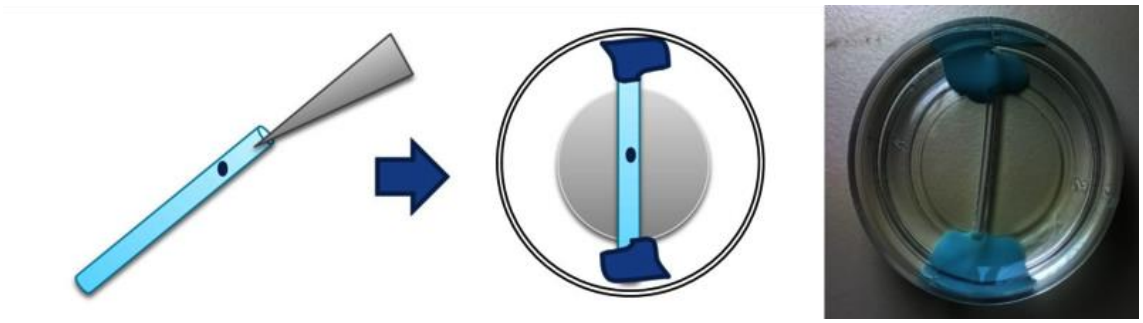

Figure 3: Positioning of specimens inside an FEP tube.

The advantages of this kind of specimen mounting are:

- easy handling and
- possibility to use low concentration of scaffolding medium (e.g., agarose or methylcellulose) which provides enough specimen confinement under physiological conditions for long-term in vivo imaging.

The disadvantage is the difficulty to align the specimens such that the region of interest is exposed to the side used for fluorescence detection.

To overcome this disadvantage, while maintaining the aforementioned advantages, a rotation device has been designed which allows the angle of the

FEP tube to be easily adjusted, so that the specimen can be optimally aligned for imaging. Such set-ups have previously been demonstrated elsewhere [1, 2, 3].

Materials and Methods

Figure 4: Sample Rotation Device

The sample rotation device (see above, **158007064**) for DLS imaging comes with:

- the DLS rotation device;
- microscope glass cover slips (21 x 26 mm); and
- FEP tubes (Camitec, outer diameter 2.00 mm, inner diameter 1.80 mm).

However, there is no silicone or other material for sealing the cover slip included with the rotation device.

Step 1: Cleaning of FEP tubes (recommended procedure)

As described in the report by Kaufmann et al. [4], FEP tubes should be treated in the following way before usage:

- first, all solutions must be degassed and syringe filtered (Millex-HV, PVDF, 0.45 µm);
- rinse with 1 M NaOH (Merck);
- place them in 0.5 M NaOH and ultrasonicate for 10 minutes;
- rinse with double-distilled H2O and 70% ethanol
- ultrasonicate in 70% ethanol for 10 minutes;
- rinse with double-distilled H2O; and
- finally, store in double-distilled H2O.

Step 2: Sealing the rotation device with the glass cover slip

Sealing of the cover slip onto the rotation device is done in the following manner:

- apply silicone to the inner edge of the recess at the bottom of the rotation device (see A below);
- add a cover glass and press the glass lightly to ensure that it sits evenly for a good seal at all points (see B below); and
- to check the chamber seal, add some distilled water to the rotation device and see if leaks occur (see C below).

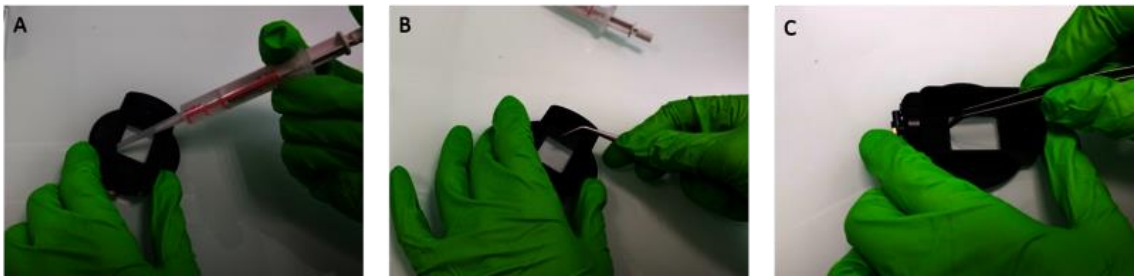

Figure 5: Sealing the DLS rotation device.

Step 3: Placing the specimen(s) into the FEP tube

Specimens are placed in the mounting medium and drawn into the tube with a pipette or syringe (shown below).

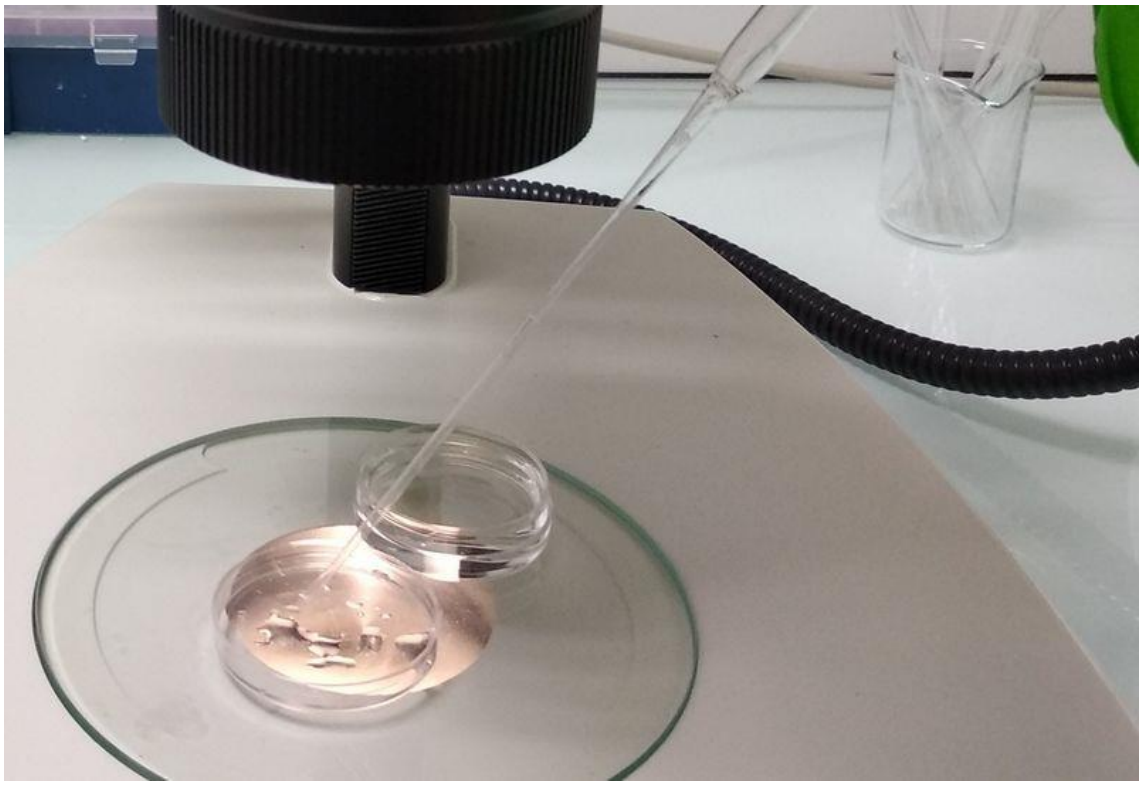

Figure 6: Drawing the specimen into an FEP tube.

The FEP tubes need to have a length of 38 mm.

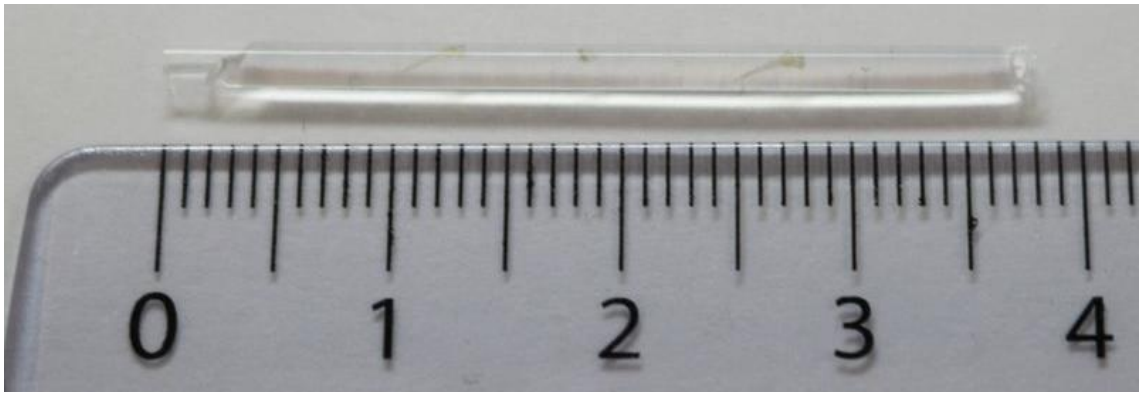

Figure 7: Length of FEP tube: 38 mm.

Step 4: Inserting the FEP tube into the rotation device

Attach the black caps on both sides of the FEP tube (see A and B below).

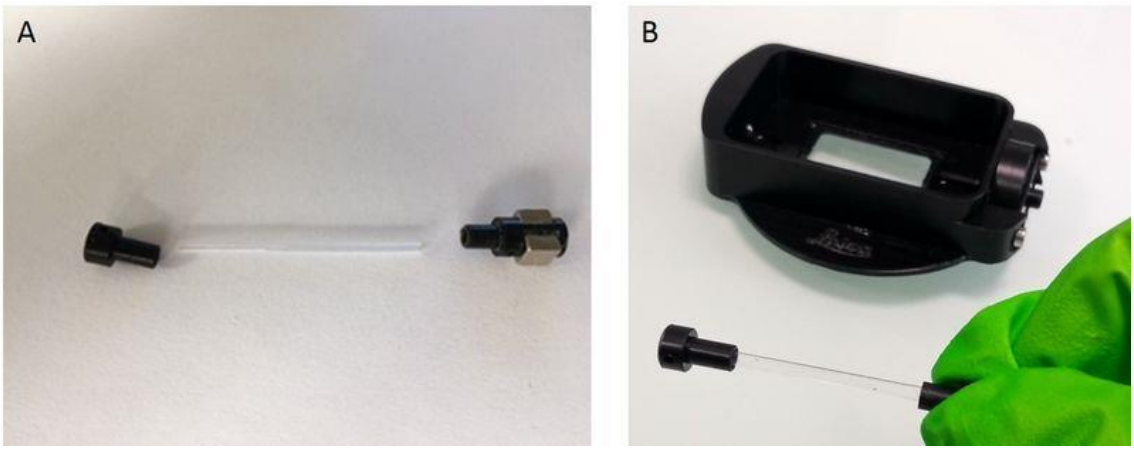

Figure 8: Attaching the black caps to the FEP tube.

As seen below, insert into the rotation device's pin (1), the end of the FEP tube with both a black cap and magnet (2).

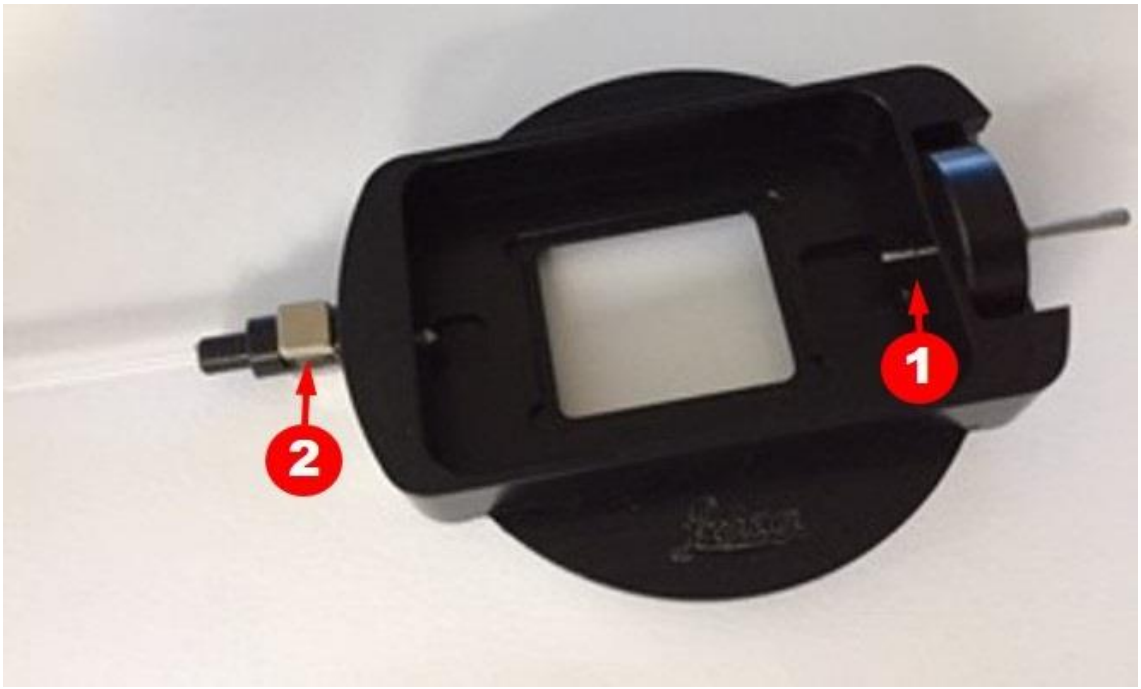

Figure 9: Placing the FEP tube in the rotation device (first step).

Finally, the opposite side of the tube is fixed in place (1 in image below).

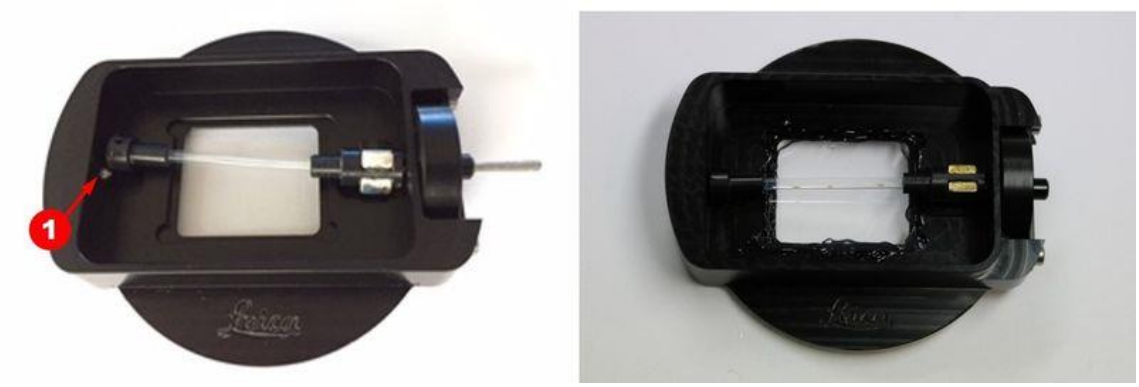

Figure 10: Placing the FEP tube in the rotation device (final step).

Step 3: Start Image Acquisition

Position the glass bottom petri dish on top of the TCS SP8 DLS scanning stage (see below).

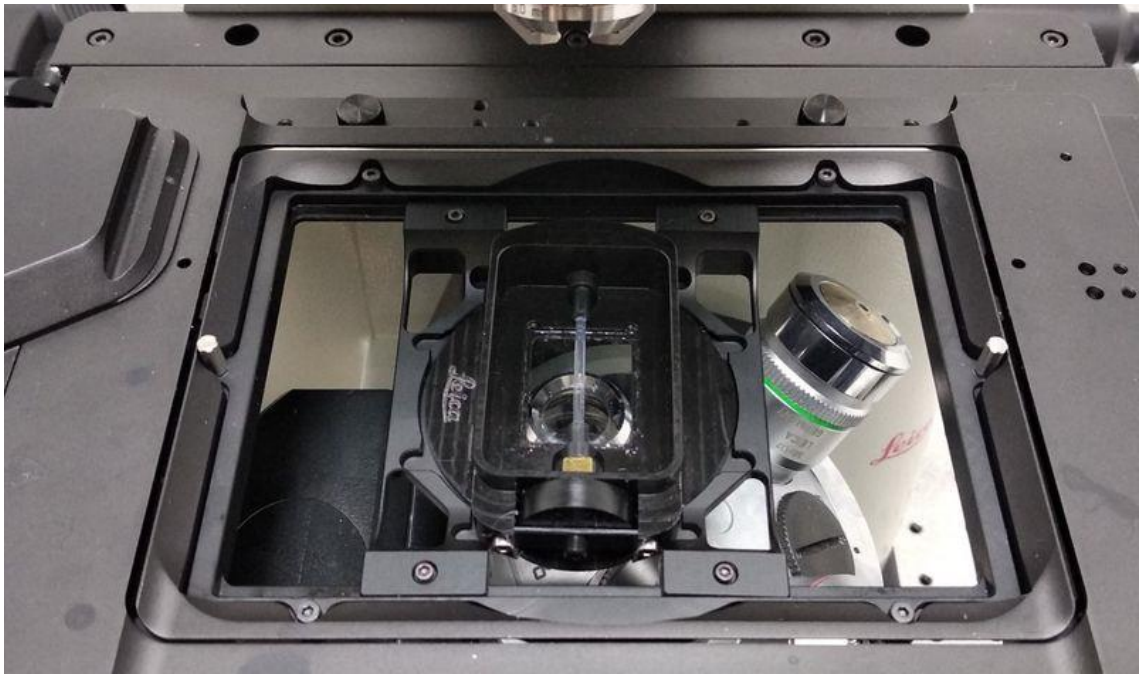

Figure 11: TCS SP8 DLS scanning stage with rotation device.

Note: The rotation device is only compatible with the following z-Galvo stage inserts:

- 158004118 Rotatable Insert Inverse and
- 158004119 Insert Universal.

Be careful: Only put the rotation device onto the z-Galvo stage after initialization. Also, pay attention when changing (illumination) objectives. The wheel for the rotation device protrudes downwards and might touch accidentally an objective (it may be best first to remove bulky objectives from the turret).

Results

Using the LightSheet Wizard, which is included with the LAS X software, you can now acquire images of your specimen(s).

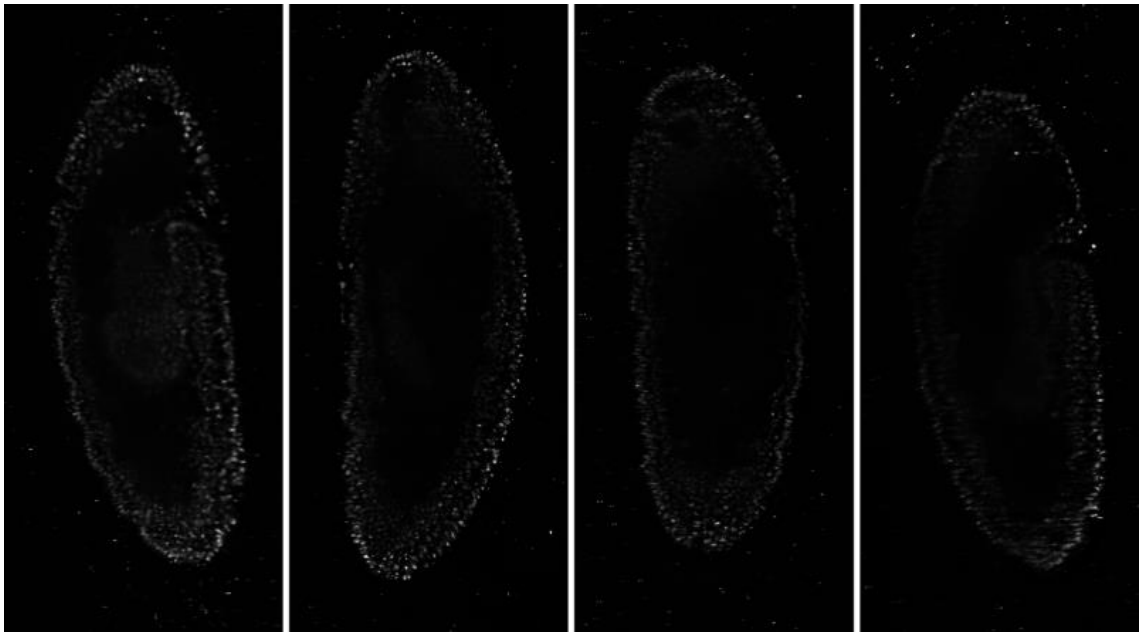

Figure 12: Drosophila embryo observed from different sides. Single planes were taken from 3D image stacks. Courtesy of Pavel Tomancak, MPI-CBG, Dresden, Germany.

References

1. Voie, A. H., Burns, D. H. & Spelman, F. A. Orthogonal-plane fluorescence optical sectioning: Three-dimensional imaging of macroscopic biological specimens. J. Microsc. 170, 229–236 (1993)
2. Preibisch S, Saalfeld S, Schindelin J, Tomancak P. Software for bead-based registration of selective plane illumination microscopy data. Nat

Methods. 2010 Jun;7(6):418-9Supplementary Material: https://imagej.net/_images/3/32/Nmeth0610-418-S1.pdf

3. T. Bruns, S. Schickinger, H. Schneckenburger, Sample holder for axial rotation of specimens in 3D microscopy, First published: 06 May 2015, https://doi.org/10.1111/jmi.12263, Cited by: 9
4. A. Kaufmann, M. Mickoleit, M. Weber, J. Huisken, Multilayer mounting enables long-term imaging of zebrafish development in a light sheet microscope, Development (2012) vol. 139, iss. 17, pp. 3242-3247; DOI: 10.1242/dev.082586.

Editor's note: This is a revised version of the protocol. It contains now a reference to the EMBO Light sheet course, additional authors, and additional publications describing similar sample holders.

In the spirit of the EMBO course, the protocol described here was pushed further by using the acquired image stacks to adapt them to the FiJi Multiview Fusion Plugin (https://imagej.net/Multiview-Reconstruction).

Intraflagellar Transport Complex B Proteins Regulate the Hippo effector Yap1 during Cardiogenesis

Preface

In this chapter I present the paper “Intraflagellar Transport Complex B Proteins Regulate the Hippo effector Yap1 during Cardiogenesis”. In this paper, we study the role of IFTB proteins during cardiogenesis. We describe how IFT proteins restrict proepicardial and myocardial development independently of cilia. Moreover, we show that this modulation is acting through BMP signalling, which tunes Yap1-Tead activity. Finally, we also show that IFT88 and IFT20 interact with Yap1 in the cytoplasm, setting Yap1-Tead activity.

I am second author and I contributed to this paper by:

- Assisting with the imaging of the proepicardial cluster in mice, using the protocol explained in the previous chaper.
- Performing immunohistochemistries against Isl1 and ctgf and helping with the analysis.
- Performing *In situ hybridization* against Bmp4 in *iguana* mutants and helping with the analysis.
- Assisting with data curation.
- Helping with the review and editing of the manuscript.

Préface en français

Dans ce chapitre, je présente l'article "Intraflagellar Transport Complex B Proteins Regulate the Hippo effector Yap1 during Cardiogenesis". Dans cet article, nous étudions le rôle des protéines IFTB pendant la cardiogenèse. Nous décrivons comment les protéines IFT limitent le développement proépicardique et myocardique indépendamment des cils. De plus, nous montrons que cette modulation agit par le biais de la signalisation BMP, qui règle l'activité de Yap1-Tead. Enfin, nous montrons également que IFT88 et IFT20 interagissent avec Yap1 dans le cytoplasme, ce qui règle l'activité de Yap1-Tead.

Je suis le deuxième auteur et j'ai contribué à cet article en :

- Aidant à l'imagerie de l'amas proépicardique chez la souris, en utilisant le protocole expliqué dans le chapitre précédent.
- Réalisant des immunohistochimies contre Isl1 et ctgf et en aidant à l'analyse.

- Réalisant les hybridations in situ contre Bmp4 chez les mutants iguanes et aide à l'analyse.
- Aidant à la conservation des données.
- Aidant à la révision et à l'édition du manuscrit.

Cell Reports

Intraflagellar Transport Complex B Proteins Regulate the Hippo Effector Yap1 during Cardiogenesis

Graphical Abstract

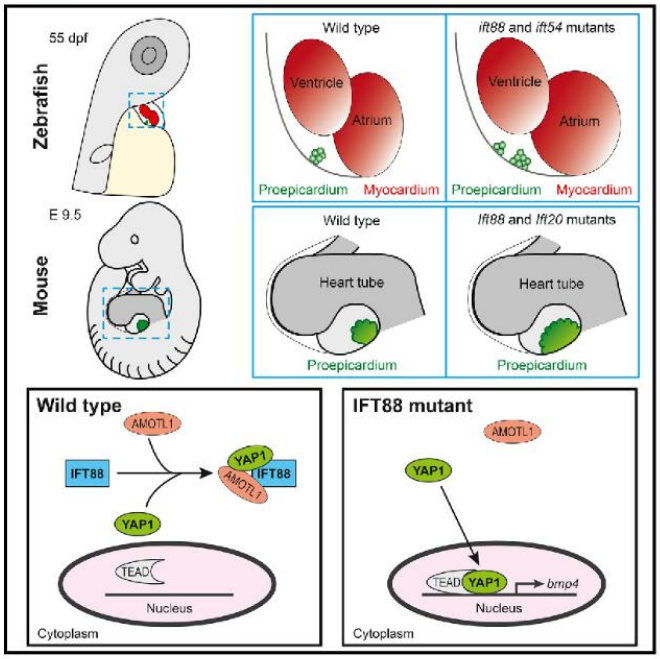

Highlights

- IFT proteins restrict proepicardial and myocardial development
- IFT proteins act independently of primary cilia in this process
- IFT proteins modulate BMP signaling by tuning Yap1-Tead activity
- IFT88 and IFT20 interact with YAP1 in the cytoplasm to set Yap1-Tead activity

Authors

Marina Peralta, Laia Ortiz Lopez, Katerina Jerabkova, ..., Benedicte Delaval, Sigolène M. Meilhac, Julien Vermot

Correspondence

jvermot@imperial.ac.uk

In Brief

Peralta et al. show that intraflagellar transport (IFT) complex B proteins (Ift88, Ift54, and Ift20) modulate the Hippo pathway effector Yap1 in zebrafish and mouse. This cytoplasmic interaction is key to restrict proepicardial and myocardial development.

Peralta et al., 2020, Cell Reports 32, 107932
July 21, 2020
https://doi.org/10.1016/j.celrep.2020.107932

Cell Reports

CellPress
OPEN ACCESS

Report

Intraflagellar Transport Complex B Proteins Regulate the Hippo Effector Yap1 during Cardiogenesis

Marina Peralta,[1,2,3,4] Laia Ortiz Lopez,[1,2,3,4,13] Katerina Jerabkova,[1,2,3,4,13] Tommaso Lucchesi,[5,6,7,13] Benjamin Vitre,[8] Dong Han,[5,6] Laurent Guillemot,[5,6] Chaitanya Dingare,[9] Izabela Sumara,[1,2,3,4] Nadia Mercader,[10,11] Virginie Lecaudey,[9] Benedicte Delaval,[8] Sigolène M. Meilhac,[5,6] and Julien Vermot[1,2,3,4,7,12,14,*]

[1]Institut de Génétique et de Biologie Moléculaire et Cellulaire, Illkirch, France
[2]Centre National de la Recherche Scientifique, UMR7104, Illkirch, France
[3]Institut National de la Santé et de la Recherche Médicale, U964, Illkirch, France
[4]Université de Strasbourg, Illkirch, France
[5]*Imagine*–Institut Pasteur, Laboratory of Heart Morphogenesis, Paris, France
[6]INSERM UMR1163, Université Paris Descartes, Paris, France
[7]Sorbonne Université, Collège Doctoral, F-75005, Paris, France
[8]Centre de Recherche en Biologie Cellulaire de Montpellier (CRBM), CNRS, Université de Montpellier, Montpellier, France
[9]Institute for Cell Biology and Neurosciences, Goethe University of Frankfurt, Frankfurt, Germany
[10]Institute of Anatomy, University of Bern, Bern, Switzerland
[11]Centro Nacional de Investigaciones Cardiovasculares (CNIC), Madrid, Spain
[12]Department of Bioengineering, Imperial College London, London, UK
[13]These authors contributed equally
[14]Lead Contact
*Correspondence: jvermot@imperial.ac.uk
https://doi.org/10.1016/j.celrep.2020.107932

SUMMARY

Cilia and the intraflagellar transport (IFT) proteins involved in ciliogenesis are associated with congenital heart diseases (CHDs). However, the molecular links between cilia, IFT proteins, and cardiogenesis are yet to be established. Using a combination of biochemistry, genetics, and live-imaging methods, we show that IFT complex B proteins (Ift88, Ift54, and Ift20) modulate the Hippo pathway effector YAP1 in zebrafish and mouse. We demonstrate that this interaction is key to restrict the formation of the proepicardium and the myocardium. *In cellulo* experiments suggest that IFT88 and IFT20 interact with YAP1 in the cytoplasm and functionally modulate its activity, identifying a molecular link between cilia-related proteins and the Hippo pathway. Taken together, our results highlight a noncanonical role for IFT complex B proteins during cardiogenesis and shed light on a mechanism of action for ciliary proteins in YAP1 regulation.

INTRODUCTION

Primary cilia are immotile microtubule-based organelles, well known for being both chemical and/or mechanical sensors (Berbari et al., 2009; Ferreira et al., 2019). Disruption of cilia function causes multiple human syndromes known as ciliopathies (Reiter and Leroux, 2017). Cilia are required for cardiac development and mutations in cilia-related proteins have been linked to congenital heart diseases (CHDs) (Klena et al., 2016; Li et al., 2015; San Agustin et al., 2016; Slough et al., 2008). Nevertheless, the specific role of cilia and cilia-related proteins during cardiogenesis is still unclear.

Intraflagellar transport (IFT) proteins are required for the transport of cilia components along the axoneme and are thus essential for cilia formation and function (Rosenbaum and Witman, 2002). The role of IFT proteins during ciliogenesis is highly conserved across organisms (Taschner et al., 2012). The IFT machinery is composed of two biochemically distinct subcomplexes, IFT-A and IFT-B (Taschner et al., 2012). The IFT complex B member IFT20, which localizes inside the cilium and at the Golgi complex in mammalian cells, participates in the sorting and/or transport of membrane proteins for the cilia (Follit et al., 2006). Within the IFT complex B, IFT20 interacts with IFT54/Elipsa (Omori et al., 2008; Zhu et al., 2017) and IFT88, which is essential for flagellar assembly in *Chlamydomonas* and ciliogenesis in vertebrates (Pazour et al., 2000). Mutations in some IFT proteins have been identified in CHDs (Li et al., 2015). IFT proteins also display noncanonical, cilia-independent functions (Hua and Ferland, 2018; Vertii et al., 2015). IFT88, for example, is needed for spindle orientation and organization, cleavage furrow ingression, or extra centrosome clustering in dividing cells (Delaval et al., 2011; Taulet et al., 2017, 2019; Vitre et al., 2020) and regulates G1-S phase transition in nonciliated cells (Robert et al., 2007). IFT20, together with IFT88 and IFT54, plays a role

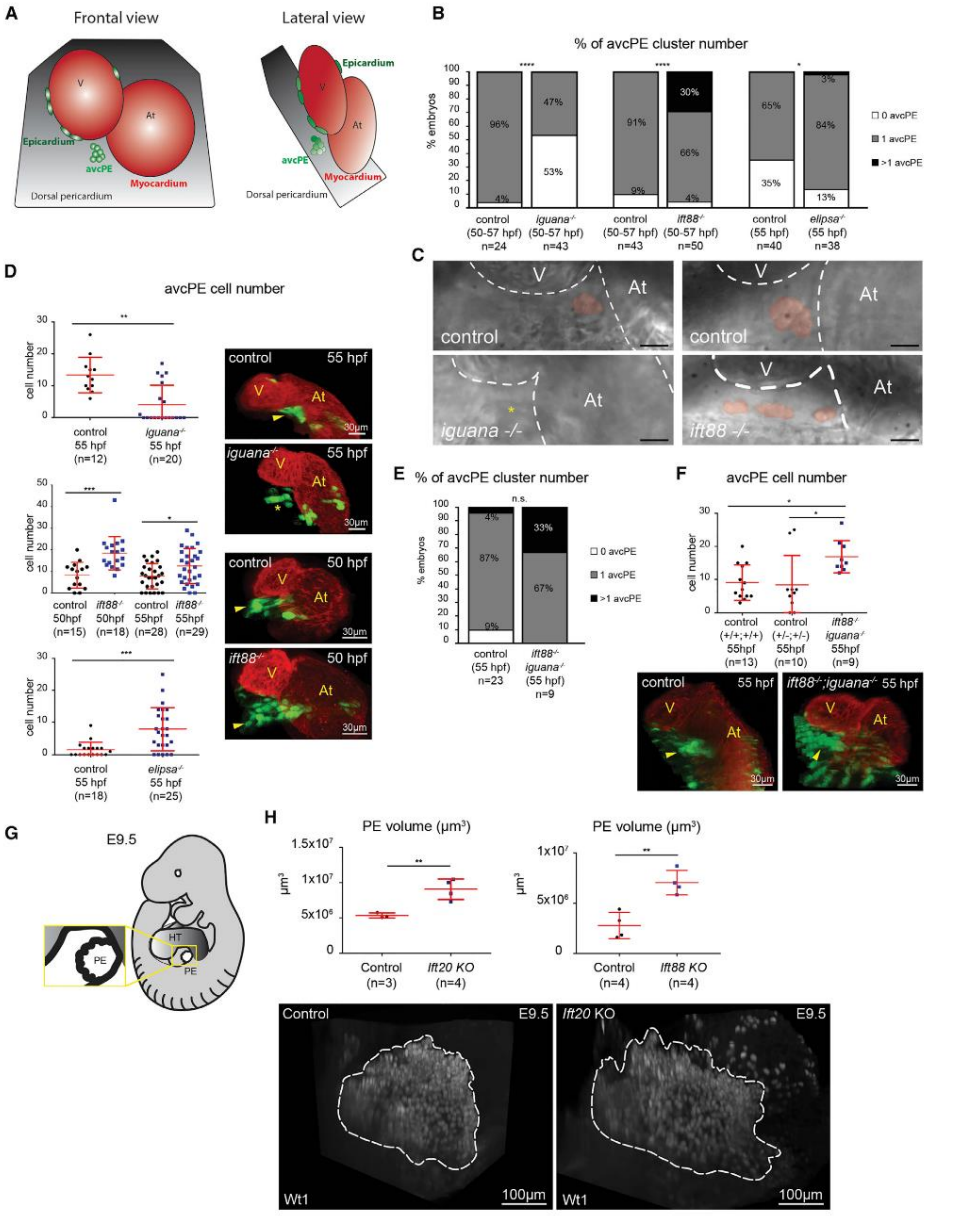

(legend on next page)

in the establishment of the immune synapse in T lymphocytes lacking cilia (Finetti et al., 2009; Galgano et al., 2017). These observations suggest that IFT proteins could play a key role in embryonic cardiogenesis through both cilia-dependent and -independent functions.

The Hippo signaling mediators, YAP1/WWTR1 (TAZ), constitute a key signaling pathway for the regulation of cardiac development (Fukui et al., 2018; Lai et al., 2018; Ragni et al., 2017; Xin et al., 2011) and cardiac regeneration (Bassat et al., 2017; Leach et al., 2017) in vertebrates. For example, YAP1/WWTR1 (TAZ) are required for epicardium and coronary vasculature development (Singh et al., 2016) in mice. In addition, Yap1 signaling has been reported to regulate the number of atrial cardiomyocytes derived from Islet1 (Isl1)-positive (+) secondary heart field (SHF) cells in the zebrafish (Fukui et al., 2018). Changes in cell shape, substrate stiffness, and tension forces activate a phosphorylation-independent YAP1/WWTR1 (TAZ) modulation (Elosegui-Artola et al., 2017), which is mediated by the Motin family (AMOT, AMOTL1, and AMOTL2) (Bratt et al., 2002; Zheng et al., 2009). Motin proteins bind to YAP/WWTR1 (TAZ), sequestering them in the cytoplasm in several cellular contexts (Agarwala et al., 2015; DeRan et al., 2014; Nakajima et al., 2017; Wang et al., 2011; Zhao et al., 2011). While it is known that ciliary proteins from the Nephrocystin family modulate the transcriptional activity of YAP1/WWTR1 (TAZ) (Frank et al., 2013; Grampa et al., 2016; Habbig et al., 2012) and that the Hippo kinases MST1/2-SAV1 promote ciliogenesis (Kim et al., 2014), the connection between the Hippo pathway and cilia function remains unclear.

Cardiogenesis involves an interplay between multiple tissue layers. The epicardium is the outermost layer covering the heart. This cardiac cell layer plays an essential role in myocardial maturation and coronary vessel formation during development (Männer et al., 2005; Moore et al., 1999; Wu et al., 2013) and has a crucial role during regeneration (González-Rosa et al., 2012; Kikuchi and Poss, 2012; Limana et al., 2011). Epicardial cells derive from the proepicardium (PE), an extracardiac transient cluster of heterogeneous cells (Katz et al., 2012). The PE, the sinoatrial node, and the atrial myocardium all derive from the SHF (Buckingham et al., 2005; Mommersteeg et al., 2010; van Wijk et al., 2009). In zebrafish, the transcription factor Isl1 marks a subset of SHF cells that give rise to part of the atrial myocardium (de Pater et al., 2009; Witzel et al., 2012). In mice, the PE is a single cell cluster located close to the venous pole of the heart (Katz et al., 2012), while in zebrafish it is composed of two cell clusters, avcPE (the main source of cells) and vpPE (Peralta et al., 2013). PE cells give rise to the epicardium, part of the coronary vasculature, and intracardiac fibroblasts (Acharya et al., 2012; Katz et al., 2012; Mikawa and Fischman, 1992; Mikawa and Gourdie, 1996). The secreted signaling molecules of the bone morphogenetic protein (BMP) family are indispensable for PE formation (Ishii et al., 2010; Liu and Stainier, 2010; Schlueter et al., 2006).

Despite the increasing evidence for the role of IFT proteins in cell signaling, it has been difficult to pinpoint the exact function of cilia-related proteins outside the cilium. Without this key information, the question of whether cilia-related proteins can affect the developmental program independently of their cilia function remains unresolved. Here, we provide a combination of *in vivo* and *in vitro* analyses of IFT protein function showing that IFT complex B proteins can modulate the Hippo pathway effector Yap1. In particular, we show that IFT88 is required to restrict PE and myocardium development through cytoplasmic activity.

RESULTS

IFT Complex B Proteins Regulate PE Development in Zebrafish and Mouse

Considering the importance of cilia during cardiogenesis, we assessed the role of several IFT complex B proteins during PE development. In order to benefit from live imaging and genetics, we used zebrafish as a model organism. We performed live-imaging focusing on the main PE cell source located near the atrioventricular canal (avcPE) in *ift88* (Tsujikawa and Malicki, 2004) and *elipsa/ift54* (Omori et al., 2008) mutants (Figures 1A–1D). Between 50 and 57 hours post fertilization (hpf), we found that *ift88* mutants display multiple avcPE clusters (either two or three), when controls have only one (Video S1). Using a *wilms tumor 1 a* (*wt1a*) enhancer trap line that marks proepicardial and epicardial cells (*Et(−26.5Hsa.WT1-gata2:EGFP)*^{cn1}; hereafter, *epi:GFP*) (Peralta et al., 2013), we quantified avcPE and epicardial cell number and found that *ift88* $^{-/-}$ have increased avcPE and

Figure 1. IFT Complex B Proteins Regulate Proepicardial Development in Zebrafish and Mice

(A) Schematic representation of the zebrafish heart at 55 hpf in frontal and lateral views. The dorsal pericardium (DP) is shown in gray, the myocardium (myoc) in red, the avcPE in light green, and the epicardial cells in dark green.

(B) Percentage of avcPE cluster number in *iguana* (n = 43), *ift88* (n = 50), and *elipsa/ift54* (n = 38) mutants and their controls (n = 24; n = 43; n = 40, respectively), between 50 and 57 hpf (Mann-Whitney test, *iguana* p value < 0.0001; *ift88* p value < 0.0001; *elipsa* p value, 0.014).

(C) High-speed avcPE imaging (digital red mask to improve visualization) of *iguana* and *ift88* mutants and their control. Scale bars: 20 μm.

(D) Graphs show avcPE cell number quantified on *iguana* (n = 20), *ift88* (n = 18 and 29), and *elipsa* (n = 25) mutants in *epi:GFP* background and their controls (n = 12; n = 15; n = 28 n = 18, respectively) (t test, *iguana* p value, 0.001; *ift88* p value, 0.0002; and p value, 0.015, respectively; *elipsa* p value, 0.0005). 3D projections of whole-mount immunofluorescence (IF) of hearts using anti-myosin heavy chain antibody (MHC) (red) and GFP (green) expression.

(E) Percentage of avcPE cluster number on *iguana* $^{-/-}$, *ift88* $^{-/-}$, *epi:GFP* (n = 9), and controls (n = 23) at 55 hpf (Mann-Whitney test, p value, 0.059).

(F) Graph shows avcPE cell number quantified in wild-type (n = 13), double-heterozygous controls (n = 10), and double *ift88; iguana* mutants (n = 9) (Kruskal-Wallis, p value, 0.014). 3D projections of whole-mount IF of hearts. MHC (red) and GFP (green) expression.

(G) Schematic representation of an E9.5 mouse embryo. Heart tube (HT) in dark gray and PE in white. Section of the PE represented inside the yellow box.

(H) Left-side graph shows quantification of PE volume (in cubic micrometers) in Ift20 KO (n = 4) and control mice (n = 3) (control, 5.35×10^6 μm^3 ± 3.63×10^5; Ift20 KO, 9.06×10^6 μm^3 ± 1.46×10^6) (t test, p value, 0.008) and that of *Ift88* KO (n = 4) and control embryo (n = 4) on the right (control, 2.78×10^6 μm^3 ± 1.3×10^6; *Ift88* KO, 7.05×10^6 μm^3 ± 1.2×10^6) (t test, p value, 0.003). In the lower panel, 3D projections of whole-mount IF performed on control and *Ift20* KO embryos. PE marked using anti-Wt1 antibody. The white dotted shapes enclose the PE area. In all graphs, red bars indicate mean ± SD. In all panels, ventral views, anterior is to the top. Arrowheads mark avcPE, and asterisk shows lack of avcPE. V, ventricle; At, atrium.

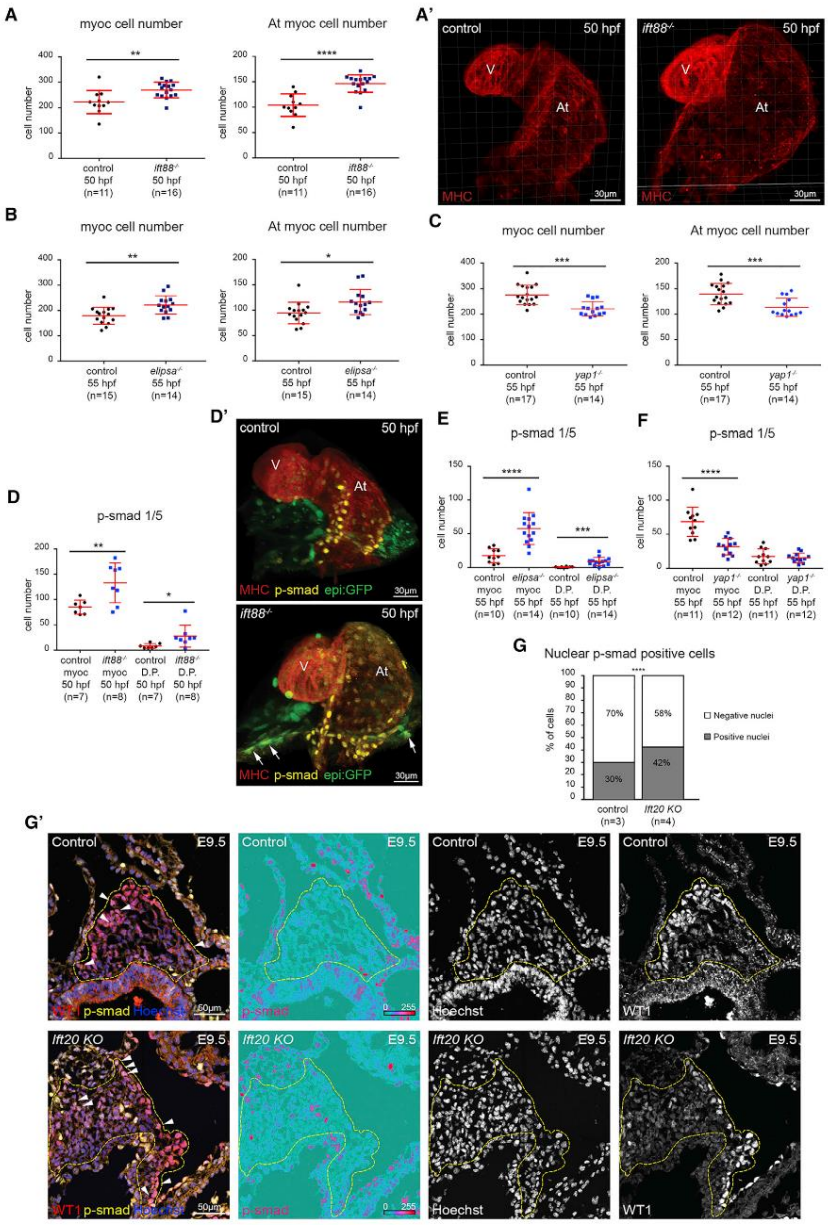

(legend on next page)

epicardial cell numbers compared to their controls at 50 and 55 hpf, respectively (Figures S1B and S2A). Similarly, we found that *elipsa* $^{-/-}$ also showed bigger avcPE compared to controls (Figures S1C and S2A″). Taken together, these data indicate that *ift88* and *elipsa/ift54* are required to restrict PE size.

To determine whether primary cilia are required for PE formation, we took advantage of the *iguana/dzip* (Tay et al., 2010) mutant, a well-established cilia mutant lacking primary cilia (Kim et al., 2010). We confirmed the absence of primary cilia in the pericardial cavity of the *iguana* $^{-/-}$ using the cilia reporter *actb2:Mmu.Arl13b-GFP* (Borovina et al., 2010; Figures S2C–S2E; Video S2). Zebrafish *ift* genes are expressed maternally (Sun et al., 2004; Figure S2E), and complete removal of both zygotic and maternal expression of *ift88* leads to the ablation of primary cilia resembling the *iguana* mutant phenotype (Huang and Schier, 2009). Live imaging revealed that a significant fraction of *iguana* mutants lacked an avcPE between 50 and 57 hpf (Figure 1B; Video S3). At 55 hpf, *iguana* $^{-/-}$ displayed decreased avcPE cell numbers (Figures 1D, S1A, and S2A′). Since the *iguana* mutants presented a phenotype opposite to that of the *ift88* mutants, we analyzed the *ift88* $^{-/-}$*; iguana* $^{-/-}$*; epi:GFP* double mutant to elucidate whether the differences could be due to a new cilia-independent function. The *ift88* $^{-/-}$*; iguana* $^{-/-}$*;* double mutant shows multiple avcPE cluster formation and an increased avcPE cell number, reminiscent of *ift88* loss of function (Figures 1E, 1F, and S1D). We conclude that Ift88 modulates the PE cell number independently of its cilia function.

We assessed whether the role of IFT complex B proteins during PE formation was conserved in mammals. We analyzed the PE in *Ift20* and *Ift88* knockout (KO) mice at mouse embryonic day 9.5 (E9.5) (Figures S3A and S3B). First, we performed immunofluorescence (IF) using an anti-Arl13b antibody to quantify the percentage of ciliated PE cells in *Ift20*, *Ift88* KO, and wild-type mice (Figures S3C–S3C″). We found that, while over 60% of the wild-type PE cells were ciliated, in *Ift88* KO mice only 3% of cells were ciliated and *Ift20* KO embryos lack cilia. We compared the PE volume of *Ift20* and *Ift88* KO mice to their controls, using an anti-Wt1 antibody (a well-established PE marker; Carmona et al., 2001). Mutant embryos showed increased PE volume (Figures 1G and 1H; Videos S5 and S6). These results suggest that IFT protein function is conserved during PE formation in mouse and zebrafish.

To test whether IFT complex B affected other cardiac tissues, we focused on the myocardium. Cell quantification showed increased myocardial cell number in *ift88* $^{-/-}$ compared to their controls at 50 hpf (Figures 2A and 2A′) and 55 hpf (Figure S4A). Interestingly, the increment was mostly affecting the atrium. Similar data were obtained with the *elipsa* mutants at 55 hpf (Figure 2B). We concluded that the absence of IFT complex B proteins also affects the myocardium.

To determine whether Isl1^{+} SHF cells were altered at earlier stages leading to the increment in avcPE and atrial myocardial cells, we quantified Isl1^{+} cells in *ift88* and *amotl2a* mutants at 36 hpf. We did not find differences between *ift88* $^{-/-}$, *amotl2a* $^{-/-}$, and their controls (Figure S1E).

BMP Signaling Is Increased in *ift88*, *elipsa/ift54*, and *Ift20* Mutants during PE Development

As it is known in zebrafish that overexpressing BMP increases PE size (Liu and Stainier, 2010), we investigated whether *ift88* loss influences BMP signaling. We first assessed *bmp4* expression by *in situ* hybridization (ISH) in *ift88* and *elipsa* mutants. We found that *ift88* $^{-/-}$ display ectopic expression of *bmp4* in the dorsal pericardium (DP) at 48 hpf (Figure S4B). To validate that the upregulation is functional *in vivo*, we quantified cellular BMP activity by using p-smad1/5 as a readout and confirmed that the absence of Ift88 leads to increased BMP signaling activity in the DP and myocardium, especially in the venous pole (Figures 2D, 2D′, and S4C). By 55 hpf, *bmp4* expression at the atrioventricular canal myocardium is reduced and the expression at the venous pole is almost undetectable in controls. By contrast, *ift88* mutants presented strong *bmp4* expression in both domains (Figure S4B). Myocardial p-smad1/5 was also increased in *ift88* $^{-/-}$ compared to controls, but not in the DP (Figures

Figure 2. BMP Signaling Is Increased in *ift88*, *elipsa/ift54*, and *Ift20* Mutants

(A) Graphs show total myocardial (myoc) and atrial-myoc cell number quantified in *ift88* (n = 16) mutants and controls (n = 11) at 50 hpf (t test, total myoc p value, 0.0034; atrial myoc p value < 0.0001).

(A′) 3D projections of whole-mount immunofluorescence (IF) of hearts using myosin heavy chain antibody (MHC) (red).

(B) Graphs show total myoc and atrial-myoc cell number quantified in *elipsa* (n = 14) mutants and controls (n = 15) at 55 hpf (t test, total myoc p value, 0.0026; atrial myoc p value, 0.017).

(C) Graphs show total myoc and atrial-myoc cell number quantified in *yap1* (n = 14) mutants and controls (n = 17) at 55 hpf (t test, total myoc p value, 0.0001; atrial myoc p value, 0.0009).

(D) Graph shows number of p-smad1/5^{+} cells in the myoc and dorsal pericardium (DP) quantified in *ift88* mutants (n = 8) and controls (n = 7) at 50 hpf. Myoc (t test, p value, 0.009) and DP (t test, p value, 0.036).

(D′) 3D projections of whole-mount IF of hearts. MHC (red), *epi:GFP* (green), and p-smad1/5 (yellow). Arrows mark dorsal pericardial cells positive for *epi:GFP* and p-smad1/5 (same embryos as in A′).

(E) Graph shows number of p-smad1/5^{+} cells in the myoc and DP quantified in *elipsa* mutants (n = 14) and controls (n = 10) at 55 hpf. Myoc (t test, p value < 0.0001) and DP (t test, p value, 0.0004).

(F) Graph shows number of p-smad1/5^{+} cells in the myoc and DP quantified in *yap1* $^{-/-}$*; tcf21:nls-GFP* (n = 12) and controls (n = 11) at 55 hpf. Myoc (t test, p value < 0.0001) and DP (t test, p value, 0.599).

(G) Graph shows that the percentage of p-smad1/5/9^{+} PE cells is higher in *Ift20* KO (n = 4 embryos: 1,862 nuclei analyzed) compared to control (n = 3 embryos: 1,414 nuclei analyzed) mice (Chi-square test of homogeneity = 51.593; p value, 6.829e-13 on 1 degree of freedom).

(G′) Control and *Ift20* KO IF confocal cryosections labeled with WT1 (red), p-smad1/5/9 (yellow), and Hoechst (blue) at E9.5. Yellow dotted lines enclose the PE area. Arrowheads mark p-smad1/5/9 and Wt1 double-positive cells. Individual channels are displayed for p-smad1/5/9 (signal is shown as ice LUT to facilitate the visualization of signal intensity, where green is the minimum and red is the maximum), Hoechst (white), and WT1 (white). In all graphs, red bars indicate mean ± SD. V, ventricle; At, atrium. Ventral views, anterior is to the top. p-smad, p-smad1/5 in (D′) and p-smad1/5/9 in (G′).

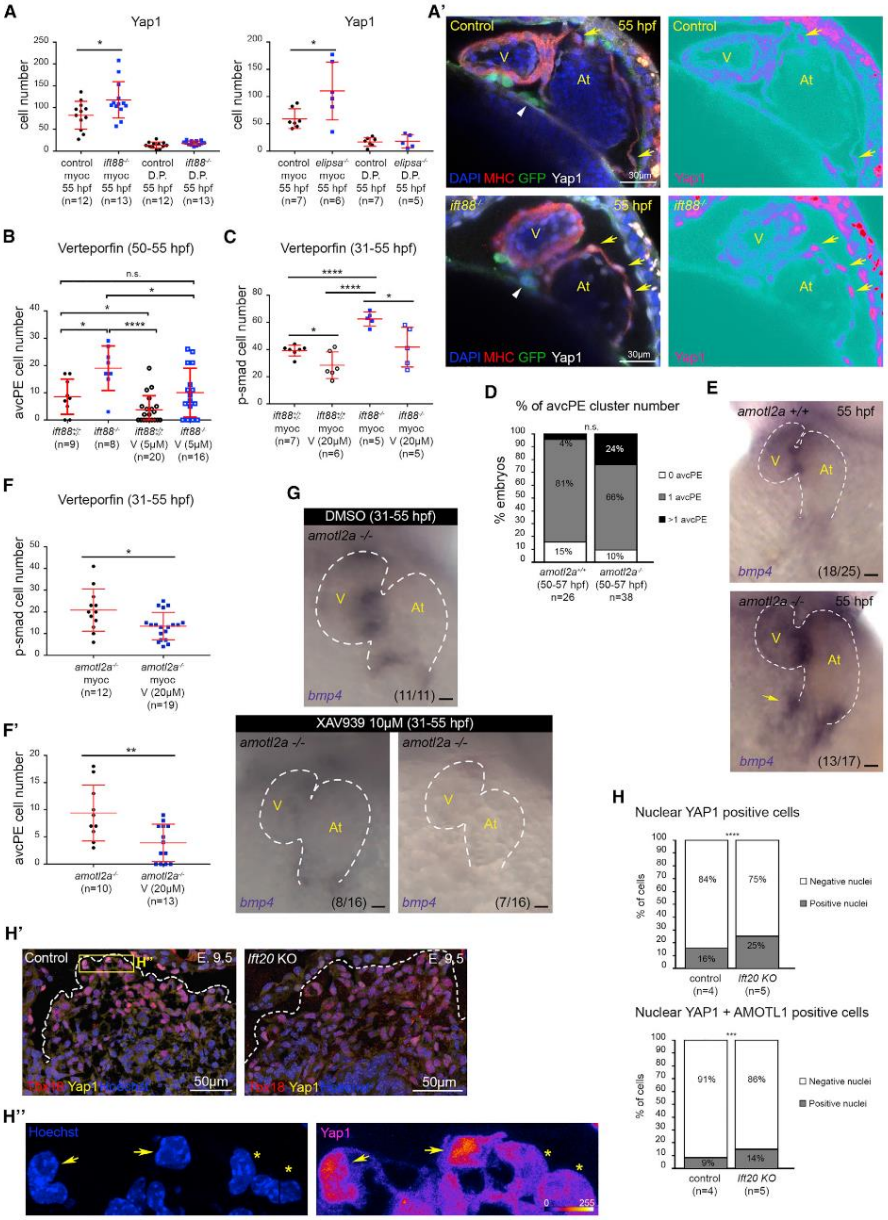

(legend on next page)

S4C and S4D). We reached similar conclusions when analyzing the *elipsa* mutants at 55 hpf (Figures 2E, S4B, and S4C). To confirm that the regulation of BMP signaling by IFT is conserved in vertebrates, we analyzed p-smad1/5/9 in *Ift20* and *Ift88* KO and control mice at E9.5 and found that only the *Ift20* mutants displayed a higher percentage of p-smad$^+$ cells compared to controls (Figures 2G, 2G′, and S3D). Together, these results suggest that Ift88 and Ift54 modulate BMP signaling activity in the myocardium and the pericardium of the zebrafish, and that IFT20 plays a similar role in the mouse PE.

Yap1-Tead Activity Is Increased in *ift88*, *elipsa/ift54*, and *Ift20* Mutants during PE Development

Yap1 participates in the regulation of Bmp signaling during SHF development (Fukui et al., 2018). This led us to assess whether Yap1/Wwtr1-Tead is active during PE formation using the *4xGTIIC:d2GFP* reporter line (Miesfeld and Link, 2014). We found that the reporter was active in the PE cluster, myocardium, pericardium, and epicardial cells at 55 hpf (Figure S5A). We performed time-lapse analysis to study the dynamics of Yap1/Wwtr1-Tead activity during PE development (Video S4). GFP quantification in PE and pericardial cells showed higher Yap1/Wwtr1-Tead activity (GFP average intensity) in the PE cells than in the pericardial cells (75% of the embryos) (Figure S5B; Table S1).

To test whether pericardial cells have differential Yap1 activity at earlier stages, before avcPE formation, we analyzed *4xGTIIC:d2GFP* reporter expression at 36 hpf (Figure S5D). We observed that some pericardial cells show stronger GFP intensity (hence higher levels of active Yap1) than others. Consistently with our data at later stages (Video S4; Figure S5B), pericardial cells at the area that will give rise to the avcPE show stronger GFP intensity. Additionally, we obtained similar data with Ctgf antibody, a well-characterized Yap1 target gene (Zhao et al., 2008; Figure S5E).

To test whether the increased avcPE cell number was due to abnormal Yap1 activity, we performed IF to quantify the number of nuclear Yap1$^+$ cells in *ift88* and *elipsa* mutants (Figures 3A, 3A′ and S5F–S5G′). At 55 hpf, *ift88* $^{-/-}$ showed more myocardial with nuclear Yap1$^+$ cells than controls, especially in the atrium (Figure 3A-A′). Similar data were obtained with the *elipsa* mutants (Figure 3A). To further validate the link between increased PE size and Yap1-Tead activity, we treated the *ift88* $^{-/-}$ with the drug Verteporfin, which binds to YAP and changes its conformation, blocking its interaction with TEAD (Liu-Chittenden et al., 2012). To assess Verteporfin specificity, we performed time-lapse imaging on Verteporfin-treated *4xGTIIC:d2GFP* embryos. We measured the Yap/Wwtr1-Tead activity (GFP average intensity) in the same PE and pericardial cells at several time points: before adding Verteporfin (t0), after 2-h treatment with Verteporfin, and 45 min after washing out (Figure S5C). We found that Yap/Wwtr1-Tead activity is significantly decreased with Verteporfin, confirming the specificity of the drug on the embryo. We next treated *ift88* $^{-/-}$ and control (*ift88*$^{+/+}$ and $^{+/-}$) embryos with Verteporfin (Figure 3B). Control embryos treated with Verteporfin showed smaller avcPE compared to untreated controls.

Figure 3. Yap1-Tead Activity Is Increased in *ift88*, *elipsa/ift54*, and *Ift20* Mutants during Proepicardium Development

(A) Graphs show number of Yap1$^+$ cells in the myocardium (myoc) and dorsal pericardium (DP) quantified in *ift88* (n = 13), *elipsa* (n = 6), and their controls (n = 12 and n = 7, respectively). *ift88* mutants show increased Yap1$^+$ myoc cell numbers (t test, p value, 0.03) and a tendency toward higher Yap1$^+$ DP cell numbers (t test, p value, 0.07). *elipsa* mutants show higher Yap1$^+$ myoc cell numbers (t test, p value, 0.036).

(A′) Control and *ift88* $^{-/-}$; *epi:GFP* immunofluorescence (IF) confocal sections labeled with anti-myosin heavy chain antibody (MHC) (red), GFP (green), -Yap1 (white), and DAPI (blue) at 55 hpf. Individual channel is displayed for Yap1 (signal is shown as ice LUT to facilitate the visualization of signal intensity, where green is the minimum and red is the maximum). Yellow arrows mark nuclear Yap1-positive atrial myocardial cells. White arrowheads mark the avcPE.

(B) Graph shows avcPE cell number quantified in control (n = 9), *ift88* $^{-/-}$; *epi:GFP* (n = 8) and Verteporfin (5 μM)-treated *ift88* $^{-/-}$; *epi:GFP* (n = 16) and control (n = 20) embryos. Control embryos treated with Verteporfin showed smaller avcPE compared to untreated controls (t test, p value, 0.04). Verteporfin-treated *ift88* $^{-/-}$; *epi:GFP* embryos presented lower avcPE cell numbers than nontreated *ift88* $^{-/-}$; *epi:GFP* embryos (t test, p value, 0.027). *ift88* $^{-/-}$; *epi:GFP* embryos showed bigger avcPE compared to untreated (t test, p value, 0.01) and treated controls (t test, p value, 0.0001).

(C) Graph shows number of p-smad1/5$^+$ cells in the myoc quantified in control (n = 7), *ift88* $^{-/-}$; *epi:GFP* (n = 5), and Verteporfin (20 μM)-treated *ift88* $^{-/-}$; *epi:GFP* (n = 5) and control (n = 6) embryos from 31 to 55 hpf. Control embryos treated with Verteporfin showed decreased p-smad1/5$^+$ cell numbers compared to untreated controls (t test, p value, 0.0219). Verteporfin-treated *ift88* $^{-/-}$; *epi:GFP* embryos presented less p-smad1/5$^+$ cells than non-treated *ift88* $^{-/-}$; *epi:GFP* embryos (t test, p value, 0.0173). *ift88* $^{-/-}$; *epi:GFP* embryos showed more p-smad1/5$^+$ cells compared to untreated (t test, p value < 0.0001) and treated controls (t test, p value < 0.0001).

(D) Percentage of avcPE cluster number in *amotl2a*$^{+/+}$ (n = 26) and *amotl2a* $^{-/-}$ (n = 38) embryos between 50 and 57 hpf (Mann-Whitney test, p value, 0.08).

(E) Whole-mount bmp4 *in situ* hybridization (ISH) in *amotl2a*$^{+/+}$ (n = 18/25) and *amotl2a* $^{-/-}$ (n = 13/17) embryos (55 hpf). Yellow arrow shows bmp4 overexpression. Scale bars: 20 μm.

(F) Graph shows number of p-smad1/5$^+$ cells in the myoc quantified in Verteporfin (20 μM)-treated *amotl2a* $^{-/-}$ (n = 19) embryos from 31 to 55 hpf and untreated *amotl2a* $^{-/-}$ (n = 12) embryos. Treated embryos showed decreased p-smad1/5$^+$ cell numbers compared to untreated ones (t test, p value, 0.0148).

(F′) Graph shows avcPE cell number quantified in Verteporfin (20 μM)-treated *amotl2a* $^{-/-}$ (n = 13) embryos from 31 to 55 hpf and untreated *amotl2a* $^{-/-}$ (n = 10) embryos. Treated embryos showed decreased avcPE cell numbers compared to untreated ones (t test, p value, 0.0059).

(G) Whole-mount bmp4 ISH in XAV939 (10 μM)-treated *amotl2a* $^{-/-}$ (n = 16) from 31 to 55 hpf and untreated embryos (n = 11). Treated embryos showed either decreased (n = 8/16) or absent (n = 7/16) bmp4 expression at the atrioventricular canal myoc and the venous pole. Scale bars: 20 μm.

(H) Graphs show percentages of YAP1$^+$ PE cells and double-YAP1-AMOTL1-positive PE cells in *Ift20* KO (n = 5 embryos: 1,196 nuclei analyzed) and control (n = 4 embryos: 929 nuclei analyzed) mice at E9.5. The percentage of nuclear YAP1$^+$ PE cells (Chi-square test of homogeneity = 25.354; p value, 4.77E-07 on 1 degree of freedom) and nuclear YAP1-AMOTL1$^+$ cells (Chi-square test of homogeneity = 12,025; p value, 5.25E-04 on 1 degree of freedom) were higher in *Ift20* KO than in control mice.

(H′) Control and *Ift20* KO IF confocal sections labeled with TBX18 (red), YAP1 (yellow), and Hoechst (blue) at E9.5. The white dotted lines enclose the PE area.

(H″) Zoomed region shows the difference between nuclear YAP1$^+$ cells (yellow arrows) and YAP1-negative cells (yellow asterisks). Hoechst signal (blue) highlights cell nuclei. YAP1 signal is shown as fire LUT to facilitate the visualization of signal intensity, where blue is the minimum and yellow is the maximum. In all graphs, red bars indicate mean ± SD. In all panels, ventral views, anterior is to the top. V, ventricle; At, atrium.

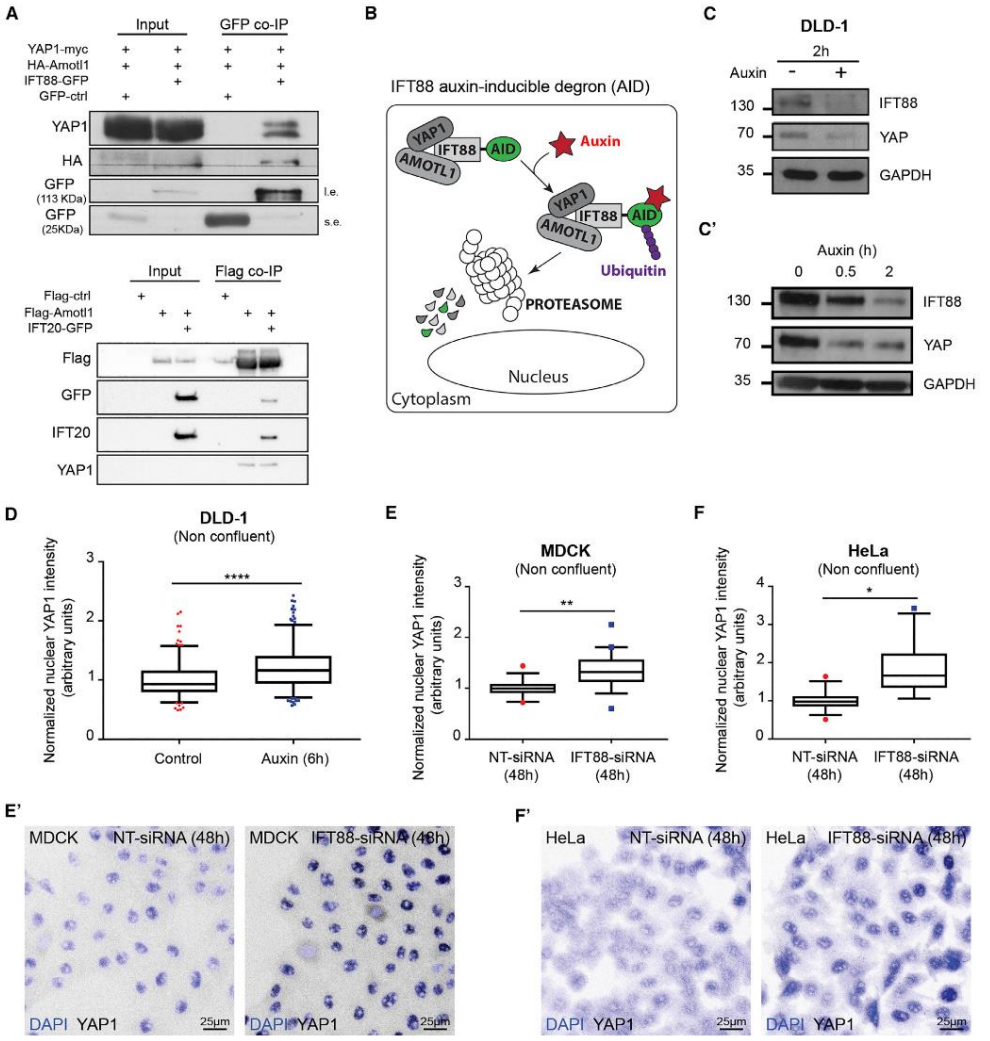

Figure 4. IFT88 and IFT20 Are Physically Associated to YAP1, and IFT88 Modulates YAP1 Activity

(A) Co-IP experiment using HeLa cells transfected with IFT88-GFP, HA-Amotl1, and YAP1-Myc (l.e., long exposure; s.e., short exposure). Co-IP experiment using HEK293 cells transfected with Flag-Amotl1 and IFT20-GFP. Endogenous levels of Yap1 are monitored.

(B) Schematic representation of the IFT88 auxin-inducible degron (AID) system.

(C) Western blot analysis of IFT88 AID DLD-1 cells after 2-h auxin treatment.

(C') Western blot analysis of IFT88 and YAP1 degradation after auxin treatment (0, 0.5, and 2 h).

(D) Graph shows the increase in normalized YAP1 nuclear signal in cells treated with auxin (6 h) (Mann–Whitney, p value < 0.0001) (controls: 2 replicates, n = 204 cells; Auxin 2 h: 2 replicates, n = 261 cells).

(E) Graph shows the increase in YAP/WWTR1 (TAZ) nuclear signal in IFT88-siRNA (48 h)-treated MDCK cells (n = 5 replicates, average cell number analyzed for each condition = 382; t test, p value, 0.004). Box and whiskers (5th–95th percentile). Outliers are represented as red dots (NT-siRNA) or blue squares (IFT88-siRNA).

(legend continued on next page)

Verteporfin-treated *ift88* $^{-/-}$ embryos presented fewer avcPE cell numbers than nontreated *ift88* $^{-/-}$ embryos. Interestingly, nontreated controls and treated *ift88* mutants did not show significant differences in avcPE cell number. Thus, the increase in avcPE cell number induced in the absence of Ift88 was rescued by Verteporfin treatment. These results suggest that Ift88 requires Yap1 activity to modulate the PE size restriction.

To explore a possible role of Yap1 in the regulation of BMP signaling by IFT, we treated *ift88* $^{-/-}$ and control (*ift88*$^{+/+}$ and $^{+/-}$) embryos with Verteporfin (Figure 3C) and quantified BMP activity. Control embryos treated with Verteporfin showed decreased p-smad1/5^{+} myocardial cell number compared to untreated controls. Verteporfin-treated *ift88* $^{-/-}$ embryos presented fewer p-smad1/5^{+} myocardial cells than nontreated *ift88* $^{-/-}$ embryos. Remarkably, nontreated controls and treated *ift88* $^{-/-}$ did not show significant differences. Thus, the increase in BMP activity induced in the absence of Ift88 was rescued by Verteporfin treatment. Likewise, ISH performed in *elipsa* $^{-/-}$ and control (*elipsa*$^{+/+}$ and $^{+/-}$) embryos treated with Verteporfin displayed decreased *bmp4* expression (Figure S6C). Furthermore, treatment with the drug XAV939, a tankyrase inhibitor that suppressed YAP-TEAD activity (Wang et al., 2015), also led to a reduction of *bmp4* expression (Figure S5H). These results suggest that Ift88 and Ift54 require Yap1 activity to modulate BMP signaling activity in the myocardium of the zebrafish. To confirm the involvement of an increased Yap1 activity in the *ift88* $^{-/-}$ phenotype, we analyzed the avcPE in *angiomotin like 2a* (*amotl2a*) mutants (Figures 3D and 3E). In zebrafish, Amotl2a physically interacts with Yap1 leading to its cytoplasmic retention in a way that *amotl2a* mutants show upregulated Yap1 activity (nuclear Yap1) (Agarwala et al., 2015; Nakajima et al., 2017). Accordingly, *amotl2a* $^{-/-}$ presented multiple avcPE formation and increased *bmp4* expression when compared to *amotl2a*$^{+/+}$ embryos at 55 hpf. When treated with Verteporfin, *amotl2a* $^{-/-}$ showed decreased myocardial p-smad1/5^{+} and avcPE cell numbers compared to untreated *amotl2a* $^{-/-}$ embryos (Figures 3F and 3F′). Likewise, *bmp4* expression at the atrioventricular canal myocardium and at the venous pole were reduced in *amotl2a* $^{-/-}$ embryos treated with XAV939 (Figure 3G). Thus, Verteporfin and XAV939 treatments rescued the increase in BMP signaling induced in the absence of Amotl2a, suggesting it acts through Yap1 activity. We next analyzed the *yap1* mutants (Agarwala et al., 2015). At 55 hpf, *yap1* $^{-/-}$ showed decreased myocardial cell number compared to their controls (Figure 2C). Besides, fewer myocardial cells were p-smad1/5^{+} (Figure 2F). Surprisingly, avcPE cell number was similar between *yap1* $^{-/-}$ and their controls (Figures S2B and S2B′). Altogether, these results suggest that Ift88 and Ift54 modulate BMP signaling activity by tuning Yap1-Tead activity in the myocardium of the zebrafish. To assess whether the upregulation of Yap1 activity observed in IFT zebrafish mutants was conserved in vertebrates, we analyzed YAP1 localization in the PE of *Ift20 KO* and control mice (Figures 3H–3H″). We quantified the proportion of nuclear YAP1^{+} cells (i.e., cells with higher signal intensity inside the nucleus than in the cytoplasm). The percentage of nuclear YAP1^{+} PE cells was higher in *Ift20 KO* than in control mice. In mouse myocardium, YAP1 and AMOTL1 translocate to the nucleus together to modulate cell response (Ragni et al., 2017). To assess AMOTL1 localization in PE cells, we performed AMOTL1 IF. Consistent with the results obtained with an anti-YAP1 antibody, the percentage of nuclear AMOTL1^{+} cells (i.e., cells with higher signal intensity inside the nucleus than in the cytoplasm) was increased in the *Ift20 KO* when compared to control mice (Figure S5I). We also found that the mutants showed an increase in the percentage of YAP1-AMOTL1 double-positive cells (Figure 3H). Together, these data show that the increased PE size in *Ift20 KO* mice is associated with increased YAP1 activity.

IFTs Interact with YAP1 and Regulate Its Activity

Taking advantage of cultured cells, we next explored the mechanism by which IFT proteins could regulate YAP1 activity. IF performed in HeLa cells transfected with IFT88-GFP showed co-localization between IFT88 and YAP1 in the cytoplasm (Figures S6A–S6C). To confirm a potential physical interaction between IFT proteins with YAP1, we performed co-immunoprecipitation (co-IP) experiments using IFT88-GFP and YAP1-Myc in HeLa cells but never obtained any clear interaction. Considering that YAP1 often necessitates the scaffold protein Angiomotin-like 1 (Amotl1) (Ragni et al., 2017), we next performed co-IP experiment using HA-Amotl1, IFT88-GFP, and YAP1-Myc in HeLa cells. The experiments revealed a clear interaction between YAP1, Amotl1, and IFT88 (Figure 4A). Similarly, physical interaction between endogenous YAP1, Flag-Amotl1, and IFT20-GFP was observed in transfected HEK293 cells (Figure 4A). These results reveal that IFT proteins, YAP1, and Amotl1 could function as part of a complex involved in the functional modulation of YAP1 activity *in vivo*.

To functionally assess the impact of endogenous IFT88 depletion on YAP1 activity, we used a DLD-1 IFT88-auxin-inducible degron (AID) cell line, in which a rapid degradation of IFT88 protein can be induced by auxin treatment (Figure 4B). Of note, DLD-1 cells do not grow cilia, allowing us to explore the cytoplasmic, cilia-independent function of IFT88 (Lancaster et al., 2011).

We observed that 2 h of auxin treatment led to IFT88 and YAP1 degradation. The rapid co-degradation further suggested that both proteins physically interact (Figure 4C). We confirmed this finding by performing shorter auxin treatments to study the progressive degradation of IFT88 and YAP1 (Figure 4C′). Importantly, as previously observed *in vivo*, longer depletion of endogenous IFT88 after 6 h of auxin treatment led to an increase in nuclear YAP1 measured by IF (Figure 4D). Consistently, the nuclear/cytoplasmic YAP1 ratio was also increased (Figure S7A). Additionally, we confirmed these results using HeLa and MDCK cell lines where IFT88 function was inactivated by IFT88-siRNA. The IFT88-siRNA efficiency was validated by IF

(E′) Immunofluorescence (IF) confocal images of MDCK cells treated with NT- or IFT88-siRNA (48 h). DAPI (blue) and YAP/WWTR1 (TAZ) (white inverted LUT). (F) Graph shows the increase in YAP/WWTR1 (TAZ) nuclear signal in IFT88-siRNA (48 h)-treated HeLa cells (n = 5 replicates, average cell number analyzed for each condition = 252; t test, p value, 0.02). Box and whiskers (5th–95th percentile). Outliers are represented as red dots (NT-siRNA) or blue squares (IFT88-siRNA). (F′) IF confocal images of HeLa cells treated with NT- or IFT88-siRNA (48 h). DAPI (blue) and YAP/WWTR1 (TAZ) (white inverted LUT).

and western blot (Figures S7E–S7G). After 48 h of IFT88-siRNA treatment, nuclear YAP1 signal was measured by IF (Figures 4E–4F′). The inactivation of IFT88 was accompanied with increased nuclear YAP1 (Figures 4E and 4F). Altogether, these data indicate that IFT88 can interact with YAP1 in the cytoplasm and is involved in modulating the activation of the Hippo pathway effector YAP1.

To confirm that increased nuclear YAP1 is specific of IFT protein function, we performed IFT88 and IFT20 overexpression assays. While the transfection of pEGFP C1 did not alter the nuclear signal between GFP-positive and GFP-negative cells (endogenous control) (Figure S6D), IFT88-GFP and IFT20-GFP overexpression caused a decrease in nuclear signal (Figures S7B–S7D). Together, these data confirm that IFT proteins modulate YAP1 activation.

DISCUSSION

IFT proteins have long been associated with ciliary functions in developmental processes. For example, *ift88* mutants display a number of phenotypes reminiscent of ciliary defects such as abnormal patterning of the neural tube, defects in the Hedgehog pathway and left-right patterning (Huang and Schier, 2009). Ift88 has also been associated with planar cell polarity (Cao et al., 2010) and cell division (Delaval et al., 2011; Taulet et al., 2017, 2019; Vitre et al., 2020). Our observations provide evidence for a role of IFT complex B proteins in cardiogenesis. Mechanistically, IFT proteins are best known for their function in ciliary transport (Ocbina et al., 2011). Here, we describe an unexpected interaction between the ciliary machinery proteins and a potent mechanosensing pathway, the Hippo pathway. The hippo effector YAP1 is known to have essential roles in cancer (Zanconato et al., 2016), regeneration (Bassat et al., 2017; Leach et al., 2017; Oh et al., 2018), and organ size control (Artap et al., 2018; Thompson and Sahai, 2015; Yu et al., 2015). Several mechanisms have been shown to regulate the shuttling of YAP1 into the nucleus, including phosphorylation by Hippo kinases. Recent studies show that YAP1 is mechanosensitive and that force applied to the nucleus can directly drive YAP1 nuclear translocation (Elosegui-Artola et al., 2017; Sun et al., 2014). Additionally, Angiomotin (AMOT) has been shown to interact physically with YAP1 and act as a buffering factor sequestering YAP1 in the cytoplasm (Zhao et al., 2011). Nevertheless, AMOTL1 has also been shown to co-localize with YAP1 in the nucleus (Ragni et al., 2017; Yi et al., 2013), demonstrating that YAP1 subcellular localization is highly regulated by Motin family proteins. Our results indicate that IFT complex B proteins are also involved in regulating YAP1 localization. We demonstrate that IFT88 interacts biochemically with YAP1 and both co-localize in the cytoplasm. We did not study TAZ, the other Hippo effector that is known to act with YAP1 (Piccolo et al., 2014), and we cannot draw general conclusions on the role of IFT88 on all the known Hippo effectors. Nevertheless, our work suggests alternative ways to interpret Ift88 mutant phenotypes, which are often interpreted based on polarity or cilia function issues, and, more generally, phenotypes of other mutants with abnormal IFT complex B proteins. Our working model is that Ift88 participates in sequestering YAP1 away from the nucleus using its cargo transport activity. Other cilia-related proteins, such as kinesin2 and IFT complex A proteins, have been shown to promote nuclear localization of β-catenin during Wnt signaling in *Drosophila* (Vuong et al., 2018), further suggesting that proteins identified for their ciliary transport functions are not always limited to that function. Future work will reveal the mechanism by which Ift88 limits nuclear translocation of YAP1 and address whether IFT complex A proteins play a role.

Importantly, while our study points toward a noncanonical function for IFT complex B proteins, our results do not exclude a role for primary cilia in PE formation. We found that *iguana/dzip* mutants display an avcPE phenotype, suggesting that primary cilia function is required for PE morphogenesis. The HH pathway is often associated with ciliary function. To date, a number of studies suggest the proepicardium and epicardium formation are not regulated by Hedgehog signaling (Rudat et al., 2013; Sugimoto et al., 2017). Indeed, dissection of zebrafish *shha* function in the PE and epicardium using a *tcf21:CreER*, a well-established PE and epicardial tissue driver (Robb et al., 1998), does not affect PE formation (Sugimoto et al., 2017). Besides, expression of *Shh*, *Dhh*, *Ihh*, and *Ptch1* was neither detected in the mouse PE nor in the epicardium at subsequent stages (Rudat et al., 2013). Thus, primary cilia certainly operate independently of the HH pathway and Yap1, which is not altered in *dzip* mutants, in the process. Our work further highlights the important role of the BMP pathway in PE formation (Andrés-Delgado et al., 2019; Liu and Stainier, 2010). Primary cilia modulate BMP pathway and, more generally, TGF beta signaling pathways (Mönnich et al., 2018; Villalobos et al., 2019). In endothelial cells, primary cilia modulate angiogenesis by altering BMP signaling (Vion et al., 2018). We speculate the situation is different in PE cells, where BMP is activated downstream of YAP1, and where IFT88 helps to limit YAP1 and BMP signaling. Similarly, Hippo signaling determines the number of atrial myocardial cells that originate from the SHF by modulating BMP signaling (Fukui et al., 2018). Interestingly, lack of Ift88 did not affect Isl1 expression at early stages, suggesting Ift88 modulates Yap1-BMP axis at later stages during PE and atrial myocardium development. While *yap1* zebrafish mutants display decreased myocardial cell number, they surprisingly display normal avcPE cell number. The zebrafish *yap1* mutants are able to develop and to reach adulthood, which can be due to the compensation between Yap1 and Wwtr1 previously described (Miesfeld et al., 2015). We speculate that similar compensation may be at work in the PE as well. Importantly, we found phenotypic difference between mouse and fish, especially regarding the heart size, which is not affected in mouse. More work will be needed to understand these interspecific differences as well as the potential mechanisms of compensation involved if any. Zebrafish, *ift88* and *elipsa*, and mouse, *Ift20* and *Ift88*, mutants are lethal at 6 dpf and E10.5–E11.5, respectively, making impossible the study of cardiovascular defects at later stages without conditional gene inactivation approaches.

In summary, our study reports the role of IFT complex B proteins during PE development by modulating YAP1 activity independently of any cilia function. Linking IFT with YAP1 activity might have important implications for understanding the etiology of ciliopathies during cardiogenesis and for the interpretation of ciliary defects in IFT mutants.

STAR★METHODS

Detailed methods are provided in the online version of this paper and include the following:

- KEY RESOURCES TABLE
- RESOURCE AVAILABILITY
  - Lead Contact
  - Materials Availability
  - Data and Code Availability
- EXPERIMENTAL MODEL AND SUBJECT DETAILS
  - Zebrafish (ZF) Models
  - Mouse Models
- METHOD DETAILS
  - *In Vivo* Imaging
  - ZF Treatments
  - ZF Immunofluorescence
  - *In Situ* Hybridization (ISH)
  - Whole Mount Immunofluorescence in the Mouse
  - Immunofluorescence on Cryosections in the Mouse
  - Cell Culture, siRNAs and Transfection
  - Generation of DLD-1 IFT88-AID Targeted Cells
  - Immunofluorescence on Cells
  - Lysates and Immunoblotting
- IMMUNOPRECIPITATION (IP) ASSAYS
  - HEK293 Cells
  - HeLa Cells
  - ZF avcPE Cell Quantification
  - ZF Myocardial Cell Quantification
  - Mice PE Volume Analysis
  - Mice Yap1- and Amotl1-Positive Cell Quantifications
  - Nuclear Yap Quantifications on Cells
  - Nuclear/cytoplasmic Yap1 Ratio
- QUANTIFICATION AND STATISTICAL ANALYSIS

SUPPLEMENTAL INFORMATION

Supplemental Information can be found online at https://doi.org/10.1016/j.celrep.2020.107932.

ACKNOWLEDGMENTS

We thank P. Lamperti, E. Steed, A. Bhat, D. Riveline, S. Harlepp, J. Godin, A. Benmerah, and the Vermot laboratory for discussion and thoughtful comments on the manuscript, in particular R. Chow for her help with editing. We thank S. Roth for technical help. We thank G. Pazour, M. Faucourt, and N. Spassky for advice, for the gift of plasmids, and for providing the *Ift20* and *Ift88* mutant mouse lines, and C. Cimper, L. Bombardelli, and C. Shea for technical assistance. We are grateful to the IGBMC fish facility, the IGBMC imaging center, and the imaging platforms of the SFR Necker. This project has received funding from the European Union's Horizon 2020 Research and Innovation Programme under the Marie Sklodowska-Curie Grant Agreement No. 708312 (M.P.) and from the European Research Council (ERC) under the European Union's Horizon 2020 Research and Innovation Programme: GA No. 682938 (J.V.). This work was supported by FRM (DEQ20140329553), by ANR (ANR-15-CE13-0015–liveheart, ANR- SNF310030E-164245-forcinregeneration), and by the Grant ANR-10-LABX-0030-INRT, a French State fund managed by the Agence Nationale de la Recherche under the frame program Investissements d'Avenir labeled ANR-10-IDEX-0002-02. B.D.'s team was supported by ANR-12-CHEX-005 and CNRS. S.M.M.'s team was supported by core funding from the Institut Imagine, Institut Pasteur, Inserm, Université Paris Descartes, and a grant from the AFM-Téléthon (Trampoline 18727). T.L. was funded by the ED515 (1691/2014). L.O.L. is supported by the European Commission (H2020-MSCA-ITN-2016 European Industrial Doctorate 4DHeart 722427).

AUTHOR CONTRIBUTIONS

Conceptualization, M.P. and J.V.; Data Curation, M.P., L.O.L., K.J., and T.L.; Formal Analysis, M.P.; Funding Acquisition, M.P., B.D., S.M.M., and J.V.; Investigation, M.P., L.O.L., K.J., T.L., B.V., D.H., and L.G.; Methodology, M.P., K.J., T.L., B.V., B.D., S.M.M., and J.V.; Project Administration, M.P. and J.V.; Resources, C.D., V.L., I.S., B.D., S.M.M., and J.V.; Supervision, J.V.; Validation, M.P., B.D., S.M.M., and J.V.; Visualization, M.P.; Writing – Original Draft, M.P. and J.V.; Writing – Review & Editing, M.P., L.O.L., K.J., T.L., D.H., C.D., B.V., N.M., V.L., B.D., S.M.M., and J.V.

DECLARATION OF INTERESTS

The authors declare no competing interests.

Received: October 24, 2019
Revised: April 30, 2020
Accepted: June 29, 2020
Published: July 21, 2020

REFERENCES

Acharya, A., Baek, S.T., Huang, G., Eskiocak, B., Goetsch, S., Sung, C.Y., Banfi, S., Sauer, M.F., Olsen, G.S., Duffield, J.S., et al. (2012). The bHLH transcription factor Tcf21 is required for lineage-specific EMT of cardiac fibroblast progenitors. Development *139*, 2139–2149.

Agarwala, S., Duquesne, S., Liu, K., Boehm, A., Grimm, L., Link, S., König, S., Eimer, S., Ronneberger, O., and Lecaudey, V. (2015). Amotl2a interacts with the Hippo effector Yap1 and the Wnt/β-catenin effector Lef1 to control tissue size in zebrafish. eLife *4*, e08201.

Andrés-Delgado, L., Ernst, A., Galardi-Castilla, M., Bazaga, D., Peralta, M., Münch, J., González-Rosa, J.M., Marques, I., Tessadori, F., de la Pompa, J.L., et al. (2019). Actin dynamics and the Bmp pathway drive apical extrusion of proepicardial cells. Development *146*, dev174961.

Artap, S., Manderfield, L.J., Smith, C.L., Poleshko, A., Aghajanian, H., See, K., Li, L., Jain, R., and Epstein, J.A. (2018). Endocardial Hippo signaling regulates myocardial growth and cardiogenesis. Dev. Biol. *440*, 22–30.

Bassat, E., Mutlak, Y.E., Genzelinakh, A., Shadrin, I.Y., Baruch Umansky, K., Yifa, O., Kain, D., Rajchman, D., Leach, J., Riabov Bassat, D., et al. (2017). The extracellular matrix protein agrin promotes heart regeneration in mice. Nature *547*, 179–184.

Berbari, N.F., O'Connor, A.K., Haycraft, C.J., and Yoder, B.K. (2009). The primary cilium as a complex signaling center. Curr. Biol. *19*, R526–R535.

Boin, A., Couvelard, A., Couderc, C., Brito, I., Filipescu, D., Kalamarides, M., Bedossa, P., De Koning, L., Danelsky, C., Dubois, T., et al. (2014). Proteomic screening identifies a YAP-driven signaling network linked to tumor cell proliferation in human schwannomas. Neuro-oncol. *16*, 1196–1209.

Borovina, A., Superina, S., Voskas, D., and Ciruna, B. (2010). Vangl2 directs the posterior tilting and asymmetric localization of motile primary cilia. Nat. Cell Biol. *12*, 407–412.

Bratt, A., Wilson, W.J., Troyanovsky, B., Aase, K., Kessler, R., Van Meir, E.G., and Holmgren, L. (2002). Angiomotin belongs to a novel protein family with conserved coiled-coil and PDZ binding domains. Gene *298*, 69–77.

Buckingham, M., Meilhac, S., and Zaffran, S. (2005). Building the mammalian heart from two sources of myocardial cells. Nat. Rev. Genet. *6*, 826–835.

Cao, Y., Park, A., and Sun, Z. (2010). Intraflagellar transport proteins are essential for cilia formation and for planar cell polarity. J. Am. Soc. Nephrol. *21*, 1326–1333.

Carmona, R., González-Iriarte, M., Pérez-Pomares, J.M., and Muñoz-Chápuli, R. (2001). Localization of the Wilm's tumour protein WT1 in avian embryos. Cell Tissue Res. *303*, 173–186.

Cong, L., Ran, F.A., Cox, D., Lin, S., Barretto, R., Habib, N., Hsu, P.D., Wu, X., Jiang, W., Marraffini, L.A., and Zhang, F. (2013). Multiplex genome engineering using CRISPR/Cas systems. Science *339*, 819–823.

de Pater, E., Clijsters, L., Marques, S.R., Lin, Y.F., Garavito-Aguilar, Z.V., Yelon, D., and Bakkers, J. (2009). Distinct phases of cardiomyocyte differentiation regulate growth of the zebrafish heart. Development *136*, 1633–1641.

Delaval, B., Bright, A., Lawson, N.D., and Doxsey, S. (2011). The cilia protein IFT88 is required for spindle orientation in mitosis. Nat. Cell Biol. *13*, 461–468.

DeRan, M., Yang, J., Shen, C.-H., Peters, E.C., Fitamant, J., Chan, P., Hsieh, M., Zhu, S., Asara, J.M., Zheng, B., et al. (2014). Energy stress regulates hippo-YAP signaling involving AMPK-mediated regulation of angiomotin-like 1 protein. Cell Rep. *9*, 495–503.

Elosegui-Artola, A., Andreu, I., Beedle, A.E.M., Lezamiz, A., Uroz, M., Kosmalska, A.J., Oria, R., Kechagia, J.Z., Rico-Lastres, P., Le Roux, A.-L., et al. (2017). Force triggers YAP nuclear entry by regulating transport across nuclear pores. Cell *171*, 1397–1410.e14.

Ferreira, RR, Fukui, H, Chow, R, Vilfan, A, Vermot, J (Eds.), 2019 Jul. The cilium as a force sensor-myth versus reality. J Cell Sci 30132, jcs213496.

Finetti, F., Paccani, S.R., Riparbelli, M.G., Giacomello, E., Perinetti, G., Pazour, G.J., Rosenbaum, J.L., and Baldari, C.T. (2009). Intraflagellar transport is required for polarized recycling of the TCR/CD3 complex to the immune synapse. Nat. Cell Biol. *11*, 1332–1339.

Follit, J.A., Tuft, R.A., Fogarty, K.E., and Pazour, G.J. (2006). The intraflagellar transport protein IFT20 is associated with the Golgi complex and is required for cilia assembly. Mol. Biol. Cell *17*, 3781–3792.

Frank, V., Habbig, S., Bartram, M.P., Eisenberger, T., Veenstra-Knol, H.E., Decker, C., Boorsma, R.A.C., Göbel, H., Nürnberg, G., Griessmann, A., et al. (2013). Mutations in NEK8 link multiple organ dysplasia with altered Hippo signalling and increased c-MYC expression. Hum. Mol. Genet. *22*, 2177–2185.

Fukui, H., Miyazaki, T., Chow, R.W.-Y., Ishikawa, H., Nakajima, H., Vermot, J., and Mochizuki, N. (2018). Hippo signaling determines the number of venous pole cells that originate from the anterior lateral plate mesoderm in zebrafish. eLife *7*, e29106.

Galgano, D., Onnis, A., Pappalardo, E., Galvagni, F., Acuto, O., and Baldari, C.T. (2017). The T cell IFT20 interactome reveals new players in immune synapse assembly. J. Cell Sci. *130*, 1110–1121.

González-Rosa, J.M., Peralta, M., and Mercader, N. (2012). Pan-epicardial lineage tracing reveals that epicardium derived cells give rise to myofibroblasts and perivascular cells during zebrafish heart regeneration. Dev. Biol. *370*, 173–186.

Grampa, V., Delous, M., Zaidan, M., Odye, G., Thomas, S., Elkhartoufi, N., Filhol, E., Niel, O., Silbermann, F., Lebreton, C., et al. (2016). Novel NEK8 mutations cause severe syndromic renal cystic dysplasia through YAP dysregulation. PLoS Genet. *12*, e1005894.

Habbig, S., Bartram, M.P., Sägmüller, J.G., Griessmann, A., Franke, M., Müller, R.-U., Schwarz, R., Hoehne, M., Bergmann, C., Tessmer, C., et al. (2012). The ciliopathy disease protein NPHP9 promotes nuclear delivery and activation of the oncogenic transcriptional regulator TAZ. Hum. Mol. Genet. *21*, 5528–5538.

Haycraft, C.J., Zhang, Q., Song, B., Jackson, W.S., Detloff, P.J., Serra, R., and Yoder, B.K. (2007). Intraflagellar transport is essential for endochondral bone formation. Development *134*, 307–316.

He, M., Subramanian, R., Bangs, F., Omelchenko, T., Liem, K.F., Jr., Kapoor, T.M., and Anderson, K.V. (2014). The kinesin-4 protein Kif7 regulates mammalian Hedgehog signalling by organizing the cilium tip compartment. Nat. Cell Biol. *16*, 663–672.

Holland, A.J., Fachinetti, D., Han, J.S., and Cleveland, D.W. (2012). Inducible, reversible system for the rapid and complete degradation of proteins in mammalian cells. Proc. Natl. Acad. Sci. USA *109*, E3350–E3357.

Hua, K., and Ferland, R.J. (2018). Primary cilia proteins: ciliary and extraciliary sites and functions. Cell. Mol. Life Sci. *75*, 1521–1540.

Huang, P., and Schier, A.F. (2009). Dampened Hedgehog signaling but normal Wnt signaling in zebrafish without cilia. Development *136*, 3089–3098.

Ishii, Y., Garriock, R.J., Navetta, A.M., Coughlin, L.E., and Mikawa, T. (2010). BMP signals promote proepicardial protrusion necessary for recruitment of coronary vessel and epicardial progenitors to the heart. Dev. Cell *19*, 307–316.

Jonassen, J.A., San Agustin, J., Follit, J.A., and Pazour, G.J. (2008). Deletion of IFT20 in the mouse kidney causes misorientation of the mitotic spindle and cystic kidney disease. J. Cell Biol. *183*, 377–384.

Katz, T.C., Singh, M.K., Degenhardt, K., Rivera-Feliciano, J., Johnson, R.L., Epstein, J.A., and Tabin, C.J. (2012). Distinct compartments of the proepicardial organ give rise to coronary vascular endothelial cells. Dev. Cell *22*, 639–650.

Kikuchi, K., and Poss, K.D. (2012). Cardiac regenerative capacity and mechanisms. Annu. Rev. Cell Dev. Biol. *28*, 719–741.

Kikuchi, K., Gupta, V., Wang, J., Holdway, J.E., Wills, A.A., Fang, Y., and Poss, K.D. (2011). tcf21^{+} epicardial cells adopt non-myocardial fates during zebrafish heart development and regeneration. Development *138*, 2895–2902.

Kim, H.R., Richardson, J., van Eeden, F., and Ingham, P.W. (2010). Gli2a protein localization reveals a role for Iguana/DZIP1 in primary ciliogenesis and a dependence of Hedgehog signal transduction on primary cilia in the zebrafish. BMC Biol. *8*, 65.

Kim, M., Kim, M., Lee, M.-S., Kim, C.-H., and Lim, D.-S. (2014). The MST1/2-SAV1 complex of the Hippo pathway promotes ciliogenesis. Nat. Commun. *5*, 5370.

Klena, N., Gabriel, G., Liu, X., Yagi, H., Li, Y., Chen, Y., Zahid, M., Tobita, K., Leatherbury, L., Pazour, G., and Lo, C.W. (2016). Role of cilia and left-right patterning in congenital heart disease. Etiology and Morphogenesis of Congenital Heart Disease: From Gene Function and Cellular Interaction to Morphology (Springer), p. 1.

Lai, J.K.H., Collins, M.M., Uribe, V., Jiménez-Amilburu, V., Günther, S., Maischein, H.-M., and Stainier, D.Y.R. (2018). The Hippo pathway effector Wwtr1 regulates cardiac wall maturation in zebrafish. Development *145*, dev159210.

Lallemand, Y., Luria, V., Haffner-Krausz, R., and Lonai, P. (1998). Maternally expressed PGK-Cre transgene as a tool for early and uniform activation of the Cre site-specific recombinase. Transgenic Res. *7*, 105–112.

Lancaster, M.A., Schroth, J., and Gleeson, J.G. (2011). Subcellular spatial regulation of canonical Wnt signalling at the primary cilium. Nat. Cell Biol. *13*, 700–707.

Leach, J.P., Heallen, T., Zhang, M., Rahmani, M., Morikawa, Y., Hill, M.C., Segura, A., Willerson, J.T., and Martin, J.F. (2017). Hippo pathway deficiency reverses systolic heart failure after infarction. Nature *550*, 260–264.

Li, Y., Klena, N.T., Gabriel, G.C., Liu, X., Kim, A.J., Lemke, K., Chen, Y., Chatterjee, B., Devine, W., Damerla, R.R., et al. (2015). Global genetic analysis in mice unveils central role for cilia in congenital heart disease. Nature *521*, 520–524.

Limana, F., Capogrossi, M.C., and Germani, A. (2011). The epicardium in cardiac repair: from the stem cell view. Pharmacol. Ther. *129*, 82–96.

Liu, J., and Stainier, D.Y.R. (2010). Tbx5 and Bmp signaling are essential for proepicardium specification in zebrafish. Circ. Res. *106*, 1818–1828.

Liu-Chittenden, Y., Huang, B., Shim, J.S., Chen, Q., Lee, S.-J., Anders, R.A., Liu, J.O., and Pan, D. (2012). Genetic and pharmacological disruption of the TEAD-YAP complex suppresses the oncogenic activity of YAP. Genes Dev. *26*, 1300–1305.

Männer, J., Schlueter, J., and Brand, T. (2005). Experimental analyses of the function of the proepicardium using a new microsurgical procedure to induce loss-of-proepicardial-function in chick embryos. Dev. Dyn. *233*, 1454–1463.

Miesfeld, J.B., and Link, B.A. (2014). Establishment of transgenic lines to monitor and manipulate Yap/Taz-Tead activity in zebrafish reveals both evolutionarily conserved and divergent functions of the Hippo pathway. Mech. Dev. *133*, 177–188.

Miesfeld, J.B., Gestri, G., Clark, B.S., Flinn, M.A., Poole, R.J., Bader, J.R., Besharse, J.C., Wilson, S.W., and Link, B.A. (2015). Yap and Taz regulate retinal pigment epithelial cell fate. Development *142*, 3021–3032.

Mikawa, T., and Fischman, D.A. (1992). Retroviral analysis of cardiac morphogenesis: discontinuous formation of coronary vessels. Proc. Natl. Acad. Sci. USA *89*, 9504–9508.

Mikawa, T., and Gourdie, R.G. (1996). Pericardial mesoderm generates a population of coronary smooth muscle cells migrating into the heart along with ingrowth of the epicardial organ. Dev. Biol. *174*, 221–232.

Mommersteeg, M.T.M., Domínguez, J.N., Wiese, C., Norden, J., de Gier-de Vries, C., Burch, J.B.E., Kispert, A., Brown, N.A., Moorman, A.F.M., and Christoffels, V.M. (2010). The sinus venosus progenitors separate and diversify from the first and second heart fields early in development. Cardiovasc. Res. *87*, 92–101.

Mönnich, M., Borgeskov, L., Breslin, L., Jakobsen, L., Rogowski, M., Doganli, C., Schrøder, J.M., Mogensen, J.B., Blinkenkjær, L., Harder, L.M., et al. (2018). CEP128 localizes to the subdistal appendages of the mother centriole and regulates TGF-β/BMP signaling at the primary cilium. Cell Rep. *22*, 2584–2592.

Moore, A.W., McInnes, L., Kreidberg, J., Hastie, N.D., and Schedl, A. (1999). YAC complementation shows a requirement for Wt1 in the development of epicardium, adrenal gland and throughout nephrogenesis. Development *126*, 1845–1857.

Nakajima, H., Yamamoto, K., Agarwala, S., Terai, K., Fukui, H., Fukuhara, S., Ando, K., Miyazaki, T., Yokota, Y., Schmelzer, E., et al. (2017). Flow-dependent endothelial YAP regulation contributes to vessel maintenance. Dev. Cell *40*, 523–536.e6.

Ocbina, P.J.R., Eggenschwiler, J.T., Moskowitz, I., and Anderson, K.V. (2011). Complex interactions between genes controlling trafficking in primary cilia. Nat. Genet. *43*, 547–553.

Oh, S.-H., Swiderska-Syn, M., Jewell, M.L., Premont, R.T., and Diehl, A.M. (2018). Liver regeneration requires Yap1-TGFβ-dependent epithelial-mesenchymal transition in hepatocytes. J. Hepatol. *69*, 359–367.

Omori, Y., Zhao, C., Saras, A., Mukhopadhyay, S., Kim, W., Furukawa, T., Sengupta, P., Veraksa, A., and Malicki, J. (2008). Elipsa is an early determinant of ciliogenesis that links the IFT particle to membrane-associated small GTPase Rab8. Nat. Cell Biol. *10*, 437–444.

Pazour, G.J., Dickert, B.L., Vucica, Y., Seeley, E.S., Rosenbaum, J.L., Witman, G.B., and Cole, D.G. (2000). *Chlamydomonas IFT88* and its mouse homologue, polycystic kidney disease gene tg737, are required for assembly of cilia and flagella. J. Cell Biol. *151*, 709–718.

Pei, Z., Bai, Y., and Schmitt, A.P. (2010). PIV5 M protein interaction with host protein angiomotin-like 1. Virology *397*, 155–166.

Peralta, M., Steed, E., Harlepp, S., González-Rosa, J.M., Monduc, F., Ariza-Cosano, A., Cortés, A., Rayón, T., Gómez-Skarmeta, J.-L., Zapata, A., et al. (2013). Heartbeat-driven pericardiac fluid forces contribute to epicardium morphogenesis. Curr. Biol. *23*, 1726–1735.

Piccolo, S., Dupont, S., and Cordenonsi, M. (2014). The biology of YAP/TAZ: hippo signaling and beyond. Physiol. Rev. *94*, 1287–1312.

Ragni, C.V., Diguet, N., Le Garrec, J.-F., Novotova, M., Resende, T.P., Pop, S., Charon, N., Guillemot, L., Kitasato, L., Badouel, C., et al. (2017). Amotl1 mediates sequestration of the Hippo effector Yap1 downstream of Fat4 to restrict heart growth. Nat. Commun. *8*, 14582.

Reiter, J.F., and Leroux, M.R. (2017). Genes and molecular pathways underpinning ciliopathies. Nat. Rev. Mol. Cell Biol. *18*, 533–547.

Robb, L., Mifsud, L., Hartley, L., Biben, C., Copeland, N.G., Gilbert, D.J., Jenkins, N.A., and Harvey, R.P. (1998). epicardin: a novel basic helix-loop-helix transcription factor gene expressed in epicardium, branchial arch myoblasts, and mesenchyme of developing lung, gut, kidney, and gonads. Dev. Dyn. *213*, 105–113.

Robert, A., Margall-Ducos, G., Guidotti, J.-E., Brégerie, O., Celati, C., Bréchot, C., and Desdouets, C. (2007). The intraflagellar transport component IFT88/polaris is a centrosomal protein regulating G1-S transition in non-ciliated cells. J. Cell Sci. *120*, 628–637.

Rosenbaum, J.L., and Witman, G.B. (2002). Intraflagellar transport. Nat. Rev. Mol. Cell Biol. *3*, 813–825.

Rudat, C., Norden, J., Taketo, M.M., and Kispert, A. (2013). Epicardial function of canonical Wnt-, Hedgehog-, Fgfr1/2-, and Pdgfra-signalling. Cardiovasc. Res. *100*, 411–421.

San Agustin, J.T., Klena, N., Granath, K., Panigrahy, A., Stewart, E., Devine, W., Strittmatter, L., Jonassen, J.A., Liu, X., Lo, C.W., and Pazour, G.J. (2016). Genetic link between renal birth defects and congenital heart disease. Nat. Commun. *7*, 11103.

Schindelin, J., Arganda-Carreras, I., Frise, E., Kaynig, V., Longair, M., Pietzsch, T., Preibisch, S., Rueden, C., Saalfeld, S., Schmid, B., et al. (2012). Fiji: an open-source platform for biological-image analysis. Nat. Methods *9*, 676–682.

Schlueter, J., Männer, J., and Brand, T. (2006). BMP is an important regulator of proepicardial identity in the chick embryo. Dev. Biol. *295*, 546–558.

Singh, A., Ramesh, S., Cibi, D.M., Yun, L.S., Li, J., Li, L., Manderfield, L.J., Olson, E.N., Epstein, J.A., and Singh, M.K. (2016). Hippo signaling mediators Yap and Taz are required in the epicardium for coronary vasculature development. Cell Rep. *15*, 1384–1393.

Slough, J., Cooney, L., and Brueckner, M. (2008). Monocilia in the embryonic mouse heart suggest a direct role for cilia in cardiac morphogenesis. Dev. Dyn. *237*, 2304–2314.

Sugimoto, K., Hui, S.P., Sheng, D.Z., and Kikuchi, K. (2017). Dissection of zebrafish *shha* function using site-specific targeting with a Cre-dependent genetic switch. eLife *6*, e24635.

Sun, Z., Amsterdam, A., Pazour, G.J., Cole, D.G., Miller, M.S., and Hopkins, N. (2004). A genetic screen in zebrafish identifies cilia genes as a principal cause of cystic kidney. Development *131*, 4085–4093.

Sun, Y., Yong, K.M.A., Villa-Diaz, L.G., Zhang, X., Chen, W., Philson, R., Weng, S., Xu, H., Krebsbach, P.H., and Fu, J. (2014). Hippo/YAP-mediated rigidity-dependent motor neuron differentiation of human pluripotent stem cells. Nat. Mater. *13*, 599–604.

Taschner, M., Bhogaraju, S., and Lorentzen, E. (2012). Architecture and function of IFT complex proteins in ciliogenesis. Differentiation *83*, S12–S22.

Taulet, N., Vitre, B., Anguille, C., Douanier, A., Rocancourt, M., Taschner, M., Lorentzen, E., Echard, A., and Delaval, B. (2017). IFT proteins spatially control the geometry of cleavage furrow ingression and lumen positioning. Nat. Commun. *8*, 1928.

Taulet, N., Douanier, A., Vitre, B., Anguille, C., Maurin, J., Dromard, Y., Georget, V., and Delaval, B. (2019). IFT88 controls NuMA enrichment at k-fibers minus-ends to facilitate their re-anchoring into mitotic spindles. Sci. Rep. *9*, 10311.

Tay, S.Y., Yu, X., Wong, K.N., Panse, P., Ng, C.P., and Roy, S. (2010). The iguana/DZIP1 protein is a novel component of the ciliogenic pathway essential for axonemal biogenesis. Dev. Dyn. *239*, 527–534.

Thisse, C., and Thisse, B. (2008). High-resolution *in situ* hybridization to whole-mount zebrafish embryos. Nat Protoc *3*, 59–69.

Thompson, B.J., and Sahai, E. (2015). MST kinases in development and disease. J. Cell Biol. *210*, 871–882.

Tsujikawa, M., and Malicki, J. (2004). Intraflagellar transport genes are essential for differentiation and survival of vertebrate sensory neurons. Neuron *42*, 703–716.

van Wijk, B., van den Berg, G., Abu-Issa, R., Barnett, P., van der Velden, S., Schmidt, M., Ruijter, J.M., Kirby, M.L., Moorman, A.F.M., and van den Hoff, M.J.B. (2009). Epicardium and myocardium separate from a common precursor pool by crosstalk between bone morphogenetic protein- and fibroblast growth factor-signaling pathways. Circ. Res. *105*, 431–441.

Vertii, A., Bright, A., Delaval, B., Hehnly, H., and Doxsey, S. (2015). New frontiers: discovering cilia-independent functions of cilia proteins. EMBO Rep. *16*, 1275–1287.

Villalobos, E., Criollo, A., Schiattarella, G.G., Altamirano, F., French, K.M., May, H.I., Jiang, N., Nguyen, N.U.N., Romero, D., Roa, J.C., et al. (2019). Fibroblast primary cilia are required for cardiac fibrosis. Circulation *139*, 2342–2357.

Vion, A.-C., Alt, S., Klaus-Bergmann, A., Szymborska, A., Zheng, T., Perovic, T., Hammoutene, A., Oliveira, M.B., Bartels-Klein, E., Hollfinger, I., et al. (2018). Primary cilia sensitize endothelial cells to BMP and prevent excessive vascular regression. J. Cell Biol. *217*, 1651–1665.

Vitre, B., Taulet, N., Guesdon, A., Douanier, A., Dosdane, A., Cisneros, M., Maurin, J., Hettinger, S., Anguille, C., Taschner, M., et al. (2020). IFT proteins interact with HSET to promote supernumerary centrosome clustering in mitosis. EMBO Rep. *21*, e49234.

Vuong, L.T., Iomini, C., Balmer, S., Esposito, D., Aaronson, S.A., and Mlodzik, M. (2018). Kinesin-2 and IFT-A act as a complex promoting nuclear localization of β-catenin during Wnt signalling. Nat. Commun. *9*, 5304.

Wang, W., Huang, J., and Chen, J. (2011). Angiomotin-like proteins associate with and negatively regulate YAP1. J. Biol. Chem. *286*, 4364–4370.

Wang, W., Li, N., Li, X., Tran, M.K., Han, X., and Chen, J. (2015). Tankyrase inhibitors target YAP by stabilizing angiomotin family proteins. Cell Rep. *13*, 524–532.

Witzel, H.R., Jungblut, B., Choe, C.P., Crump, J.G., Braun, T., and Dobreva, G. (2012). The LIM protein Ajuba restricts the second heart field progenitor pool by regulating Isl1 activity. Dev. Cell *23*, 58–70.

Wu, S.-P., Dong, X.-R., Regan, J.N., Su, C., and Majesky, M.W. (2013). Tbx18 regulates development of the epicardium and coronary vessels. Dev. Biol. *383*, 307–320.

Xin, M., Kim, Y., Sutherland, L.B., Qi, X., McAnally, J., Schwartz, R.J., Richardson, J.A., Bassel-Duby, R., and Olson, E.N. (2011). Regulation of insulin-like growth factor signaling by Yap governs cardiomyocyte proliferation and embryonic heart size. Sci. Signal. *4*, ra70.

Yi, C., Shen, Z., Stemmer-Rachamimov, A., Dawany, N., Troutman, S., Showe, L.C., Liu, Q., Shimono, A., Sudol, M., Holmgren, L., et al. (2013). The p130 isoform of angiomotin is required for Yap-mediated hepatic epithelial cell proliferation and tumorigenesis. Sci. Signal. *6*, ra77.

Yu, F.-X., Zhao, B., and Guan, K.-L. (2015). Hippo pathway in organ size control, tissue homeostasis, and cancer. Cell *163*, 811–828.

Zanconato, F., Cordenonsi, M., and Piccolo, S. (2016). YAP/TAZ at the roots of cancer. Cancer Cell *29*, 783–803.

Zhao, B., Ye, X., Yu, J., Li, L., Li, W., Li, S., Yu, J., Lin, J.D., Wang, C.Y., Chinnaiyan, A.M., et al. (2008). TEAD mediates YAP-dependent gene induction and growth control. Genes Dev. *22*, 1962–1971.

Zhao, B., Li, L., Lu, Q., Wang, L.H., Liu, C.-Y., Lei, Q., and Guan, K.-L. (2011). Angiomotin is a novel Hippo pathway component that inhibits YAP oncoprotein. Genes Dev. *25*, 51–63.

Zheng, Y., Vertuani, S., Nyström, S., Audebert, S., Meijer, I., Tegnebratt, T., Borg, J.-P., Uhlén, P., Majumdar, A., and Holmgren, L. (2009). Angiomotin-like protein 1 controls endothelial polarity and junction stability during sprouting angiogenesis. Circ. Res. *105*, 260–270.

Zhu, X., Liang, Y., Gao, F., and Pan, J. (2017). IFT54 regulates IFT20 stability but is not essential for tubulin transport during ciliogenesis. Cell. Mol. Life Sci. *74*, 3425–3437.

STAR★METHODS

KEY RESOURCES TABLE

REAGENT or RESOURCE	SOURCE	IDENTIFIER
Antibodies		
anti-myosin heavy chain	DSHB	Cat. # MF20; RRID:AB_2147781
anti-GFP	AVES	Cat. # GFP 1020; RRID:AB_10000240
anti-phospho-Smad 1/5 (Ser463/465)	Cell signaling	Cat. # 9516S; RRID:AB_491015
anti-phospho- Smad1/5/9	Cell signaling	Cat. #13820; RRID:AB_2493181
anti-Tbx18	Santa Cruz	Cat. # sc-17869; RRID:AB_2200374
anti-Yap1	Santa Cruz	Cat. # sc-101199; RRID:AB_1131430
anti-Yap1	Lecaudey laboratory	N/A
anti-Wt1	Santa Cruz	Cat. # sc-192; RRID:AB_632611
anti- Amotl1	Sigma	Cat. # HPA001196; RRID:AB_1078147
anti-γ-tubulin	Santa Cruz	Cat. # sc-17787; RRID:AB_628417
anti-α-tubulin	Sigma	Cat. # T6199; RRID:AB_477583
anti-IFT88	Euromedex	Cat. # 13967-1-AP; RRID:AB_2121979
anti-Islet1	Genetex	Cat. # GTX128201; RRID:AB_11179180
anti-Yap1	Cell signaling	Cat. # 4912; RRID:AB_2218911
anti-Yap/Taz	Cell signaling	Cat. # D24E4; RRID:AB_2799044
goat anti-chicken Alexa Fluor 488 IgY (H+L)	Invitrogen	Cat. # A-11039; RRID:AB_142924
goat anti-mouse IgG Cy3 conjugate (H+L)	Life technologies	Cat. # M30010; RRID:AB_2536619
goat anti-rabbit Alexa Fluor 647	ThermoFisher	Cat. # A-21244; RRID:AB_2535812
4′,6-diamidino-2-phenylindole (DAPI)	Invitrogen	Cat. # D1306; RRID:AB_2629482
anti-GFP	ThermoFisher	Cat. # CAB421; RRID AB_10709851
anti-FLAG	Sigma	Cat. # F7425; RRID:AB_439687
anti-Ift20	Proteintech	Cat. # 13615-1-AP; RRID:AB_2280001
anti-GFP	Abcam	Cat. # ab290; RRID:AB_303395
anti-HA	Roche	Cat. # 11867423001; RRID:AB_390918
Chemicals, Peptides, and Recombinant Proteins		
1-phenyl-2-thiourea (PTU)	Sigma-Aldrich	Cat. # P7629
Tricaine/MS-222	Sigma-Aldrich	Cat. # A-5040
UltraPure™ Low Melting Point Agarose	Invitrogen	Cat. # 16520-050
Verteporfin	Sigma-Aldrich	Cat. # SML0534
XAV939	Tocris Bioscience	Cat. # 3748
Phosphate buffered saline (PBS)	Sigma-Aldrich	Cat. # P4417
Indole-3-acetic acid sodium salt (Heteroauxin)	Sigma-Aldrich	Cat. # I5148
Lipofectamine® 2000 Transfection Reagent	ThermoFisher SCIENTIFIC	Cat. # 11668030
cOmpleteTM Protease Inhibitor Cocktail	Roche	Cat. # 11697498001
Opti-MEM	GIBCO	Cat. # 51985-026
Oligofectamine	Invitrogen	Cat. # 12252-01
Hoechst	ThermoFisher	Cat. # 62249
Experimental Models: Cell Lines		
HEK293 cells	Q-BIOgene	AES0503
MDCK cells	Sumara laboratory	N/A
HeLa cells	Sumara laboratory	N/A
DLD-1 IFT88-AID	Vitre et al., 2020	N/A

(Continued on next page)

Continued

REAGENT or RESOURCE	SOURCE	IDENTIFIER
Experimental Models: Organisms/Strains		
Zebrafish: *Et(−26.5Hsa.WT1-1gata2:EGFP)^{cn1}* (*epi:GFP*)	Peralta et al., 2013	ZFIN ID: ZDB-ALT-170823-7
Zebrafish: *iguana^{ts294e}*	Tay et al., 2010	ZFIN ID: ZDB-FISH-150901-16040
Zebrafish: *ift88 $^{tz288/ovaI}$*	Tsujikawa and Malicki, 2004	ZFIN ID: ZDB-ALT-980413-526
Zebrafish: *elipsa ^{tp49d}*	Omori et al., 2008	ZFIN ID: ZDB-ALT-980413-466
Zebrafish: *yap1 ^{fu48}*	Agarwala et al., 2015	ZFIN ID: ZDB-ALT-160413-4
Zebrafish: *amotl2a ^{fu46}*	Agarwala et al., 2015	ZFIN ID: ZDB-ALT-160412-2
Zebrafish: *4xGTIIC:d2GFP*	Miesfeld and Link, 2014	ZFIN ID: ZDB-ALT-150928-6
Zebrafish: *actb2:Mmu.Arl13b-GFP*	Borovina et al., 2010	ZFIN ID: ZDB-ALT-100721-1
Zebrafish: *tcf21:NLS-EGFP*	Kikuchi et al., 2011	ZFIN ID: ZDB-ALT-110914-2
Mice: *Ift20$^{null/+}$* (*C57BL* background)	Jonassen et al., 2008	MGI: 12565
Mice: PGK-Cre	Lallemand et al., 1998	PMID: 9608738
Mice: *Ift88$^{null/+}$* (*6JRj* background)	Haycraft et al., 2007	MGI:5505911
Oligonucleotides		
siRNA ON-Target plus - Control pool Non-targeting	Dharmacon	D-001810-10-05
siRNA ON-Target plus - SMART pool human IFT88	Dharmacon	L-012281-01
Recombinant DNA		
Flag-Amotl1	Pei et al., 2010	N/A
Ift20-GFP	Follit et al., 2006	N/A
YAP1-Myc	Boin et al., 2014	N/A
pEGFP-C1	Ragni et al., 2017	N/A
HA-Amotl1	Ragni et al., 2017	N/A
IFT88-GFP	He et al., 2014	N/A
Software and Algorithms		
FIJI	Schindelin et al., 2012	RRID:SCR_002285
Imaris	Bitplane	RRID: SCR_007370
MATLAB	MathWorks	RRID: SCR_001622
Microsoft Excel	Microsoft	RRID: SCR_016137
GraphPad Prism 7	GraphPad Software	RRID: SCR_002798
Other		
GFP-Trap	ChromoTek	Cat. # gta-10
anti-FLAG M2 Affinity gel	Sigma	Cat. # A2220

RESOURCE AVAILABILITY

Lead Contact

Further information and requests for reagents may be directed to and will be fulfilled by the Lead Contact, Julien Vermot (jvermot@imperial.ac.uk).

Materials Availability

This study did not generate new unique reagents.

Data and Code Availability

This study did not generate any unique datasets or code.

EXPERIMENTAL MODEL AND SUBJECT DETAILS

Zebrafish (ZF) Models

Animal experiments were approved by the Animal Experimentation Committee of the Institutional Review Board of the IGBMC. ZF lines used in the study were *Et(−26.5Hsa.WT1-1gata2:EGFP)*^{cn1} transgenic line (referred to as *epi:GFP*) (Peralta et al., 2013), *amotl2a* ^{fu46} (Agarwala et al., 2015), *elipsa* ^{tp49d} (Omori et al., 2008), *ift88* $^{tz288/oval}$ (Tsujikawa and Malicki, 2004), *iguana* ^{ts294e} (Tay et al., 2010), *yap1* ^{fu48} (Agarwala et al., 2015), *4xGTIIC:d2GFP* (Miesfeld and Link, 2014), *actb2:Mmu.Arl13b-GFP* (Borovina et al., 2010) and *tcf21:NLS-EGFP* (Kikuchi et al., 2011). Male and female samples were mixed. All animals were incubated at 28.5°C for 24h before treatment with 1-phenyl-2-thiourea (PTU) (Sigma Aldrich) to prevent pigment formation.

Mouse Models

Ift20$^{flox/+}$ (Jonassen et al., 2008) were crossed to PGK-Cre mice (Lallemand et al., 1998) to generate *Ift20*$^{null/+}$ maintained on a C57BL/6JRj genetic background. *Ift88*$^{null/+}$ (Haycraft et al., 2007) mice were maintained on a B6D2 genetic background. Animal procedures were approved by the ethical committee of the Institut Pasteur and the French Ministry of Research. E9.5 embryos were isolated in 200ng/ml cold heparin, incubated in cold 250mM KCl and fixed in 4% paraformaldehyde in PBS inside a rotative oven at 37°C overnight to remove excess of blood. Male and female samples were mixed.

METHOD DETAILS

In Vivo Imaging

ZF embryos were staged, anaesthetized with 0.02% tricaine solution and mounted in 0.7% low melting-point agarose (Sigma Aldrich). Confocal imaging was performed on a Leica SP8 confocal microscope. Images were acquired bidirectionally with a low-magnification water immersion objective (Leica HCX IRAPO L, 25X, N.A. 0.95). For time lapse, z stacks were acquired each 15 or 30 min, depending on the experiment. The optical plane was moved 15 μm between z sections.

Bright field experiments were performed on a Leica DMIRBE inverted microscope using a Photron SA3 high speed CMOS camera (Photron, San Diego, CA) and water immersion objective (Leica 20X, NA 0.7). Image sequences were acquired at a frame rate of 150 frames per second.

ZF Treatments

Verteporfin (5 μM) (Sigma Aldrich) and XAV939 (10 μM) were diluted in fish tank water with 0.0033% PTU, in which larvae were incubated in darkness at 28.5°C for the required time.

ZF Immunofluorescence

Embryos were fixed at the desired stages in 4% paraformaldehyde (PFA) overnight at 4°C. After washing in 0.1% PBS Tween 20, embryos were permeabilized in 0.5% PBS Triton X-100 for 20 min at room temperature (RT). Samples were washed and then blocked (3% albumin from bovine serum (BSA), 5% goat serum, 20 mM MgCl2, 0.3% Tween 20 in PBS) during 2h at RT. Primary antibodies were added in the blocking solution and incubated overnight at 4°C. Secondary antibodies were added in 0.1% PBS Tween20 after thorough washing and incubated overnight at 4°C. Embryos were washed and incubated with DAPI (Invitrogen), 1:1000, for 15 min at RT. After being thoroughly washed, samples were mounted for imaging on a Leica SP8 confocal with a dipping immersion objective (Leica HCX IRAPO L, 25X, N.A. 0.95). Z stacks were taken every 10 μm. 3D images were reconstructed using IMARIS software (Bitplane Scientific Software). The ventral pericardium was digitally removed to provide a clearer view of the heart.

Antibodies used were as follows: anti-myosin heavy chain (MF20, DSHB) 1:20, anti-GFP (AVES) 1:500, anti-phospho-Smad 1/5 (Ser463/465) (Cell signaling) 1:50, anti-Islet1 (Genetex) 1:100, anti-Yap1 (Lecaudey laboratory) 1:200. Secondary antibodies: goat anti-chicken Alexa Fluor 488 IgY (H+L) (*In vitro*gen), goat anti-mouse IgG Cy3 conjugate (H+L) (Life technologies) and goat anti-rabbit Alexa Fluor 647 (ThermoFisher) were used at 1:500.

To test the effects of Verteporfin treatment, embryos were rinsed in fish tank water before being fixed and processed as described above.

In Situ Hybridization (ISH)

ISH was performed in whole embryos according to Thisse and Thisse, 2008, with minor modifications. Antisense mRNA probe used was against full coding sequence of *bmp4*. To test the effects of Verteporfin and XAV939 treatments, embryos were rinsed in fish tank water before being fixed and processed as described above.

Whole Mount Immunofluorescence in the Mouse

Embryos were fixed in paraformaldehyde. The cardiac region was dissected, permeabilized in 0.75% Triton. Aldehydes were quenched with 2.6mg/ml NH4Cl. Immunostaining was performed in 10% inactivated horse serum, 0.5% Triton with a primary antibody against Wt1 (Santa Cruz sc-192, 1:50), and with Alexa Fluor conjugated secondary antibodies (1:300) and counterstained with Hoechst (1:400). 80% glycerol was used to make the samples transparent.

Immunofluorescence on Cryosections in the Mouse

Embryos were embedded in 7% gelatin, 15% sucrose, frozen in cold isopentane and sectioned on a cryostat (10 μm). Immunostaining was performed on cryosections as described above, with permeabilization in 0.5% Triton, and with an additional incubation in 0.2 mg/mL goat anti-mouse IgG Fab fragment to reduce non-specific reactivity of antibodies raised in the mouse. Primary antibodies against Tbx18 (Santa Cruz sc-17869, 1:100), Wt1 (Santa Cruz sc-192, 1:50), Yap1 (Santa Cruz sc-101199, 1:100), Amotl1 (Sigma HPA001196, 1:50) and p-Smad1/5/9 (Cell signaling 13820, 1:250) were used, with Alexa Fluor conjugated secondary antibodies (1:500) and Hoechst nuclear counterstaining (1:1000). Samples were imaged in DAKO mounting medium on a LSM700 (Zeiss) confocal microscope with a 40X/1.3 objective. Z stacks were taken every 0.9 μm.

Cell Culture, siRNAs and Transfection

Cells were cultured in appropriate conditions: MDCK (MEM Eagle - Earle's BSS, 10% FCS, AANE 0.1 mM, Sodium Pyruvate 1mM, Gentamicin 40 μg/ml), HeLa (DMEM 4.5 g/l glucose, 10% FCS, Penicillin 100 UI/ml, Streptomycin 100 μg/ml), HEK293 cells (DMEM 1g/L glucose, FCS 10%, Penicillin 100 UI/ml, Streptomycin 100 μg/ml) and DLD-1 (DMEM 4.5 g/l glucose, 10% FCS, Penicillin 100 UI/ml, Streptomycin 100 μg/ml). siRNA (Dharmacon) ON-Target plus - Control pool Non-targeting (D-001810-10-05) and SMART pool human IFT88 (L-012281-01) were used at 50 nM working concentration. Cells were transfected 16h after splitting using Opti-MEM medium and Oligofectamine reagent.

Generation of DLD-1 IFT88-AID Targeted Cells

DLD-1 IFT88-AID cells were generated by adding an AID tag followed by a YFP tag at the 3′ end of the last exon on the IFT88 genomic locus. In detail, a clonal population of DLD-1 cells stably expressing TIR1-9xMyc protein was used for targeting (Holland et al., 2012). sgRNA targeting two regions adjacent to the 3′ end of IFT88 gene were introduced under the control of U6 transcription promoter into two separate vectors encoding for the expression of the Cas9 nickase (D10A) (Cong et al., 2013) (addgene 42335). A donor construct containing ≈600 bp recombination arms surrounding the 3′ end of IFT88 locus, in frame with a sequence encoding for an AID-YFP-Stop sequence, was generated. All three vectors were transfected into DLD-1 TIR1 cells using Xtreme Gene 9 DNA transfection reagent (Roche). Cells were sorted based on their YFP fluorescence and single clones were isolated. Homozygous targeted clones were identified by PCR. Targeting of IFT88 and degradation of IFT88-AID-YFP was confirmed by immunoblot following addition of Auxin (Sigma-Aldrich) at 500 μM in the culture medium for the indicated times.

Immunofluorescence on Cells

Cells were fixed in 100% MeOH for 6 min at −20°C (Ift88 and γ-tubulin antibodies), in 4% PFA for 7 min at RT (DLD-1 cells. Yap1 antibody) or in PFA 4% for 17 min at RT (MDCK and HeLa cells. Yap/Taz antibody). After washing in 0.1% PBS Tween20, cells were permeabilized in 0.5% PBS-NP40 and blocked in 5% BSA 1h at RT. Primary antibodies were added in the blocking solution and incubated overnight at 4°C. Secondary antibodies were added in 0.1% PBS Tween20 after washing and incubated for 2h at RT. Then cells were incubated with DAPI (Invitrogen), 1:1000, for 15 min at RT. After being thoroughly washed, samples were mounted for imaging on a Leica SP5 (siRNA experiments) or SP8 (DLD-1 experiments and experiments to assess subcellular localization) confocal microscope with an oil immersion objective (Leica HCX PL APO lambda blue, 63X, N.A. 1.4). Z stacks were taken every 1 μm.

Antibodies used were as follows: anti-γ-tubulin (Santa Cruz) 1:500, anti-α-tubulin (Sigma, 1:2000), anti-IFT88 (Euromedex) 1:50, anti-Yap1 (4912) (Cell signaling) 1:50 (DLD-1 experiments), and anti-Yap/Taz (D24E4) (Cell signaling) 1:50 (MDCK and HeLa siRNA experiments). Secondary antibodies: goat anti-mouse IgG Cy3 conjugate (H+L) (Life technologies) and goat anti-rabbit Alexa Fluor 647 (*In vitro*gen) were used at 1:500.

Lysates and Immunoblotting

DLD-1 cell extracts were obtained after lysis with Laemmli sample buffer of an equal number of cells for each sample. Proteins were resolved by SDS-PAGE, transferred to nitrocellulose membranes and revealed by immunoblot using Western Lightning Plus-ECL kit (PerkinElmer).

IMMUNOPRECIPITATION (IP) ASSAYS

HEK293 Cells

HEK293 cells (Q-BIOgene AES0503) were co-transfected with plasmids Flag-Amotl1 (Pei et al., 2010) and Ift20-GFP (Follit et al., 2006), or a Flag-control plasmid using Lipofectamine® 2000 Transfection Reagent (ThermoFisher SCIENTIFIC) and cultured for 48h. Proteins were extracted in a lysis buffer (10mMTris-Cl pH 7.5, 5mM EDTA, 150mM NaCl, 10% glycerol and 5% CHAPS) in the presence of protease inhibitors (cOmpleteTM Protease Inhibitor Cocktail, Roche). Immunoprecipitation of protein extracts was performed using a monoclonal anti-Flag antibody covalently attached to agarose (Anti-FLAG M2 Affinity gel, Sigma). Proteins were eluted in 2xNuPAGE LDS Sample Buffer (ThermoFisher). Proteins were separated on SDS–polyacrylamide gel electrophoresis and transferred to a nitrocellulose membrane. Proteins were detected with the primary antibodies against Flag (1:1000, Sigma

F7425), GFP (1:1000, ThermoFisher CAB421), Ift20 (1:500, Proteintech, 13615-1-AP), Yap1 (1:1000, Cell Signaling 4912S) and Amotl1 (1:1000, Sigma HPA001196), followed by HRP-conjugated secondary antibodies (1:5000, Jackson ImmunoResearch) and the ECL detection reagent.

HeLa Cells

We performed IPs using GFP-Trap (ChromoTek) agarose beads in two conditions: Control IP (YAP1-Myc (Boin et al., 2014), pEGFP-C1 and HA-Amotl1 (Ragni et al., 2017)) and IFT88 IP (YAP1-Myc, IFT88-GFP (He et al., 2014) and HA-Amotl1). HeLa cells (2x 10cm dish/ condition) were transfected with Lipofectamine 2000. Experiments were performed using the following setup: Cells were seeded at high density into 10cm dishes and transfected 16 hr after seeding at 95% confluency. Twenty-four hours post-transfection, cells were seeded into 15cm dishes in order to achieve culture of isolated cells (10x 15cm dish/ condition). Proteins were extracted 60 hr post-transfection in a lysis buffer (10mM TrisHCl, pH7.5; 150mM NaCl; 0.5mM EDTA; 0.5% NP-40; protease inhibitors Complete). GFP beads were washed once in lysis buffer and incubated with 16 mg of the protein lysate for 16 hr at 4°C. Beads were washed four times in buffer without detergent and proteins were eluted by boiling for 10 mins. The input (1%) and IP were analyzed using immunoblot and the membranes were probed with anti-GFP (Abcam), anti-Yap/TAZ (D24E4, Cell Signaling) and anti-HA (Sigma Aldrich) antibodies.

ZF avcPE Cell Quantification

We performed whole-mount immunofluorescent staining on control and mutant embryos in the *epi:GFP* reporter line background and imaged the heart using a confocal microscope with a z-step of 10 μm. The different tissues were labeled using anti-myosin heavy chain (MHC) (myocardium) and anti-GFP (*epi:GFP*) antibodies, and DAPI dye to stain for nuclei. We then manually quantified the number of avcPE cells per z slice. We identified the avcPE clusters anatomically: avcPE clusters form in the dorsal pericardium, close to the atrio-ventricular canal (avc). PE cells were identified by their rounded morphology in conjunction with their expression of GFP (although some pericardial cells are also GFP-positive, they can be excluded due to their flat morphology). In order to count each cell only once in the z stack, we only counted a cell when its nucleus was visible.

ZF Myocardial Cell Quantification

We performed whole-mount immunofluorescent staining on control and mutant embryos using anti-myosin heavy chain (MHC) (myocardium) antibody and DAPI dye (nuclei). We imaged the heart using a confocal microscope with a z-step of 10 μm. We then manually quantified the number of myocardial cells per z slice (nuclei surrounded by MHC signal).

Mice PE Volume Analysis

Whole mount embryos stained with Wt1 antibody (Santa Cruz) were scanned on TCS SP8 DLS (Digital Light Sheet) Leica with a water immersion objective (HC APO L, 10X, 0.3). Z stacks were taken every 2 μm. Both, coronal and sagittal views were acquired, if possible, for a more precise analysis (Figure S2F). Using MATLAB software, the contour of the PE was manually drawn (Wt1 signal) for each z plane and the area (A) was calculated. Volume (V) was estimated as:

$$V = \Sigma zn\ Ai \times dz\ ;\ i = 1\ ;\ zn = \text{number of planes};\ dz = 2\ \mu m$$

We performed a double-blind quantitative analysis. 3D images were reconstructed using IMARIS software (Bitplane Scientific Software).

Mice Yap1- and Amotl1-Positive Cell Quantifications

Nuclei positions on the slides were defined using IMARIS (Bitplane Scientific Software) Spots detection function. The results were manually corrected if needed. Nuclei positions were exported from Imaris and imported to MATLAB. Each cell was assigned a unique index. The intensity of Tbx18 signal was evaluated in correspondence with the nuclei positions. Cells where the intensity was found higher than a threshold were considered positive. The threshold was established according to the background noise intensity. Results were manually corrected if needed and Tbx18-positive cells were automatically counted. Yap1 signal was visualized in fire LUT to facilitate perception of signal intensity. Nuclear Yap1-positive cells (higher signal in the nucleus than in the cytoplasm) were manually defined through index identification of cells and counted automatically. The same procedure was followed for Amotl1 signal. The outline of the outer PE region was manually drawn and areas of the two regions were calculated automatically. MATLAB provided the total positive cell number for each signal and area, including signal co-localization. We performed a double-blind quantitative analysis.

Nuclear Yap Quantifications on Cells

Analyses were performed using Fiji (Schindelin et al., 2012). Nuclei areas were selected manually using DAPI signal as reference on z-projection images (sum slices for DLD-1 experiment and maximum intensity projection for siRNA experiments). Yap average nuclear signal intensity was measured for the selected areas. In experiments in DLD-1 cells the values were measured for each individual nucleus, while in the case of siRNA experiments, all the nuclei in a slice were measured together. Values were normalized to their controls in order to merge data from different experiments.

Nuclear/cytoplasmic Yap1 Ratio

Analyses were performed using Fiji. Nuclei areas were selected manually using DAPI signal as reference on z-projection images (sum slices). Cytoplasmic areas were selected using α-tubulin signal as reference. Yap average nuclear signal intensity was measured for the nuclear ROI. Yap average cytoplasmic signal intensity was measured after subtracting nuclear ROI from the cytoplasmic ROI.

QUANTIFICATION AND STATISTICAL ANALYSIS

We applied D'Agostino & Pearson and Shapiro-Wilk normality tests to assess whether the samples fit a normal distribution and F test to compare variances. For normal distributed and homoscedastic samples, we used t test or ANOVA. For non-parametric samples, we applied Man-Whitney or Kruskal-Wallis. The pertinent statistical analyses for each experiment were performed using GraphPad Prism 7 software. For the analysis of nuclear p-smad 1/5/9 and YAP1 signal in mice we used the non-parametric Chi-square test of homogeneity to test whether the observed frequency of positive nuclei was equally distributed across the *wild-type* and mutant embryos. In each figure legend is stated the number of embryos (n), as well as the meaning of error bars and p values.

Cell Reports, Volume *32*

Supplemental Information

Intraflagellar Transport Complex B Proteins Regulate the Hippo Effector Yap1 during Cardiogenesis

Marina Peralta, Laia Ortiz Lopez, Katerina Jerabkova, Tommaso Lucchesi, Benjamin Vitre, Dong Han, Laurent Guillemot, Chaitanya Dingare, Izabela Sumara, Nadia Mercader, Virginie Lecaudey, Benedicte Delaval, Sigolène M. Meilhac, and Julien Vermot

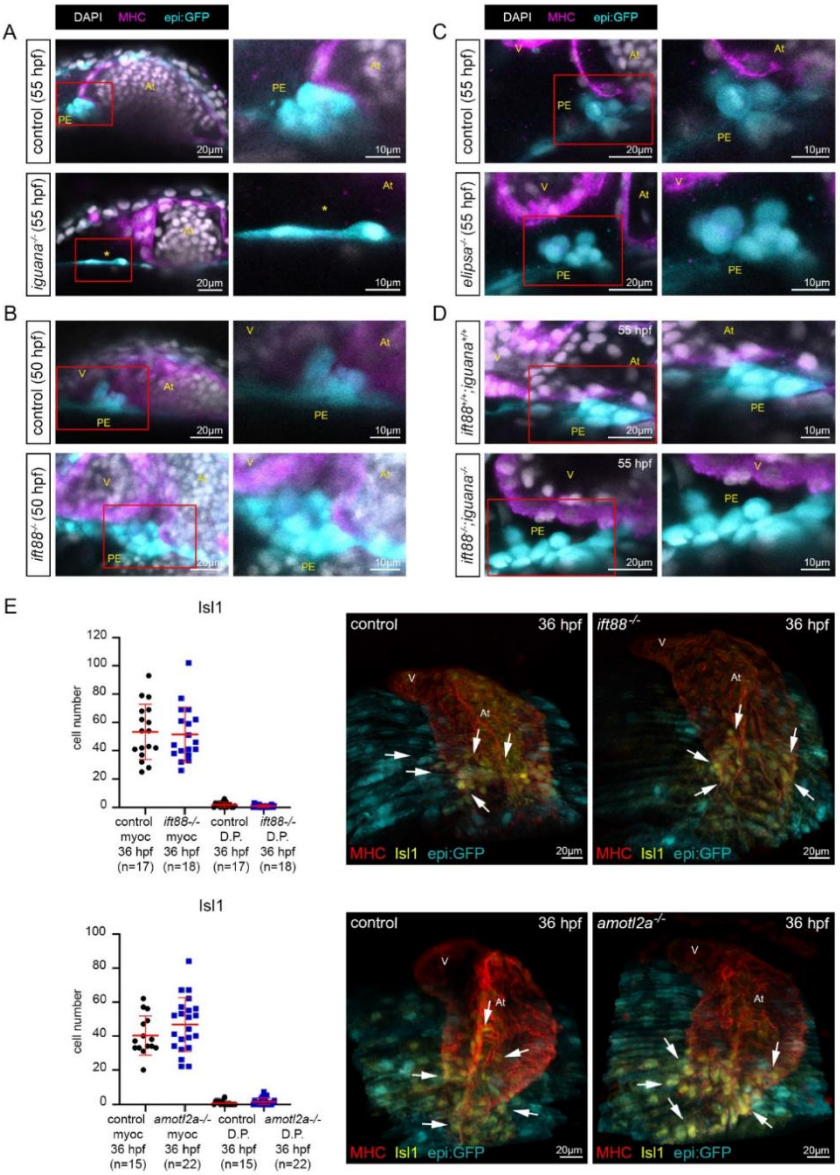
A
DAPI MHC epi:GFP
control (55 hpf)
iguana-/- (55 hpf)
B
control (50 hpf)
ift88-/- (50 hpf)
C
elipsa-/- (55 hpf)
D
ift88+/+;iguana+/+
ift88-/-;iguana-/-
55 hpf
E
Isl1
cell number
control myoc 36 hpf (n=17)
ift88-/- myoc 36 hpf (n=18)
control D.P. 36 hpf (n=17)
ift88-/- D.P. 36 hpf (n=18)
amotl2a-/- myoc 36 hpf (n=22)
amotl2a-/- D.P. 36 hpf (n=22)
control myoc 36 hpf (n=15)
control 36 hpf
ift88-/- 36 hpf
amotl2a-/- 36 hpf
MHC Isl1 epi:GFP
V
At
PE
20μm
10μm

Figure S1. IFT complex B mutants show increased proepicardial size without affecting Islet1 cell number in zebrafish. Related to Figures 1 and 2.

(A-D) *Confocal sections of whole mount immunofluorescence (IF) of iguana$^{-/-}$, epi:GFP* ***(A)****, ift88$^{-/-}$, epi:GFP* ***(B)****, elipsa$^{-/-}$, epi:GFP* ***(C)*** *and ift88$^{-/-}$, iguana$^{-/-}$, epi:GFP* ***(D)*** *and their controls using anti-myosin heavy chain antibody (MHC) (magenta), anti-GFP (cyan) and DAPI (white) antibodies. Asterisk shows lack of avcPE as there is only one rounded PE cell. Zoomed regions contained inside the red boxes are showed on the right side.* ***(E)*** *The top graph shows number of Isl1-positive cells in the myocardium and dorsal pericardium (D.P.) quantified in ift88-/-, epi:GFP (n=18) and control (n=17) embryos at 36 hpf (t-test myocardium p value 0.785 and Mann Whitney test D.P. p value 0.216). Bottom graph shows number of Isl1-positive cells in the myocardium and D.P. quantified in amotl2a-/-, epi:GFP (n=15) and control (n=22) embryos at 36 hpf (t-test myocardium p value 0.188 and Mann Whitney test D.P. p value 0.167). In all graphs, red bars indicate mean ± standard deviation. 3D projections of whole mount IF of hearts using MHC (red), epi:GFP (cyan) and Isl1 (yellow) antibody. White arrows mark Isl –positive cells. All images are ventral views, anterior is to the top. V, ventricle; At, atrium; PE, avcPE.*

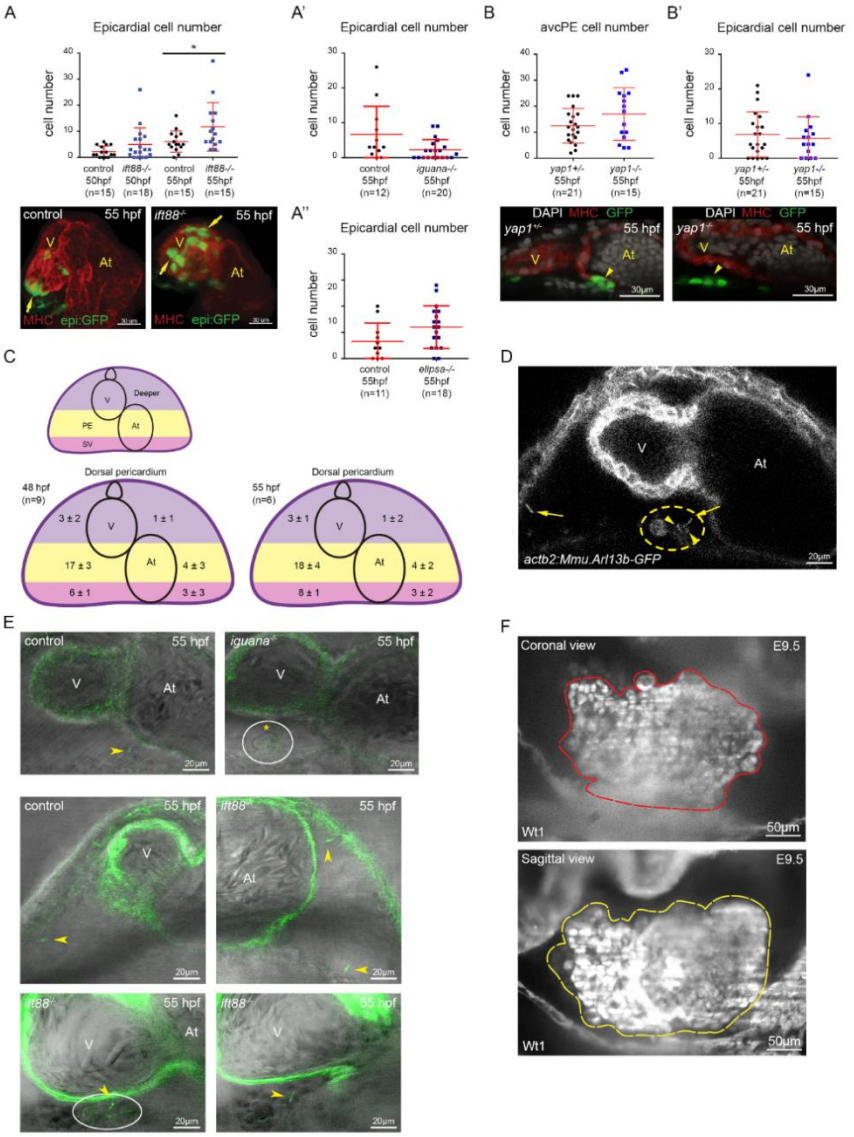

Figure S2. Cilia protruding into the pericardial cavity are distributed heterogeneously in zebrafish during proepicardial development. Related to Figures 1 and 3 and STAR methods.

(A-A'') *Graphs show epicardial cell numbers quantified in ift88, iguana and elipsa mutants in epi:GFP background.* ***(A)*** *At 55 hpf, ift88 mutants (n=15) showed increased epicardial cell numbers (t-test p value 0.04). 3D projections of whole mount immunofluorescence (IF) of hearts using anti-myosin heavy chain antibody (MHC) (red) and GFP (green) expression. Arrows mark some epicardial cells;* ***(A')*** *iguana mutants (n=20) showed a tendency towards decreased epicardial cell numbers (t-test p value 0.055), while* ***(A'')*** *elipsa mutants (n=18) showed a tendency towards increased epicardial cell number (t-test p value 0.08).* ***(B)*** *Graph shows avcPE cell numbers quantified in yap1$^{-/-}$ (n=15) and control (n=21) embryos in tcf21:nsl-GFP background at 55 hpf. (t-test p-value 0.12) Control and yap1$^{-/-}$ IF confocal sections labelled with MHC (red), GFP (green), DAPI (white). Yellow arrowheads point at the avcPE.* ***(B')*** *Graph shows epicardial cell numbers quantified in yap1$^{-/-}$ (n=15) and control (n=21) embryos in tcf21:nsl-GFP background at 55 hpf. (Mann Whitney p-value 0.63)* ***(C)*** *For cilia quantification, we divided the dorsal pericardial wall in to three different regions: SV region, including the sinus venosus (pink); PE region, where the avcPE forms (yellow) and Deeper region (purple). These three regions were subdivided in to right and left halves, containing the ventricle or the atrium respectively. At 48 hpf (n=9 larvae), prior to PE formation, cilia protruding from the dorsal pericardium showed a heterogeneous distribution. Interestingly, the right half of the SV (6 ± 1) and the PE (17 ± 3) regions, where both PE clusters will form, presented higher cilia number than the rest of the regions. At 55 hpf, when the avcPE is formed, the cilia distribution was similar to that observed at 48 hpf (n= 6 larvae).* ***(D)*** *Confocal section of actb2:Mmu.Arl13b-GFP embryo (55 hpf). Yellow dotted circle encloses the avcPE. Yellow arrows point to cilia protruding from the ventral and dorsal pericardium. Yellow arrowheads point at immotile and bent cilia protruding from a few avcPE cells.* ***(E)*** *Confocal sections of iguana; actb2:Mmu.Arl13b-GFP, ift88; actb2:Mmu.Arl13b-GFP and control embryos. In controls, yellow arrowhead points at cilium protruding into the*

pericardial cavity. In iguana yellow asterisk shows lack of cilia in the avcPE (enclosed in the white circle). Confocal section of ift88; actb2:Mmu.Arl13b-GFP and control embryos. In ift88 mutant embryo, yellow arrowheads point at cilia protruding from ventral and dorsal pericardium and the avcPE (enclosed in the white circle). ***(F)*** *Coronal and sagittal sections acquired by light sheet microscopy to illustrate the methods used to measure PE volume (labeled with anti-Wt1 antibody). Red and yellow dotted shapes enclose the PE area. In all the images ventral views, anterior is to the top. V, ventricle; At, atrium. In all graphs, red bars indicate mean ± standard deviation.*

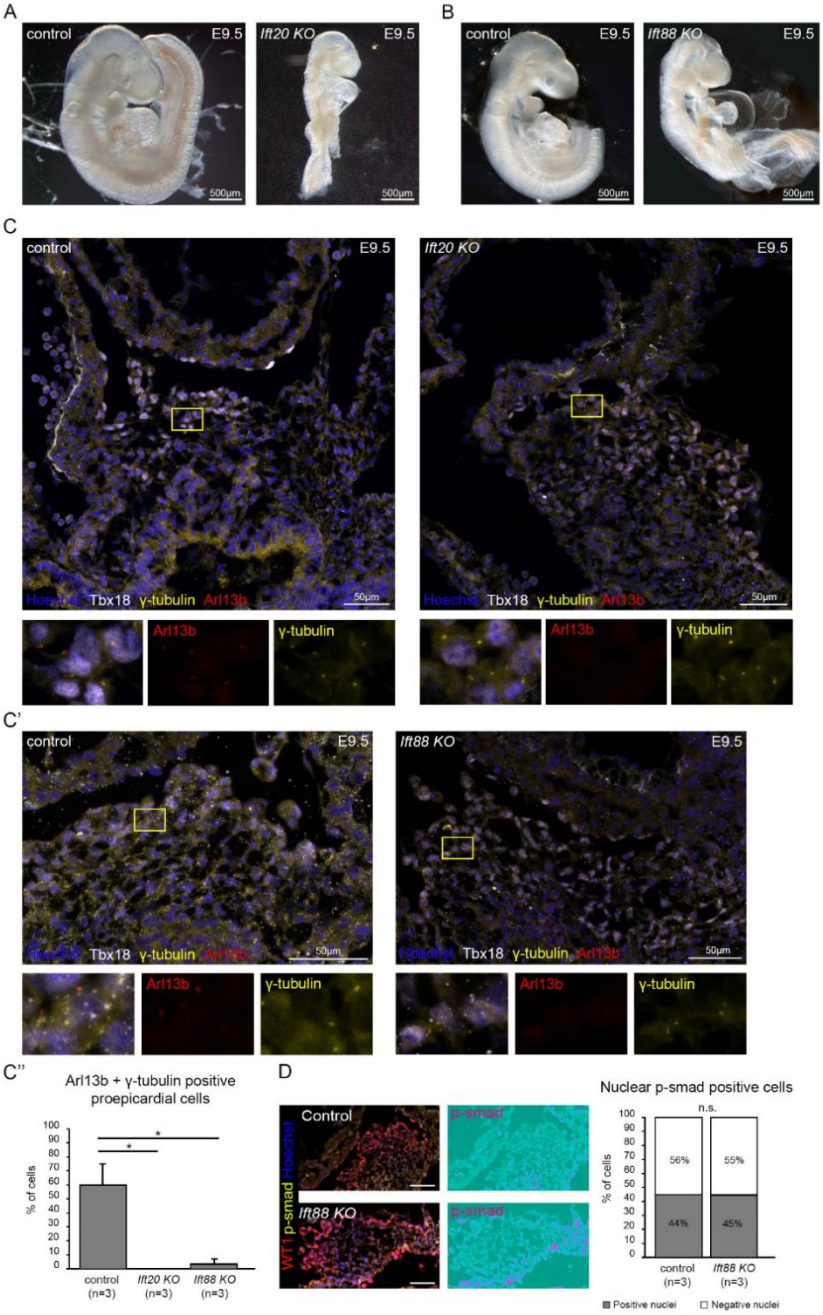
A
control
E9.5
Ift20 KO
E9.5
500µm
B
control
E9.5
Ift88 KO
E9.5
500µm
C
control
E9.5
Ift20 KO
E9.5
Hoechst Tbx18 γ-tubulin Arl13b
50µm
Arl13b
γ-tubulin
C'
control
E9.5
Ift88 KO
E9.5
Hoechst Tbx18 γ-tubulin Arl13b
50µm
Arl13b
γ-tubulin
C''
Arl13b + γ-tubulin positive proepicardial cells
% of cells
control (n=3)
Ift20 KO (n=3)
Ift88 KO (n=3)
D
Control
Ift88 KO
WT1 p-smad Hoechst
p-smad
Nuclear p-smad positive cells
n.s.
56%
55%
44%
45%
% of cells
control (n=3)
Ift88 KO (n=3)
Positive nuclei
Negative nuclei

Figure S3. Ift20 KO mice proepicardial cells lack cilia. Related to Figures 1 and 2.

(A,B) *Ift20 and Ift88 KO mice show left-right patterning defects including heart looping defects at E9.5.* ***(C)*** *Control and Ift20 KO cryosections imaged by confocal microscopy after labelling with anti-TBX18 (white), anti-Arl13b (red) and anti-γ-tubulin (yellow) antibodies and Hoechst (blue) at E9.5. Zoomed region (enclosed in yellow box) shows the lack of Arl13b signal in Ift20 KO mice. Individual channels are shown for Arl13b (red), γ-tubulin (yellow).* ***(C')*** *Control and Ift88 KO cryosections labelled with anti-TBX18 (white), anti-Arl13b (red) and anti-γ-tubulin (yellow) antibodies and Hoechst (blue) at E9.5. Zoomed region (enclosed in yellow box) shows the decrease of Arl13b signal in Ift88 KO mice. Individual channels are shown for Arl13b (red), γ-tubulin (yellow).* ***(C'')*** *Graph shows the percentage of ciliated PE cells in Ift20 KO (n=3, Ift88 KO (n=3) and control (n=3) mice. The percentage of ciliated PE cells is severely reduced in Ift20 KO (n=3) and Ift88 KO (n=3) when compared to control (n=3) mice. (t-test Ift20 p-value 0.024; t-test Ift88 p-value 0.025). Error bars indicate standard deviation.* ***(D)*** *Control and Ift88 KO cryosections labelled with WT1 (red), p-smad 1/5/9 (yellow) and Hoechst (blue) at E9.5. Individual channel is displayed for p-smad 1/5/9 as ice LUT to facilitate the visualization of signal intensity (green is the minimum and red is the maximum).Graph shows that the percentage of p-smad 1/5/9 positive PE cells is similar in Ift88 KO (n=3 embryos: 1477 nuclei analyzed) and controls (n=3 embryos: 1514 nuclei analyzed) (Chi-square test* of homogeneity *=0.15225, p-value 0.6964 on 1 degree of freedom).*

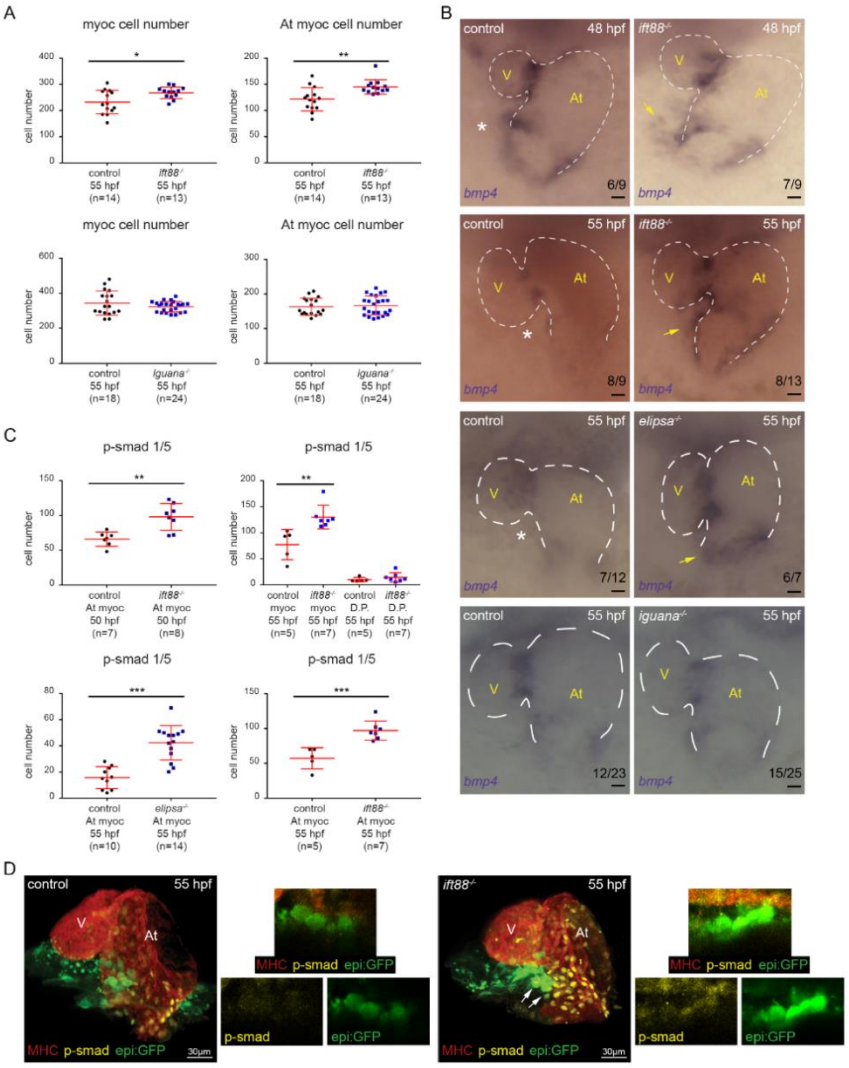

Figure S4. bmp4 is overexpressed in ift88, elipsa/ift54 and Ift20 mutants. Related to Figure 2.

(A) *The top two graphs show total myocardial and atrial-myocardial cell numbers quantified in ift88 (n=13) mutants and controls (n=14) at 55 hpf. (t-test total myocardium p-value 0.016;*

atrial myocardium p-value 0.003). The bottom two graphs show total myocardial and atrial-myocardial cell number quantified in iguana (n=24) mutants and controls (n=18) at 55 hpf. (t-test total myocardium p-value 0.2; atrial myocardium p-value 0.68). ***(B)*** *Whole mount bmp4 in situ hybridization performed on control and ift88 mutant embryos at 48 hpf and at 55 hpf on ift88, elipsa and iguana mutants and their controls. Yellow arrows point to bmp4 overexpression, while white asterisks mark reduced or absent expression. Ventral views, anterior is to the top. V, ventricle; At, atrium. Scale bars 20 µm.* ***(C)*** *Graphs show number of p-smad1/5 positive cells in the atrial myocardium quantified in ift88 (at 50 hpf n=8; at 55 hpf n=7), elipsa (n=14) mutants and their controls (n=7; n=5; n=10 respectively). At 50 hpf, ift88 mutants show p-smad 1/5 increased cell number on the atrial myocardium (t-test p value 0.0017). Similar data were obtained at 55 hpf (t-test p value 0.0008). At 55 hpf, elipsa mutants also show p-smad 1/5 increased cell number in the atrial myocardium (t-test p value 0.0003). At 55 hpf, ift88 mutants show p-smad 1/5 increased cell numbers in the myocardium (t-test p value 0.005).* ***(D)*** *3D projections of whole mount immunofluorescence of hearts using anti-myosin heavy chain antibody (MHC) (red), epi:GFP (green) and anti-p-smad1/5 (yellow) antibody. Arrows mark avcPE cells positive for epi:GFP and p-smad1/5. Zoomed confocal sections show avcPE in ift88 mutant and control embryos. Individual channels are displayed for p-smad 1/5 and GFP. Ventral views, anterior is to the top. In all graphs, red bars indicate mean ±standard deviation.*

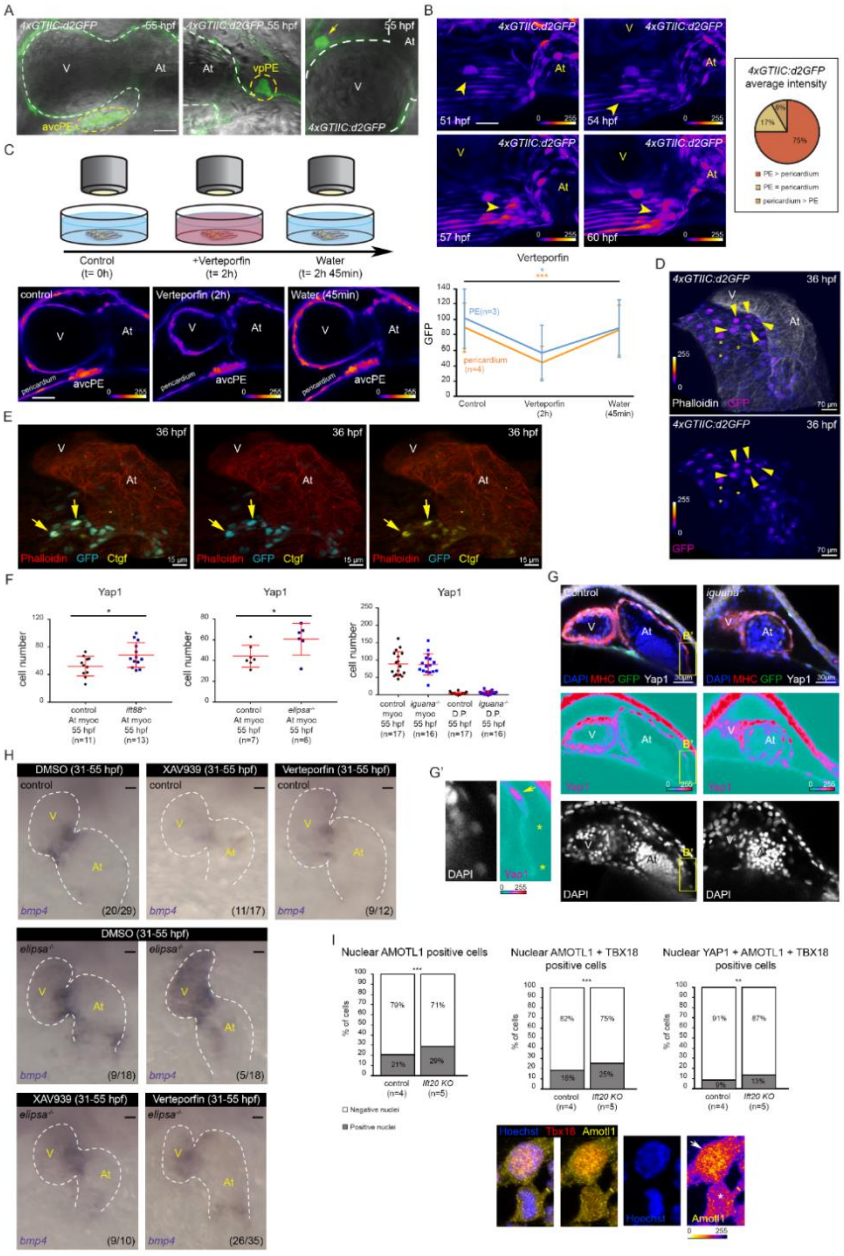

Figure S5 Yap1 activity is increased in the myocardium of ift88 and elipsa/ift54 zebrafish

mutants and AMOTL1 activity is increased in IFT20 KO mice proepicardium. Related to Figure 3.

(A) *Confocal sections of 4xGTIIC:d2GFP signal merged with bright-field, showing Yap/Wwtr1-Tead interaction in avcPE, vpPE, epicardial, myocardial and pericardial cells (n=12). Yellow dashed circles enclose the avcPE and the vpPE. Arrow shows an epicardial cell. Scale bar 20 µm.* ***(B)*** *Maximum projection 4xGTIIC:d2GFP time lapse (51-60 hpf) snapshots (n=6). Arrowheads point at the avcPE. GFP signal is shown as fire LUT where blue is the minimum and yellow is the maximum to facilitate visualization of the intensity changes through the experiment. Scale bar 20 µm. Graph shows 75% of the embryos displayed higher average GFP intensity in PE cells than in pericardial cells (n=12, 7-15 cells of each type).* ***(C)*** *Scheme of the experiment to assess Verteporfin specificity. Time lapse performed on 4xGTIIC:d2GFP embryos at 55 hpf. Yap/Wwtr1-Tead activity (average GFP intensity) was measured on the same PE (3 cells in each embryo, n=3) and pericardial (3 cells in each embryo, n=4) cells at three timepoints: before adding Verteporfin (5µM) (t=0h), after 2 hours of treatment (t=2h) and 45 min after washing out the Verteporfin with fish water (t=2h45 min). Graph shows the decrease in Yap/Wwtr1-Tead activity due to Verteporfin treatment on PE (blue) and pericardial (orange) cells, which is rescued after removing the inhibitor. (Pericardial cells ANOVA p value 0.0007. PE cells ANOVA p value 0.05). Example of 4xGTIIC:d2GFP embryo confocal sections used for the experiment. GFP signal is shown as fire LUT. Scale bar 20 µm.* ***(D)*** *3D projection of 4xGTIIC:d2GFP signal and phalloidin (white) at 36 hpf. GFP signal is shown as fire LUT. Yellow arrowheads show pericardial cells with stronger GFP intensity. Asterisks show pericardial cells with weaker GFP intensity. Individual GFP channel is displayed to facilitate visualization of the dorsal pericardium.* ***(E)*** *3D projection of tcf21:nls-EGFP signal,phalloidin (red) and Ctgf (yellow) at 36 hpf. Yellow arrows show Ctgf and GFP double-positive pericardial cells. Individual channels are*

displayed for GFP (cyan) and Ctgf (yellow) with phalloidin (red). ***(F)*** *The graphs show number of Yap1+ cells in the atrial myocardium (myoc) quantified in ift88$^{-/-}$, epi:GFP (n=13) and elipsa$^{-/-}$, epi:GFP (n=6) mutants and their controls (n=11 and n=7 respectively) at 55 hpf. Mutants show increased Yap1+ cell numbers (t-test ift88 p value 0.024 and elipsa p value 0.042). The last graph shows number of Yap1+ cells in the myoc and dorsal pericardium (D.P.) quantified in iguana$^{-/-}$, epi:GFP (n=16) mutants and their controls (n=17) at 55 hpf (t-test myoc p value 0.875 and D.P. p value 0.312).* ***(G)*** *Control and iguana$^{-/-}$, epi:GFP immunofluorescence (IF) confocal sections labelled with anti-myosin heavy chain antibody (MHC) (red), GFP (green), anti-Yap1 antibody (white) and DAPI (blue) at 55 hpf. Individual channels are displayed for Yap1 (signal is shown as ice LUT to facilitate visualization of signal intensity, where green is the minimum and red is the maximum) and DAPI (white).* ***(G')*** *Zoomed region (yellow box in panel* ***G****) shows Yap1 and DAPI channels to illustrate the method used to quantify Yap1+ (Yap1 signal in the nucleus: yellow arrow) and –negative (yellow asterisks) cells.* ***(H)*** *Whole mount bmp4 in situ hybridization in untreated elipsa mutant (n=18) and control (n=29) embryos and treated with XAV939 (10µM) (elipsa mutant, n=10 and control, n=17) or Verteporfin (20µM) (elipsa mutant, n=35 and control, n=12) from 31 to 55 hpf. Treated embryos showed either decreased or absent bmp4 expression at the atrioventricular canal myocardium and the venous pole. Scale bars 20 µm.* ***(I)*** *Graphs show the percentages of AMOTL1-positive PE cells, double AMOTL1-TBX18-positive PE cells and triple YAP1-AMOTL1-TBX18-positive PE cells in Ift20 KO (n=5 embryos: 1196 nuclei analyzed) and control (n=4 embryos: 929 nuclei analyzed) mice at E9.5. The percentage of nuclear AMOTL1-positive cells (Chi-square test* of homogeneity *= 14,748, p-value 1,23E-04 on 1 degree of freedom), nuclear AMOTL1-TBX18-positive cells (Chi-square test* of homogeneity *= 12,506, p-value 4,06E-04 on 1 degree of freedom) and nuclear YAP1-AMOTL1-TBX18-positive cells (Chi-square test* of homogeneity *= 6,9059, p-value 8,59E-03 on 1 degree of freedom) were*

higher in Ift20 KO than in control mice. Control (n=4) and Ift20 KO (n=5) sections labelled with TBX18 (red), Amotl1 (yellow) and Hoechst (blue). Individual AMOTL1 channel shows the difference between nuclear AMOTL1-positive cells (white arrow) and AMOTL1-negative cells (white asterisk). AMOTL1 signal is shown as fire LUT. In all the images ventral views, anterior is to the top. V, ventricle; At, atrium. In all graphs, red bars indicate mean ±standard deviation.

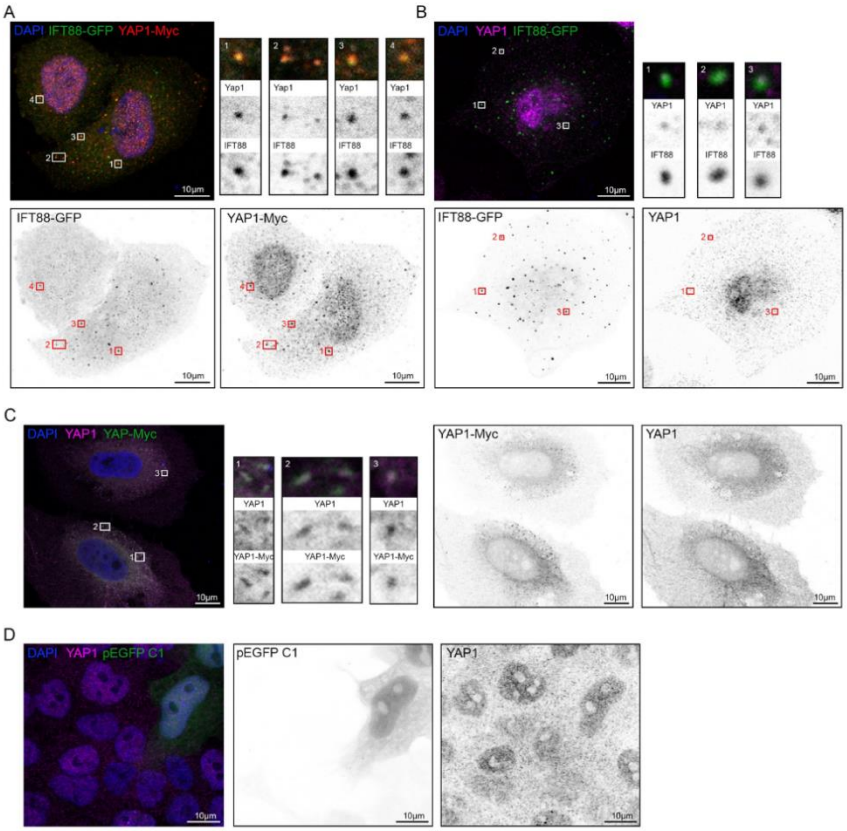

Figure S6. IFT88-GFP co-localize with YAP1 in the cytoplasm. Related to Figure 4.

(A) *Confocal section of HeLa cells transfected with IFT88-GFP and Yap1-Myc plasmids (48h). DAPI (blue), IFT88-GFP (green) and Yap1 (visualized using anti-Myc antibody) (red).*

Individual channels are displayed for IFT88-GFP and Yap1-Myc. ***(1-4)*** *Zoom of selected areas inside boxes showing co-localization.* ***(B)*** *Confocal sections of HeLa cells transfected with IFT88-GFP (48h) showing co-localization with endogenous YAP (visualized using anti-YAP/WWTR1 (TAZ) antibody). DAPI (blue), IFT88-GFP (green) and YAP1 (magenta).* ***(1-3)*** *Zoom of the selected areas inside white boxes showing co-localization of IFT88 and YAP1. Individual channels are displayed for IFT88-GFP and YAP1 signals.* ***(C)*** *Confocal sections of HeLa cells transfected with Yap1-Myc (48h) showing co-localization with endogenous YAP1 (visualized using anti-YAP/WWTR1 (TAZ) antibody). DAPI (blue), Yap1-Myc (green) and YAP1 (magenta).* ***(1-3)*** *Zoom of the selected areas inside white boxes showing examples of co-localization between Yap1-Myc (visualized using anti-Myc antibody) and endogenous YAP1 (using YAP/WWTR1 (TAZ) antibody) signals. Individual channels are displayed for Yap1-Myc and YAP1 signals.* ***(D)*** *Confocal sections of HeLa cells transfected with pEGFP C1 (48h) do not show co-localization with endogenous YAP1 (visualized using anti-YAP/WWTR1 (TAZ) antibody). DAPI (blue), pEGFP C1 (green) and YAP1 (magenta). Individual channels are displayed for pEGFP C1 and YAP1 signals.*

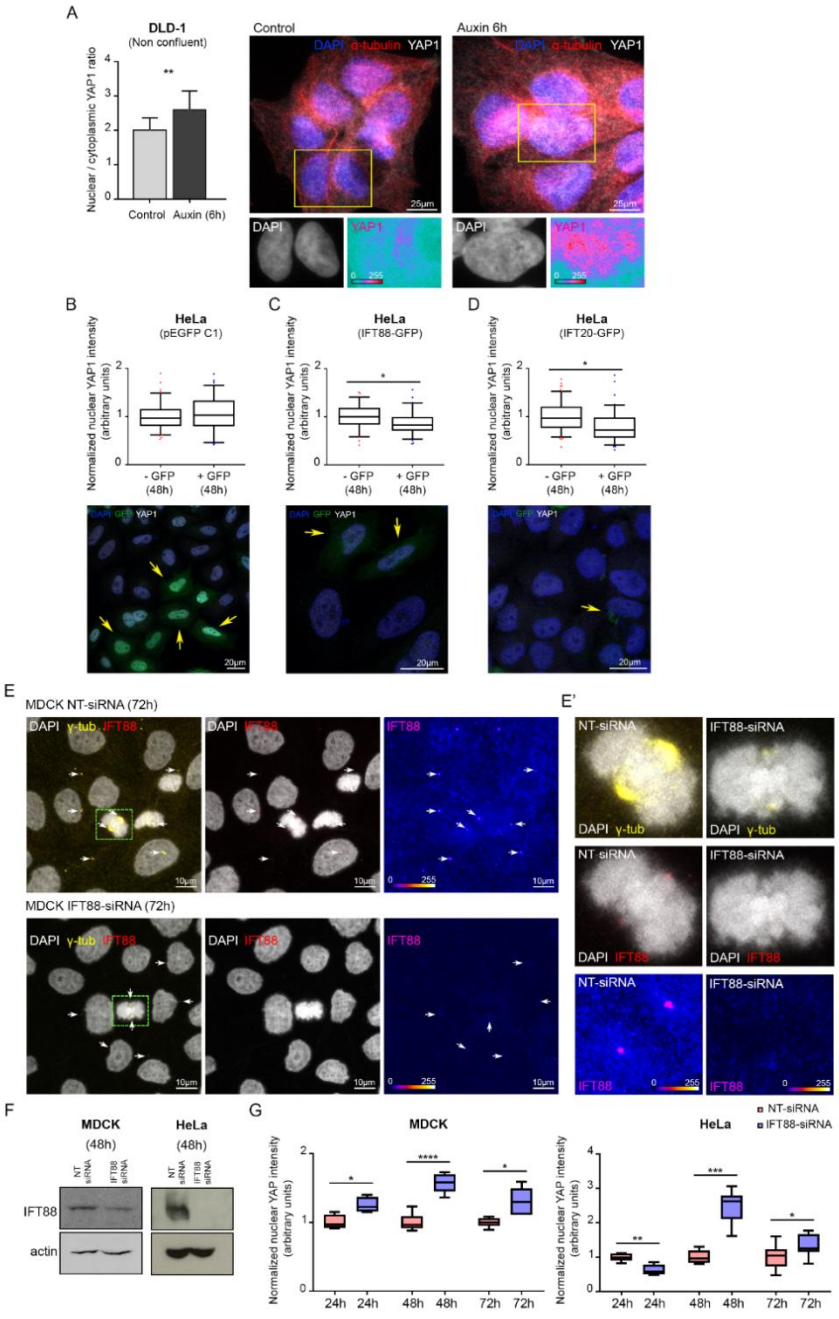
A
DLD-1
(Non confluent)
Nuclear / cytoplasmic YAP1 ratio
Control
Auxin (6h)
Control
Auxin 6h
DAPI α-tubulin YAP1
DAPI
YAP1
B
HeLa
(pEGFP C1)
C
HeLa
(IFT88-GFP)
D
HeLa
(IFT20-GFP)
Normalized nuclear YAP1 intensity
(arbitrary units)
- GFP
(48h)
+ GFP
(48h)
DAPI GFP YAP1
E
MDCK NT-siRNA (72h)
MDCK IFT88-siRNA (72h)
DAPI γ-tub IFT88
DAPI IFT88
IFT88
E'
NT-siRNA
IFT88-siRNA
DAPI γ-tub
DAPI IFT88
F
MDCK
(48h)
HeLa
(48h)
NT siRNA
IFT88 siRNA
IFT88
actin
G
MDCK
HeLa
NT-siRNA
IFT88-siRNA
Normalized nuclear YAP intensity
(arbitrary units)
24h 24h 48h 48h 72h 72h

Figure S7. IFT88 and IFT20 regulate YAP1 activity. Related to Figure 4.

(A) *YAP1 nuclear/cytoplasmic ratio is increased in cells treated with auxin (6h) (Mann-Whitney p-value 0.004). (controls: 2 replicates, n=102 cells; Auxin 6h: 2 replicates, n=104 cells). Error bars indicate standard deviation. Immunofluorescence (IF) confocal images of DLD-1 cells treated with auxin (6 h) and controls. DAPI (blue), YAP1 (white) and α-tubulin (red). Zoomed regions show DAPI and YAP1 channels. YAP1 channel is shown in ice LUT where green is the minimum and red is the maximum to facilitate the visualization of signal intensity increases after treatment.* ***(B-D)*** *IFT88 and IFT20 overexpression assays performed in HeLa cells (48h). Graphs show nuclear YAP/WWTR1 (TAZ) signal in GFP-positive cells (+ GPF), compared to GFP-negative cells (- GPF: endogenous control) in cells transfected with pEGFP C1 (GFP control) (n=4 replicates, average cell number analyzed for each condition = 22, t-test p-value 0.5)* ***(B)****, IFT88-GFP (n=3 replicates, average cell number analyzed for each condition = 23, t-test p-value 0.01)* ***(C)*** *or IFT20-GFP (n=4 replicates, average cell number analyzed for each condition = 27, t-test p-value 0.03)* ***(D)****. Box and whiskers (5-95 percentile). Outliers are represented as red dots (-GFP) or blue squares (+GFP). IF confocal images of cells transfected with pEGFP C1 (GFP control), IFT88-GFP or IFT20-GFP. DAPI (blue) and YAP/WWTR1 (TAZ) (white). Yellow arrows mark GFP signal.* ***(E)*** *IF confocal images of MDCK cells treated with NT- or IFT88-siRNA (72h). DAPI (white), γ-tubulin (yellow) and IFT88 (red). White arrows highlight IFT88-positive centrosomes facilitating the visualization of IFT88 signal depletion upon IFT88-siRNA treatment.* ***(E')*** *Zoom of dividing cells (green boxes) treated with NT-siRNA and IFT88-siRNA respectively. Centrosomes show reduced IFT88 (red) and γ-tubulin (yellow) signal after IFT88 depletion. DAPI (white). IFT88 channel is shown in fire LUT where blue is the minimum and yellow is the maximum to facilitate the visualization of the intensity reduction after the treatment.* ***(F)*** *Western blot analysis of HeLa and MDCK cells after 48h NT- and IFT88-siRNA treatments respectively.* ***(G)*** *Graphs*

show the increase in nuclear YAP/WWTR1 (TAZ) signal in IFT88-siRNA treated cells (blue), compared to NT-siRNA controls (red) at 24, 48 and 72h. Box and whiskers (5-95 percentile). (MDCK: 24h: n=1 replicate, average cell number analyzed for each condition = 42, t-test p-value 0.02; 48h: n=1 replicate, average cell number analyzed for each condition = 52, t-test p-value <0.0001; 72h: n=1 replicate, average cell number analyzed for each condition = 126, t-test p-value 0.01) (HeLa: 24h: n=1 replicate, average cell number analyzed for each condition = 12, t-test p-value 0.001; 48h: n=1 replicate, average cell number analyzed for each condition = 12, t-test p-value 0.0002; 72h: n=1 replicate, average cell number analyzed for each condition = 32, t-test p-value 0.047).

Average intensity	Embryo_01	Embryo_02	Embryo_03	Embryo_04	Embryo_05	Embryo_06
PE cells	71,37	72,42	30,84	89,57	69,72	49,63
St-Dev	11,91	21,49	26,85	20,56	24,85	13,35
Pericardial cells	52,45	45,17	55,81	94,08	49,98	29,95
St-Dev	21,16	9,76	18,25	29,84	14,67	7,51
t-test	**0,0325**	**0,0084**	0,0101	0,7309	0,0608	**0,0001**

Average intensity	Embryo_07	Embryo_08	Embryo_09	Embryo_10	Embryo_11	Embryo_12
PE cells	63,69	60,99	115,45	64,67	56,23	107,03
St-Dev	26,92	18,28	6,52	11,43	10,46	21,14
Pericardial cells	28,76	31,59	74,03	36,44	30,05	68,40
St-Dev	16,68	7,78	22,14	6,82	8,85	28,52
t-test	**0,0055**	**0,0005**	**0,0001**	**0,0000**	**0,0002**	**0,0024**

Table S1. Yap/Wwtr1-Tead activity (GFP average intensity) in PE and pericardial cells. Related to Figure 3.

Statistically significant results are highlighted in bold.

Study of Yap1/Taz-Tead activity during PE cluster formation

Preface

In this chapter I present my main work during my PhD, the study of Yap1/Taz-Tead activity during PE cluster formation. The conceptualization of the project was done by me, Marina Peralta and Julien Vermot. Investigation, data curation and writing of the original draft were done by me.

Préface en français

Dans ce chapitre, je présente le travail principal de mon doctorat, l'étude de l'activité de Yap1/Taz-Tead pendant la formation du PE. La conceptualisation du projet a été faite par moi, Marina Peralta et Julien Vermot. La recherche, la conservation des données et la rédaction de la version originale ont été effectuées par moi-même.

Introduction

The epicardium is the mesothelial cell layer covering the myocardium. It is essential for proper heart development, as it has several key functions such as promoting myocardial growth, coronary vasculature formation, and intracardiac fibroblast generation (Olivey and Svensson 2010; Ruiz-Villalba and Pérez-Pomares 2012; Schlueter and Brand 2012). Furthermore, the epicardium is critical during heart regeneration. Following a cardiac injury, epicardial cells turn on embryonic genes and contribute to new coronary vascular cells and the maintenance of the survived heart muscle (Simões and Riley 2018).

Epicardial cell progenitors arise from the DP, the cell layer surrounding the heart and forming the pericardial cavity. Around the time of heart looping, cells from the dorsal pericardium round up and form the PE cluster (Maya-Ramos et al. 2013). In zebrafish, PE formation depends on DP constriction and extrusion of PE cells to the pericardial cavity. After PE cluster formation, PE cells are released into the pericardial cavity and are advected by the pericardial flow until they attach to the myocardium. Once on the myocardium, cells spread and proliferate until they cover the whole heart by around 6 dpf (Peralta et al. 2013; Andrés-Delgado et al. 2019).

Several epicardial markers have been described, such as *tcf21*, *wt1*, or *tbx18*. Nevertheless, the epicardial layer is very heterogeneous and there are different subsets of cells with different gene expression within it (Y. Cao and Cao 2018; Plavicki et al. 2014; González-Rosa, Peralta, and Mercader 2012; Weinberger et al. 2020). Several regulation pathways have been described as important regulators of this process, such as the Bmp pathway (Andrés-Delgado et al. 2019). However, it is still unknown why some specific cells from the dorsal pericardium will acquire PE-like identity, undergoing major cell shape changes to form the PE cluster.

One crucial regulator of cardiovascular development is the Hippo pathway, a signalling pathway involved in the regulation of organ size and cell proliferation among others (Zhao, Tumaneng, and Guan 2011). Yap1 and Wwrt1 (or Taz) are the main effectors of the Hippo pathway, as activation of the Hippo pathway results in Yap/Taz phosphorylation and cytoplasmatic retention (Yu, Zhao, and Guan 2015). However, changes in mechanical cues such as extracellular matrix rigidity, shear stress, or biomechanical forces of blood flow can also regulate Yap/Taz nuclear translocation independently from the Hippo pathway (Lundin et al. 2020; Elosegui-Artola et al. 2017). In zebrafish, the Hippo pathway promotes venous pole identity and increases atrial cardiomyocyte number through BMP (Fukui et al. 2018). Moreover, it has been described that intraflagellar transport complex B proteins can regulate the Hippo effector Yap1 during cardiogenesis (Peralta et al. 2020). In mice, Yap1 is colocalizing with Wt1 in epicardial cells. Moreover, epicardial inactivation of Yap/Wwrt1 causes embryonic death (Singh et al. 2016). Although Yap1/Wwrt1-Tead activity is involved in different steps of cardiac development, its impact during the process of PE cluster formation remains elusive.

Here, we used zebrafish to study the role of Yap1/Taz-Tead activation during PE cluster formation. We found that Yap1/Taz is active in DP cells from early timepoints and activity is maintained in PE and epicardial cells. Chemical modulation of Yap1/Taz activity affects PE formation and we describe Lkb1 as a new regulator in PE cluster formation.

Results

Yap/Taz-Tead activity during PE cluster formation

To investigate in detail PE formation, represented in Figure 2A, we sought to describe Yap1/Taz-Tead activity during this process. Since *wt1* is an epicardial marker and its promoter is downstream of TEAD (Singh et al. 2016), we used the Yap1/Taz-TEAD reporter line *4xGTIIC:d2GFP* (Miesfeld and Link 2014) to follow Yap1/Taz-TEAD activation in the epicardium before and during PE cluster formation.

For this purpose, we fixed *4xGTIIC:d2GFP* embryos at 36, 48, and 55 hpf and stained them with phalloidin (cell shape readout) to image them with confocal microscopy (Figure 1A). At 36 hpf, cells from the pericardium are flat and expression in the DP is low. At 48 hpf, before the PE is formed, pericardial cells are flat but we see some cells in the atrioventricular channel area with high GFP expression. At 55 hpf, cells from the PE are rounded and have high GFP expression and there are some high GFP flat cells next to the PE (Figure 1B). We believe that these are the cells that will be incorporated into the PE cluster.

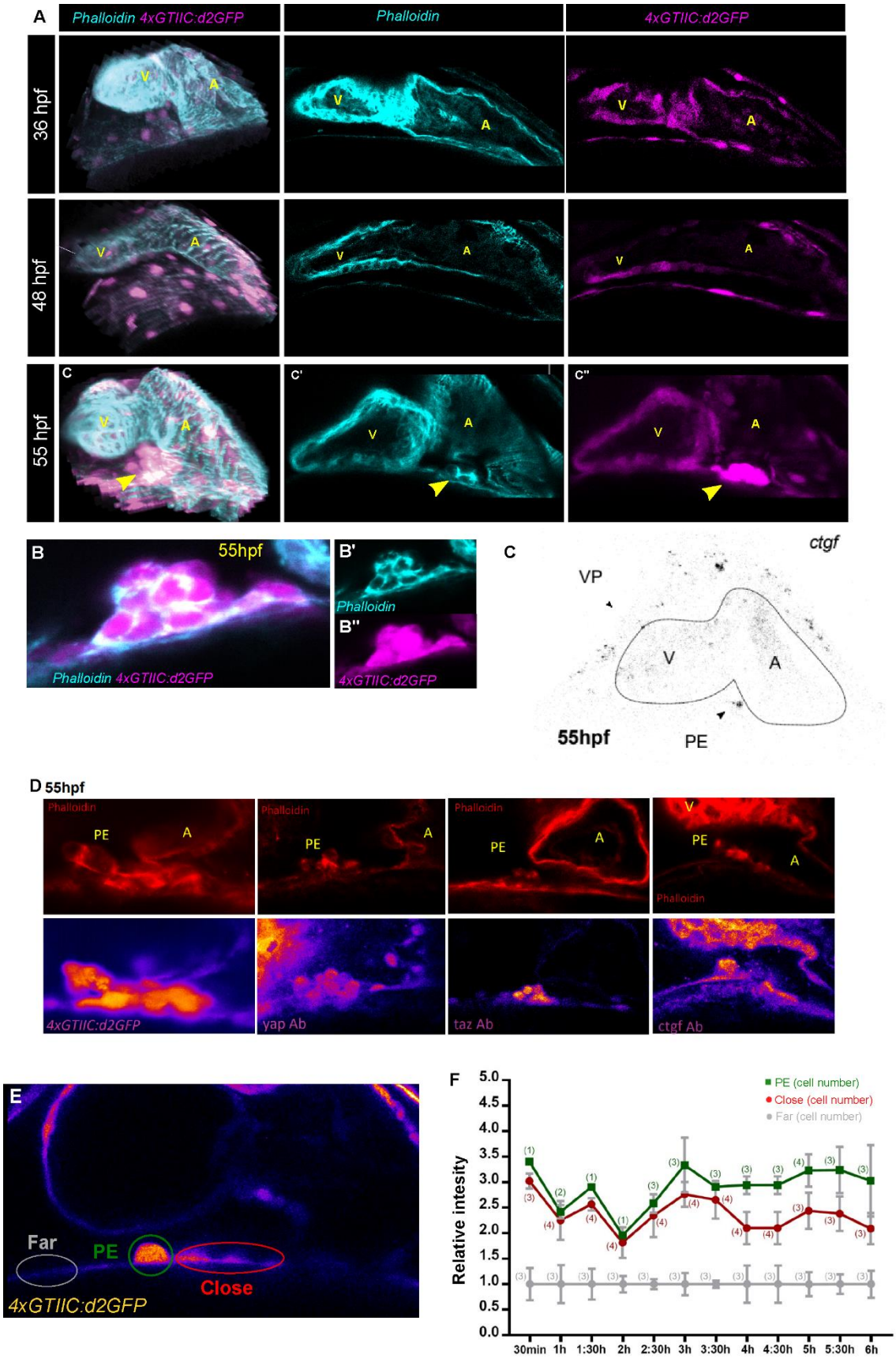

Figure 1. Yap1/Taz-Tead in the dorsal pericardium. A. Confocal imaging of 4xGTIIC:d2FP embryos stained with phalloidin at 36, 48, and 55 hpf. Arrowheads mark

the PE cluster. B. Confocal imaging of 4xGTIIC:d2GFP embryos stained with phalloidin. Zoomed in image of the PE cluster. C. Confocal imaging of a wild type fish after RNA scope with ctgf probe. The heart is indicated in the image. PE cells have high ctgf expression. D. Confocal imaging of wild type fish comparing the PE of 4xGTIIC:d2GFP fish against wild type fish after IMHC against Yap, Taz, and ctgf. E. Plane of a timelapse of a 4xGTIIC:d2GFP embryo with confocal microscopy. F. Graphic showing relative intensity (intensity normalized to pericardial cells far from the cluster) of the PE cells and cells close to the pericardium. PE cells, followed by cells close to the cluster, have higher intensity.

To confirm that *4xGTIIC:d2GFP* was specifically labelling Yap1/Taz-Tead activation, we performed RNAscope at 55 hpf to check *ctgf* expression, a known read-out of Yap1/Taz-Tead activity (Totaro, Panciera, and Piccolo 2018). We confirmed that *ctgf* is specifically expressed in PE cells, as well as in some cells in the ventral pericardium, consistent with the results that we previously obtained (Figure 1C).

Furthermore, we performed IMHC against yap, taz, and ctgf at 55 hpf. We confirmed that the localization of these antibodies is consistent with the GFP expression from the reporter line *4xGTIIC:d2GFP*, thereby confirming that GFP expression is specific to Yap1/Taz-Tead activity (Figure 1D).

To further describe Yap-Taz/Tead activation, we measured quantitatively GFP intensity in different areas of the DP. We performed confocal *in vivo* imaging every 30 minutes starting at 50 hpf. For every time point, we measured the intensity of PE cells and pericardial cells close to the PE cluster, and we normalized it to the intensity of the pericardial cells far from the PE cluster (Figure 1E). As expected, cells from the PE cluster have GFP intensity higher than nearby pericardial cells (Figure 1F), confirming that cells from the PE have increased Yap/Taz-Tead activity compared to other areas of the DP.

To investigate in more detail PE formation we sought to follow it *in vivo* using lightsheet microscopy. For this purpose, we imaged *actb2:lifeAct-RFP* (Behrndt et al. 2012) embryos crossed with *Et(-26.5Hsa.WT1-gata2:EGFP)cn1* or *epi:GFP* (Peralta et al. 2013), a reporter line of *Wt1a* where around 70% of PE cells express GFP. Imaging at 48 hpf every 30 seconds (Figure 2B), we

observed that some cells from the pericardium express GFP before they start to round up and the PE cluster is not completely formed. Since the PE expresses different known markers, we next wanted to confirm if *tcf21* was also expressed before cells extrude from the DP. We imaged *tcf21:nls-GFP* embryos starting at 36 hpf every 15 minutes. We observe that similarly to wt1a, tcf21 is present in PE cells before they round up and after in the formed PE (Figure 2C).

Next we image *4xGTIIC:d2GFP* embryos (n=2) starting at 36 hpf every 15 minutes (Figure 2D). In earlier time points, GFP expression is weak in all the pericardium. At around 40 hpf, some cells in the atrioventricular channel area in the DP increased their GFP intensity. These cells keep increasing their GFP expression through time and at 48 hpf they start to round up, possibly being the ones that will form the PE cluster.

We then imaged an embryo starting at 48 hpf every 15 minutes (Figure 2E). We observed flat cells in the dorsal pericardium with high GFP expression, that when followed in time, gives rise to the PE cluster.

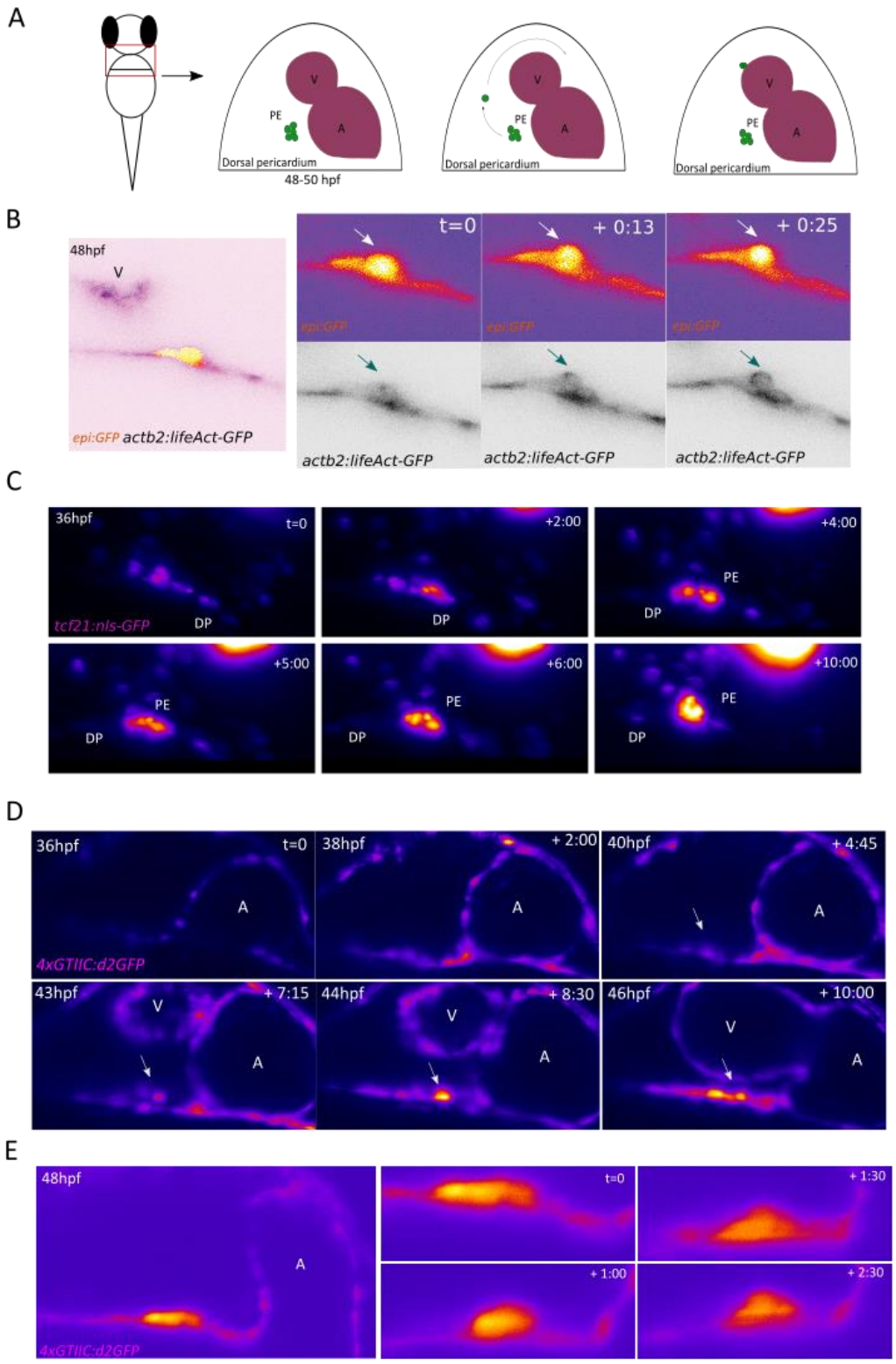

Figure 2. Yap1/Taz-TEAD in vivo activation during PE cluster formation. A. Schematic representation of PE cluster formation. At approximately 48 hpf cells from the dorsal pericardium protrude in the atrioventricular channel area forming the PE cluster. Cells from the cluster are released to the pericardial cavity until they attach to the myocardium. B. Lightsheet timelapse analysis of an actb2:lifeAct-RFP; epi:GFP

embryo starting at 48 hpf. One plane per timepoint. Rounded cells express epicardial markers (arrowhead). C. Lightsheet timelapse imaging of a tcf21:nls-GFP embryo starting at 36 hpf. Maximum intensity projection. D. Lightsheet timelapse imaging of a 4xGTIIC:d2GFP embryo starting at 36 hpf. One plane per time point. Cells from the dorsal pericardium increase their GFP expression through time and eventually form the PE cluster (arrowhead). D. Lightsheet timelapse analysis of a 4xGTIIC:d2GFP embryo starting at 48 hpf. One plane per timepoint.

Overall, our results show that Yap1/Taz-Tead is specifically active in the first steps of epicardial development.

Chemical modification of Yap1/Taz nuclear activity has an impact on PE cluster formation

We then sought to test the role of Yap1/Taz-Tead in PE formation upregulating and downregulating its activity. For this purpose, we used dexamethasone and XAV939. Dexamethasone is a glucocorticoid that activates *in vivo* Yap1/Taz-Tead mediated transcription (Sorrentino et al. 2017; Astone et al. 2018), while XAV939 is a compound that inhibits tankyrase stabilizing AMOT proteins, resulting in a decrease of Yap1 nuclear translocation (W. Wang et al. 2015).

We first treated *4xGTIIC:d2GFP* embryos from 50 to 55 hpf with a solution containing 25 µM of dexamethasone and fixed them to image them with a confocal microscope after phalloidin staining. Dexamethasone treated embryos show no differences in terms of PE cell number compared to non-treated embryos. However, there is an increase of fluorescence in PE cells from dexamethasone-treated embryos compared to non-treated embryos (Sup. figure 3A, B).

Taking into consideration these results, we decided to increase the time of treatment and treated *4xGTIIC:d2GFP* embryos from 36 to 55 hpf (Figure 3A, C). Dexamethasone treated embryos have an increased percentage of GFP cells in the pericardium (Figure 3B) and myocardium (Figure 3B'), showing a general increase of Yap1/Taz-Tead activity. PE cell number is increased in dexamethasone-treated embryos compared to non-treated siblings (Figure 3B''). However, epicardial cell number does not significantly change (Figure 3B''').

Next, we then treated *4xGTIIC:d2GFP* embryos with a solution containing 5 µM of XAV939 and treated them from 36 to 55 hpf to fix them and image them with a confocal microscope after phalloidin staining (Figure 3A, D). Although the percentage of GFP positive cells in the pericardium is not significantly different in XAV939 treated embryos (Figure 3E), they do have a decreased percentage of GFP cells in the myocardium compared to non-treated embryos (Figure 3E'), showing a decrease of Yap1/Taz-Tead activity. In addition, PE cell number is lower in XAV939 treated embryos compared to non-treated embryos (Figure 3E''), as well as the epicardial cell number (Figure 3E''').

Taken together, our results indicate that increasing Yap1/Taz-Tead activity starting at 36 hpf increases the number of PE cluster cells, while decreasing Yap1 nuclear translocation has the opposite effect.

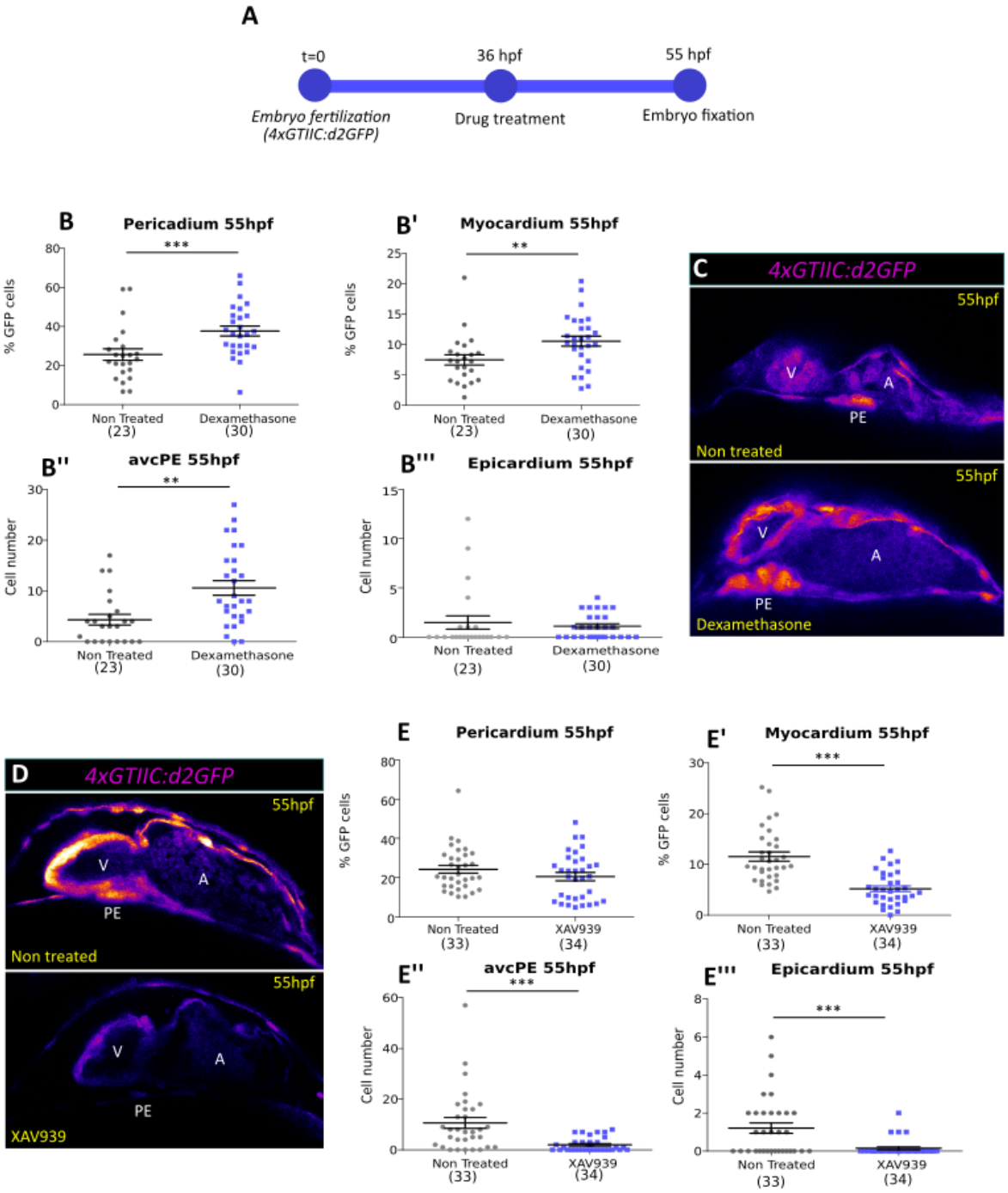

Figure 3. Modifying Yap1/Taz-Tead activity chemically impacts PE cluster formation. A. 4xGTIIC:d2GFP embryo treatment with dexamethasone and XAV939. B-B'-B''-B'''. Quantification in non-treated and dexamethasone-treated embryos of: GFP positive cells in the dorsal pericardium and the myocardium, PE cell number, and epicardial cell number. C. Confocal plane of a non-treated and a dexamethasone-treated embryo showing PE cluster. D. Confocal plane of a non-treated and a XAV939 treated embryo showing PE cluster. E-E'-E''-E'''. Quantification in non-treated and XAV939 treated

embryos of: GFP positive cells in the dorsal pericardium and the myocardium, PE cell number, and epicardial cell number.

We next sought to test whether a *Yap1* mutation would induce the same phenotype as XAV939 treatment with the zebrafish line *Yap1-/-;tcf21:nls-GFP*. Surprisingly, PE cluster cell number and epicardial cell number is not significantly different in *Yap1* mutants compared to wild type (Figure Sup 3 C-D).

These results contradict our main hypothesis, since we were expecting the PE cluster formation to be somewhat impaired in *Yap1* mutants. However, since it is already known that Yap1 and Taz have some overlapping functions, these results could be the result of compensation by Taz. To check this, we performed immunohistochemistry against Taz in *Yap1* mutants and controls and saw that Taz protein is present in the zebrafish heart, PE, some DP cells, and in some epicardial cells (Figure Sup 3 E). To avoid any possible compensation, we used Taz MO at 2ng concentration in *Yap1* mutants. In *Yap1* mutants and Taz morphants, as expected, the number of Taz cells in the myocardium (Fig Sup 3 F) and pericardium (Fig Sup 3 G) is decreased compared to *Yap1* mutants and controls. However, the number of PE cluster cells is not significantly different (Fig Sup 3 H).

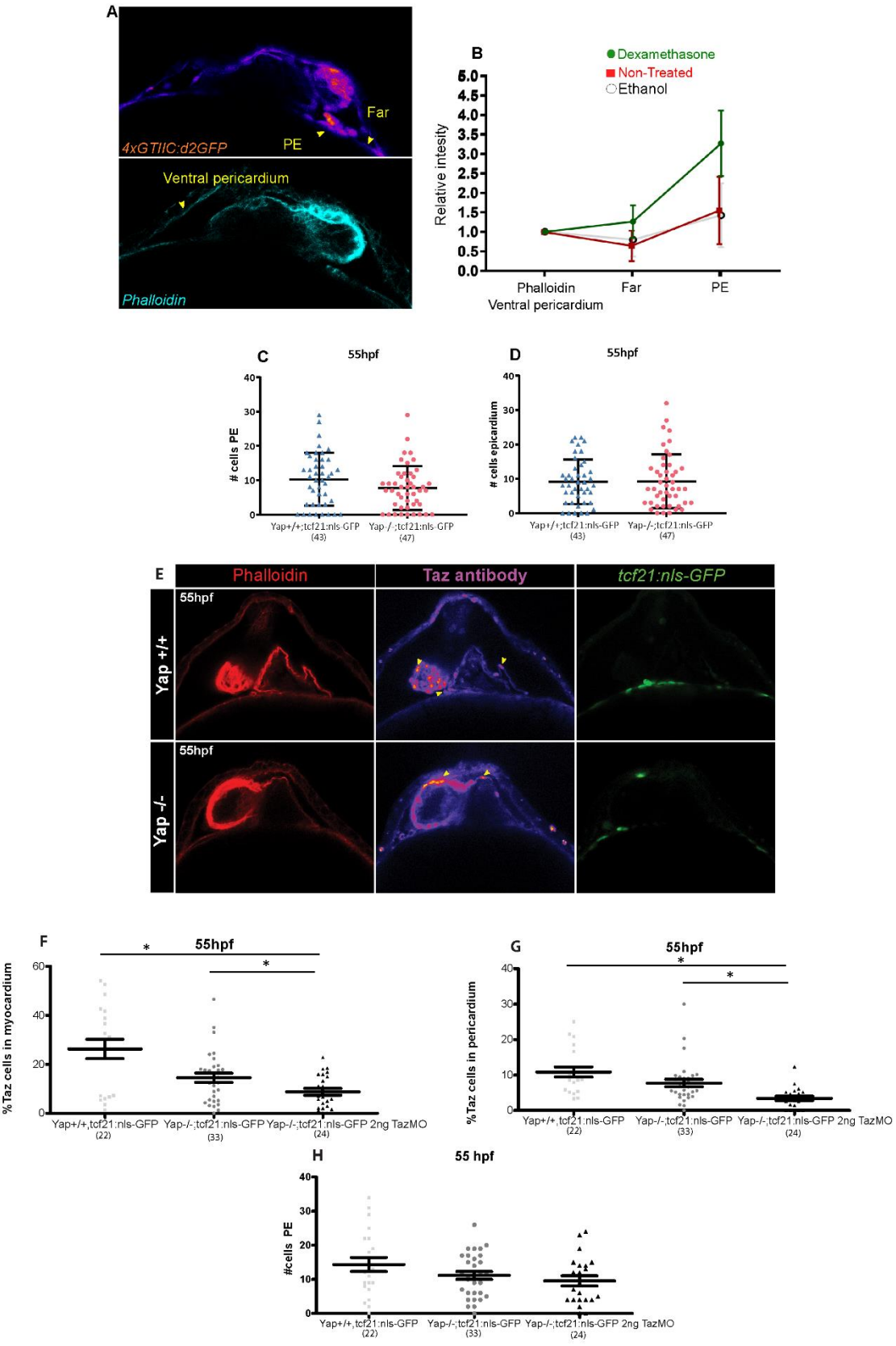
A
Far
PE
4xGTIIC:d2GFP
Ventral pericardium
Phalloidin
B
Dexamethasone
Non-Treated
Ethanol
Relative intesity
Phalloidin
Far
PE
Ventral pericardium
C
55hpf
cells PE
Yap+/+;tcf21:nls-GFP (43)
Yap-/-;tcf21:nls-GFP (47)
D
55hpf
cells epicardium
Yap+/+;tcf21:nls-GFP (43)
Yap-/-;tcf21:nls-GFP (47)
E
Phalloidin
Taz antibody
tcf21:nls-GFP
Yap +/+
Yap -/-
55hpf
F
55hpf
% Taz cells in myocardium
Yap+/+,tcf21:nls-GFP (22)
Yap-/-;tcf21:nls-GFP (33)
Yap-/-;tcf21:nls-GFP 2ng TazMO (24)
G
55hpf
% Taz cells in pericardium
Yap+/+,tcf21:nls-GFP (22)
Yap-/-;tcf21:nls-GFP (33)
Yap-/-;tcf21:nls-GFP 2ng TazMO (24)
H
55 hpf
#cells PE
Yap+/+,tcf21:nls-GFP (22)
Yap-/-;tcf21:nls-GFP (33)
Yap-/-;tcf21:nls-GFP 2ng TazMO (24)

Figure Supplementary 3. Dexamethasone increases GFP intensity in 4xGTIIC:d2GFP embryos but Yap1 mutations are not affecting PE formation. A. Confocal plane of a treated 4xGTIIC:d2GFP embryo. Top image is the 4xGTIIC:d2GFP channel and the bottom one is phalloidin. B. Intensity measurement of PE cells and pericardial cells far from the cluster normalized to phalloidin in the ventral pericardium. Treated embryos have increased GFP intensity in both of the measurements compared to non-treated and ethanol-treated embryos. C. Quantification in Yap1+/+;tcf21:nls-GFP and Yap1-/-;tcf21:nls-GFP of myocardial cell number at 55 hpf. D. Quantification in Yap1+/+;tcf21:nls-GFP and Yap1-/-;tcf21:nls-GFP of epicardial cell number at 55 hpf. G. Confocal imaging of Yap1+/+;tcf21:nls-GFP and Yap1-/-;tcf21:nls-GFP at 55 hpf with Taz Ab. Arrowheads mark the positive cells in the Taz channel. H. Quantification of percentage of Taz positive cells in the myocardium in Yap1+/+;tcf21:nls-GFP, Yap1-/-;tcf21:nls-GFP and Yap1-/-;tcf21:nls-GFP with Taz MO at 2ng of concentration. I. Quantification of percentage of Taz positive cells in the pericardium in Yap1+/+;tcf21:nls-GFP, Yap1-/-;tcf21:nls-GFP and Yap1-/-;tcf21:nls-GFP with Taz MO at 2ng of concentration. J. Quantification of PE cell number in Yap1+/+;tcf21:nls-GFP, Yap1-/-;tcf21:nls-GFP and Yap1-/-;tcf21:nls-GFP with Taz MO at 2ng of concentration.

Altogether, we see that although Yap1/Taz-Tead is active specifically in PE cells, when we inhibit this pathway starting at the 1 cell stage the PE cluster formation is not affected. Since the epicardial layer is essential, it is possible that there are compensatory ways to ensure proper epicardial formation that can overcome Yap1 and Taz inhibition.

Lkb1 mutants have bigger PE clusters at 72 hpf

Given that Dexamethasone increases Yap1/Taz-Tead activity and results in a bigger PE cluster, we hypothesized that mutations in Yap1/Taz-Tead inhibitors would result too in a bigger cluster. Since *lkb1* has been previously described as a regulator of Yap1 nuclear translocation *in vitro* (Mohseni et al. 2014), we sought to investigate the impact of *lkb1* loss-of-function during PE cluster formation. We fixed *lkb1* mutants (van der Velden et al. 2011) crossed to *tcf21:nls-GFP* at 36, 55, 72 hpf, and 5 dpf and performed immunohistochemistry against GFP and phalloidin.

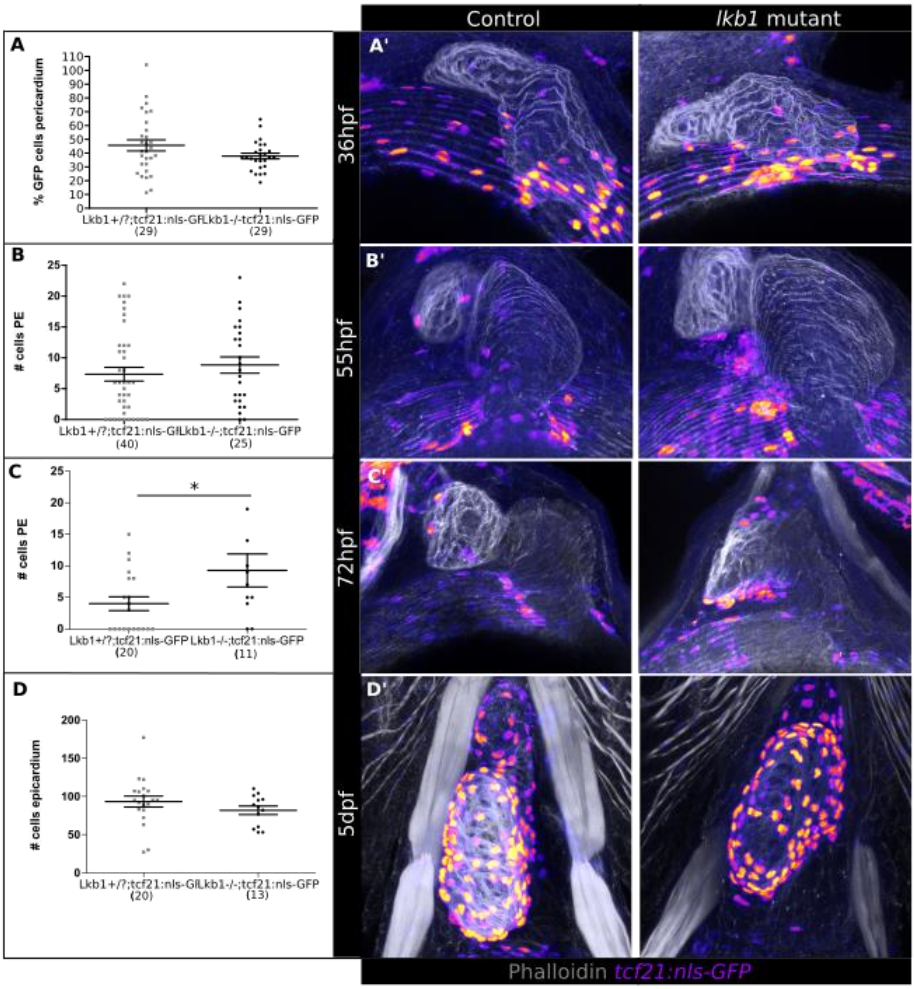

Figure 4. Description of lkb1 mutants at key points of PE cluster formation. A. Percentage of positive GFP cells in the dorsal pericardium at 36 hpf. B. Quantification of PE cluster cell number at 55 hpf. C. Quantification of PE cluster cell number at 72 hpf. D. Quantification of epicardial cell number at 5dpf. A'-D'. Confocal imaging of Lkb1-/-;tcf21:nls-GFP and control siblings at 36, 55, 72 hpf and 5dpf.

At 36 hpf there are no apparent differences between controls and mutants in terms of GFP positive cells in the pericardium (Figure 4A) or myocardium cell number (Figure Sup 4A). At 55 hpf, there no significant differences between *lkb1* mutants and controls in terms of PE cluster cell number (Figure 4B). Mutants did not show either any difference in terms of myocardial cell number or epicardial cell number (Figure Sup 4B-C). At 72 hpf mutants have an increased number of PE cells compared to controls (Figure 4C). As it happened in earlier time points, there were no differences in terms of myocardial and epicardial cell numbers (Figure Sup 4 D-E). Finally, we checked at 5 dpf, and

there are no apparent differences between controls and mutants in terms of epicardial (Figure 4D) or myocardial cell number (Figure Sup 3F).

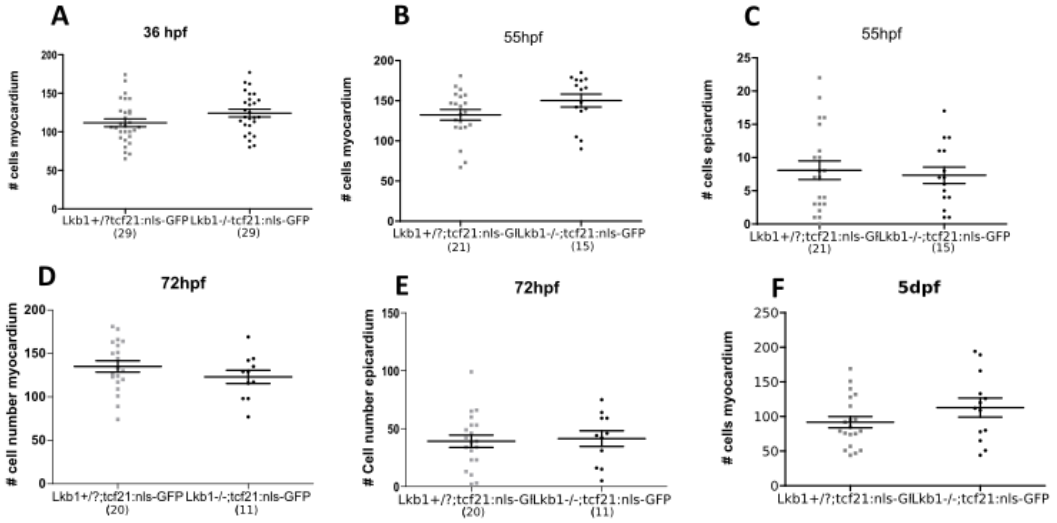

Figure Supplementary 4. Description of lkb1 mutants at key points of PE cluster formation. A. Quantification of myocardial cell number in lkb1-/-;tcf21:nls-GFP and controls at 36 hpf. B. Quantification of myocardial cell number in lkb1-/-;tcf21:nls-GFP and controls at 55 hpf. C. Quantification of epicardial cell number in lkb1-/-;tcf21:nls-GFP and controls at 55 hpf. D. Quantification of myocardial cell number in lkb1-/-;tcf21:nls-GFP and controls at 72 hpf. E. Quantification of epicardial cell number in lkb1-/-;tcf21:nls-GFP and controls at 72 hpf. F. Quantification of myocardial cell number in lkb1-/-;tcf21:nls-GFP and controls at 5 dpf.

Thus, *lkb1* mutants show differences in terms of PE cell number at 72 hpf.

Discussion

In this chapter we study Yap1/Taz-Tead activity during PE cluster formation. We describe *in vivo* Yap1/Taz-Tead activity in the heart from 36 hpf to 55 hpf using the reporter line *4xGTIIC:d2GFP*. We see GFP expressed specifically in the PE cluster. Moreover, GFP expression is on before PE cells extrude to the proepicardial cavity, suggesting that it is involved somehow in PE cluster formation.

PE cells change their shape from flat to round, breaking their cell adhesions. Although this process is not a complete epithelial to mesenchymal transition (EMT), it shares many similarities (Andrés-Delgado et al. 2019). Moreover, PE cells express *twist1a* (Peralta 2014), a bHLH transcription factor involved in

EMT and a regulator of lineage specification and differentiation (Lamouille, Xu, and Derynck 2014). It is also interesting to mention that Yap has been described as a promoter of EMT in several cancers, such as colorectal cancer (Cheng et al. 2020). *In vitro*, it has also been seen that Yap-mediated responses to changes in ECM organization promote EMT (Park et al. 2019). This would be consistent with a model in which Yap1/Taz-Tead activity promotes PE cluster formation: Yap1/Taz-Tead is active in DP cells from early time points and these cells will extrude, in an EMT-like process, to form the PE cluster.

Consistent with this, in our chapter we show that modifying Yap1/Taz-Tead activity using drugs results in dysregulation of the PE formation process: an increase in Yap1/Taz-Tead activity results in more PE cell in the cluster while a decrease results in a decreased PE cell number. All of this suggests that Yap1/Taz-Tead activity promotes PE-like cell identity. This is consistent with what has been previously published in the field. It has been published that IFT complex B proteins inhibit Yap1 activity during PE cluster formation and a lack of IFT88 results in an increase in PE cell cluster (Peralta et al. 2020). Motin proteins have also been shown to regulate PE cluster formation. In zebrafish, Amot proteins bind to Yap/Taz in the cytoplasm sequestering it (Agarwala et al. 2015). *Amotl2a* mutants, which would have increased nuclear Yap1/Taz, have bigger PE clusters (Peralta et al. 2020). However, although when we chemically decrease Yap1/Taz-Tead activity in zebrafish results in a smaller PE cluster, we do not see the same results in *Yap1* mutants or *Yap1* mutants and Taz morphants.

This could be due to different events. In our model, we did not completely eliminate Taz from the system. Double mutants for Yap1/Taz exhibit severe developmental defects and die by 30 hpf (Nakajima et al. 2017). We tried to overcome this by treating our *Yap1* mutants with a low concentration of Taz MO. The resultant fish had decreased, but not absent, levels of Taz protein. However, we found that the PE cluster is still formed in these fish. One possibility could be that even low amounts of Taz is enough to promote PE cluster formation and compensate for the loss of Yap1. For instance, it has been described in retinal development in mice that in *Yap* heterozygous mice

models, depletion of one *Yap* allele leads to transient TAZ compensatory mechanisms at postnatal stages, associated with a gain of function-like phenotype (Masson et al. 2020). However, this hypothesis is very hard to prove since we reached the limit of our model: we need some levels of Taz in order to have viable fish and so we cannot study the consequences of completely deleting the activity of both.

One way to try to answer our question would be to create conditional mutants of *Yap1* or *Taz*. While traditional mutants have a mutation in all cells at all times, conditional mutants allow inactivation of genes in somatic cells in a temporal or tissue specific manner (Maddison, Lu, and Chen 2012). It is still challenging to create zebrafish conditional mutants due to the unavailability of gene targeting techniques for zebrafish embryonic stem cells and the low efficiency of homologous recombination in fertelized zebrafish eggs (Dai et al. 2010; Robles, Martí, and Belmonte 2011). Although challenging, several labs have created conditional mutants restricting expression in a tissue specific manner, for example, Cre lines specific for cardiomyocytes (Jopling et al. 2010) among others. However, this approach would not be suitable for our study. First of all, there are no specific genes only expressed in the PE or epicardium. We could not completely restrict *Yap1* or *Taz* expression only in the PE, other organs of the zebrafish would be affected. For instance, if we used the promoter of one of the most used epicardical markers, *wt1a,* and conditionally mutate genes under this promoter, we would also be affecting kidney development (Perner, Englert, and Bollig 2007). Another issue that we would face is that *Yap1* and *Taz* are necessary for development and double mutants die at 30 hpf (Nakajima et al. 2017). If we tried to restrict Yap1 or Taz expression before the PE cluster is formed, the embryos would most likely not survive. A way to overcome these issues would be to change animal model. In mice conditional mutant are widely available and a conditional line with a double mutation in *Yap1* and *Taz* specifically in epicardial cells already exists (Singh et al. 2016). Although in this paper they already described that this double mutants do not survive, it would be useful for our project to try different conditions with this line and study PE cluster formation.

Another explanation could be that other pathways involved in PE formation are compensating for the loss of Yap1/Taz. Since the heart is essential for survival and the epicardium is key for heart development, it is possible that there exists several signalling pathways to ensure PE cluster formation. These pathways might not be effective when we chemically modify Yap1/Taz-Tead activity because we treat from 36 hpf and it is too late to compensate. For instance, it is known that PE is regulated by BMP signalling (Liu and Stainier 2012) and that endothelial Notch signalling activates bmp expression, inducing PE cluster formation (Andrés-Delgado et al. 2020). In the future, it should be studied if *Yap1* mutants show any differences in Bmp or Notch levels that could explain why they do not have any differences in terms of PE cell number.

Another possibility is that, although we do see some change in PE cluster formation after drug treatment targeting Yap1/Taz-Tead activity, this pathway is not essential for PE cluster formation and it would have more importance at later points of epicardial development. For instance, it is known that epicardial cells undergo EMT transition and give rise to non-myocardial cardiac cells. It is possible that PE cells activate Yap1 when they acquire their identity but Yap1 function is not relevant until after the cells are attached to the myocardium. However, to prove this hypothesis we face the same issues as before – we cannot completely delete Yap1 and Taz as double mutants die at early time points.

Previously it has been described that cells from the DP collectively move towards the DP midline, where the cluster will be formed (Andrés-Delgado et al. 2019). In this same paper they propose a model in which Bmp promotes actin polymerization leading to PE formation. Our hypothesis that Yap1/Taz-Tead activity is involved in PE cluster formation is compatible with this model. Yap1/Taz are known mechanosensors that can respond to F-actin polymerization, as it has been seen that triggering F-actin polymerization promoted Yap1/Taz activity (Dupont et al. 2011). It is possible that the promotion of actin polymerization, as well as the reduction in cell area that cells in the DP midline experience, increases Yap1/Taz-Tead activity.

Finally, we also describe a new possible regulator for PE cluster formation*, lkb1*. *In vitro* it has been described that it inhibits Yap1 nuclear translocation (Mohseni et al. 2014). We show that *lkb1* mutants have bigger clusters at later points of proepicardial formation. At 55 hpf there are no differences between controls and mutants. However, at 72 hpf *lkb1* mutants have increased PE cell number compared to controls. Since epicardial cell number is not changed, it could mean that time of cell extrusion from the DP is increased. However, further studies about the role of *lkb1* during PE cluster formation should be done.

In summary, our study reports specific Yap1/Taz-Tead activation during PE cells. Further studies are needed to understand the exact function of this pathway during PE formation.

Discussion en français

Dans ce chapitre, nous étudions l'activité de Yap1/Taz-Tead pendant la formation du PE. Nous décrivons l'activité *in vivo* de Yap1/Taz-Tead dans le cœur de 36 hpf à 55 hpf en utilisant la lignée rapporteur *4xGTIIC:d2GFP*. Nous constatons que la GFP est exprimée spécifiquement dans le PE. De plus, l'expression de la GFP est présente avant l'extrusion des cellules PE vers la cavité proépicardique, ce qui suggère qu'elle est impliquée d'une manière ou d'une autre dans la formation du PE.

Les cellules PE changent de forme, passant d'une forme plate à ronde, en rompant leurs adhésions cellulaires. Bien que ce processus ne soit pas une transition épithéliale à mésenchymateuse (EMT) complète, il présente de nombreuses similitudes (Andrés-Delgado et al. 2019). De plus, les cellules PE expriment *twist1a* (Peralta 2014), un facteur de transcription bHLH impliqué dans l'EMT et un régulateur de la spécification et de la différenciation des lignées (Lamouille, Xu et Derynck 2014). Il est également intéressant de mentionner que Yap a été décrit comme un promoteur de l'EMT dans plusieurs cancers, comme le cancer colorectal (Cheng et al. 2020). *In vitro*, il a également été observé que les réponses médiées par Yap aux changements dans l'organisation de l'ECM favorisent l'EMT (Park et al. 2019). Cela serait cohérent avec un modèle dans lequel l'activité de Yap1/ Taz-Tead favorise la formation du PE: Yap1/Taz-Tead

est actif dans les cellules DP dès les premiers stades et ces cellules vont s'extruder, dans un processus de type EMT, pour former le PE.

Dans notre chapitre, nous montrons que la modification de l'activité de Yap1/Taz-Tead à l'aide de médicaments entraîne une dérégulation du processus de formation du PE: une augmentation de l'activité de Yap1/Taz-Tead entraîne une augmentation du nombre de cellules PE, tandis qu'une diminution entraîne une diminution du nombre de cellules PE. Tout ceci suggère que l'activité de Yap1/Taz-Tead favorise l'aquisition de l'identité des cellules de type PE. Ceci est cohérent avec ce qui a été publié précédemment dans le domaine. Il a été publié que les protéines du complexe B de l'IFT inhibent l'activité de Yap1 pendant la formation des PE et que l'absence d'IFT88 entraîne une augmentation des cellules du PE (Peralta et al. 2020). Il a également été démontré que les protéines Motin régulent la formation du PE. Chez le poisson zèbre, les protéines Amot se lient à Yap/Taz dans le cytoplasme en le séquestrant (Agarwala et al. 2015). Les mutants Amotl2a, qui auraient une augmentation de Yap1/Taz au niveau nucléaire, ont de PE plus grands (Peralta et al. 2020). Cependant, bien que lorsque nous diminuons chimiquement l'activité de Yap1/Taz-Tead chez le poisson zèbre, nous obtenons un PE plus petit, nous ne voyons pas les mêmes résultats chez les mutants *Yap1* ou les mutants *Yap1* et les morphants *Taz*.

Cela pourrait être dû à différents événements. Dans notre experience, nous n'avons pas complètement éliminé Taz du système. Les mutants doubles pour *Yap1/Taz* présentent de graves défauts de développement et meurent avant 30 hpf (Nakajima et al. 2017). Nous avons essayé de surmonter ce problème en traitant nos mutants *Yap1* avec une faible concentration de *Taz* MO. Les poissons résultants présentaient des niveaux diminués, mais pas absents, de protéine Taz. Cependant, nous avons constaté que le PE est toujours formé chez ces poissons. Une possibilité pourrait être que même de faibles quantités de Taz sont suffisantes pour promouvoir la formation du PE et compenser la perte de Yap1. Par exemple, il a été décrit dans le développement de la rétine chez la souris que dans les modèles de souris hétérozygotes Yap, la déplétion d'un allèle Yap entraîne des mécanismes compensatoires TAZ transitoires aux stades postnatals, associés à un phénotype de type gain de fonction (Masson

et al. 2020). Cependant, cette hypothèse est très difficile à prouver car nous avons atteint la límite de notre modèle: nous avons besoin de certains niveaux de Taz pour avoir des poissons viables et nous ne pouvons donc pas étudier les conséquences de la suppression totale de l'activité des deux.

Une façon d'essayer de répondre à notre question serait de créer des mutants conditionnels de *Yap1* ou de *Taz*. Alors que les mutants traditionnels présentent une mutation dans toutes les cellules à tout moment, les mutants conditionnels permettent l'inactivation de gènes dans les cellules somatiques d'une manière temporelle ou tissulaire spécifique (Maddison, Lu et Chen 2012). Il est encore difficile de créer des mutants conditionnels de poisson zèbre en raison de l'indisponibilité de techniques de ciblage de gènes pour les cellules souches embryonnaires de poisson zèbre et de la faible efficacité de la recombinaison homologue dans les œufs de poisson zèbre fertilisés (Dai et al. 20 10 ; Robles, Martí et Belmonte 2011). Bien qu'il s'agisse d'un défi, plusieurs laboratoires ont créé des mutants conditionnels limitant l'expression d'une manière spécifique aux tissus, par exemple, des lignées Cre spécifiques aux cardiomyocytes (Jopling et al. 2010), entre autres. Cependant, cette approche ne serait pas adaptée à notre étude. Tout d'abord, il n'existe pas de gènes spécifiques expresées uniquement dans le PE ou l'épicarde. Nous ne pourrions pas restreindre complètement l'expression de *Yap1* ou *Taz* uniquement dans le PE, d'autres organes du poisson zèbre seraient affectés. Par exemple, si nous utilisons le promoteur de l'un des marqueurs épicardiques les plus utilisés, *wt1a*, et que nous mutons conditionnellement les gènes sous ce promoteur, nous affecterions également le développement des reins (Perner, Englert et Bollig 2007). Un autre problème auquel nous serions confrontés est que Yap1 et Taz sont nécessaires au développement et que les doubles mutants meurent à 30 hpf (Nakajima et al. 2017). Si nous essayions de restreindre l'expression de *Yap1* ou de *Taz* avant la formation du PE, les embryons ne survivraient probablement pas. Un moyen de surmonter ces problèmes serait de changer de modèle animal. Chez la souris, les mutants conditionnels sont largement disponibles et une lignée conditionnelle avec une double mutation de *Yap1* et *Taz* spécifiquement dans les cellules épicardiques existe déjà (Singh et al. 2016). Bien que dans cet article ils décrivent déjà que ces doubles mutants ne

survivent pas, il serait utile pour notre projet d'essayer différentes conditions avec cette lignée et d'étudier la formation du PE.

Une autre explication pourrait être que d'autres voies impliquées dans la formation du PE compensent la perte de Yap1/Taz. Comme le cœur est essentiel à la survie et que l'épicarde est la clé du développement du cœur, il est possible qu'il existe plusieurs voies de signalisation pour assurer la formation du PE. Ces voies pourraient ne pas être efficaces lorsque nous modifions chimiquement l'activité de Yap1/Taz-Tead car nous traitons à partir de 36 hpf et il est trop tard pour compenser. Par exemple, il est connu que le PE est régulé par la signalisation BMP (Liu et Stainier 2012) et que la signalisation Notch endothéliale active l'expression de bmp, induisant la formation du PE (Andrés-Delgado et al. 2020). À l'avenir, il faudrait étudier si les mutants *Yap1* présentent des différences dans les niveaux de Bmp ou de Notch qui pourraient expliquer pourquoi ils ne présentent pas de différences en termes de nombre de cellules PE.

Une autre possibilité est que, bien que nous observions un certain changement dans la formation du PE après un traitement médicamenteux ciblant l'activité de Yap1/Taz-Tead, cette voie n'est pas essentielle pour la formation du PE et elle aurait plus d'importance à des moments ultérieurs du développement épicardique. Par exemple, il est connu que les cellules épicardiques subissent une transition EMT et donnent naissance à des cellules cardiaques non myocardiques. Il est possible que les cellules PE activent Yap1 lorsqu'elles acquièrent leur identité mais que la fonction de Yap1 ne soit pertinente qu'après la fixation des cellules au myocarde. Cependant, pour prouver cette hypothèse, nous sommes confrontés aux mêmes problèmes que précédemment - nous ne pouvons pas supprimer complètement Yap1 et Taz car les mutants doubles meurent à des moments précoces.

Auparavant, il a été décrit que les cellules du DP se déplacent collectivement vers la ligne médiane du DP, où le cluster sera formé (Andrés-Delgado et al. 2019). Dans ce même article, ils proposent un modèle dans lequel Bmp favorise la polymérisation de l'actine conduisant à la formation du PE. Notre hypothèse selon laquelle l'activité de Yap1/Taz-Tead est impliquée dans la

formation du PE est compatible avec ce modèle. Yap1/Taz sont des mécanosenseurs connus qui peuvent répondre à la polymérisation de la F-actine, car il a été vu que le déclenchement de la polymérisation de la F-actine favorisait l'activité de Yap1/Taz (Dupont et al. 2011). Il est possible que la promotion de la polymérisation de l'actine, ainsi que la réduction de la surface cellulaire que subissent les cellules de la ligne médiane DP, augmente l'activité de Yap1/Taz-Tead.

Enfin, nous décrivons également un nouveau régulateur possible de la formation du PE, lkb1. *In vitro*, il a été décrit qu'il inhibe la translocation nucléaire de Yap1 (Mohseni et al. 2014). Nous montrons que les mutants *lkb1* ont de PE plus grands à des points plus tardifs de la formation du proépicarde. A 55 hpf, il n'y a pas de différences entre les contrôles et les mutants. Cependant, à 72 hpf, les mutants *lkb1* ont un nombre accru de cellules PE par rapport aux témoins. Comme le nombre de cellules épicardiques n'est pas modifié, cela pourrait signifier que le temps d'extrusion des cellules du DP est augmenté. Cependant, d'autres études sur le rôle de lkb1 pendant la formation des grappes PE devraient être menées.

En résumé, notre étude rapporte une activation spécifique de Yap1/Taz-Tead au cours des cellules PE. Des études supplémentaires sont nécessaires pour comprendre la fonction exacte de cette voie pendant la formation des PE.

How is PE cluster formation affected by changes in fluid forces?

Preface

In this chapter I present a study on how fluid forces are affecting PE cluster formation. The conceptualization of the project was done by me, Marina Peralta and Julien Vermot. Investigation, data curation and writing of the original draft were done by me.

Préface en français

Dans ce chapitre, je présente une étude sur la façon dont les forces fluides affectent la formation du PE. La conceptualisation du projet a été faite par moi, Marina Peralta et Julien Vermot. La recherche, la conservation des données et la rédaction de la version originale ont été effectuées par moi-même.

Introduction

The heart is the first functional organ to form in the embryo, ensuring a supply of oxygen and nutrients to de developing tissues (Lindsey, Butcher, and Yalcin 2014). The cardiovascular system is constantly subjected to the mechanical forces generated by the beating heart, and changes form considerably during development and disease (Garoffolo and Pesce 2019; Andrés-Delgado and Mercader 2016).

It is known that mechanical forces influence chamber formation, trabeculation, cardiomyocyte proliferation, and valve formation (Granados-Riveron and Brook 2012). However, the role of fluid forces during PE formation remains elusive.

Pericardial advections, formed by the heartbeat, are necessary for the release of PE cells. Moreover, avcPE and vpPE are located in areas of high flow forces (Peralta et al. 2013). However, mutants without heartbeat still form the PE cluster, although it is misplaced (Serluca 2008; Andrés-Delgado et al. 2019).

Since it has been described that subcellular localization and activity of Yap1/Taz can be regulated by cell substrate rigidity, actin cytoskeleton remodelling, and by specific regimens of cell stretching (Low et al. 2014), we thought that specific Yap1/Taz-Tead activity in the DP could be due to mechanical forces caused by heartbeat and this could, in turn, regulate PE cluster formation.

In this chapter we ought to examine further how changes in fluid forces within the pericardial cavity affect PE cluster formation and Yap1/Taz-Tead activity in the dorsal pericardium.

Results

Modifying heartbeat results in affected PE cluster formation

To assess the role of pericardial fluid forces during PE formation, we modified them by treating *4xGTIIC:d2GFP* embryos with drugs that affect the heartbeat.

We treated embryos with caffeine (concentration100 µM) from 50 to 55 hpf, which leads to a nonhomogeneous contraction. Immunohistochemistry experiments performed on caffeine treated embryos and non-treated embryos (Figure 1A) showed that caffeine treatment does not significantly change the number of GFP positive cells in the myocardium or the DP. In caffeine treated embryos there is an increase of PE cluster cells (Figure 1B), as previously published (Peralta et al. 2013). Nevertheless, the number of epicardial cells is not changed between treated embryos and controls, suggesting that caffeine is affecting specifically PE cluster formation.

To further study PE formation when heartbeat is altered, we used isoprenaline, a drug that increases heart rate (Kossack et al. 2017). We treated *4xGTIIC:d2GFP* embryos from 50 to 55 hpf with isoprenaline (concentration 300 µM) and fixed them for imaging (Figure 1F). Isoprenaline treated embryos also have increased PE cluster cell number (Figure 1D) and no differences in terms of epicardial cell number (Figure 1E).

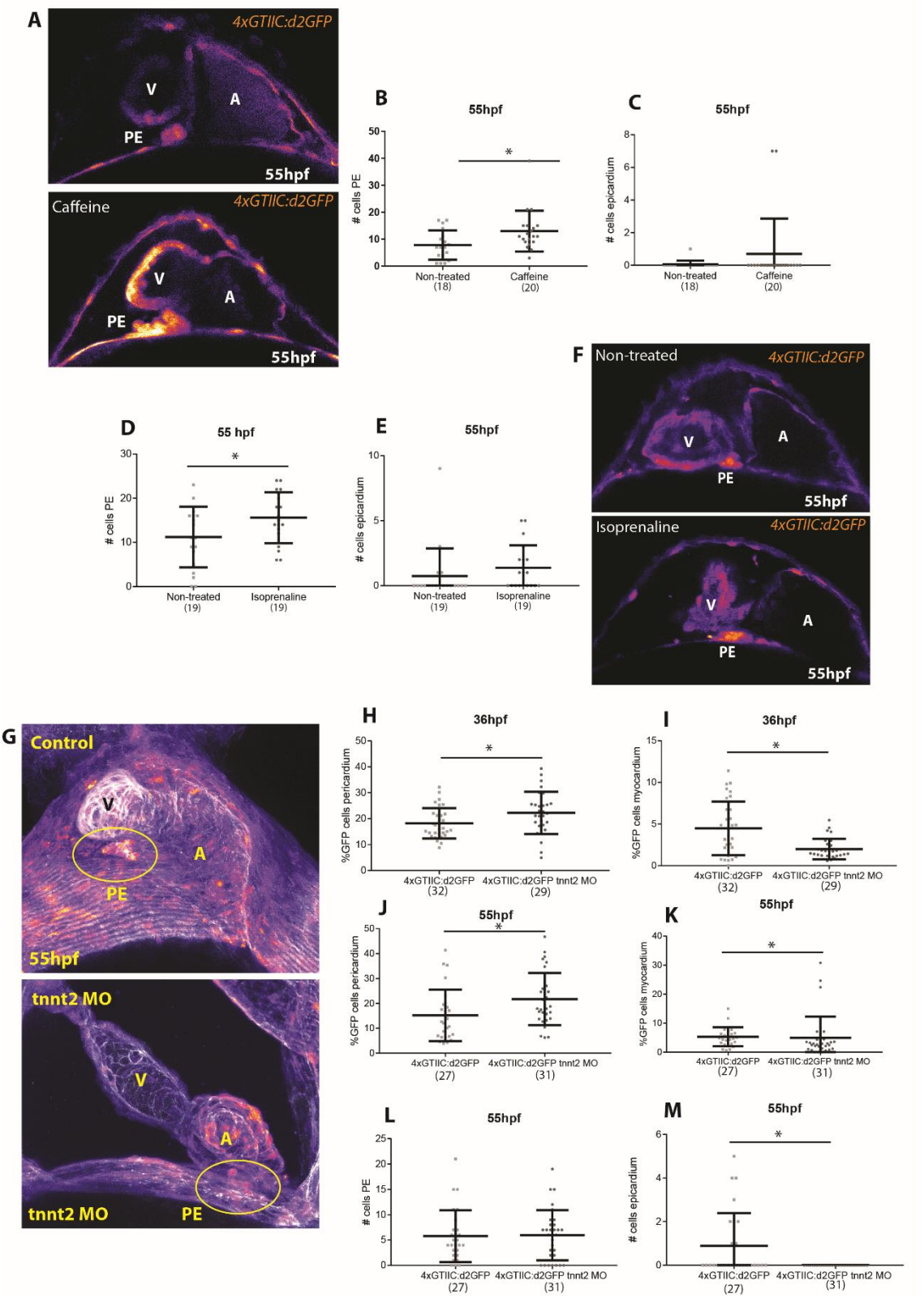

Figure 1. Modifying heartbeat affects PE cluster formation. A. Confocal plane of non-treated and caffeine treated 4xGTIIC:d2GFP embryos at 55hpf. B. Quantification of PE cell number at 55hpf of caffeine treated embryos and non-treated. C. Quantification of epicardial cell number at 55hpf of caffeine treated embryos and non-treated. D.

Quantification of PE cell number at 55hpf of isoprenaline treated embryos and non-treated. E. Quantification of epicardial cell number at 55hpf of isoprenaline treated embryos and non-treated. F. Confocal plane of non-treated and caffeine treated 4xGTIIC:d2GFP embryos at 55hpf. G. Confocal maximum intensity projection of tnnt2a MO and controls 4xGTIIC:d2GFP embryos at 55hpf. H. Quantification of percentage of GFP positive cells in DP at 36hpf of tnnt2a MO and controls. I. Quantification of percentage of GFP positive cells in myocardium at 36hpf of tnnt2a MO and controls. J. Quantification of percentage of GFP positive cells in DP at 55hpf of tnnt2a MO and controls. K. Quantification of percentage of GFP positive cells in myocardium at 55hpf of tnnt2a MO and controls. L. Quantification of PE cells at 55hpf of tnnt2a MO and controls. M. Quantification of epicardial cells at 55hpf of tnnt2a MO and control.

We next sought to study PE formation and Yap1/Taz-Tead activity in models without heartbeat. We injected *tnnt2a*-morpholino (5.8ng concentration) to *4xGTIIC:d2GFP* embryos at the 1 cell stage and fixed them either at 36 or at 55 hpf. At 36 hpf, when there already are GFP positive cells in the DP and the myocardium, we observe that the percentage of GFP positive cells is increased in the DP of the *tnnt2a* morphant (Figure 1H), while it is decreased in the myocardium (Figure 1I). Consistently with what has been previously published, we also see that while the number of PE cluster cells is not significantly different, its position is shifted towards the VP.

Yap1 mutants without heartbeat do not have impaired PE cluster formation

To further study the role of Yap1/Taz-Tead activity in PE cluster formation related to the sensing of mechanical forces, we injected *tnnt2a*-morpholino (5.8ng concentration) to *Yap1-/-:tcf21:nls-GFP* and *Yap1+/+:tcf21:nls-GFP* embryos at the 1 cell stage and fixed them at 55 hpf (Figure 2A). Although heart morphology in *Yap1-/-* and *tnnt2a* morphants seems more affected than in the *tnnt2a* morphants alone, there are no differences in terms of PE cluster number (Figure 2B). As expected, since there are no pericardial advections to transfer PE cells to the myocardium, the tnnt2a MO have significantly less epicardial cells than the controls (Figure 2C).

We conclude that arresting the heartbeat affects Yap1/Taz-Tead activity.

BDM treatment in *4xGTIIC:d2GFP* embryos

Since it has been published that BDM treatment arrests PE cluster formation due to the disruption of the actin-myosin network (Andrés-Delgado et al. 2019), we wanted to check if there were any changes in Yap1/Taz-Tead activity after BDM treatment. To do so, we performed live imaging in *4xGTIIC:d2GFP* embryos. We imaged the embryos starting at 48 or 52 hpf every 15 minutes for 4 hours. We imaged first in fish medium with tricaine and after we added BDM to the medium. We also imaged control fish without treatment starting at the same timepoints, as is explained in figure 2D. To measure changes in Yap1/Taz-Tead activity we measured GFP intensity expressed as CTCF (CTCF = Integrated Density – (Area of selected cell X Mean fluorescence of background readings)) and we plotted the ratio of CTCF of every timepoint compared to the first one. We measured separately the fluorescence intensity in the PE (selecting one plane where the PE cross-section appears largest) and in the pericardium (DP intensity of every fish is an average of 3 different planes) and plotted it through time.

When we start the treatment at 48 hpf (Figure 2E), the changes in GFP intensity are not significantly different between treated and non-treated embryos. Both in the PE and in the DP, the intensity decreases through time (Figure 2G-H).

However, when we start the treatment at 52 hpf (figure 2F), the results are very different. Although it is very variable between fish, after BDM treatment intensity in the PE and the DP increases compared to non-treated embryos (Figure 2I-J).

Overall we see that disrupting the actin-myosin network also results in a change in Yap1/Taz-Tead activity but it is highly dependent on the time of the treatment.

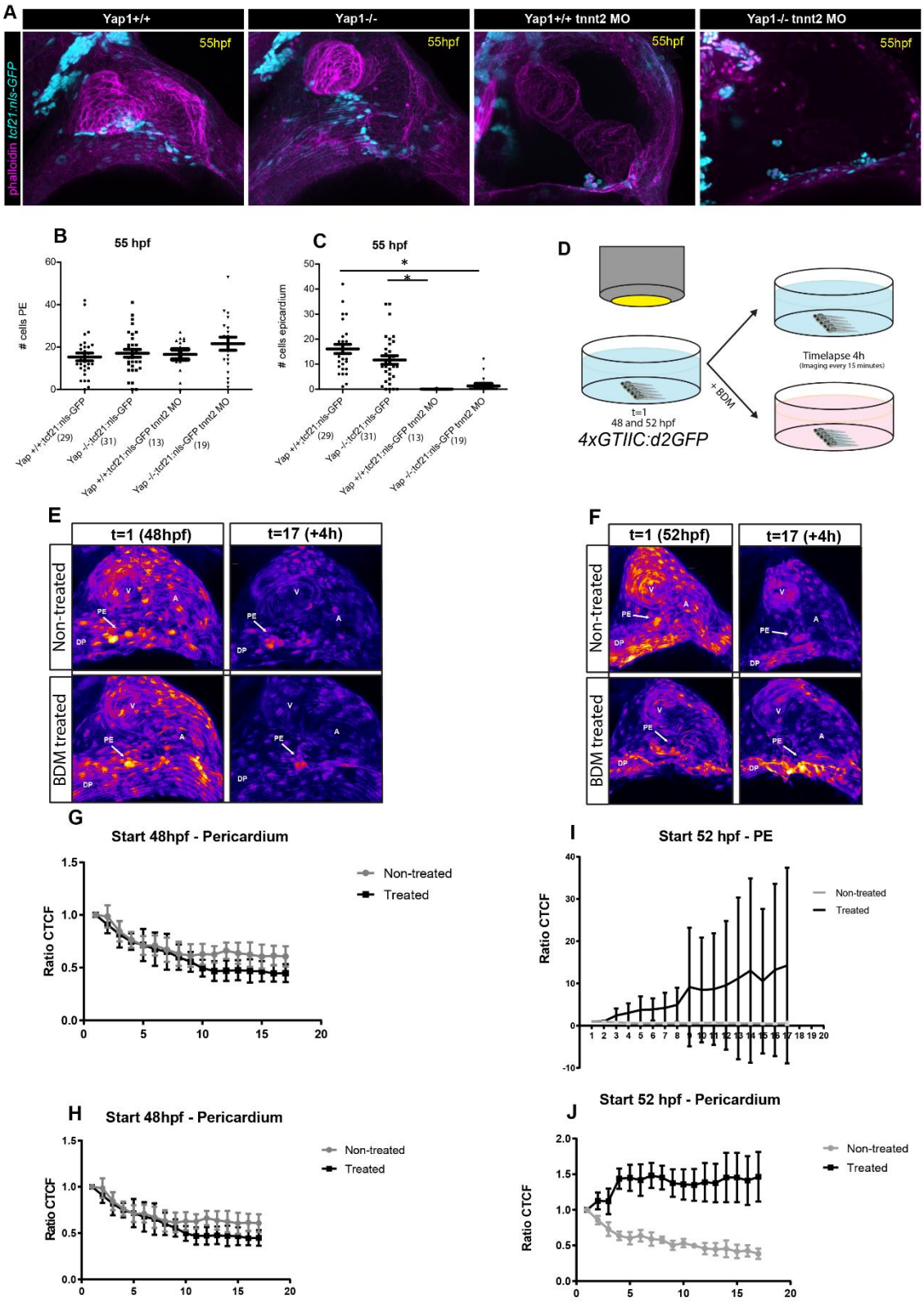

Figure 2. PE cluster in Yap1 injected with tnnt2a MO and changes in 4xGTIIC:d2GFP after BDM treatment. A. Confocal imaging of Yap1 mutants with tnnt2a MO at 55hpf.Maximum intensity projection. B. Quantification of PE cell number in Yap1 mutants, Yap1 injected with tnnt2a MO and controls in tcf21:nls-GFP background at

55hpf. C. Quantification of epicardial cell number in Yap1 mutants, Yap1 injected with tnnt2a MO and controls in tcf21:nls-GFP background at 55hpf. D. Schematic representation of in vivo timelapse imaging after BDM treatment. E. Confocal imaging of a timelapse with 4xGTIIC:d2GFP starting at 48hpf. Maximum intensity projection.1 image per timepoint. F. Confocal imaging of a timelapse with 4xGTIIC:d2GFP starting at 52hpf. Maximum intensity projection.1 image per timepoint. G. Graphic representation of intensity changes through time in the PE cluster starting at 48hpf in controls (n=4) and fish treated with BDM (n=5). Intensity is shown as a ratio of CTCF compared to the first one. H. Graphic representation of intensity changes through time in the DP starting in controls (n=4) and fish treated with BDM (n5) at 48hpf. Intensity is shown as a ratio of CTCF compared to the first one. I. Graphic representation of intensity changes through time in the PE cluster starting in controls (n=4) and fish treated with BDM (n=5) at 52hpf. Intensity is shown as a ratio of CTCF compared to the first one. J. Graphic representation of intensity changes through time in the DP in controls (n=4) and fish treated with BDM (n=5) starting at 52 hpf. Intensity is showed as a ratio of CTCF compared to the first one.

Discussion

In this chapter we explore further the role of heartbeat during PE cluster formation related to Yap1/Taz-Tead activity.

We see that affecting the heartbeat, either increasing the heart rate or arresting the heart, results in changes in Yap1/Taz-Tead activity. This is consistent with the fact that Yap1/Taz are known mechanosensors whose subcellular localization can be regulated by changes in cell stretching, such as the ones caused by heartbeat.

After we treat with caffeine and isoprenaline, two drugs that affect heart beating, we obtain similar results: an increase in PE cell number without changes in epicardial cell number. However, after caffeine treatment, we see an increase in GFP positive cells that we do not see after isoprenaline treatment. Although both drugs act similarly, their consequences in the zebrafish embryo are not exactly the same. Overall these results suggest that a change in heart rate results in a bigger PE cluster. However, it has to be taken into account that these drugs might not be specific and they could be promoting cell extrusion in the DP independently of the heartbeat. One possible experiment to be done in

the future could be to treat fish lacking heartbeat with caffeine and isoprenaline and analyse the changes in *4xGTIIC:d2GFP* fish. If the change in cluster cell size is due to changes in heartbeat, we should not see any difference compared to controls once we eliminate heartbeat. Moreover, although we do not see any change in epicardial cell number, we cannot discard that the cluster increased cell size could be due to a change in cell release.

As it has been previously described, arresting the heart does not affect PE cluster size but it affects PE cluster position. We also describe a general decrease in GFP positive cells in the myocardium and an increase of GFP positive cells in the DP. The decrease in the myocardium could be explained by the fact that cell stretching of myocardial cells due to the heartbeat could be translocating Yap1/Taz to the nuclei. In *tnnt2a* morphants, we lose this cell stretching and consequently also Yap1/Taz-Tead activity. However, we saw an increased number of GFP positive cells in the DP. This could be related to the displacement of the PE cluster. In order to test this hypothesis, one experiment that could be done would be treating *tnnt2a* morphants with drugs that reduce Yap1/Taz-Tead activity, such as XAV939 or Verteporfin. If we do see a decrease in the number of GFP positive cells in the DP after treatment, we could study were is the cluster formed in these embryos and assess if the misplacement is due to the increase of Yap1/Taz-Tead activity in DP cells.

We also wanted to address whether Yap1 would be important to regulate PE formation in embryos that lack heartbeat. Although Yap1 mutants and *tnnt2a* morphants seem to have a stronger phenotype in terms of heart shape as heart morphology is more affected than in *tnnt2a* morphants alone, the PE cluster still forms and there are no significant differences compared to *tnnt2a* morphants.

Finally, we performed *in vivo* imaging of *4xGTIIC:d2GFP* embryos for 4 hours to monitor changes in GFP expression in the heart after BDM treatment. Our results show that changes in Yap1/Taz-Tead activity after BDM treatment are very dependent on the stage of the treatment. Treating embryos starting at 48 hpf does not change significantly Yap1/Taz -Tead activation. However, treating after 52 hpf gives similar results to embryos injected with *Tnnt2a* MO: we see a general increase of GFP intensity in the DP, as well as in the PE cells. It was

previously published that BDM treatment, due to the disruption of the actin-myosin network (Andrés-Delgado et al. 2019), avoids PE cluster formation. In our embryos, an early PE cluster was present already at 48 hpf. We did not see a regression of this initial cluster, but we did see an arrest in cell extrusion: no more cells were incorporated in the cluster after BDM treatment.

Overall, we show that Yap1/Taz-Tead activity is sensitive to changes in heartbeat and that PE cluster formation is affected, either in size or place, when we modify heartbeat. Further studies are needed to deduce how mechanical forces are regulating PE cluster formation.

Discussion en français

Dans ce chapitre, nous explorons plus avant le rôle du rythme cardiaque pendant la formation du PE en relation avec l'activité de Yap1/Taz-Tead.

Nous constatons que le fait d'affecter le rythme cardiaque, que ce soit en augmentant la fréquence cardiaque ou en arrêtant le cœur, entraîne des changements dans l'activité de Yap1/Taz-Tead. Ceci est cohérent avec le fait que Yap1/Taz sont des mécanosenseurs connus dont la localisation subcellulaire peut être régulée par des changements dans l'étirement des cellules, tels que ceux provoqués par les battements cardiaques.

Après avoir traité avec de la caféine et de l'isoprénaline, deux médicaments qui affectent les battements du cœur, nous obtenons des résultats similaires: une augmentation du nombre de cellules PE sans changement du nombre de cellules épicardiques. Cependant, après le traitement à la caféine, nous constatons une augmentation des cellules positives pour la GFP que nous ne voyons pas après le traitement à l'isoprénaline. Bien que les deux médicaments agissent de manière similaire, leurs conséquences dans l'embryon de poisson zèbre ne sont pas exactement les mêmes. Dans l'ensemble, ces résultats suggèrent qu'une modification de la fréquence cardiaque entraîne une augmentation du nombre de cellules PE. Cependant, il faut tenir compte du fait que ces médicaments ne sont peut-être pas spécifiques et qu'ils pourraient favoriser l'extrusion des cellules dans le PE indépendamment du rythme cardiaque. Une expérience possible à réaliser dans le futur pourrait être de traiter des poissons sans rythme cardiaque avec de la caféine et de

l'isoprénaline et d'analyser les changements chez les poissons *4xGTIIC:d2GFP*. Si le changement de la taille du PE est dû aux changements du rythme cardiaque, nous ne devrions pas voir de différence par rapport aux contrôles une fois que nous avons éliminé le rythme cardiaque. De plus, bien que nous n'observions aucun changement dans le nombre de cellules épicardiques, nous ne pouvons pas exclure que l'augmentation de les cellules du PE puisse être due à un changement dans la libération des cellules.

Comme cela a été décrit précédemment, l'arrêt du cœur n'affecte pas le nombre des cellules du PE mais il affecte la position du PE. Nous décrivons également une diminution générale des cellules positives pour la GFP dans le myocarde et une augmentation des cellules positives pour la GFP dans le DP. La diminution dans le myocarde pourrait être expliquée par le fait que l'étirement des cellules du myocarde dû aux battements du cœur pourrait transloquer Yap1/Taz vers les noyaux. Chez les morphants *tnnt2a*, nous perdons cet étirement cellulaire et par conséquent aussi l'activité Yap1/Taz-Tead. Cependant, nous avons observé un nombre accru de cellules positives pour la GFP dans le DP. Ceci pourrait être lié au déplacement du PE. Afin de tester cette hypothèse, une expérience qui pourrait être réalisée serait de traiter les morphants *tnnt2a* avec des médicaments qui réduisent l'activité de Yap1/Taz-Tead, tels que XAV939 ou Verteporfin. Si nous constatons une diminution du nombre de cellules positives pour la GFP dans le DP après le traitement, nous pourrions étudier où se forme le PE dans ces embryons et évaluer si le mauvais placement est dû à l'augmentation de l'activité Yap1/Taz-Tead dans les cellules du DP.

Nous avons également voulu savoir si Yap1 serait important pour réguler la formation du PE dans les embryons dépourvus de battements cardiaques. Bien que les mutants *Yap1* et les morphants *tnnt2a* semblent avoir un phénotype plus fort en termes de forme du cœur, la morphologie du cœur étant plus affectée que chez les morphants *tnnt2a* seuls, le groupe PE se forme toujours et il n'y a pas de différences significatives par rapport aux morphants *tnnt2a*.

Enfin, nous avons réalisé une imagerie in vivo d'embryons *4xGTIIC:d2GFP* pendant 4 heures pour suivre les changements de l'expression de la GFP dans

le cœur après le traitement par BDM. Nos résultats montrent que les changements de l'activité de Yap1/Taz-Tead après le traitement BDM sont très dépendants du stade du traitement. Le traitement des embryons à partir de 48 hpf ne change pas significativement l'activation de Yap1/Taz-Tead. Cependant, le traitement après 52 hpf donne des résultats similaires à ceux des embryons injectés avec la MO *Tnnt2a*: on observe une augmentation générale de l'intensité de la GFP dans les cellules DP, ainsi que dans les cellules PE. Il a été publié précédemment que le traitement par BDM, en raison de la perturbation du réseau actine-myosine (Andrés-Delgado et al. 2019), évite la formation du PE. Chez nos embryons, un PE précoce était déjà présent à 48 hpf. Nous n'avons pas observé de régression de ce cluster initial, mais nous avons constaté un arrêt de l'extrusion cellulaire: plus aucune cellule n'était incorporée dans le cluster après le traitement par BDM.

Dans l'ensemble, nous montrons que l'activité de Yap1/Taz-Tead est sensible aux changements du rythme cardiaque et que la formation du PE est affectée, que ce soit en taille ou en lieu, lorsque nous modifions le rythme cardiaque. D'autres études sont nécessaires pour déduire comment les forces mécaniques régulent la formation du PE.

Looking for possible mechanoregulators of PE cluster formation

Preface

In this chapter we assess the role of several known mechanosensors in PE cluster formation. The conceptualization of the project was done by me, Marina Peralta and Julien Vermot. Investigation, data curation and writing of the original draft were done by me.

Preface en français

Dans ce chapitre, nous évaluons le rôle de plusieurs mécanosenseurs connus dans la formation du PE. La conceptualisation du projet a été faite par moi, Marina Peralta et Julien Vermot. La recherche, la conservation des données et la rédaction de la version originale ont été effectuées par moi-même.

Introduction

Mechanical forces play a big role during heart development: the heartbeat, as well as the blood flow, regulate cell behaviour in the cardiac system (Andrés-Delgado and Mercader 2016). As we showed in the last chapter, changes in mechanical forces in the heart can also affect PE cluster formation.

Mechanical forces are sensed by cells via mechanosensors, which induce downstream signalling cascades. It is likely that different types of cells use different mechanisms and that multiple mechanisms are working together to sense and respond to mechanical forces (Trubelja and Bao 2018). Some known mechanosensors are cilia, integrin signalling components, cell membrane receptor kinases, stretch-sensitive ion channels, intercellular junction proteins, and membrane lipids (Lyon et al. 2015; Andrés-Delgado and Mercader 2016).

In this chapter we chose some of these already known mechanosensors and evaluated if their disruption affected PE cluster formation.

Results

Primary cilia during PE cluster formation

It has been previously published that *iguana* mutants, which lack Dzip protein located in the basal body and subsequently also lack primary cilia, have smaller PE clusters compared to controls (Peralta et al. 2020). Moreover, in the context of epidermis development in mice, cilia presence stimulates canonical Notch

signalling (Ezratty et al. 2011). Since Notch is also involved in PE cluster formation (Andrés-Delgado et al. 2020) and cilia number in the DP where the cluster is formed is higher than in other areas (Peralta et al. 2020), we wanted to further study which role could primary cilia have during this process.

First of all we sought to investigate the role of Yap1/Taz-Tead signalling in early steps of development in *iguana* mutants to investigate if the reduced cluster size is due to changes in Yap1/Taz-Tead activity. We crossed *iguana* mutants with the reporter line *4xGTIIC:d2GFP* and analysed them at 36 hpf. We did not see any change in terms of the percentage of GFP positive cells in the pericardium (Figure 1B) or the pericardium (Figure 1C).

Next, we studied two different mutants to investigate further the possible role of primary cilia in PE cluster formation: *Kif3a* and *Pkd2* mutants (its position in the primary cilia is shown in figure 1A).

Kinesin family member 3A (Kif3a) is the ciliary kinase part of the anterograde IFT kinesin motor, required for ciliogenesis (Sipe and Lu 2011). Mutations in *Kif3a* cause embryonic lethality (Marszalek et al. 1999) and typical phenotypes of ciliogenesis defects, such as curved body axis. Consistently, mutant embryos lack cilia in the nasal pit, lateral line, spinal canal, and the kidney. In other organs of the embryos, cilia were still present but in a decreased number and some of these cilia were shorter than in wild type (Pooranachandran and Malicki 2016).

We studied *Kif3a-/-;epi:GFP* and controls at 55 hpf. We performed immunohistochemistry analysis by counting the number of cells in the PE and in the epicardium (Figure 1B-C). We did not detect any significant differences between controls and mutants.

Pkd2 is a calcium-sensitive cation channel located in the cilia. Calcium signalling depends on Pkd2 in several ciliated structures, such as the left-right organizer or kidney epithelial cells (Schottenfeld, Sullivan-Brown, and Burdine 2007). It has been suggested that Pkd2 is mechanosensor in endothelial cells (Goetz et al. 2014).

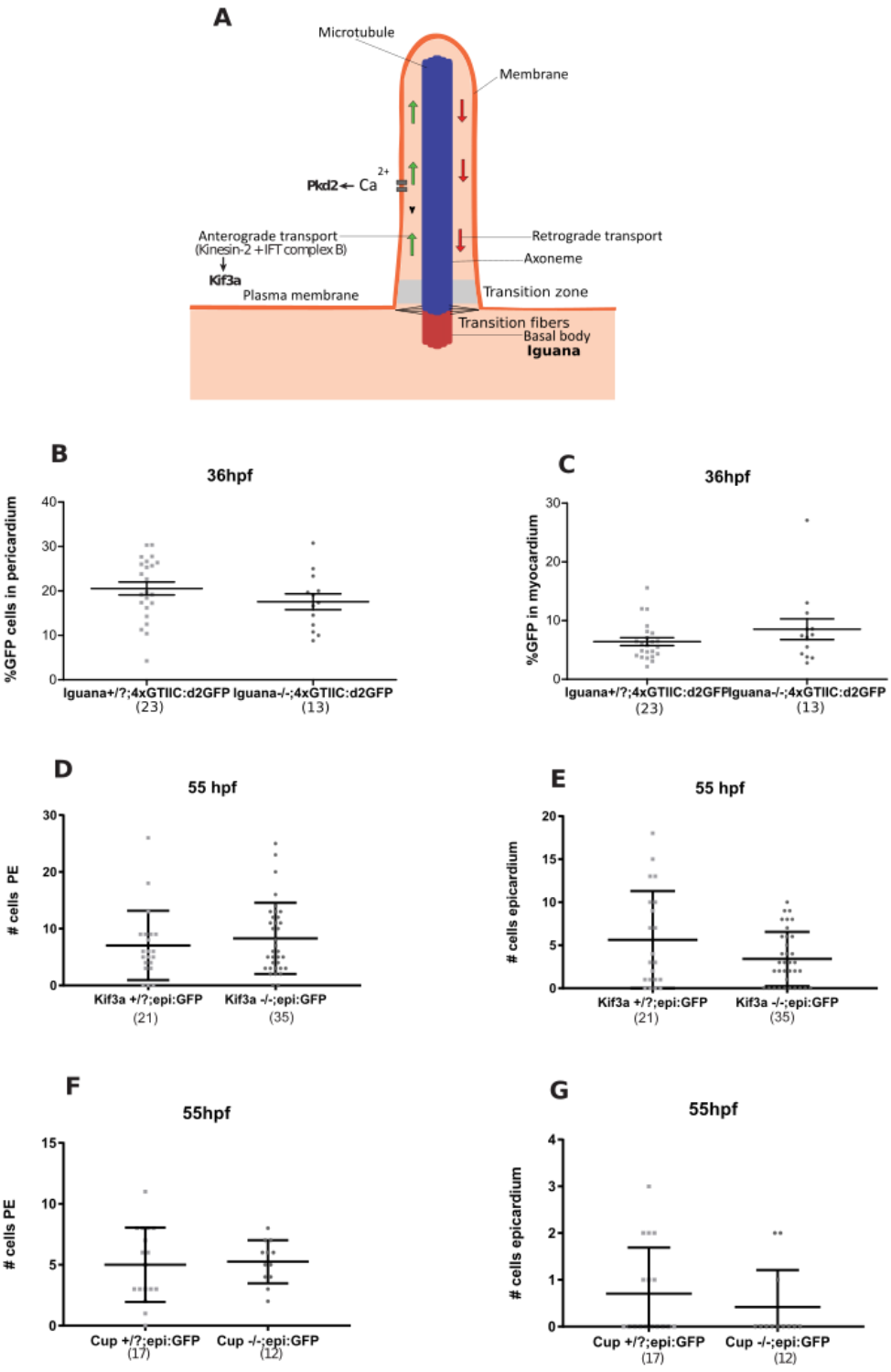

Figure 1. Study of PE cluster in mutants with primary cilia defects. A. Schematic representation of a primary cilia showing the localization of Pkd2, Kif3a, and Iguana. B. Percentage of GFP positive cells in the pericardium in iguana mutants and controls in 4xGTIIC:d2GFP background at 36 hpf. C. Percentage of GFP positive cells in the myocardium in iguana mutants and controls in 4xGTIIC:d2GFP background at 36 hpf. D. Quantification of PE cell number in Kif3a mutants and controls at 55 hpf. E.

Quantification of epicardial cell number in Kif3a mutants and controls at 55 hpf. F. Quantification of PE cell number in Cup mutants and controls at 55 hpf. G. Quantification of epicardial cell number in Cup mutants and controls at 55 hpf.

In zebrafish, *Pkd2* mutants are also known as *Curly* up or *Cup* mutants (Schottenfeld, Sullivan-Brown, and Burdine 2007). In order to assess the possible role of Pkd2 during PE cluster formation, we used the same protocol as with the *Kif3a* mutants and counted to the number of PE and epicardial cells in *Cup-/-;epi:GFP* and controls. We found again that there is no significant difference between mutants and controls (Figure 1D-E).

Klf2a/b during PE cluster formation

Klf2a/b are flow-responsive transcription factors that become expressed in the zebrafish heart at 36 hpf (Vermot et al. 2009). Endothelial klf2a expression has been shown to be flow-dependent and knockdown by antisense morpholino affects cardiac valve development (Steed et al. 2016). Since pericardial cells are exposed to flow within the pericardial cavity, we investigated the role of Klf2a/b during PE formation. We used *klf2a* and *klf2b* double mutants and performed live imaging to determine if these mutants have PE clusters (Figure 2A). *klf2a* and *klf2b* double mutants presented no differences in terms of PE cluster presence (Figure 2B). We conclude that klf2a and klf2b have not a major role in the regulation of the PE cluster formation.

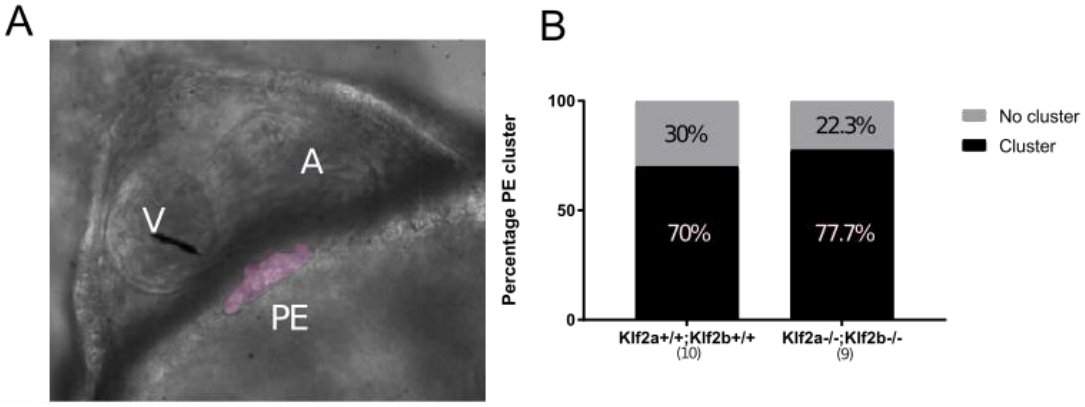

Figure 2. Study of PE cluster in Klf2a/b mutants. A. Brightfield image of zebrafish heart. PE masked in pink. B. Percentage of PE cluster presence in Klf2a/b mutants and controls.

Discussion

In this chapter, we assessed the role of several known mechanosensors in the regulation of PE cluster formation.

Since primary cilia are important mechanosensors involved in different steps of development (R Ferreira et al. 2019), we studied further its role in PE cluster formation. Since *iguana* mutants have reduced PE cluster size and it has been seen than Verteporfin and XAV939 treatment, two drugs that inhibit Yap1/Taz-Tead activity, results in a similar phenotype, we studied Yap1/Taz-Tead activity at early developmental timepoints. However, we do not see a decrease in Yap1/Taz-Tead activity, so we must conclude that the reduced size of PE in these mutants is not due to a decrease in Yap1/Taz-Tead.

We further studied the role of primary cilia in this process by investigating PE cluster size in *Kif3a* mutants, which lack primary cilia, and *Pkd2* mutants. Pkd2 is a known mechanosensor in endothelial cells and endocardial cells during valve morphogenesis (Goetz et al. 2014; Heckel et al. 2015). We did not see any change in terms of PE cluster formation. Although there mechanosensors are not involved in PE cluster formation, since *iguana* mutants have smaller cluster size, we cannot conclude that primary cilia are not important for PE cluster formation. *Iguana* encodes for Dzip1, a zinc-finger protein required for the proper regulation of Hedgehog signalling (Sekimizu et al. 2004). Further studies should be made to determine if the *iguana* mutant phenotype is due to the lack of primary cilia or due to misregulation of the Hedgehog signalling pathway. Furthermore, since epicardial regeneration can be regulated by Hedgehog signalling, it would be interesting to further analyse if Hedgehog signalling has an important role also during earlier steps of epicardial formation when the PE cluster is being formed.

Finally, we also conclude that Klf2a/b are not relevant for PE cluster formation.

Although we did not find any new mechanosensors involved in PE cluster formation, there are still many other mechanosensors that have not been studied and more should be done in the future to understand why PE cluster formation is sensitive to mechanical forces and how DP cells sense these changes and differentiate to form epicardial precursor cells.

Discussion en français

Dans ce chapitre, nous avons évalué le rôle de plusieurs mécanosenseurs connus dans la régulation de la formation du PE.

Les cils primaires étant d'importants mécanosenseurs impliqués dans différentes étapes du développement (R. Ferreira et al. 2019), nous avons étudié plus avant leur rôle dans la formation du PE. Puisque les mutants d'iguane ont une taille réduite du PE et qu'il a été vu que le traitement par Verteporfin et XAV939, deux médicaments qui inhibent l'activité de Yap1/Taz-Tead, entraîne un phénotype similaire, nous avons étudié l'activité de Yap1/Taz-Tead à des points de temps précoces du développement. Cependant, nous ne constatons pas de diminution de l'activité de Yap1/Taz-Tead, nous devons donc conclure que la taille réduite du PE chez ces mutants n'est pas due à une diminution de Yap1/Taz-Tead.

Nous avons étudié plus avant le rôle des cils primaires dans ce processus en examinant la taille du PE chez les mutants *Kif3a*, qui sont dépourvus de cils primaires, et chez les mutants *Pkd2*. Pkd2 est un mécanosenseur connu dans les cellules endothéliales et les cellules endocardiques pendant la morphogenèse des valves (Goetz et al. 2014 ; Heckel et al. 2015). Nous n'avons pas observé de changement en termes de formation du PE. Bien que les mécanosenseurs ne soient pas impliqués dans la formation du PE, puisque les mutants d'iguana ont une taille de PE plus petite, nous ne pouvons pas conclure que les cils primaires ne sont pas importants pour la formation du PE. Iguana code pour Dzip1, une protéine à doigts de zinc nécessaire à la régulation correcte de la signalisation Hedgehog (Sekimizu et al. 2004). D'autres études devraient être menées pour déterminer si le phénotype mutant d'iguana est dû à l'absence de cils primaires ou à une mauvaise régulation de la voie de signalisation Hedgehog. De plus, étant donné que la régénération épicardique peut être régulée par la signalisation Hedgehog, il serait intéressant d'analyser plus en détail si la signalisation Hedgehog joue un rôle important également au cours des premières étapes de la formation épicardique, lorsque le PE est en cours de formation.

Enfin, nous concluons également que Klf2a/b ne sont pas nécessaire pour la formation du PE.

Bien que nous n'ayons pas trouvé de nouveaux mécanosenseurs impliqués dans la formation du PE, il existe encore de nombreux autres mécanosenseurs qui n'ont pas été étudiés et il faudrait faire davantage à l'avenir pour comprendre pourquoi la formation du PE est sensible aux forces mécaniques et comment les cellules DP détectent ces changements et se différencient pour former des cellules précurseurs épicardiques.

Final discussion

In this thesis we provide new studies about PE cluster formation, focusing on the role of Yap1/Taz-Tead activity during this process.

First, we created a protocol for in vivo imaging using the DLS, which allows us to follow zebrafish heart development.

Next, I participated in the paper “Intraflagellar Transport Complex B Proteins Regulate the Hippo Effector Yap1 during Cardiogenesis”, were we prove for the first time that IFTB proteins can regulate Yap1-Tead activity through BMP signalling independently of cilia. This restricts proepicardial and myocardial development. Every day new functions for ciliary proteins are being discovered and we found a novel role forIFTB proteins.

We also described Yap1/Taz-Tead activity through all the process of PE cluster formation. Using *in vivo* and fixed imaging, we show that Yap1/Taz-Tead is active before PE cells extrude from the DP and how this activity is maintained when cells are already attached to the myocardium. Currently, many details about PE cluster formation remain elusive. In this thesis we propose Yap1/Taz-Tead activity as a new pathway involved in epicardial development and cell identity.

Although we do see a change in PE cluster formation when we modify Yap1/Taz-Tead activity using drugs, we do not obtain the same results when we study Yap1 mutants injected with Taz MO. Consequently, we cannot conclude that Yap1/Taz-Tead activity leads to PE cluster formation. However, it should be noted that this activity is specific to PE cluster cells and that it is not possible to completely eliminate Yap1 and Taz in our model since this would cause embryonic death. More studies should be done to try to decipher Yap1/Taz role in epicardial development.

Following previous studies (Peralta et al. 2013), we also investigated further the role of mechanical forces in PE cluster formation and tried to find mechanosensors involved in this process. We do show that changing fluid forces in the pericardial cavity affect PE cluster formation, either changing its size or its position, and Yap1/Taz-Tead signalling. However, we did not find new mechanosensors involved in this process.

The epicardial layer is key for proper heart function and it has been widely ignored until recent studies. In this thesis we present an exhaustive study of PE cluster formation in zebrafish, focusing in Yap1/Taz-Tead activity. We hope that this thesis helps to further our knowledge of PE cluster formation. Although we were unable to pinpoint Yap1/Taz-Tead function or find new regulators involved in PE cluster formation, we hope that our results will help to redirect future studies about PE cluster formation.

Discussion finale

Dans cette thèse, nous fournissons de nouvelles études sur la formation du PE, en nous concentrant sur le rôle de l'activité de Yap1/Taz-Tead pendant ce processus.

Tout d'abord, nous avons créé un protocole d'imagerie in vivo utilisant le DLS, qui nous permet de suivre le développement du cœur du poisson zèbre.

Ensuite, j'ai participé à l'article "Intraflagellar Transport Complex B Proteins Regulate the Hippo Effector Yap1 during Cardiogenesis", où nous prouvons pour la première fois que les protéines IFTB peuvent réguler l'activité de Yap1-Tead par la signalisation BMP indépendamment des cils. Cela limite le développement proépicardique et myocardique. Chaque jour, de nouvelles fonctions pour les protéines ciliaires sont découvertes et nous avons trouvé un nouveau rôle pour les protéines IFTB.

Nous avons également décrit l'activité de Yap1/Taz-Tead tout au long du processus de formation du PE. En utilisant l'imagerie in vivo et fixe, nous montrons que Yap1/Taz-Tead est actif avant que les cellules PE n'extrudent du DP et comment cette activité est maintenue lorsque les cellules sont déjà attachées au myocarde. Actuellement, de nombreux détails sur la formation du PE restent insaisissables. Dans cette thèse, nous proposons l'activité de Yap1/Taz-Tead comme une nouvelle voie impliquée dans le développement épicardique et l'identité cellulaire.

Bien que nous observions un changement dans la formation du PE lorsque nous modifions l'activité Yap1/Taz-Tead à l'aide de médicaments, nous n'obtenons pas les mêmes résultats lorsque nous étudions des mutants *Yap1* injectés avec la MO Taz. Par conséquent, nous ne pouvons pas conclure que l'activité Yap1/Taz-Tead entraîne la formation du PE. Cependant, il faut noter que cette activité est spécifique aux cellules du PE et qu'il n'est pas possible d'éliminer complètement Yap1 et Taz dans notre modèle car cela provoquerait la mort embryonnaire. D'autres études devraient être menées pour essayer de déchiffrer le rôle de Yap1/Taz dans le développement épicardique.

Suite à des études précédentes (Peralta et al. 2013), nous avons également étudié le rôle des forces mécaniques dans la formation du PE et essayé de

trouver des mécanosenseurs impliqués dans ce processus. Nous montrons que le changement des forces fluides dans la cavité péricardique affecte la formation du PE, soit en changeant leur taille ou leur position, et la signalisation Yap1/Taz-Tead. Cependant, nous n'avons pas trouvé de nouveaux mécanosenseurs impliqués dans ce processus.

La couche épicardique est essentielle au bon fonctionnement du cœur et elle a été largement ignorée jusqu'à des études récentes. Dans cette thèse, nous présentons une étude exhaustive de la formation du PE chez le poisson zèbre, en nous concentrant sur l'activité de Yap1/Taz-Tead. Nous espérons que cette thèse contribuera à approfondir nos connaissances sur la formation du PE. Bien que nous n'ayons pas été en mesure d'identifier la fonction de Yap1/Taz-Tead ou de trouver de nouveaux régulateurs impliqués dans la formation du PE, nous espérons que nos résultats aideront à réorienter les études futures sur la formation du PE.

Bibliography

Agarwala, Sobhika, Sandra Duquesne, Kun Liu, Anton Boehm, Lin Grimm, Sandra Link, Sabine König, Stefan Eimer, Olaf Ronneberger, and Virginie Lecaudey. 2015. “Amotl2a Interacts with the Hippo Effector Yap1 and the Wnt/β-Catenin Effector Lef1 to Control Tissue Size in Zebrafish.” *ELife* 4 (September). https://doi.org/10.7554/eLife.08201.

Andrés-Delgado, Laura, Alexander Ernst, María Galardi-Castilla, David Bazaga, Marina Peralta, Juliane Münch, Juan Manuel González-Rosa, et al. 2019. “Actin Dynamics and the Bmp Pathway Drive Apical Extrusion of Proepicardial Cells.” *Development (Cambridge, England)*, June, dev.174961. https://doi.org/10.1242/dev.174961.

Andrés-Delgado, Laura, and Nadia Mercader. 2016. “Interplay between Cardiac Function and Heart Development.” *Biochimica et Biophysica Acta - Molecular Cell Research* 1863 (7): 1707–16. https://doi.org/10.1016/j.bbamcr.2016.03.004.

Andrés- Delgado, Laura, María Galardi- Castilla, Juliane Münch, Marina Peralta, Alexander Ernst, Juan Manuel González- Rosa, Federico Tessadori, et al. 2020. “Notch and Bmp Signaling Pathways Act Coordinately during the Formation of the Proepicardium.” *Developmental Dynamics* 249 (12): 1455–69. https://doi.org/10.1002/dvdy.229.

Aragona, Mariaceleste, Tito Panciera, Andrea Manfrin, Stefano Giulitti, Federica Michielin, Nicola Elvassore, Sirio Dupont, and Stefano Piccolo. 2013. “A Mechanical Checkpoint Controls Multicellular Growth through YAP/TAZ Regulation by Actin-Processing Factors.” *Cell* 154 (5): 1047–59. https://doi.org/10.1016/j.cell.2013.07.042.

Astone, Matteo, Jason Kuan Han Lai, Sirio Dupont, Didier Y. R. Stainier, Francesco Argenton, and Andrea Vettori. 2018. “Zebrafish Mutants and TEAD Reporters Reveal Essential Functions for Yap and Taz in Posterior Cardinal Vein Development.” *Scientific Reports* 8 (1): 10189. https://doi.org/10.1038/s41598-018-27657-x.

Bakkers, Jeroen. 2011. “Zebrafish as a Model to Study Cardiac Development and Human Cardiac Disease.” *Cardiovascular Research* 91 (2): 279–88. https://doi.org/10.1093/cvr/cvr098.

Behrndt, Martin, Guillaume Salbreux, Pedro Campinho, Robert Hauschild, Felix Oswald, Julia Roensch, Stephan W Grill, and Carl-Philipp Heisenberg. 2012. “Forces Driving Epithelial Spreading in Zebrafish Gastrulation.” *Science (New York, N.Y.)* 338 (6104): 257–60. https://doi.org/10.1126/science.1224143.

Berbari, Nicolas F., Amber K. O’Connor, Courtney J. Haycraft, and Bradley K. Yoder. 2009. “The Primary Cilium as a Complex Signaling Center.” *Current Biology*. NIH Public Access. https://doi.org/10.1016/j.cub.2009.05.025.

Bimber, Benjamin, Robert W. Dettman, and Hans Georg Simon. 2007. “Differential Regulation of Tbx5 Protein Expression and Sub-Cellular Localization during Heart Development.”

Developmental Biology 302 (1): 230–42. https://doi.org/10.1016/j.ydbio.2006.09.023.

Bodmer, Rolf, and Paul M. Wassarman. 2008. *Cardiovascular Development*. Edited by Rolf Bodmer and Paul M. Wassarman. Elsevier.

Borok, Matthew J., Virginia E. Papaioannou, and Lori Sussel. 2016. “Unique Functions of Gata4 in Mouse Liver Induction and Heart Development.” *Developmental Biology* 410 (2): 213–22. https://doi.org/10.1016/j.ydbio.2015.12.007.

Braitsch, Caitlin M., Michelle D. Combs, Susan E. Quaggin, and Katherine E. Yutzey. 2012. “Pod1/Tcf21 Is Regulated by Retinoic Acid Signaling and Inhibits Differentiation of Epicardium-Derived Cells into Smooth Muscle in the Developing Heart.” *Developmental Biology* 368 (2): 345–57. https://doi.org/10.1016/j.ydbio.2012.06.002.

Bressan, Michael, Gary Liu, and Takashi Mikawa. 2013. “Early Mesodermal Cues Assign Avian Cardiac Pacemaker Fate Potential in a Tertiary Heart Field.” *Science* 340 (6133): 744–48. https://doi.org/10.1126/science.1232877.

Brown, Daniel, Leigh Samsa, Li Qian, and Jiandong Liu. 2016. “Advances in the Study of Heart Development and Disease Using Zebrafish.” *Journal of Cardiovascular Development and Disease* 3 (2): 13. https://doi.org/10.3390/jcdd3020013.

Bruneau, Benoit G. 2008. “The Developmental Genetics of Congenital Heart Disease.” *Nature* 451 (7181): 943–48. https://doi.org/10.1038/nature06801.

Buckingham, Margaret, Sigolène Meilhac, and Stéphane Zaffran. 2005. “Building the Mammalian Heart from Two Sources of Myocardial Cells.” *Nature Reviews Genetics*. Nat Rev Genet. https://doi.org/10.1038/nrg1710.

Cao, Jingli, and Kenneth D Poss. 2018. “The Epicardium as a Hub for Heart Regeneration.” *Nature Reviews. Cardiology* 15 (10): 631–47. https://doi.org/10.1038/s41569-018-0046-4.

Cao, Yingxi, and Jingli Cao. 2018. “Covering and Re-Covering the Heart: Development and Regeneration of the Epicardium.” *Journal of Cardiovascular Development and Disease* 6 (1). https://doi.org/10.3390/jcdd6010003.

Carmona, R., M. González-Iriarte, J. M. Pérez-Pomares, and R. Muñoz-Chápuli. 2001. “Localization of the Wilms’ Tumour Protein WT1 in Avian Embryos.” *Cell and Tissue Research* 303 (2): 173–86. https://doi.org/10.1007/s004410000307.

Cheng, Dan, Lan Jin, Yunhe Chen, Xueyan Xi, and Yang Guo. 2020. “YAP Promotes Epithelial Mesenchymal Transition by Upregulating Slug Expression in Human Colorectal Cancer Cells.” *International Journal of Clinical and Experimental Pathology* 13 (4): 701–10.

Cossette, Stephanie, and Ravi Misra. 2011. “The Identification of Different Endothelial Cell

Populations within the Mouse Proepicardium." *Developmental Dynamics* 240 (10): 2344–53. https://doi.org/10.1002/dvdy.22724.

Dai, Jun, Xiaojuan Cui, Zuoyan Zhu, and Wei Hu. 2010. "Non-Homologous End Joining Plays a Key Role in Transgene Concatemer Formation in Transgenic Zebrafish Embryos." *International Journal of Biological Sciences* 6 (7): 756–68. https://doi.org/10.7150/ijbs.6.756.

Dong, Jixin, Georg Feldmann, Jianbin Huang, Shian Wu, Nailing Zhang, Sarah A. Comerford, Mariana F F. Gayyed, Robert A. Anders, Anirban Maitra, and Duojia Pan. 2007. "Elucidation of a Universal Size-Control Mechanism in Drosophila and Mammals." *Cell* 130 (6): 1120–33. https://doi.org/10.1016/j.cell.2007.07.019.

Duchemin, Anne Laure, Héléne Vignes, and Julien Vermot. 2019. "Mechanically Activated Piezo Channels Modulate Outflow Tract Valve Development through the Yap1 and KLF2-Notch Signaling Axis." *ELife* 8 (September). https://doi.org/10.7554/eLife.44706.

Dupont, Sirio, Leonardo Morsut, Mariaceleste Aragona, Elena Enzo, Stefano Giulitti, Michelangelo Cordenonsi, Francesca Zanconato, et al. 2011. "Role of YAP/TAZ in Mechanotransduction." *Nature* 474 (7350): 179–84. https://doi.org/10.1038/nature10137.

Elosegui-Artola, Alberto, Ion Andreu, Amy E.M. Beedle, Ainhoa Lezamiz, Marina Uroz, Anita J. Kosmalska, Roger Oria, et al. 2017. "Force Triggers YAP Nuclear Entry by Regulating Transport across Nuclear Pores." *Cell* 171 (6): 1397-1410.e14. https://doi.org/10.1016/J.CELL.2017.10.008.

Ezratty, Ellen J., Nicole Stokes, Sophia Chai, Alok S. Shah, Scott E. Williams, and Elaine Fuchs. 2011. "A Role for the Primary Cilium in Notch Signaling and Epidermal Differentiation during Skin Development." *Cell* 145 (7): 1129–41. https://doi.org/10.1016/j.cell.2011.05.030.

Fransen, Margaret E., and Larry F. Lemanski. 1990. "Epicardial Development in the Axolotl,Ambystoma Mexicanum." *The Anatomical Record* 226 (2): 228–36. https://doi.org/10.1002/ar.1092260212.

Fukui, Hajime, Takahiro Miyazaki, Renee Wei-Yan Chow, Hiroyuki Ishikawa, Hiroyuki Nakajima, Julien Vermot, and Naoki Mochizuki. 2018. "Hippo Signaling Determines the Number of Venous Pole Cells That Originate from the Anterior Lateral Plate Mesoderm in Zebrafish." *ELife* 7 (May). https://doi.org/10.7554/eLife.29106.

Garoffolo, Gloria, and Maurizio Pesce. 2019. "Mechanotransduction in the Cardiovascular System: From Developmental Origins to Homeostasis and Pathology." *Cells*. NLM (Medline). https://doi.org/10.3390/cells8121607.

Goetz, Jacky G., Emily Steed, Rita R. Ferreira, Stéphane Roth, Caroline Ramspacher,

Francesco Boselli, Gilles Charvin, et al. 2014. “Endothelial Cilia Mediate Low Flow Sensing during Zebrafish Vascular Development.” *Cell Reports* 6 (5): 799–808. https://doi.org/10.1016/j.celrep.2014.01.032.

González-Rosa, Juan Manuel, Marina Peralta, and Nadia Mercader. 2012. “Pan-Epicardial Lineage Tracing Reveals That Epicardium Derived Cells Give Rise to Myofibroblasts and Perivascular Cells during Zebrafish Heart Regeneration.” *Developmental Biology* 370 (2): 173–86. https://doi.org/10.1016/j.ydbio.2012.07.007.

Granados-Riveron, Javier T., and J. David Brook. 2012. “The Impact of Mechanical Forces in Heart Morphogenesis.” *Circulation: Cardiovascular Genetics* 5 (1): 132–42. https://doi.org/10.1161/CIRCGENETICS.111.961086.

Haas, Petra. 2017. “DLS Sample Preparation: Using U-Shaped Glass Capillaries for Sample Mounting.”

Haas, Petra, Elena Remacha Motta, Laia Ortiz Lopez, Bruno Cossermelli Vellutini, Pavel Tomancak, and Emmanuel Reynaud. 2019. “Using a Rotation Device for DLS Sample Mounting | Learn & Share | Leica Microsystems.” 2019. https://www.leica-microsystems.com/science-lab/using-a-rotation-device-for-dls-sample-mounting/.

Hami, Danyal, Adrian C. Grimes, Huai Jen Tsai, and Margaret L. Kirby. 2011. “Zebrafish Cardiac Development Requires a Conserved Secondary Heart Field.” *Development* 138 (11): 2389–98. https://doi.org/10.1242/dev.061473.

Hatcher, Cathy J., Nata Y.S.-G. Diman, Min-Su Kim, David Pennisi, Yan Song, Marsha M. Goldstein, Takashi Mikawa, and Craig T. Basson. 2004. “A Role for Tbx5 in Proepicardial Cell Migration during Cardiogenesis.” *Physiological Genomics* 18 (2): 129–40. https://doi.org/10.1152/physiolgenomics.00060.2004.

Heckel, Emilie, Francesco Boselli, Stéphane Roth, Alice Krudewig, Heinz Georg Belting, Gilles Charvin, and Julien Vermot. 2015. “Oscillatory Flow Modulates Mechanosensitive Klf2a Expression through Trpv4 and Trpp2 during Heart Valve Development.” *Current Biology* 25 (10): 1354–61. https://doi.org/10.1016/j.cub.2015.03.038.

Higgins, Michael, Ismael Obaidi, and Tara McMorrow. 2019. “Primary Cilia and Their Role in Cancer (Review).” *Oncology Letters*. Spandidos Publications. https://doi.org/10.3892/ol.2019.9942.

Hildebrandt, Friedhelm, Thomas Benzing, and Nicholas Katsanis. 2011. “Ciliopathies.” *New England Journal of Medicine*. Massachussetts Medical Society. https://doi.org/10.1056/NEJMra1010172.

Hilman, Dror, and Uri Gat. 2011. “The Evolutionary History of YAP and the Hippo/YAP Pathway.” *Molecular Biology and Evolution* 28 (8): 2403–17.

https://doi.org/10.1093/molbev/msr065.

Hirakow, R. 1992. “Epicardial Formation in Staged Human Embryos.” *Kaibogaku Zasshi. Journal of Anatomy* 67 (5): 616–22.

Hsiao, Yi Chun, Karina Tuz, and Russell J. Ferland. 2012. “Trafficking in and to the Primary Cilium.” *Cilia*. Cilia. https://doi.org/10.1186/2046-2530-1-4.

Huang, Jianbin, Shian Wu, Jose Barrera, Krista Matthews, and Duojia Pan. 2005. “The Hippo Signaling Pathway Coordinately Regulates Cell Proliferation and Apoptosis by Inactivating Yorkie, the Drosophila Homolog of YAP.” *Cell* 122 (3): 421–34. https://doi.org/10.1016/j.cell.2005.06.007.

Huisken, J., and D. Y. R. Stainier. 2009. “Selective Plane Illumination Microscopy Techniques in Developmental Biology.” *Development*. https://doi.org/10.1242/dev.022426.

Icardo, José M., Alejandro Guerrero, Ana C. Durán, Elvira Colvee, Alberto Domezain, and Valentín Sans-Coma. 2009. “The Development of the Epicardium in the Sturgeon *Acipenser Naccarii*.” *The Anatomical Record: Advances in Integrative Anatomy and Evolutionary Biology* 292 (10): 1593–1601. https://doi.org/10.1002/ar.20939.

Ishikawa, Hiroaki, and Wallace F. Marshall. 2011. “Ciliogenesis: Building the Cell’s Antenna.” *Nature Reviews Molecular Cell Biology*. Nature Publishing Group. https://doi.org/10.1038/nrm3085.

Ivanovitch, Kenzo, Susana Temiño, and Miguel Torres. 2017. “Live Imaging of Heart Tube Development in Mouse Reveals Alternating Phases of Cardiac Differentiation and Morphogenesis.” *ELife* 6. https://doi.org/10.7554/eLife.30668.

Iyer, Dharini, Laure Gambardella, William G. Bernard, Felipe Serrano, Victoria L. Mascetti, Roger A. Pedersen, Amarnath Talasila, and Sanjay Sinha. 2015. “Robust Derivation of Epicardium and Its Differentiated Smooth Muscle Cell Progeny from Human Pluripotent Stem Cells.” *Development (Cambridge)* 142 (8): 1528–41. https://doi.org/10.1242/dev.119271.

Jahr, Maike, Jan Schlueter, Thomas Brand, and Jörg Männer. 2008. “Development of the Proepicardium in Xenopus Laevis.” *Developmental Dynamics* 237 (10): 3088–96. https://doi.org/10.1002/dvdy.21713.

Jopling, Chris, Eduard Sleep, Marina Raya, Merce Marti, Angel Raya, and Juan Carlos Izpisua Belmonte. 2010. “Zebrafish Heart Regeneration Occurs by Cardiomyocyte Dedifferentiation and Proliferation.” *Nature* 464 (7288): 606–9. https://doi.org/10.1038/nature08899.

Kirschner, Karin M., Nicole Wagner, Kay Dietrich Wagner, Sven Wellmann, and Holger Scholz.

2006. “The Wilms Tumor Suppressor Wt1 Promotes Cell Adhesion through Transcriptional Activation of the A4integrin Gene.” *Journal of Biological Chemistry*. https://doi.org/10.1074/jbc.M602668200.

Komiyama, Masatoshi, Kintoku Ito, and Yutaka Shimada. 1987. “Origin and Development of the Epicardium in the Mouse Embryo.” *Anatomy and Embryology* 176 (2): 183–89. https://doi.org/10.1007/BF00310051.

Kossack, Mandy, Selina Hein, Lonny Juergensen, Mauro Siragusa, Alexander Benz, Hugo A. Katus, Patrick Most, and David Hassel. 2017. “Induction of Cardiac Dysfunction in Developing and Adult Zebrafish by Chronic Isoproterenol Stimulation.” *Journal of Molecular and Cellular Cardiology* 108 (July): 95–105. https://doi.org/10.1016/j.yjmcc.2017.05.011.

Köster, Isabelle, and Petra Haas. 2015. “Light Sheet Microscopy Turned Vertically.” *Optik & Photonik* 10 (4): 39–43. https://doi.org/10.1002/opph.201500028.

Kraus, Florian, Bénédicte Haenig, and Andreas Kispert. 2001. “Cloning and Expression Analysis of the Mouse T-Box Gene Tbx18.” *Mechanisms of Development* 100 (1): 83–86. https://doi.org/10.1016/S0925-4773(00)00494-9.

Kuhn, Hans Jürg, and Gisela Liebherr. 1988. “The Early Development of the Epicardium in Tupaia Belangeri.” *Anatomy and Embryology* 177 (3): 225–34. https://doi.org/10.1007/BF00321133.

Kurkiewicz, and T. 1909. “O Histogenezie Miesna Sercowego Zwierzat Kregowych-Zur Histogenese Des Herzmuskels Der Wirbeltiere.” *Bull Int Acad Sci Cracovie*.

Lai, Jason K.H., Michelle M. Collins, Veronica Uribe, Vanesa Jiménez-Amilburu, Stefan Gü Nther, Hans Martin Maischein, and Didier Y.R. Stainier. 2018. “The Hippo Pathway Effector Wwtr1 Regulates Cardiac Wall Maturation in Zebrafish.” *Development (Cambridge)* 145 (10). https://doi.org/10.1242/dev.159210.

Lamouille, Samy, Jian Xu, and Rik Derynck. 2014. “Molecular Mechanisms of Epithelial-Mesenchymal Transition.” *Nature Reviews Molecular Cell Biology*. NIH Public Access. https://doi.org/10.1038/nrm3758.

Leung, Chuen Yan, and Magdalena Zernicka-Goetz. 2013. “Angiomotin Prevents Pluripotent Lineage Differentiation in Mouse Embryos via Hippo Pathway-Dependent and-Independent Mechanisms.” *Nature Communications* 4. https://doi.org/10.1038/ncomms3251.

Lindsey, Stephanie E., Jonathan T. Butcher, and Huseyin C. Yalcin. 2014. “Mechanical Regulation of Cardiac Development.” *Frontiers in Physiology*. Frontiers Research Foundation. https://doi.org/10.3389/fphys.2014.00318.

Liu, Jiandong, Michael Bressan, David Hassel, Jan Huisken, David Staudt, Kazu Kikuchi, Kenneth D. Poss, Takashi Mikawa, and Didier Y.R. Stainier. 2010. “A Dual Role for ErbB2 Signaling in Cardiac Trabeculation.” *Development* 137 (22): 3867–75. https://doi.org/10.1242/dev.053736.

Liu, Jiandong, and Didier Y.R. Stainier. 2012. “Zebrafish in the Study of Early Cardiac Development.” *Circulation Research*. NIH Public Access. https://doi.org/10.1161/CIRCRESAHA.111.246504.

Liu, Jiandong, and Didier Y R Stainier. 2010. “Tbx5 and Bmp Signaling Are Essential for Proepicardium Specification in Zebrafish.” *Circulation Research*. https://doi.org/10.1161/CIRCRESAHA.110.217950.

Low, Boon Chuan, Catherine Qiurong Pan, G.V. Shivashankar, Alexander Bershadsky, Marius Sudol, and Michael Sheetz. 2014. “YAP/TAZ as Mechanosensors and Mechanotransducers in Regulating Organ Size and Tumor Growth.” *FEBS Letters* 588 (16): 2663–70. https://doi.org/10.1016/j.febslet.2014.04.012.

Lundin, Vanessa, Wade W. Sugden, Lindsay N. Theodore, Patricia M. Sousa, Areum Han, Stephanie Chou, Paul J. Wrighton, et al. 2020. “YAP Regulates Hematopoietic Stem Cell Formation in Response to the Biomechanical Forces of Blood Flow.” *Developmental Cell* 52 (4): 446-460.e5. https://doi.org/10.1016/j.devcel.2020.01.006.

Lyon, Robert C., Fabian Zanella, Jeffrey H. Omens, and Farah Sheikh. 2015. “Mechanotransduction in Cardiac Hypertrophy and Failure.” *Circulation Research*. Lippincott Williams and Wilkins. https://doi.org/10.1161/CIRCRESAHA.116.304937.

Maddison, Lisette A., Jianjun Lu, and Wenbiao Chen. 2012. “Generating Conditional Mutations in Zebrafish Using Gene-Trap Mutagenesis.” *Methods Cell Biology* 104: 1–22. https://doi.org/10.1016/B978-0-12-374814-0.00001-X.Generating.

Männer, Jörg. 1993. “Experimental Study on the Formation of the Epicardium in Chick Embryos.” *Anatomy and Embryology* 187 (3): 281–89. https://doi.org/10.1007/BF00195766.

Männer, Jörg. 1999. “Does the Subepicardial Mesenchyme Contribute Myocardioblasts to the Myocardium of the Chick Embryo Heart? A Quail- chick Chimera Study Tracing the Fate of the Epicardial Primordium.” *The Anatomical Record* 255 (2): 212–26. https://doi.org/10.1002/(SICI)1097-0185(19990601)255:2<212::AID-AR11>3.0.CO;2-X.

Marszalek, Joseph R., Pilar Ruiz-Lozano, Elizabeth Roberts, Kenneth R. Chien, and Lawrence S.B. Goldstein. 1999. “Situs Inversus and Embryonic Ciliary Morphogenesis Defects in Mouse Mutants Lacking the KIF3A Subunit of Kinesin-II.” *Proceedings of the National Academy of Sciences of the United States of America* 96 (9): 5043–48.

https://doi.org/10.1073/pnas.96.9.5043.

Masson, Christel, Diana García-García, Juliette Bitard, Élodie Kim Grellier, Jérôme E. Roger, and Muriel Perron. 2020. “Yap Haploinsufficiency Leads to Müller Cell Dysfunction and Late-Onset Cone Dystrophy.” *Cell Death and Disease* 11 (8): 1–15. https://doi.org/10.1038/s41419-020-02860-9.

Mateus, Rita, Raquel Lourenço, Yi Fang, Gonçalo Brito, Ana Farinho, Fabio Valerio, and Antonio Jacinto. 2015. “Control of Tissue Growth by Yap Relies on Cell Density and F-Actin in Zebrafish Fin Regeneration.” *Development (Cambridge)* 142 (16): 2752–63. https://doi.org/10.1242/dev.119701.

Maya-Ramos, Lisandro, James Cleland, Michael Bressan, and Takashi Mikawa. 2013. “Induction of the Proepicardium.” *Journal of Developmental Biology*. https://doi.org/10.3390/jdb1020082.

MB INFO. 2016. “What Is the Hippo-YAP/TAZ Tumor-Suppressor Pathway? | MBInfo.” 2016. https://www.mechanobio.info/what-is-mechanosignaling/signaling-pathways/what-is-the-hippo-yaptaz-tumor-suppressor-pathway/.

Meilhac, Sigolène M., and Margaret E. Buckingham. 2018. “The Deployment of Cell Lineages That Form the Mammalian Heart.” *Nature Reviews Cardiology* 15 (11): 705–24. https://doi.org/10.1038/s41569-018-0086-9.

Meng, Zhipeng, Toshiro Moroishi, and Kun Liang Guan. 2016. “Mechanisms of Hippo Pathway Regulation.” *Genes and Development*. Cold Spring Harbor Laboratory Press. https://doi.org/10.1101/gad.274027.115.

Miesfeld, Joel B, and Brian A Link. 2014. “Establishment of Transgenic Lines to Monitor and Manipulate Yap/Taz-Tead Activity in Zebrafish Reveals Both Evolutionarily Conserved and Divergent Functions of the Hippo Pathway.” *Mechanisms of Development* 133 (August): 177–88. https://doi.org/10.1016/j.mod.2014.02.003.

Mikawa, T., and D. A. Fischman. 1992. “Retroviral Analysis of Cardiac Morphogenesis: Discontinuous Formation of Coronary Vessels.” *Proceedings of the National Academy of Sciences of the United States of America* 89 (20): 9504–8. https://doi.org/10.1073/pnas.89.20.9504.

Mohseni, Morvarid, Jianlong Sun, Allison Lau, Stephen Curtis, Jeffrey Goldsmith, Victor L Fox, Chongjuan Wei, et al. 2014. “A Genetic Screen Identifies an LKB1-MARK Signalling Axis Controlling the Hippo-YAP Pathway.” *Nature Cell Biology* 16 (1): 108–17. https://doi.org/10.1038/ncb2884.

Moore, Adrian W., Lesley McInnes, Jordan Kreidberg, Nicholas D. Hastie, and Andreas Schedl. 1999. “YAC Complementation Shows a Requirement for Wt1 in the Development of

Epicardium, Adrenal Gland and throughout Nephrogenesis." *Development* 126 (9): 1845–57.

Moriyama, Yuuta, Fumihiro Ito, Hiroyuki Takeda, Tohru Yano, Masataka Okabe, Shigehiro Kuraku, Fred W. Keeley, and Kazuko Koshiba-Takeuchi. 2016. "Evolution of the Fish Heart by Sub/Neofunctionalization of an Elastin Gene." *Nature Communications* 7 (January). https://doi.org/10.1038/ncomms10397.

Nakajima, Hiroyuki, Kimiko Yamamoto, Sobhika Agarwala, Kenta Terai, Hajime Fukui, Shigetomo Fukuhara, Koji Ando, et al. 2017. "Flow-Dependent Endothelial YAP Regulation Contributes to Vessel Maintenance." *Developmental Cell* 40 (6): 523-536.e6. https://doi.org/10.1016/j.devcel.2017.02.019.

Nakano, Atsushi, Haruko Nakano, Kelly A. Smith, and Nathan J. Palpant. 2016. "The Developmental Origins and Lineage Contributions of Endocardial Endothelium." *Biochimica et Biophysica Acta - Molecular Cell Research*. Elsevier B.V. https://doi.org/10.1016/j.bbamcr.2016.01.022.

Nesbitt, Tresa, Aubrey Lemley, Jeff Davis, Michael J. Yost, Richard L. Goodwin, and Jay D. Potts. 2006. "Epicardial Development in the Rat: A New Perspective." *Microscopy and Microanalysis*. Cambridge University Press. https://doi.org/10.1017/S1431927606060533.

Nguyen, H. B., J. T. Babcock, C. D. Wells, and L. A. Quilliam. 2013. "LKB1 Tumor Suppressor Regulates AMP Kinase/MTOR-Independent Cell Growth and Proliferation via the Phosphorylation of Yap." *Oncogene* 32 (35): 4100–4109. https://doi.org/10.1038/onc.2012.431.

Olivey, Harold E., and Eric C. Svensson. 2010. "Epicardial-Myocardial Signaling Directing Coronary Vasculogenesis." *Circulation Research*. NIH Public Access. https://doi.org/10.1161/CIRCRESAHA.109.209197.

OMIM. 2006. "OMIM Entry - # 142900 - HOLT-ORAM SYNDROME; HOS." 2006. https://www.omim.org/entry/142900.

Park, Jin Seok, Deok Ho Kim, Sagar R. Shah, Hong Nam Kim, Kshitiz, Peter Kim, Alfredo Quiñones-Hinojosa, and Andre Levchenko. 2019. "Switch-like Enhancement of Epithelial-Mesenchymal Transition by YAP through Feedback Regulation of WT1 and Rho-Family GTPases." *Nature Communications* 10 (1): 1–15. https://doi.org/10.1038/s41467-019-10729-5.

Pater, Emma de, Linda Clijsters, Sara R. Marques, Yi Fan Lin, Zayra V. Garavito-Aguilar, Deborah Yelon, and Jeroen Bakkers. 2009. "Distinct Phases of Cardiomyocyte Differentiation Regulate Growth of the Zebrafish Heart." *Development* 136 (10): 1633–41. https://doi.org/10.1242/dev.030924.

Pennisi, David J., Victoria L.T. Ballard, and Takashi Mikawa. 2003. “Epicardium Is Required for the Full Rate of Myocyte Proliferation and Levels of Expression of Myocyte Mitogenic Factors FGF2 and Its Receptor, FGFR-1, but Not for Transmural Myocardial Patterning in the Embryonic Chick Heart.” *Developmental Dynamics* 228 (2): 161–72. https://doi.org/10.1002/dvdy.10360.

Peralta, Marina. 2014. “Dissecting the Role of Heartbeat- Driven Pericardiac Fluid Forces on Epicardium Morphogenesis Through.” Universidad Autonoma de Madrid.

Peralta, Marina, Juan Manuel González-Rosa, Inês Joao Marques, Nadia Mercader, and Author Manuscript. 2014. “The Epicardium in the Embryonic and Adult Zebrafish Europe PMC Funders Group.” *Es (I.J.M.) J Dev Biol J Dev Biol. April* 11 (22): 101–16. https://doi.org/10.3390/jdb2020101.

Peralta, Marina, Laia Ortiz Lopez, Katerina Jerabkova, Tommaso Lucchesi, Benjamin Vitre, Dong Han, Laurent Guillemot, et al. 2020. “Intraflagellar Transport Complex B Proteins Regulate the Hippo Effector Yap1 during Cardiogenesis.” *Cell Reports* 32 (3): 107932. https://doi.org/10.1016/j.celrep.2020.107932.

Peralta, Marina, Emily Steed, Sébastien Harlepp, Juan Manuel González-Rosa, Fabien Monduc, Ana Ariza-Cosano, Alfonso Cortés, et al. 2013. “Heartbeat-Driven Pericardiac Fluid Forces Contribute to Epicardium Morphogenesis.” *Current Biology : CB* 23 (18): 1726–35. https://doi.org/10.1016/j.cub.2013.07.005.

Pérez-Pomares, José María, and José Luis de la Pompa. 2011. “Signaling during Epicardium and Coronary Vessel Development.” *Circulation Research* 109 (12): 1429–42. https://doi.org/10.1161/CIRCRESAHA.111.245589.

Perner, Birgit, Christoph Englert, and Frank Bollig. 2007. “The Wilms Tumor Genes Wt1a and Wt1b Control Different Steps during Formation of the Zebrafish Pronephros.” *Developmental Biology* 309 (1): 87–96. https://doi.org/10.1016/j.ydbio.2007.06.022.

Peshkovsky, Courtney, Ronald Totong, and Deborah Yelon. 2011. “Dependence of Cardiac Trabeculation on Neuregulin Signaling and Blood Flow in Zebrafish.” *Developmental Dynamics* 240 (2): 446–56. https://doi.org/10.1002/dvdy.22526.

Piccolo, Stefano, Sirio Dupont, and Michelangelo Cordenonsi. 2014. “The Biology of YAP/TAZ: Hippo Signaling and Beyond.” *Physiological Reviews* 94 (4): 1287–1312. https://doi.org/10.1152/physrev.00005.2014.

Plavicki, Jessica S, Peter Hofsteen, Monica S Yue, Kevin A Lanham, Richard E Peterson, and Warren Heideman. 2014. “Multiple Modes of Proepicardial Cell Migration Require Heartbeat.” *BMC Developmental Biology*. https://doi.org/10.1186/1471-213X-14-18.

Pooranachandran, Niedharsan, and Jarema J. Malicki. 2016. “Unexpected Roles for Ciliary

Kinesins and Intraflagellar Transport Proteins." *Genetics* 203 (2): 771–85. https://doi.org/10.1534/genetics.115.180943.

Qiu, Bijun, Wei Wei, Jianwen Zhu, Guangshun Fu, and Dahai Lu. 2018. "EMT Induced by Loss of LKB1 Promotes Migration and Invasion of Liver Cancer Cells through ZEB1-Induced YAP Signaling." *Oncology Letters* 16 (5): 6465–71. https://doi.org/10.3892/ol.2018.9445.

R Ferreira, Rita, Hajime Fukui, Renee Chow, Andrej Vilfan, and Julien Vermot. 2019. "The Cilium as a Force Sensor-Myth versus Reality." *Journal of Cell Science*. NLM (Medline). https://doi.org/10.1242/jcs.213496.

Ragni, Chiara V., Nicolas Diguet, Jean-François Le Garrec, Marta Novotova, Tatiana P. Resende, Sorin Pop, Nicolas Charon, et al. 2017. "Amotl1 Mediates Sequestration of the Hippo Effector Yap1 Downstream of Fat4 to Restrict Heart Growth." *Nature Communications*. https://doi.org/10.1038/ncomms14582.

Rash, John E., Jerry W. Shay, and John J. Biesele. 1969. "Cilia in Cardiac Differentiation." *Journal of Ultrasructure Research* 29 (5–6): 470–84. https://doi.org/10.1016/S0022-5320(69)90067-7.

Rasouli, S. Javad, and Didier Y.R. Stainier. 2017. "Regulation of Cardiomyocyte Behavior in Zebrafish Trabeculation by Neuregulin 2a Signaling." *Nature Communications* 8 (May). https://doi.org/10.1038/ncomms15281.

Robb, Lorraine, Lisa Mifsud, Lynne Hartley, Christine Biben, Neal G. Copeland, Debra J. Gilbert, Nancy A. Jenkins, and Richard P. Harvey. 1998. "Epicardin: A Novel Basic Helix-loop- helix Transcription Factor Gene Expressed in Epicardium, Branchial Arch Myoblasts, and Mesenchyme of Developing Lung, Gut, Kidney, and Gonads." *Developmental Dynamics* 213 (1): 105–13. https://doi.org/10.1002/(SICI)1097-0177(199809)213:1<105::AID-AJA10>3.0.CO;2-1.

Robles, Vanesa, Mercé Martí, and Juan Carlos Izpisua Belmonte. 2011. "Study of Pluripotency Markers in Zebrafish Embryos and Transient Embryonic Stem Cell Cultures." *Zebrafish* 8 (2): 57–63. https://doi.org/10.1089/zeb.2010.0684.

Rodgers, Laurel S., Sofia Lalani, Ray B. Runyan, and Todd D. Camenisch. 2008. "Differential Growth and Multicellular Villi Direct Proepicardial Translocation to the Developing Mouse Heart." *Developmental Dynamics* 237 (1): 145–52. https://doi.org/10.1002/dvdy.21378.

Rojas, Anabel, Sarah De Val, Analeah B. Heidt, Shan Mei Xu, James Bristow, and Brian L. Black. 2005. "Gata4 Expression in Lateral Mesoderm Is Downstream of BMP4 and Is Activated Directly by Forkhead and GATA Transcription Factors through a Distal Enhancer Element." *Development* 132 (15): 3405–17. https://doi.org/10.1242/dev.01913.

Ruiz-Villalba, Adrián, and José M Pérez-Pomares. 2012. "The Expanding Role of the

Epicardium and Epicardial-Derived Cells in Cardiac Development and Disease." *Current Opinion in Pediatrics* 24 (5): 569–76. https://doi.org/10.1097/MOP.0b013e328357a532.

Sainier, Didier Y. R., Robert K. Lee, and Mark C. Fishman. 1993. "Cardiovascular Development in the Zebrafish I. Myocardial Fate Map and Heart Tube Formation." *Development* 119: 31–40.

Schlueter, Jan, and Thomas Brand. 2012. "Epicardial Progenitor Cells in Cardiac Development and Regeneration." *Journal of Cardiovascular Translational Research* 5 (5): 641–53. https://doi.org/10.1007/s12265-012-9377-4.

Schlueter, Jan, Thomas Brand, and Gail R Martin. 2009. "A Right-Sided Pathway Involving FGF8/Snai1 Controls Asymmetric Development of the Proepicardium in the Chick Embryo." *PNAS* 106 (18): 7485–90.

Schottenfeld, Jodi, Jessica Sullivan-Brown, and Rebecca D. Burdine. 2007. "Zebrafish Curly up Encodes a Pkd2 Ortholog That Restricts Left-Side-Specific Expression of Southpaw." *Development* 134 (8): 1605–15. https://doi.org/10.1242/dev.02827.

Schulte, Inga, Jan Schlueter, Radwan Abu-Issa, Thomas Brand, and Jörg Männer. 2007. "Morphological and Molecular Left–Right Asymmetries in the Development of the Proepicardium: A Comparative Analysis on Mouse and Chick Embryos." *Developmental Dynamics* 236 (3): 684–95. https://doi.org/10.1002/dvdy.21065.

Sehnert, Amy J., Anja Huq, Brant M. Weinstein, Charline Walker, Mark Fishman, and Didier Y.R. Stainier. 2002. "Cardiac Troponin T Is Essential in Sarcomere Assembly and Cardiac Contractility." *Nature Genetics* 31 (1): 106–10. https://doi.org/10.1038/ng875.

Sekimizu, Kohshin, Noriyuki Nishioka, Hiroshi Sasaki, Hiroyuki Takeda, Rolf O. Karlstrom, and Atsushi Kawakami. 2004. "The Zebrafish Iguana Locus Encodes Dzip1, a Novel Zinc-Finger Protein Required for Proper Regulation of Hedgehog Signaling." *Development*. The Company of Biologists Ltd. https://doi.org/10.1242/dev.01059.

Serluca, Fabrizio C. 2008. "Development of the Proepicardial Organ in the Zebrafish." *Developmental Biology*. https://doi.org/10.1016/j.ydbio.2007.10.007.

Simões, Filipa C., and Paul R. Riley. 2018. "The Ontogeny, Activation and Function of the Epicardium during Heart Development and Regeneration." *Development (Cambridge)*. Company of Biologists Ltd. https://doi.org/10.1242/dev.155994.

Singh, Anamika, Sindhu Ramesh, Dasan Mary Cibi, Lim Sze Yun, Jun Li, Li Li, Lauren J. Manderfield, Eric N. Olson, Jonathan A. Epstein, and Manvendra K. Singh. 2016. "Hippo Signaling Mediators Yap and Taz Are Required in the Epicardium for Coronary Vasculature Development." *Cell Reports* 15 (7): 1384. https://doi.org/10.1016/J.CELREP.2016.04.027.

Sipe, Conor W., and Xiaowei Lu. 2011. “Kif3a Regulates Planar Polarization of Auditory Hair Cells through Both Ciliary and Non-Ciliary Mechanisms.” *Development* 138 (16): 3441–49. https://doi.org/10.1242/dev.065961.

Sorrentino, Giovanni, Naomi Ruggeri, Alessandro Zannini, Eleonora Ingallina, Rebecca Bertolio, Carolina Marotta, Carmelo Neri, et al. 2017. “Glucocorticoid Receptor Signalling Activates YAP in Breast Cancer.” *Nature Communications* 8: 14073. https://doi.org/10.1038/ncomms14073.

Stainier, Didier Y. R., Robert K. Lee, and Mark C. Fishman. 1993. “Cardiovascular Development in the Zebrafish. I. Myocardial Fate Map and Heart Tube Formation - PubMed.” *Development* 119 (1): 31–40.

Staudt, David W., Jiandong Liu, Kurt S. Thorn, Nico Stuurman, Michael Liebling, and Didier Y.R. Stainier. 2014. “High-Resolution Imaging of Cardiomyocyte Behavior Reveals Two Distinct Steps in Ventricular Trabeculation.” *Development (Cambridge)* 141 (3): 585–93. https://doi.org/10.1242/dev.098632.

Steed, Emily, Francesco Boselli, and Julien Vermot. 2016. “Hemodynamics Driven Cardiac Valve Morphogenesis.” *Biochimica et Biophysica Acta - Molecular Cell Research*. https://doi.org/10.1016/j.bbamcr.2015.11.014.

Steed, Emily, Nathalie Faggianelli, Stéphane Roth, Caroline Ramspacher, Jean Paul Concordet, and Julien Vermot. 2016. “Klf2a Couples Mechanotransduction and Zebrafish Valve Morphogenesis through Fibronectin Synthesis.” *Nature Communications* 7 (1): 1–14. https://doi.org/10.1038/ncomms11646.

Svensson, Eric C. 2010. “Deciphering the Signals Specifying the Proepicardium.” *Circulation Research*. NIH Public Access. https://doi.org/10.1161/CIRCRESAHA.110.222216.

Taha, Zaid, Helena J. Janse van Rensburg, and Xiaolong Yang. 2018. “The Hippo Pathway: Immunity and Cancer.” *Cancers*. MDPI AG. https://doi.org/10.3390/cancers10040094.

Tanaka, Mikiko, and Cheryll Tickle. 2004. “Tbx18 and Boundary Formation in Chick Somite and Wing Development.” *Developmental Biology* 268 (2): 470–80. https://doi.org/10.1016/j.ydbio.2003.12.036.

Tandon, P., Y. V. Miteva, L. M. Kuchenbrod, I. M. Cristea, and F. L. Conlon. 2013. “Tcf21 Regulates the Specification and Maturation of Proepicardial Cells.” *Development*. https://doi.org/10.1242/dev.093385.

Taschner, Michael, Sagar Bhogaraju, and Esben Lorentzen. 2012. “Architecture and Function of IFT Complex Proteins in Ciliogenesis.” *Differentiation* 83 (2): S12. https://doi.org/10.1016/j.diff.2011.11.001.

Totaro, Antonio, Tito Panciera, and Stefano Piccolo. 2018. “YAP/TAZ Upstream Signals and Downstream Responses.” *Nature Cell Biology*. Nature Publishing Group. https://doi.org/10.1038/s41556-018-0142-z.

Trubelja, Alen, and Gang Bao. 2018. “Molecular Mechanisms of Mechanosensing and Mechanotransduction in Living Cells.” *Extreme Mechanics Letters*. Elsevier Ltd. https://doi.org/10.1016/j.eml.2018.01.011.

Tzahor, Eldad, and Kenneth D. Poss. 2017. “Cardiac Regeneration Strategies: Staying Young at Heart.” *Science*. American Association for the Advancement of Science. https://doi.org/10.1126/science.aam5894.

Varelas, Xaralabos. 2014. “The Hippo Pathway Effectors TAZ and YAP in Development, Homeostasis and Disease.” *Development (Cambridge)*. Company of Biologists Ltd. https://doi.org/10.1242/dev.102376.

Velden, Yme U van der, Liqin Wang, John Zevenhoven, Ellen van Rooijen, Maarten van Lohuizen, Rachel H Giles, Hans Clevers, and Anna-Pavlina G Haramis. 2011. “The Serine-Threonine Kinase LKB1 Is Essential for Survival under Energetic Stress in Zebrafish.” *Proceedings of the National Academy of Sciences of the United States of America* 108 (11): 4358–63. https://doi.org/10.1073/pnas.1010210108.

Venkatesh, Deepak. 2017. “Primary Cilia.” *Journal of Oral and Maxillofacial Pathology* 21 (1): 8–10. https://doi.org/10.4103/jomfp.JOMFP_48_17.

Vermot, Julien, Arian S. Forouhar, Michael Liebling, David Wu, Diane Plummer, Morteza Gharib, and Scott E. Fraser. 2009. “Reversing Blood Flows Act through Klf2a to Ensure Normal Valvulogenesis in the Developing Heart.” Edited by Hiroshi Hamada. *PLoS Biology* 7 (11): e1000246. https://doi.org/10.1371/journal.pbio.1000246.

Vincent, Stéphane D., and Margaret E. Buckingham. 2010. “How to Make a Heart. The Origin and Regulation of Cardiac Progenitor Cells.” In *Current Topics in Developmental Biology*, 90:1–41. Academic Press Inc. https://doi.org/10.1016/S0070-2153(10)90001-X.

Viragh, Szabolcs, and Cyril E. Challice. 1981. “The Origin of the Epicardium and the Embryonic Myocardial Circulation in the Mouse.” *The Anatomical Record* 201 (1): 157–68. https://doi.org/10.1002/ar.1092010117.

Voltes, Adrià, Covadonga F. Hevia, Carolyn Engel-Pizcueta, Chaitanya Dingare, Simone Calzolari, Javier Terriente, Caren Norden, Virginie Lecaudey, and Cristina Pujades. 2019. “Yap/Taz-TEAD Activity Links Mechanical Cues to Progenitor Cell Behavior during Zebrafish Hindbrain Segmentation.” *Development (Cambridge, England)* 146 (14). https://doi.org/10.1242/dev.176735.

Wang, Chao, Xiaoyong Zhu, Weiwei Feng, Yinhua Yu, Kangjin Jeong, Wei Guo, Yiling Lu, and

Gordon B. Mills. 2016. “Verteporfin Inhibits YAP Function through Up-Regulating 14-3-3σ Sequestering YAP in the Cytoplasm.” *American Journal of Cancer Research* 6 (1): 27–37.

Wang, Jinhu, Daniela Panáková, Kazu Kikuchi, Jennifer E Holdway, Matthew Gemberling, James S Burris, Sumeet Pal Singh, et al. 2011. “The Regenerative Capacity of Zebrafish Reverses Cardiac Failure Caused by Genetic Cardiomyocyte Depletion.” *Development (Cambridge, England)* 138 (16): 3421–30. https://doi.org/10.1242/dev.068601.

Wang, Wenqi, Nan Li, Xu Li, My Kim Tran, Xin Han, and Junjie Chen. 2015. “Tankyrase Inhibitors Target YAP by Stabilizing Angiomotin Family Proteins.” *Cell Reports* 13 (3): 524–32. https://doi.org/10.1016/j.celrep.2015.09.014.

Watt, Alistair J., Michele A. Battle, Jixuan Li, and Stephen A. Duncan. 2004. “GATA4 Is Essential for Formation of the Proepicardium and Regulates Cardiogenesis.” *Proceedings of the National Academy of Sciences of the United States of America* 101 (34): 12573–78. https://doi.org/10.1073/pnas.0400752101.

Weinberger, Michael, Filipa C. Simões, Roger Patient, Tatjana Sauka-Spengler, and Paul R. Riley. 2020. “Functional Heterogeneity within the Developing Zebrafish Epicardium.” *Developmental Cell* 52 (5): 574-590.e6. https://doi.org/10.1016/j.devcel.2020.01.023.

Wessels, Andy, Maurice J.B. van den Hoff, Richard F. Adamo, Aimee L. Phelps, Marie M. Lockhart, Kimberly Sauls, Laura E. Briggs, et al. 2012. “Epicardially Derived Fibroblasts Preferentially Contribute to the Parietal Leaflets of the Atrioventricular Valves in the Murine Heart.” *Developmental Biology* 366 (2): 111–24. https://doi.org/10.1016/j.ydbio.2012.04.020.

WHO. 2016. “WHO | Cardiovascular Diseases (CVDs).” *WHO*. http://www.who.int/mediacentre/factsheets/fs317/en/.

Xin, Mei, Eric N. Olson, and Rhonda Bassel-Duby. 2013. “Mending Broken Hearts: Cardiac Development as a Basis for Adult Heart Regeneration and Repair.” *Nature Reviews Molecular Cell Biology*. NIH Public Access. https://doi.org/10.1038/nrm3619.

Yu, Fa-Xing, Bin Zhao, and Kun-Liang Guan. 2015. “Hippo Pathway in Organ Size Control, Tissue Homeostasis, and Cancer.” *Cell* 163 (4): 811–28. https://doi.org/10.1016/j.cell.2015.10.044.

Zhao, Bin, Li Li, Qing Lu, Lloyd H. Wang, Chen Ying Liu, Qunying Lei, and Kun Liang Guan. 2011. “Angiomotin Is a Novel Hippo Pathway Component That Inhibits YAP Oncoprotein.” *Genes and Development* 25 (1): 51–63. https://doi.org/10.1101/gad.2000111.

Zhao, Bin, Karen Tumaneng, and Kun-Liang Guan. 2011. “The Hippo Pathway in Organ Size Control, Tissue Regeneration and Stem Cell Self-Renewal.” *Nature Cell Biology* 13 (8): 877–83. https://doi.org/10.1038/ncb2303.

Zhao, Bin, Xiaomu Wei, Weiquan Li, Ryan S. Udan, Qian Yang, Joungmok Kim, Joe Xie, et al. 2007. “Inactivation of YAP Oncoprotein by the Hippo Pathway Is Involved in Cell Contact Inhibition and Tissue Growth Control.” *Genes and Development* 21 (21): 2747–61. https://doi.org/10.1101/gad.1602907.

Annex 1. TauSense: a fluorescence lifetime-based toolset for everyday imaging

Leica MICROSYSTEMS

TauSense: a fluorescence lifetime-based tool set for everyday imaging

The TauSense technology from Leica Microsystems is a new, straightforward way to generate images using lifetime-based information. Measuring changes in the fluorescence arrival times gives an extra layer of information for understanding the functions of molecules within the cellular environment, increasing image quality, and expanding the number of probes that can be visualized in a specimen. This technology enables the acquisition of lifetime-based information with smaller data size and computational load compared to fluorescence lifetime imaging (FLIM). Moreover, the implementation of different tools (TauConstrast, TauGating, TauScan and TauSeparation) allows exploration of this extra dimension of information at different levels.

Fluorescence microscopy allows researchers to gain unprecedented insights into cellular mechanisms. An intrinsic phenomenon of the fluorescence process is the characteristic time between the excitation of the molecule and the photon emission (Fig. 1a). This time is known as fluorescence lifetime and corresponds to the time that the molecule stays in the excited state (S_1) before going back to the ground state (S_0). It is typically in the sub-nanosecond-to-nanosecond range. In this last step a photon is generated, as portrayed in the Jablonski-Perrin diagram (Fig. 1a)[1]. The average fluorescence lifetime is a characteristic value for each fluorophore, but it can vary if there are changes in the fluorophore's close vicinity (less than 10 nm)[2]. The changes in the fluorophore microenvironment that translate into changes in fluorescence lifetime make it a powerful analysis tool in life sciences. These changes have been used, for example, in the design of fluorescence-lifetime-based biosensors[3].

It is possible to probe lifetime-based changes by measuring the photon arrival times[4]. A straightforward way of determining arrival times is by measuring the difference between the time when a photon is detected and the time of the excitation laser pulse (Fig. 1a). The zero value of the measurement can be calibrated using the reflection signal from the excitation laser reaching each detector. Having access to the arrival times can reveal information complementary to the fluorescence intensity, which allows characterization of a specimen or a process of interest. As an example (Fig. 1b), lifetime-based information in images of an *Arabidopsis thaliana* root–hypocotyl junction expressing an actin fluorescent marker[5] and labeled with propidium iodide shows three distinct structures—actin network, cell wall and chloroplasts—that are difficult to identify when only the intensity information is available.

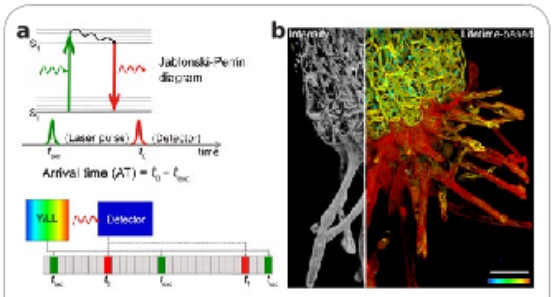

Figure 1 | Basic concepts of TauSense a | Jablonski-Perrin diagram: fluorescence process, from fluorophore excitation (green arrow, up) to emission of a photon (red arrow, down). It is possible to measure the photon arrival time (AT) as the difference between the time the emitted photon is detected and the time the excitation laser pulse from the white light laser (WLL) occurs (see text). **b**, Intensity and lifetime-based image of *Arabidopsis thaliana* root–hypocotyl junction expressing an actin fluorescent marker[5] and labeled with propidium iodide. Actin, cell wall and chloroplasts show different characteristics as observed in the lifetime-based image. Scale bar, 250 µm; look-up table, 0–2.8 ns. (Sample courtesy of M. Krebs, COS University of Heidelberg.)

Lifetime-based measurements, carried out on a point-scanning microscope, require a pulsed-laser excitation source; fast, low-noise photon counting detectors; and electronics with appropriate time-resolution capabilities. This is the basic concept underlying the TauSense technology for fluorescence imaging: the use and handling of photon arrival times to generate lifetime-based information for

M. Julia Roberti[1], Laia Ortiz Lopez[1,2,3], Giulia Ossato[1], Irmtraud Steinmetz[1], Petra Haas[1], Frank Hecht[1] and Luis A. J. Alvarez[1*]

[1]Leica Microsystems CMS GmbH, Mannheim, Germany. [2]Institut de Génétique et de Biologie Moléculaire et Cellulaire (IGBMC), Centre National de la Recherche Scientifique, UMR 7104, and Institut National de la Santé et de la Recherche Médicale, U964, Illkirch, France. [3]Université de Strasbourg, Illkirch, France. *e-mail: luis.alvarez@leica-microsystems.com

different applications. The scan head electronics, supported by a field-programmable gate array, sort the detected photons into digitally preset gates depending on their arrival times. This architecture enables TauSense to use the photon time-tagged information only for online calculations—for example, to estimate the average photon arrival time (AAT) values on the fly. The resulting images come from the evaluation of lifetime-based information, but no longer carry the time dimension at the single-photon level. This efficient handling of the data translates into a smaller file size and computational load compared to fluorescence lifetime imaging microscopy (FLIM) methods. As such, TauSense does not aim to replace FLIM methods. The motivation for TauSense is to provide access to a lifetime-based level of information with every point-scanning microscope in a guided way and obtain a result in a straightforward manner. With this in mind, TauSense is a set of tools that enable exploring lifetime-based information at different levels: TauContrast, TauGating, TauScan and TauSeparation.

A first approach to accessing lifetime-based information using TauSense comes from the analysis of photon arrival times for every pixel. The arrival times are handled at the level of the scan head electronics. Taking these together with the pixel information, it is possible to calculate the average photon arrival time per pixel and to generate an image that contains both the intensity (photon counts) and the AAT information for every pixel (Fig. 2a). This approach yields an extra, lifetime-based dimension or contrast that can be used to elucidate more characteristics of a fluorescent signal of biological relevance. This is referred to as TauContrast in TauSense (Fig. 2a). A typical example is the assessment of intracellular pH changes through lifetime-based measurements using suitable fluorescent probes, as shown here for a near infrared membrane stain (Fig. 2b). In addition to staining the plasma membrane, the probe is internalized over time, and the vesicles carrying the probe appear as bright spots in the fluorescence intensity image (Fig. 2b). That is all we can tell about the internalization process using intensity-based information. The corresponding TauContrast image (Fig. 2c) reveals another level of information: the AAT values at the plasma membrane are different than those in the vesicles. These variations in TauContrast correlate with the different environment the dye encounters when transitioning from the plasma membrane first into endosomes and then into lysosomes of different levels of maturation. TauContrast differs within the vesicles and reports on the different pH values present.

Because of the way TauContrast is generated (calibration relative to the timing of the excitation pulse, determined by on-the-fly calculation of the AAT at the scan head electronics), the lifetime-based information is qualitative and can be used in a semi-quantitative way relative to an appropriate control[6]. Like other lifetime-based tools, TauContrast measurements are independent of fluorescence intensities. TauContrast not only allows the monitoring of changes relative to a control sample but is also a precise tool for observing changes within a given sample.

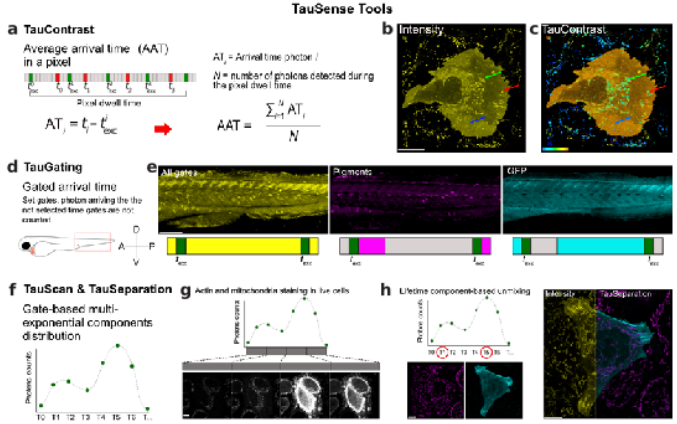

Figure 2 | TauSense tools. a, TauContrast. The contrast in each pixel is given by the average arrival times of the photons detected during the pixel dwell time. **b**,**c**, Mammalian cell labeled with near infrared membrane stain. The arrows indicate vesicles with different pH (red higher, blue lower, green intermediate). **b**, The intensity image, with higher intensity from vesicles. **c**, TauContrast image. Scale bar, 20 µm; look-up table, 0–1.5 ns. Changes in AAT highlight changes in pH in the vesicles during internalization. **d**, TauGating enables splitting photons arriving at different times. **e**, Zebrafish image; photons with short arrival times (pigments) are separated from photons with longer arrival times (GFP signal). Scale bar, 200 µm (see text for details). **f**–**h**, TauScan and TauSeparation. **f**, Schematic of the lifetime components distribution. **g**,**h**, TauScan (**g**) and TauSeparation (**h**) of mammalian cells expressing LifeAct-GFP (manufactured by ibidi GmbH) and labeled with a green mitochondrial stain. Scale bars, 10 µm.

A different use of the arrival times consists of using them to assign photons to 'categories' defined according to certain rules and to generate different populations as a result. The classic example of this approach is gating. TauSense offers this possibility with the TauGating tool. TauGating (Fig. 2d) enables the positioning of multiple digital gates (up to 16) with precise and flexible time definitions. TauGating delivers images that contain the number of photons (intensity) detected in one gate (or a set of gates, if several gates are pooled) during the pixel dwell time. A classic application for TauGating is the isolation of a signal of interest from intrinsic or spurious contributions to fluorescence in a specimen. As an example, we imaged zebrafish of the *4xGTIIC:d2GFP* line[7] still containing their native pigments. The fluorescence signal of interest provides a readout of Yap1/Taz-Tead activity and is used here to visualize the striated muscle of the trunk at 55 hpf (Fig. 2e). Using TauGating, we can extract the signal of interest from the contributions of the endogenous pigments. It is worth noting that we generated not only a gated image containing the relevant signal, but also an image with the 'gated-out' information to ensure the quality and accuracy of the result.

In addition to providing information based on AAT (TauContrast) and splitting signals into gates (TauGating), TauSense opens the door to a detailed characterization of a specimen in terms of the lifetime-based populations of the detected photons. Previous efforts to harness such information from fluorescence signals have described the use of so-called lifetime distributions to assess the potential lifetime components that constitute a given sample[8,9]. To this end, we have developed two TauSense tools, TauScan and TauSeparation, to take full advantage of our ability to characterize the distribution of mean lifetime components (Fig. 2f). Using TauScan, it is possible to scan these distributions and separate them into a predetermined number of temporal windows (Fig. 2g). We use digitally preset gates followed by a multi-exponential components fit to generate an online view (Fig. 2g, top) of the distribution of such lifetime components from the arrival times. The distribution of components enables one to work with the arrival time information in an analogous way to the spectral distribution of a fluorescence signal. Here we obtain the temporal dispersion of the signal, and by positioning the appropriate temporal windows we can split the photon signal according to the arrival time information contained in the photon flux. After such splitting of the signal, the spatial coding of the photons leads to the corresponding images. The images that result from a TauScan experiment are intensity images containing discrete temporal information (the temporal windows as explained above) across the lifetime component distribution. An example of TauScan describes the lifetime-based distributions in live cells expressing LifeAct-GFP (ibidi GmbH)[10] that were labeled with a green mitochondrial stain (Fig. 2g).

The second tool, TauSeparation, uses the lifetime-based distributions for a different application, namely species separation. Although spectral separation in fluorescence imaging has become routine[11] and a powerful tool for distinguishing multiple fluorophores, there are still instances in which fluorophore choices are limited and the necessary spectral differences are difficult to achieve. This can happen, for example, in experiments with animal models in which GFP or similar fluorescent protein reporters are used to track specific mutations and ensure the correct phenotypes. In this the case, the spectral windows of such labels are unavailable for fluorophores with overlapping emission spectra. This result can limit flexibility for probing additional structures or functions. Lifetime-based information can offer a way to tackle such dilemmas. We applied TauSeparation on the cells expressing LifeAct-GFP and stained with the green mitochondrial marker, previously used for TauScan. With TauSeparation, we obtained a well-defined signal from both the mitochondria and the actin filaments in separated intensity images. In TauSeparation, the user decides on the values of the most representative mean lifetime components with the aid of the online diagram. Then TauSeparation selects appropriate temporal windows and fits the lifetime-based information in these windows to generate separated images.

In summary, we present TauSense and show typical applications that benefit from this technology. The TauSense tool set allows one to integrate lifetime-based information and adds freedom for the multiplexing of several probes in everyday fluorescence imaging. TauSense is one of the pillars of the STELLARIS microscopes.

REFERENCES

1. Valeur, B. *Molecular Fluorescence: Principles and Applications*. *Methods* vol. 8 (2001).
2. Förster, T. Transfer Mechanisms of Electronic Excitation Energy. *Radiat. Res. Suppl.* **2**, 326–339 (1960).
3. Greenwald, E. C., Mehta, S. & Zhang, J. Genetically encoded fluorescent biosensors illuminate the spatiotemporal regulation of signaling networks. *Chem. Rev.* **118**, 11707–11794 (2018).
4. Becker, W. *The bh TCSPC Handbook*. Photon Counting Histograms. 580 (Becker & Hickl, 2017).
5. Era, A. et al. Application of lifeact reveals F-actin dynamics in *Arabidopsis thaliana* and the liverwort, *Marchantia polymorpha*. *Plant Cell Physiol.* **50**, (2009).
6. Jerome, W. G. J. & Price, R. L., eds. *Basic Confocal Microscopy* (Springer International, 2018); https://doi.org/10.1007/978-3-319-97454-5
7. Miesfeld, J. B. & Link, B. A. Establishment of transgenic lines to monitor and manipulate Yap/Taz-Tead activity in zebrafish reveals both evolutionarily conserved and divergent functions of the Hippo pathway. *Mech. Dev.* **133**, 177–188 (2014).
8. James, D. R. & Ware, W. R. Recovery of underlying distributions of lifetimes from fluorescence decay data. *Chem. Phys. Lett.* **126**, 7–11 (1986).
9. Mérola, F., Rigler, R., Holmgren, A. & Brochon, J. C. Picosecond tryptophan fluorescence of thioredoxin: evidence for discrete species in slow exchange. *Biochemistry* **28**, 3383–3398 (1989).
10. Riedl, J. et al. Lifeact: a versatile marker to visualize F-actin. *Nat. Methods* **5**, 605–607 (2008).
11. Zimmermann, T. Spectral imaging and linear unmixing in light microscopy. in *Microscopy Techniques* (ed. Rietdorf, J.) 245–265 (Springer, 2005); https://doi.org/10.1007/b102216

Résumé de la thèse

Introduction

Dans la population humaine, 1% des naissances présentent des maladies cardiaques congénitales. Le cœur est le premier organe à acquérir sa fonction dans l'embryon en développement, fournissant aux organes en formation l'oxygène et les nutriments nécessaire a la croissance et la survie. Le développement du cœur est un processus complexe, hautement régulé, qui n'a pas encore été entièrement caractérisé. Il est fondamental de mieux comprendre comment le cœur se développe pour améliorer notre connaissance des maladies cardiovasculaires.

L'épicarde est la couche de cellules mésothéliales qui recouvre le myocarde. Il est essentiel au bon développement du cœur en favorisant la croissance du myocarde, la formation de la vascularisation coronaire et la génération de fibroblastes intracardiaques. L'épicarde joue un rôle majeur dans la régénération. Plusieurs marqueurs épicardiques ont été décrits, tels que Wt1 ou tcf21 ont été identifié dans plusieurs espèces de vertébrés.

Notre projet est basé sur l'étude du poisson zèbre, qui est un modèle animal largement utilisé pour étudier le développement et la régénération. Le poisson zèbre a la capacité de régénérer un muscle cardiaque blessé à l'âge adulte. Il est particulièrement utile en raison de ses propriétés optiques optimales pour l'imagerie in vivo, car les embryons peuvent être rendu transparents jusqu'à 5 jours après la fécondation (dpf).

Chez le poisson-zèbre, les progéniteurs des cellules épicardiques proviennent du péricarde, la couche cellulaire qui entoure le cœur et forme la cavité péricardique. Les cellules péricardiques dorsales convergent en une ligne entre le pôle veineux et la zone du pôle artériel, où les cellules péricardiques s'arrondissent et forment une saillie vers la cavité péricardique. Ce groupe de cellule se regroupe et forment le proépicarde (PE) environ 48 heures après la fécondation (hpf). Les cellules de l'EP sont libérées dans la cavité péricardique et se déplacent en suivant le flux péricardique provoqué par les battements du cœur, jusqu'à ce qu'elles se fixent au myocarde. Chez d'autres espèces de vertébrés, l’epicarde présente un développement similaire, bien que les

mécanismes de libération et d'attachement des cellules puissent varier (Peralta et al, Current Biology, 2013).

Plusieurs voies de signalisation jouent un rôle important dans le processus de formation du proepicarde, dont la voie Bone Morphogenetique Protein (BMP). En outre, les voies Yap1/Wwtr1 jouent également un rôle important dans le développement de l'EP. Yap1 et Wwrt1 sont le nœud central de la voie Hippo, une voie de signalisation impliquée dans la régulation de la taille des organes et de la prolifération cellulaire, entre autres. Dans une étude précédente réalisée sur des embryons de souris, il a été démontré que Yap et Wt1 se co-localisent dans les cellules épicardiques. Ils ont également montré que l'inactivation épicardique de Yap/Taz provoque la mort embryonnaire. En outre, Yap/Taz modulent l'activité du promoteur Wt1. Bien que l'activité de Yap1/Wwrt1-Tead soit impliquée dans différentes étapes du développement cardiaque chez le poisson-zèbre, son impact au cours du processus de formation du proepicarde reste très mal connu.

Pour toutes ces raisons, nous souhaitons étudier la relation entre la signalisation de Yap1/Wwtr1-Tead et la formation de PE, ainsi que les différentes manières dont Yap1/Wwtr1-Tead pourrait être régulé.

Objectifs

Les principaux objectifs de ce projet sont les suivants :

1. Étudier le rôle de la signalisation de Yap1 dans le contexte de la formation du proepicarde

2. Étudier la formation de PE dans les modèles ou l’activité de Yap1 est altérée

3. Trouver de nouveaux régulateurs pour la formation du proepicarde

Résultats

1. Activité de Yap/Taz-Tead pendant la formation du proepicarde

Pour étudier plus en détail la formation du PE, nous avons cherché à suivre la formation du proepicarde in vivo en utilisant la microscopie à feuille de lumière. Pour ce faire, nous avons utilisé la ligne de reportage Yap1/Taz-TEAD

4xGTIIC:d2GFP (Miesfeld et Link, 2014) pour suivre l'activation de Yap1/Taz-TEAD dans l'épicarde avant et pendant la formation des amas de PE.

Nous avons donc imagé des embryons à partir de 36 heures après fertilisation (hours post fertilization, hpf). Avant ce stade, l'expression de la GFP est faible dans tout le péricarde. À environ 40 hpf, certaines cellules de la zone proche du canal atrio-ventriculaire du Cœur dans la partie du péricarde dorsal augmentent leur intensité de GFP. Ces cellules continuent d'augmenter leur expression de la GFP au fil du temps et à 48 hpf, elles commencent à s'arrondir pour former le proepicarde.

Nous avons ensuite analyse l'expression du rapporteur à partir de 48hpf. Nous avons observé des cellules plates dans le péricarde dorsal avec une expression élevée de la GFP, qui donneront naissance au proepicarde.

Dans l'ensemble, nos résultats suggèrent que les cellules qui formeront l'amas PE ont une activité Yap1/Taz-Tead avant de commencer à changer de forme et que l'activité Yap1-Taz/Tead est plus élevée dans les cellules PE.

2. La modification de l'activité nucléaire de Yap1/Taz a un impact sur la formation des grappes de PE

Nous avons ensuite cherché à tester le rôle de Yap1/Taz-Tead dans la formation des PE en régulant à la hausse et à la baisse son activité. Pour ce faire, nous avons utilisé la dexaméthasone et le XAV939. La dexaméthasone est un glucocorticoïde qui active in vivo la transcription médiée par Yap1/Taz-Tead (Sorrentino et al., 2017 ; Astone et al., 2018) et XAV939 est un composé qui inhibe les protéines AMOT stabilisatrices de la tankyrase, entraînant une diminution de la translocation nucléaire de Yap1 (Wang et al., 2015).

Nous avons traité des embryons 4xGTIIC:d2GFP de 36 à 55 hpf avec de la dexaméthasone et les avons fixés pour les imager avec un microscope confocal après coloration à la phalloïdine. Les embryons traités à la dexaméthasone ont un pourcentage accru de cellules GFP dans le péricarde et le myocarde, ce qui montre une augmentation générale de l'activité Yap1/Taz-Tead. Le nombre de cellules PE est plus élevé chez les embryons traités à la dexaméthasone que chez les contrôles non traités.

Ensuite, nous avons quantifie l'effet du traitement au XAV939 sur le nombre de cellules du proepicarde. Bien que le pourcentage de cellules GFP positives dans le péricarde ne soit pas significativement différent chez les embryons traités avec XAV939, ils ont un pourcentage de cellules GFP dans le myocarde inférieur à celui des embryons non traités, ce qui montre une diminution de l'activité Yap1/Taz-Tead. En outre, le nombre de cellules PE est plus faible chez les embryons traités par le XAV939 que chez les embryons non traités, de même que le nombre de cellules épicardiques.

Ces résultats indiquent que l'augmentation de l'activité de Yap1/Taz-Tead à des moments précoces augmente le nombre de cellules du groupe PE et que la diminution de la translocation nucléaire de Yap1 a l'effet inverse.

3. Lkb1 pourrait être un régulateur de la formation des amas de PE

Comme il a été décrit précédemment que lkb1 peut réguler la translocation nucléaire de Yap1 (Mohseni et al., 2014), nous avons cherché à étudier l'impact de la perte de fonction de lkb1 lors de la formation de proepicarde. Nous avons analysé le nombre cellules du proepicarde chez les mutants lkb1 (van der Velden et al., 2011) a différents stades embryonnaires.

À 36 hpf, il n'y a pas de différences apparentes entre les témoins et les mutants en termes du nombre de cellules proepicardiques. Cependant, à 72 hpf, les mutants lkb1 présentent un nombre accru de cellules proepicardiques par rapport aux témoins.

Conclusions

Les principales conclusions qui seront examinées plus en détail dans la thèse sont les suivantes :

- Les cellules péricardiques qui donneront naissance au proepicarde ont une activité Yap1/Taz-Tead avant que le groupe ne soit formé.
- L'augmentation de l'activité Yap1/Taz-Tead entraîne une augmentation du nombre de cellules PE.
- Une diminution de l'activité de Yap1/Taz-Tead entraîne une diminution du nombre de cellules PE.
- Les mutants Lkb1 présentent un proepicarde plus grand à 72 hpf.

Université de Strasbourg

Laia ORTIZ LÓPEZ

Étude des effecteurs de la voie Hippo, Yap1 et Wwrt1, pendant la formation du proépicarde

Résumé en français

L'épicarde est une couche de cellules mésothéliales recouvrant le myocarde. L' épicarde est essentiel pour le développement cardiaque, car il favorise la croissance myocardique, la formation de la vascularisation coronaire et la génération de fibroblastes intracardiaques. Chez le poisson zèbre, les progéniteurs épicardiques proviennent du péricarde dorsal. Lors du développement des progéniteurs épicardiques certaines cellules du péricarde dorsal s'arrondissent et font saillie pour former le cluster proépicardique (PE). Yap1 et Wwrt1 sont des protéines essentielles de la voie Hippo qui sont exprimées dans l'épicarde en développement chez la souris. Bien que l'activité Yap1 / Wwrt1 soit impliquée dans le développement cardiaque chez le poisson zèbre, son impact pendant la formation du PE reste inexploré. Nous avons caractérisé une lignée rapportant l'activité transcriptionelle de Yap1 / Wwrt1-Tead lors de la formation du PE. Ensuite, nous avons évalué le rôle de Yap1 / Wwr1-Tead lors de la formation du PE en modifiant l'activité Yap1 / Wwrt1-Tead. Nous avons également étudié le développement de PE en réponse aux forces mécaniques. Enfin, nous avons également recherché un nouveau régulateur de la formation de cluster PE. Nos travaux suggèrent que Yap1 / Wwrt1 est nécessaire pour la formation du cluster PE bien que les mutants yap1 ne présentent aucun phénotype PE. Nos travaux suggèrent également que les forces mécaniques sont essentielles pour moduler la localisation PE lors de sa formation dans la cavité péricardique.

Résumé en anglais

The epicardium, a mesothelial cell layer covering the myocardium, is essential for heart development, as it promotes myocardial growth, coronary vasculature formation and intracardiac fibroblast generation. In zebrafish, epicardial progenitors arise from the dorsal pericardium (DP). Some DP cells round up and protrude forming the proepicardial (PE) cluster. Yap1 and Wwrt1, central nodes of the Hippo pathway, are localized in the developing epicardium in mice. Although Yap1/Wwrt1-Tead activity is involved in cardiac development in zebrafish, its impact during PE cluster formation remains elusive. We characterized Yap1/Wwrt1-Tead reporter line during PE cluster formation. Next, we assessed the role of Yap1/Wwrt1-Tead activity in this process modifying it. We further studied PE cluster development and how it is affected by changes in mechanical forces. Finally, we searched as well for new regulators of PE cluster formation. Our work suggests that Yap1/Taz-Tead activity is involved during PE cluster formation although Yap1 mutants do no present any PE phenotype. Our work also suggests that fluid forces are key to modulate PE localisation and formation in the pericardial cavity.